University of Nottingham
UK | CHINA | MALAYSIA

Dynamics of cytokine induced E-selectin expression in endothelial cells

Lydia C. Ogrodzinski, BSc (Hons)

School of Life Sciences

Thesis submitted to the University of Nottingham for degree of Doctor of Philosophy

NOVEMBER 2022

i. ABSTRACT

E-selectin is a cell adhesion molecule, expressed on the cell surface of endothelial cells in response to inflammatory cytokines. Once expressed, E-selectin mediates tethering and rolling of circulating leukocytes so that they can be extravasated to inflamed tissue. Excessive recruitment of leukocytes is often a symptom of inflammatory disease, therefore the study of cytokine regulation of expression would aid understanding of how to combat this process in cases where there is over stimulation. In addition, targeting and inhibiting E-selectin expression has been a popular route to repress inflammatory progression in many diseases. Unfortunately, E-selectin - targeting therapeutics that have reached clinical trials have not been efficacious in ameliorating inflammatory symptoms or targeting E-selectin specifically. This thesis explored E-selectin regulation by key inflammatory cytokines, considered membrane organisation of expressed E-selectins and created multiple *in vitro* models to measure expression, aid detection of specific E-selectin drug binding and quantify E-selectin internalisation.

To begin, E-selectin expression was studied in human umbilical vein endothelial cells (HUVECs), using an anti-E-selectin monoclonal antibody. Binding of fluorescent secondary antibody enabled detection of expression over time using confocal microscopy, and alkaline phosphatase secondary antibody binding enabled quantification of E-selectin using principles of enzyme-linked immunosorbent assay (ELISA) in fixed cells. Here, TNF alpha time course and concentration responses were quantified, and it was discovered that $VEGF_{165}a$ and histamine enhanced the TNF alpha response as well as induced E-selectin expression alone at lower levels.

An improved model was then created with increased sensitivity and the ability to measure E-selectin expression in real time in live cells using a split NanoLuciferase binary technology (NanoBiT). A multitude of inflammatory cytokines could then be ranked in order of potency for inducing E-selectin expression and kinetics assays over 15 hr were performed to detect expression dynamics. Here it was found that TNF alpha was the most potent cytokine which exhibited maximal expression over 15 hr, contrary to other cytokines where expression decreased by 50% after 8 hr stimulation.

The E-selectin membrane organisation was then defined using principles of bioluminescence resonance energy transfer (BRET) between NanoLuc tagged E-selectin and fluorescent tagged

selectin family. Here, E-selectin homodimers were identified and heterodimers between E- and L-selectin was discovered, whereas no interactions were quantified between E-selectin and P-selectin.
Finally, BRET interactions between a fluorescently conjugated E-selectin binding peptide (Esbp) were quantified for two fluorescent conjugations; Alexa Fluor (AF) 633 and AF488, however, no interactions were observed most likely due to steric hindrance of fluorophores. However, unlabelled Esbp induced E-selectin internalisation in models using fluorescently labelled SNAP-tag E-selectin in human embryonic kidney (HEK)293T cells and HiBiT tagged E-selectin in HUVECs.

The findings demonstrated the graded stimulation of E-selectin expression by inflammatory cytokines, and further observed interactions of E-selectin with selectin family members on the membrane. In addition, peptide induced internalisation of E-selectin was observed, and the potential for all *in vitro* systems created to determine specific drug binding is discussed in detail.

ii. ACKNOWLEDGMENTS

I have been so lucky to gain diverse perspectives from my amazing supervisors on their specialities in neuroscience, polymer chemistry, cardiovascular physiology and pharmacology from Prof. Tracy Farr, Prof. Cameron Alexander, Prof. Jeanette Woolard, and Dr. Laura Kilpatrick. This project has had many potential destinations that have been altered by prolonged optimisations, external constraints and pandemics! But what hadn't waivered was the support I received from all four corners. Thank you all for keeping up with the twists and turns and remaining enthusiastic throughout. I'd like to thank Tracy for introducing me to the *in vivo* world where I had the ability to witness multiple *in vivo* experiments and even hold a human brain! I would like to thank Cameron for my short-lived but exciting introduction to polymer chemistry, being included in your lab meetings and discussions on nanoparticle and polymer chemistry was so inspiring. I'd also like to sincerely thank Prof. Steve Hill, who not only allowed me to stay in his laboratory for 4 years (compared to the originally agreed 3 months!) but invested his time and money in my project and was a source of constant encouragement and inspiration which directed the project to where it is now. Because of our 'Steve-Laura-Jeanette' (SLJ) meetings I would feel re-energised with positivity to keep going even when faced with the *numerous* experimental challenges. Jeanette, thank you for our long university park walks and for caring about my future and mental well-being above all – I've never been thrown out of the lab and assigned to 'have fun' before, but it definitely helped get out of my 'flumps'. Laura, I quite simply would not have been able to do anything without you. You are the reason I learnt anything and everything in the lab, thank you for your award-winning kindness, patience, humour and dance moves that kept me going throughout. I feel so blessed to have learnt from all of you.

Secondly, I want to thank everyone in the Institute of Cell Signalling (ICS) and COMPARE. Thank you to the SLIM team; Tim Self, Seema Bagia and Robert Markus as well as Joelle Goulding for microscopy guidance. Thank you Marleen Groenen for maintaining the lab, and being my HUVEC sensai. I want to thank Mark Soave who guided me endlessly with all things molecular biology, Leigh Stoddart for pharmacology pep talks, Liz Rosethorne for career pep talks and Rick Proudman for his hilarious and passionate outbursts about everything and anything in front of him that entertained endlessly. In addition, a special thank you to Simon Platt, who only arrived in the latter part of my PhD but who's intelligence and never ending CRISPR help was paramount to our success. I need to thank our wonderful C floor cleaners

who I grew so close to after many early starts and late nights in the lab; thank you Glennis for never failing to make me laugh and boosting moral and Cecilia for acting as my mum from home, feeding me chicken and rice and giving the best hugs. Finally, thank you to the whole team who are the reason why ICS is so great; the 'older' crew; Chloe Peach, Desislava Nesheva, Nicola Dijon, Jack Lochray, Eddy Wragg, Charlie Lay, Clare Harwood, Alistair Keen, Bradley Hoare, Laura Humphrys, Sean Cullum, Jordana Rodrigues, Leire Borrega Roman, Ben Fiedler, Laura Lemel, Julie Sanchez and the 'newer' crew: Eleonora Comeo, Owen Underwood, Noemi Karsai, George Coney, Marieke Van Daele, Patrizia Pannucci, Dehan Comez, James Farmer, Hannah Lockington and Kelvin Cheung. For the stimulating lab meetings, infectious enthusiasm on all things pharmacology, tissue culture karaoke, lab dance battles and excellent fuddles, Christmas dinners and trips to the JA. ICS always will hold a very special place in my heart.

Thirdly, I'd like to thank the EPSRC, who through the BMHA grant, headed by Felicity Rose, awarded me with this PhD. I'd like to thank our small cohort as well as the preceding years; Inas Mohd, Charlie Whitehead, Christopher Main, Benjamin Milborne, Ilona Vitkauskaite, Jason Hutchinson and Joshua Jones for providing a warm welcome into the postgraduate world.

Finally, a massive thank you to my friends and family. Thank you to my Mum and Dad for always being so loving and supportive, and for being the reason I pushed myself to go beyond what I thought I could achieve. Thank you to the rest of the Ogrodzinski (and Mastroddi) clan who have supported me throughout, Tomasz and Adam as well as Hania and Rob and their three wonderful boys Leonardo, Jovani and Massimo who cheered me on and made me laugh all the way from Toronto, Canada. I want to thank my dearest friends; Lydia Beeken, Yasmin Feuozi, Shreena Shah, Faray and Jehochanan Lawal, Ryan Lee, Rania Hamdi, Esther Ehirim, Lizzie Riby-Williams, and Emily and Serena Fathers. You've never stopped believing in me and I am so grateful for your endless cheerleading.

ABBREVIATIONS

A3	Adenosine-A3
AF	Alexa Fluor
AP	Alkaline Phosphatase
AU	Airy Unit
BRET	Bioluminescence resonance energy transfer
BSA	Bovine serum albumin
CAM	Cell Adhesion Molecule
CD	Cluster of differentiation
CLA	Cutaneous lymphocyte-associated antigen
CR	Consensus repeats
CRISPR	Clustered regularly interspaced palindromic repeats
crRNA	CRISPR RNA
CS	Chicken serum
CV	Coefficient of variation
CXCR4	C-X-C Chemokine Receptor 4
DAPI	4',6-diamidino-2-phenylindole
DMEM	Dulbecco's modified Eagle's medium
DMSO	Dimethyl sulfoxide
dNTP	Deoxynucleoside triphosphate
ECs	Endothelial cells
EDTA	Ethylenediamine tetraacetic acid
EGF	Epidermal growth factor
ELAM-1	Endothelial leukocyte adhesion molecule -1
ELISA	Enzyme linked immunosorbant assay
eNOS	Endothelial nitric oxide synthase
Esbp	E-selectin binding peptide
ESL-1	E-selectin ligand-1
Fab	Fragment antigen binding
FCS	Foetal calf serum
FITC	fluorescein isothiocyanate

GFP	Green fluorescent protein
GPCR	G-protein-coupled Receptor
gRNA	guide RNA
HBSS	Hanks' balanced salt solution
HCELL	Hematopoietic cell E- and L-selectin ligand
HEK293T	Human embryonic kidney clone 293, SV40 large T antigen
HL-60	Human leukemia-60 cells
HUVEC	Human umbilical vein endothelial cells
ICAM-1	Intracellular adhesion molecule 1
Ig	Immunoglobulin
IL	Interleukin
ILR1	IL Receptor-1
LAMP-1	lysosomal-associated membrane protein 1
LB	Luria Broth
LFA-1	Lymphocyte function associated antigen-1
LPS	Lipopolysaccharide
LSM	Laser Scanning Microscope
LU	Luminescence units
LVES	Large vessel endothelial supplement
M200	Medium 200
MAPK	Mitogen Activated Protein Kinase
NanoBiT	NanoLuc binary technology
NanoLuc	Nanoluciferase
NF-κB	Nuclear Factor Kappa Beta
NHEJ	Non-homologous end-joining
NOS	Nitric oxide synthase
NOX	NADPH oxidase
NRP-1	Neuropilin -1
OD	Optical Density
PAM	Protospacer adjacent motif
PASI	Psoriasis area and severity index
PBS	Phosphate Buffered Saline

PCR	Polymerase chain reaction
PD	Poly-D-lysine
PECAM	Platelet Endothelial Cell Adhesion Molecule
PFA	Paraformaldehyde
PMN	Polymorphonuclear cells
pNPP	p-nitrophenyl phosphate
PSGL-1	P-selectin glycoprotein ligand-1
RI	Refractive index
RNP	Ribonucleoprotein
ROI	Region of interest
ROS	Reactive oxygen species
RT	Room temperature
SEM	Standard error of the mean
sE-selectin	Soluble E-selectin
sLex	Sialyl Lewis X
sL-selectin	Soluble L-selectin
SNP	Single nucleotide polymorphism
sP-selectin	Soluble P-selectin
ssODN	single strabded oligo DNA nucleotide
TACE	TNF alpha-converting enzyme
TAE	Tris-acetate-EDTA
TERT2	Telomerase reverse transcriptase
TLR4	Toll-like receptor-4
TNF	Tumour Necrosis Factor
TNFR	TNF receptor
TNFSF	TNF superfamily
tracrRNA	trans-activating CRISPR RNA
VCAM-1	Vascular cell adhesion molecule -1
VE-cadherin	Vascular Endothelial cadherin
VEGF	Vascular endothelial growth factor
VEGFR2	VEGF Receptor 2
VLA-4	Very late antigen-4

VSMCs	Vascular smooth muscle cells
vWF	von Willebrand factor
WPB	Weibel Palade Body
WT	Wildtype

Table of Contents

Chapter 1 General Introduction

1.1 The vascular system

The vascular system (also termed the circulatory system) is an organisation of vessels that carries blood and lymph throughout the body (Tucker and Mahajan, 2019). It can be broken down into the arterial system, which provides a blood distribution network to the capillaries (the main site of interchange between blood tissues), and the venous system that returns de-oxygenated blood from the capillaries to the heart (Wheater, Burkitt and Daniels, 1982). The vascular system is vital for the survival of tissues and organs.

1.1.1 Vascular system structure

In general, blood vessels have a common basic, layered structure. The *tunica intima* is the innermost layer, and it is composed of a luminal lining of flat, cobblestone-like endothelial cells (ECs) supported by a basement membrane and connective tissue. Connective tissue fibres such as collagen provide tensile strength and elastic fibres are arranged in sheets as lamina to allow flexibility (Berridge, Van Vleet and Herman, 2018). The basement membrane also contains pericytes, which are small, thin cells (2 μm diameter) with contractile proteins, though they lack dense bodies and have fewer myofilaments (Braverman, 2000). The *tunica media* is composed of a muscular layer of smooth muscle cells (SMCs). SMCs are spindle-shaped and have elongated nuclei. They contain cytoskeletal, thin (actin) and thick (myosin) contractile filaments and regulate the vessel's ability to contract and relax (Brozovich *et al.*, 2016). The outermost layer is the *tunica externa*, consisting of a connective tissue and elastic fibres. There are great variations in this layered structure depending on the function of each vessel, including the luminal diameter, layer thickness and order, and the presence of other anatomic features such as valves (Berridge, Van Vleet and Herman, 2018).

1.1.1.1 Arteries

Arterial structures consist of thicker SMC layers and smaller lumens so that the vessels can maintain and withstand the large pressures exerted by blood flowing from the heart (Wheater, Burkitt and Daniels, 1982). Arteries are classified into three types: elastic and muscular arteries (ranging from 100 – 10,000 μm in diameter), and arterioles (30μm diameter) (Ostadfar, 2016) (Figure 1.1). Elastic arteries, such as the aorta and pulmonary arteries, are situated in close proximity to the heart, they have a relatively large diameter and an elastic property that helps

withstand high blood pressure (Ostadfar, 2016). In muscular arteries such as the radial and femoral, the connective tissue layers (internal and external elastic lamina) are reduced (Wheater, Burkitt and Daniels, 1982). Their lumen diameter is smaller and the smooth muscle layer is thicker compared to elastic arteries to better assist with blood flow regulation as their contraction and relaxation of the muscle layer allows adjustment of diameter to maintain blood pressure and control blood flow (Ostadfar, 2016). Arterioles have a lumen less than 30µm in diameter and function as resistors in the vascular system to regulate blood flow to end organs and tissue, helping to establish and maintain vasoactive tone (Ostadfar, 2016).

1.1.1.2 Capillaries

Capillaries make up the microcirculation (5-10µm). Capillaries have no tunica media and consist only of a single layer of ECs and a subendothelial cell layer of connective tissue. Therefore, muscular precapillary sphincters at the arteriolar-capillary junctions control blood flow within the capillary networks. They are responsible for the exchange of gases, fluids, nutrients and metabolic waste products, and their dense networks around tissue allows a high surface area for materials to be exchanged (Wheater, Burkitt and Daniels, 1982). Blood eventually drains into a series of post-capillary venules and veins (Wheater, Burkitt and Daniels, 1982) (Figure 1.1).

1.1.1.3 Veins

The veins collect deoxygenated blood and waste from tissues and organs (Ostadfar, 2016). Veins are mainly classed based on their size, ranging from venules (8 – 100µm) to medium and large veins up to 30,000µm in diameter. The *tunica externa* is thick (Wheater, Burkitt and Daniels, 1982) and the *tunica media* is thin compared with that of arteries and it consists of two or more layers of SMCs (Figure 1.1). This allows veins to store small or large amounts of blood by constricting and enlarging. Veins also contain valves; two flap-like structures of the *tunica intima*, which prevent the backflow of blood and maintain flow to the heart (Ostadfar, 2016).

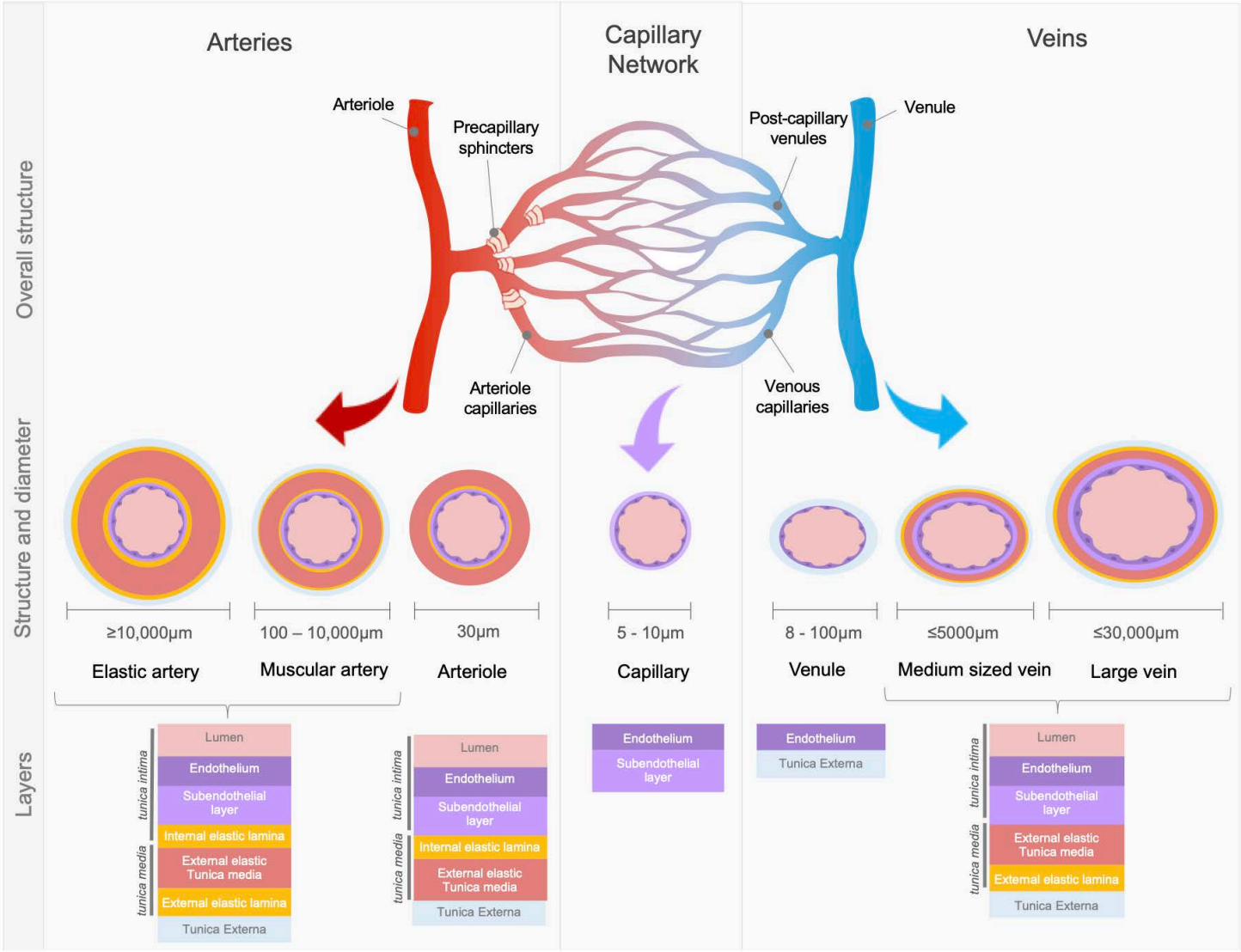

Figure 1.1 The structure of the vascular tree, from arteries to capillaries to veins. The vascular tree consists of arteries which carry oxygenated blood, capillaries which transport the blood components to the tissues that need them, and veins which transport deoxygenated blood away from tissues. Arteries lead to arterioles, where blood flows through precapillary sphincters before the capillary bed. Blood then flows through post capillary venules before venules and veins. Each type of vessel consists of different thicknesses of layers of tunica externa, tunica media and tunica intima. Arteries contain two elastic lamina layers (internal and external) within the tunica intima and media, respectively, with a thick smooth muscle layer, whereas veins only contain the external elastic lamina layer and a thin tunica media layer. As a consequence, arteries have a smaller lumen than veins.

1.2 Endothelial cells

Arguably, the most important cell type in vasculature are ECs which line all blood vessels (Figure 1.1). There are up to ten trillion ECs, covering a surface area of more than 1000 square metres, and collectively weighing up to 1 kg (Galley and Webster, 2004; Mai *et al.*, 2013). ECs were considered to be an inert monolayer forming a barrier separating blood from parenchyma (Galley and Webster, 2004) and it wasn't until the late 1960s that the understanding of EC cell biology was transformed.

In addition to providing a barrier, ECs are the first point of contact for circulating blood components and therefore mediate transport of nutrients and molecules into the parenchyma (Sturtzel, 2017a). ECs also regulate vascular tone, thrombosis and vascular inflammation, by exerting significant autocrine, paracrine and endocrine actions and interacting with circulating blood cells (Roitt *et al.*, 2017).

1.2.1 Regulation of vascular tone

ECs can regulate vasoconstriction and vasodilation of blood vessel walls independent of heartbeat, innervation and respiration, by releasing various vasoactive factors (Godo and Shimokawa, 2017). ECs produce nitric oxide (NO), prostacyclin (PGI_2) and endothelium derived hyperpolarizing factor (EDHF) to induce vasodilation, and produce thromboxane (TXA_2) and endothelin-1 (ET-1) to induce vasoconstriction of vascular smooth muscle cells (VSMCs) (Sandoo *et al.*, 2010; Kostov, 2021).

The most common method by which vasodilation is initiated is via NO; a potent vasodilator produced from the cationic amino acid L-arginine (Michel and Vanhoutte, 2010; Krüger-Genge *et al.*, 2019) (Figure 1.2). The activation of endothelial nitric oxide synthase (eNOS) is critically dependent on the inhibition of caveolin-eNOS interaction by calcium ions (Godo and Shimokawa, 2017). An influx of calcium ions is induced by a diverse group of agonists including bradykinin, acetylcholine, histamine and thrombin which activate a G-protein-dependent signalling pathway which releases intracellular calcium ion stores (Godo and Shimokawa, 2017). eNOS catalyses the production of NO, which then diffuses into vascular smooth muscle cells (VSMCs) and causes SMC relaxation and vasodilation (Godo and Shimokawa, 2017) (Figure 1.2). Click or tap here to enter text.

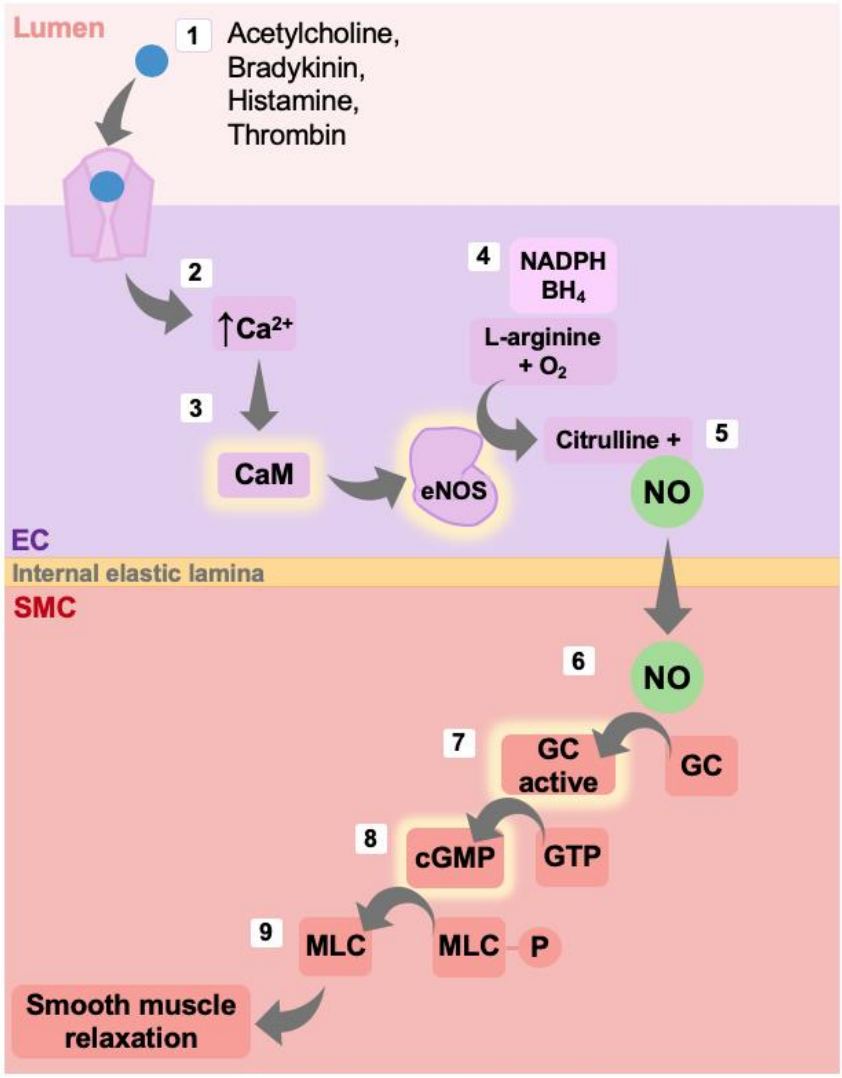

Figure 1.2 ***The production of Nitric Oxide (NO) in endothelial cells (ECs) and the method of action of NO inducing vasodilation in smooth muscle cells (SMCs).*** *Based on Michel and Vanhoutte, 2010.*

1) Stimulation of ECs with mediators such as acetylcholine, bradykinin, histamine and thrombin causes an increase in intercellular Ca^{2+}. 2) Ca^{2+} displaces the inhibitor, caveolin, from calmodulin (CaM) (11). 3) and 4) CaM in turn activates the endothelial isoform of nitric oxide synthase (eNOS), which, with the assistance of nicotinamide adenine dinucleotide phosphate (NADPH) and tetrahydrobiopterin (BH4), catalyses the conversion of L-arginine, to produce nitric oxide (NO) and citrulline (11). 5) and 6) NO diffuses into SMCs and activates guanyl cyclase (GC) enzyme. 7) GC activates the conversion of guanosine triphosphate (GTP) to cyclic guanosine monophosphate (GMP) (11). 8) Cyclic GMP (cGMP) facilitates the dephosphorylation of myosin light chains. 9) This causes the dissociation of myosin and actin filaments and results in smooth muscle relaxation (11). SMC relaxation causes vasodilation and increased blood flow (12).

Other isoforms of NOS exist to catalyse production of NO in different cell types. Neuronal NOS (nNOS) catalyses NO production in the cells of central and peripheral nervous system, epithelial cells, pancreatic islet cells and VSMCs, whereas inducible NOS (iNOS) is expressed after inflammatory stimulation in monocytes, macrophages, dendritic cells, neutrophils, epithelial cells, SMCs, microglial cells, astrocytes, neurons and endothelial cells of the blood brain barrier (Sonar and Lal, 2019; Doulias and Tenopoulou, 2020b). All three isoforms bind calmodulin (CaM) after an increase in intracellular Ca2+, however iNOS has the ability to bind at extremely low Ca^{2+} levels (below 40nM) due to a different amino acid structure of the CaM binding site (Förstermann and Sessa, 2012). All isoforms utilise L-arginine, molecular oxygen, nicotinamide adenine dinucleotide (NADPH) and BH4 to produce NO as shown in Figure 1.2 with eNOS.

Recent studies suggest that EDHF is the predominant endothelium-dependent vasorelaxation pathway in the absence of NO (Tomioka *et al.*, 1999; Krüger-Genge *et al.*, 2019). The nature of EDHF is not yet clear, however it is known to cause hyperpolarisation of smooth muscle cells via a K^+ efflux propogated from ECs via myoendothelial gap junctions to the underlying smooth muscle (Chen, Raouf and Khalil, 2017).

1.2.2 Mediation of transport

As well as regulating vascular tone, ECs also regulate transport of substances to tissues. Endothelium selectively enables or inhibits molecules to pass through the endothelial layer to the parenchyma on the basis of size, polarity and lipophilicity (Campbell, Maiers and DeMali, 2017). Molecules $\leq$ 3nm in diameter such as glucose, water and ions can pass via interendothelial junctions (termed paracellular pathway), and molecules exceeding this diameter can pass via caveolae; small invaginations of the EC plasma membrane which engulf molecules and allow transcellular transport (Hubert, Larsson and Lundmark, 2020).

a)

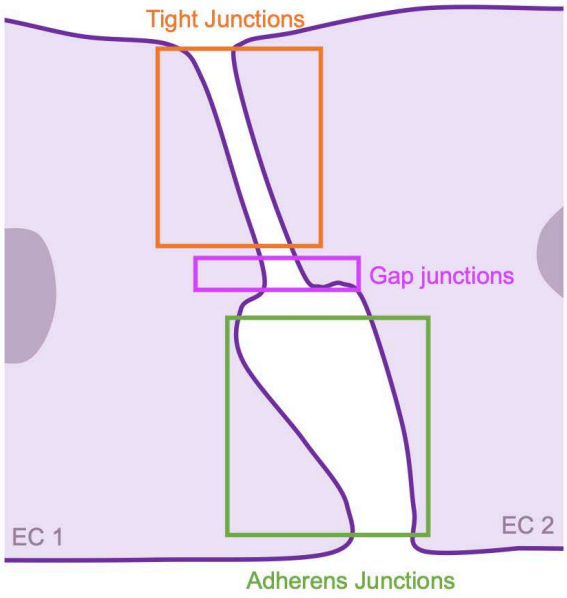

b)

Membrane protein expression

Tight Junctions	Gap Junctions	Adherens Junctions
Claudin	Connexins	VE-cadherin
Occludin		PECAM
JAM		Nectin
ESAM		
Nectin		

Figure 1.3 ***The junctional domains between ECs.*** *a) Consisting of tight junctions in the most apical side, adherens junctions in the most basal side and gap junctions in between. b) Claudins, occludins, junctional adhesion molecules (JAMs) and endothelial cell selective adhesion molecules (ESAMs) are typically found in tight junctions. Connexins are found in gap junctions and vascular endothelial cadherin (VE-cadherin) and platelet endothelial cell adhesion molecule (PECAM) are expressed in adherens junctions. Nectin is found in both gap junctions and adherens junctions.*

1.2.2.1 Paracellular transport

The best recognised junctional domains between ECs are tight junctions, typically on the apical side of ECs, adherens junctions, located basally and gap junctions in between (Figure 1.3a) (Wallez and Huber, 2008; Campbell, Maiers and DeMali, 2017). Each domain expresses a particular set of transmembrane proteins, that interact with transmembrane molecules (Figure 1.3b) (Lampugnani, 2012; Campbell, Maiers and DeMali, 2017). Often adhesive links are formed between ECs as there is identical expression of proteins and molecules in adjoining adjacent ECs (Campbell, Maiers and DeMali, 2017).

1.2.2.2 Transcellular transport

Caveolae are small lipid rafts that form on the endothelial cell surface, ranging from 50 - 100nm, that enable transcytosis of molecules such as albumin and insulin (Sukriti *et al.*, 2014; Hubert, Larsson and Lundmark, 2020). Molecules circulating in the lumen bind to their receptor found in endothelial caveolae and induce the endocytosis of caveolae vesicles (Matthaeus and Taraska, 2021). The vesicles are then transported to the subendothelial space (Matthaeus and Taraska, 2021). The endothelial transcytosis pathway has been shown to direct

the transfer of proteins and solutes, thereby acting as a filtering system essential for regulating transport of substances to tissues.

1.2.3 Regulation of vascular inflammation

As ECs are the first cell type in contact with blood circulation, they are responsible in responding to 'stress' stimuli and regulating the first stages of inflammation. ECs become 'active' in response to inflammatory cytokines which are increased in number due to inflammation.

Activation of ECs entails a series of processes which mutually interact in causing local inflammation, and an increase in transcellular and paracellular transport of leukocytes to tissue via a process called extravasation (Filippi, 2016). ECs can respond within 10 - 20 minutes to inflammatory stimuli; this is typically mediated by G-protein-coupled receptors (GPCRs) such as histamine H1 receptors, which cause NO production and vasodilation as described previously (Figure 1.2), causing increased blood flow and thereby increased interaction with circulating leukocytes (Branco *et al.*, 2018). Within this short timeframe ECs can also express cell adhesion molecules (CAMs) which mediate the tethering, rolling, and extravasation of leukocytes to tissues (Pober and Sessa, 2007; Filippi, 2016). P-selectin is a cell adhesion molecule stored in Weibel Palade bodies (WPBs) that is rapidly exocytosed to the EC surface after stimulation with inflammatory cytokines (Vinogradova, Roudnik, V. B. Bystrevskaya, *et al.*, 2000; De Wit *et al.*, 2003). ECs also retract, causing increased leakage of plasma proteins into tissue; this later on helps to create a provisional matrix to support leukocyte extravasation (Pober and Sessa, 2007; Filippi, 2016). This fast response is termed type I activation.

Type II activation of ECs is mediated by pro-inflammatory cytokines such as tumour necrosis factor (TNF) alpha, and interleukin-1 (IL-1), which, like type I activation enhance local blood flow and recruitment of leukocytes, but unlike the previous classification, is reliant on gene transcription and protein translation (Sturtzel, 2017b). Because of this, type II activation responses are slower in onset and can last from hours to days (Pober and Sessa, 2007; Sturtzel, 2017b). Type II activation is essential for a sustained inflammatory response, as after 10-20 minutes ECs become desensitized preventing re-stimulation (Gainetdinov *et al.*, 2004). The prototypic mediators of this response are TNF alpha and IL-1.

Interleukin-1 (IL-1) is a general name for two subtypes, IL-1 alpha and IL-1 beta. Both IL-1 subtypes bind to the receptors IL-1 receptor 1 (IL1R1) and IL-1 receptor accessory protein (IL1RAP) presented on ECs (Kaneko *et al.*, 2019). TNF alpha is a multifunctional cytokine secreted by activated macrophages, natural killer cells and lymphocytes and is one cytokine of over 20 belonging to the TNF superfamily (TNFSF) (Dembic, 2015). Three TNF alpha molecules form a molecular triangle (Dembic, 2015); the homotrimer is first synthesised as a membrane bound cytokine, before it is cleaved by a TNF alpha-converting enzyme (TACE) to aid its secretion (Jang *et al.*, 2021). Both IL-1 and TNF alpha stimulate MAPK and NF-κB pathways in ECs, which upregulate the expression of CAMs such as P- and E-selectin, ICAM-1 and VCAM-1 (Acuner Ozbabacan *et al.*, 2014).

1.2.4 Endothelial dysfunction

Because of the pivotal role that ECs play in vascular tone, mediation of transport and vascular inflammation, the dysfunction of ECs can lead to many complications, and disease. In some cases, due to vascular risk factors such as increased cholesterol levels, hyperglycaemia, hypertension, aging and NO dysfunction, inflammatory stimuli fail to be eradicated and the adaptive immune response is persistently stimulated which will cause development of chronic inflammation (Pober and Sessa, 2007; Sturtzel, 2017b). This can lead to EC dysfunction, which precedes the development of vascular diseases such as coronary heart disease (CHD), stroke, chronic obstructive pulmonary disease (COPD), and Alzheimer's disease, all of which were the top causes of death in 2016 globally (Kerr *et al.*, 2000a; Ohta *et al.*, 2001a; Ulbrich *et al.*, 2006a; Japp *et al.*, 2013a; Rajendran *et al.*, 2013). According to British Heart Foundation (2022), 9.1 million people died of CHD, followed by 6.6 million people who died from stroke and 3.3 million people died from COPD in 2022 alone (British Heart Foundation, 2022). These statistics highlight the importance of understanding and treating endothelial dysfunction.

Reduced production and/or bioavailability of NO is considered the central mechanism responsible for endothelial dysfunction. Obesity, high glucose intake, microbial infections, smoking and exposure to metals and air pollutants can all increase the number of free radicals in the body (Rajendran *et al.*, 2013). Free radicals can disrupt the balance of NO, damage the endothelium and leave it overly permeable which will allow toxins to pass through to tissues and cause tissue damage (Di Meo and Venditti, 2020). Increased permeability of ECs in the blood brain barrier, can lead to cerebrovascular diseases. In the periphery, loss of NO in

skeletal muscle vessels impairs the dilatation of blood vessels during exercise and ischaemia, which limits the delivery of oxygen to tissues under conditions of increased demand and impairs flow-mediated dilatation (Rajendran *et al.*, 2013). Reactive oxygen species (ROS) also plays a role in EC dysfunction. ROS is generated at sites of inflammation and low concentrations function as signalling molecules to regulate cell growth and adaptation responses (Hadi, Carr and Al Suwaidi, 2005; Aggarwal *et al.*, 2019). Higher concentrations, however, cause endothelial permeability, over-recruit leukocytes to tissues, alter endothelial signal transduction and redox-regulated transcription factors and lead to EC death (Alhayaza *et al.*, 2020). In dysfunctional endothelium, the superoxide-producing enzyme NADPH oxidase (NOX) promotes overproduction of ROS as well as superoxide anion ($O_2\bullet^-$).

As endothelial dysfunction is an early sign of many vascular diseases, its early detection would decrease the chance of vascular disease progression. One family of proteins that are expressed early in activation of ECs are the selectin family.

1.3 The selectin family

Selectins are single chain transmembrane glycoproteins consisting of an N-terminal calcium dependent (C-type) lectin domain, an epidermal growth factor (EGF) domain, a chain of consensus repeats (around 60 amino acids each), a transmembrane domain, and an intracellular cytoplasmic tail (McEver, 2015a; Kappelmayer and Nagy, 2017a) (Figure 1.4). The lectin and epidermal growth factor domains mediate interactions within the lumen of the blood vessels. Members of the selectin family include L-selectin (expressed on leukocytes) and P- and E-selectin (expressed on ECs) (Tu *et al.*, 2002; Kappelmayer and Nagy, 2017a; Tinoco *et al.*, 2017) (Figure 1.4). They structurally differ in length by varying numbers of consensus repeats (CR) units (2, 9, and 6 for L-, P- and E-selectin, respectively). The consensus repeat units' role

is not yet defined but is likely to act as a spacer between the active units and the lectin and epidermal growth factor domain mediate interactions within the lumen of the blood vessels.

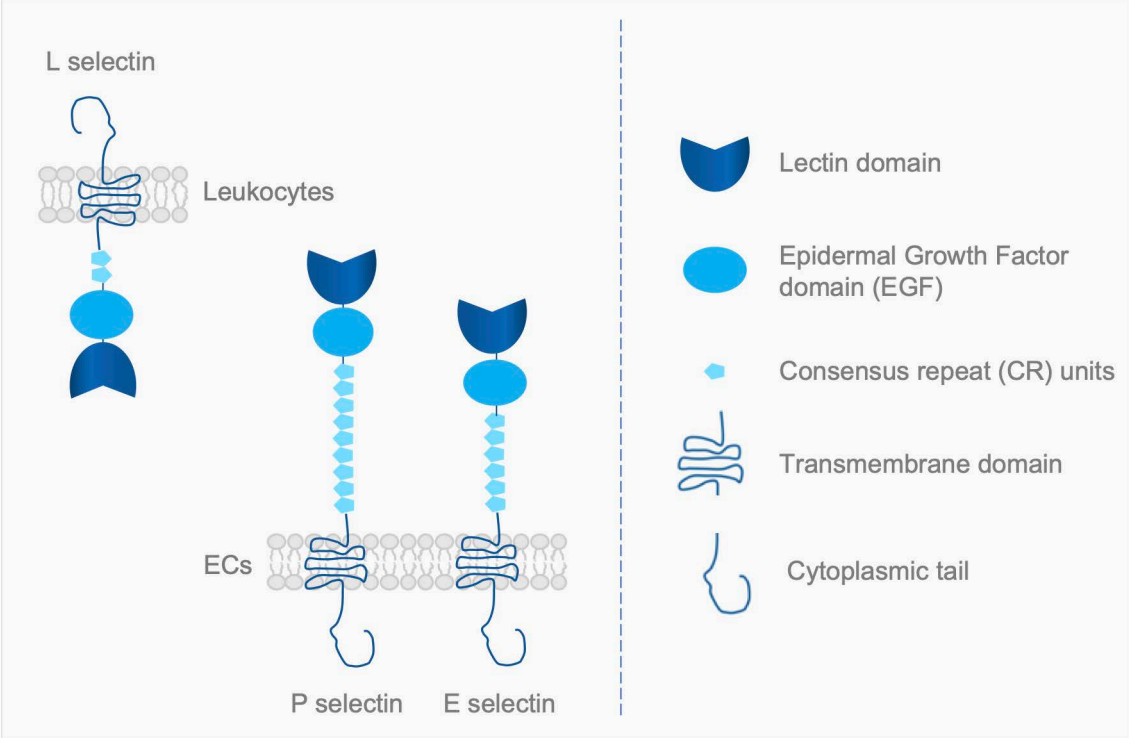

Figure 1.4 ***The structure of the selectin family****. Endothelium express both P selectin and E selectin, and leukocytes express L selectin. All selectins have the same domains; lectin, EGF, consensus repeat (CR) units, transmembrane and cytoplasmic tail domains. They differ in structure by the number of CR units; therefore, P selectin is the longest of the selectin family and L selectin is the shortest.*

1.3.1 L-selectin

L-selectin is constitutively expressed on most types of leukocytes (Tu *et al.*, 2002). It is one of the earliest surface markers to be expressed in response to inflammatory stimuli, suggesting that its role extends to hematopoietic cell trafficking and differentiation (Ivetic, Green and Hart, 2019). Upon inflammatory stimulation, L-selectin is rapidly proteolytically cleaved from the leukocyte cell surface, leaving soluble L-selectin (sL-selectin) (Tu *et al.*, 2002), which plays a role in downregulation of leukocyte adhesion to ECs (Kappelmayer and Nagy, 2017a). *In vitro*, sL-selectin has been shown to reduce leukocyte migration by 30%, as well as L-selectin specific attachment to ECs in a dose dependent manner (Schleiffenbaum, Spertini and Tedder, 1992; Tu *et al.*, 2002).

1.3.2 P-selectin

P-selectin is expressed by ECs. It is decorated with carbohydrates in the Golgi apparatus and then stored in cytoplasmic secretory vesicles that are unique to ECs named weibel palade bodies (WPBs) (Figure 1.5).

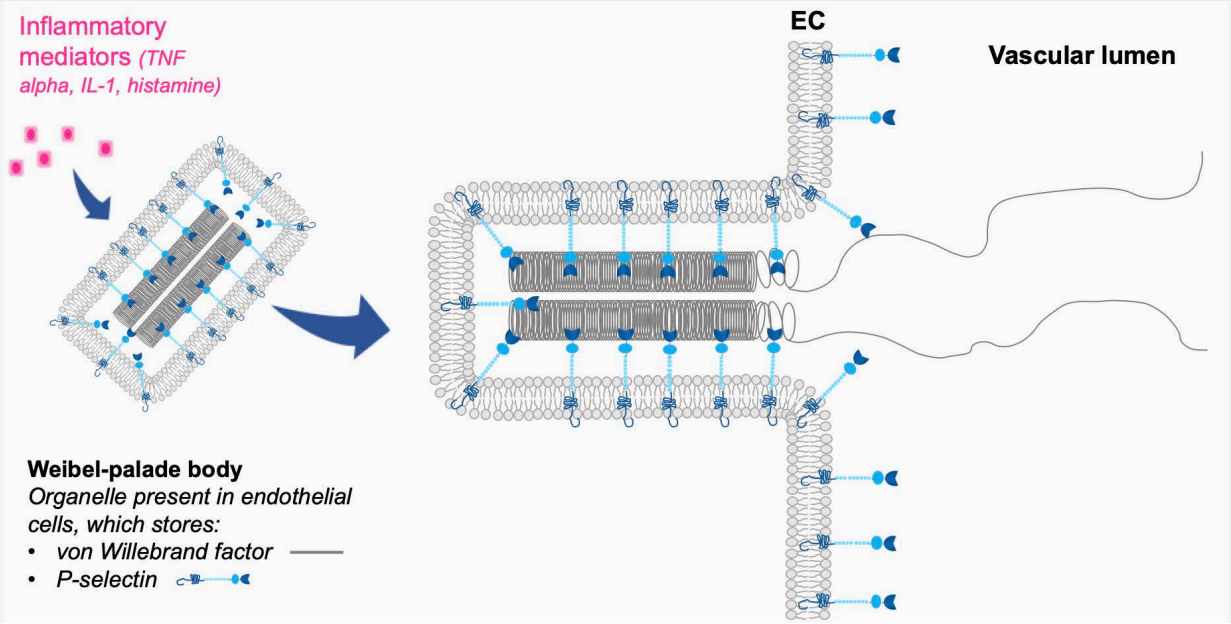

Figure 1.5 ***P-selectin storage and secretion.*** *P-selectin is contained in weibel palade bodies (WPBs), alongside von Willebrand factor (vWf). Upon inflammatory mediator stimulation, WPBs translocate to the EC surface, hypothesised by microtubule network transport. P selectin endocytoses at the EC membrane as well as vWf; both aiding the adhesion of circulating leukocytes.*

When ECs are activated, WPBs rapidly exocytose P-selectin to the luminal surface (Figure 1.5) (Vinogradova, Roudnik, V. Bystrevskaya, *et al.*, 2000; De Wit *et al.*, 2003). The cell microtubule network (actin and vimentin filaments) is essential for WPB exocytosis (Vinogradova, Roudnik, V. Bystrevskaya, *et al.*, 2000). In inflamed human aortic endothelial cells (HAECs), WPBs were shown to exhibit one of two fates: accumulation at the microtubule-organising centre, or translocation to the plasma membrane and exocytosis (Vinogradova, Roudnik, V. Bystrevskaya, *et al.*, 2000). Movement towards the microtubule-organising centre is thought to be mediated via interaction with microtubules whereas movement towards the membrane is thought to be dependent on vimentin filaments (Vinogradova, Roudnik, V. Bystrevskaya, *et al.*, 2000). de Wit and colleagues (2003) used real-time imaging to study the dynamics of WPB exocytosis after incubation with various inflammatory cytokines; thrombin, phorbol myristate acetate, forskolin and epinephrine (De Wit *et al.*, 2003). The group were able to track von Willebrand factor (vWF) secretion in human umbilical vein endothelial cells (HUVECs), and therefore movement of WPBs, by

fluorescently tagging vWF with a viral vector carrying green fluorescent protein (GFP). Consequentially, the vWF-GFP positive cells revealed rod shaped vesicles, later confirmed as WPBs, that were heterogeneously distributed throughout the cell and colocalised with P-selectin (De Wit *et al.*, 2003). WPBs in resting HUVECs either showed stochastic movement in all directions that were reminiscent of microtubule associated granules, or were motionless, appearing tethered. In HUVECs, WPBs are hypothesised to be 'docked' at the plasma membrane or trapped in the actin network (Wacker *et al.*, 1997; De Wit *et al.*, 2003). Stimulation of the HUVECs with either thrombin or phorbol myristate acetate caused a series of events: slight cell contraction which coincided with WPB movement towards the centre of the cell, then bright stationary WPB patch formation and disappearance of vesicles, followed by the appearance of vWF-GFP 'clouds'. The bright stationary WPB patch was indicative of WPB fusion to the endothelial plasma membrane and the formation of vWF-GFP 'clouds' was the result of vWF diffusion into the extracellular space. These events were slightly delayed in phorbol myristate acetate stimulated cells.

It is important to note that P-selectin can also be transcriptionally regulated. For example, pro-inflammatory cytokines interleukin 3 and 4 (IL-3 and IL-4) and Oncostatin M have been shown to increase P-selectin mRNA synthesis and protein production in ECs (Modur *et al.*, 1997; Woltmann *et al.*, 2000). A soluble form of P-selectin (sP-selectin) has also been described, which could either represent a soluble splice variant or a proteolytic fragment of membrane bound P-selectin lacking the transmembrane domain (Ushiyama *et al.*, 1993; Dunlop, 2004). Dimerized sP-selectin has been shown to help trigger integrin dependent leukocyte adhesion in vitro, as well as inducing increased thrombus frequency in the inferior vena cava in mice (Panicker *et al.*, 2017).

1.3.3 E-selectin

E-selectin (also known as CD62E or ELAM-1) is a 115 kDa protein (McEver, 2015a), though there are different glycosylated forms: 64kDa and 100kDa (Ehrhardt, Kneuer and Bakowsky, 2004a). Unlike P-selectin, E-selectin is *de novo* synthesized when ECs are activated by inflammatory mediators, such as TNF alpha, IL-1, histamine, LPS and NO. Although this is required in most organs, it is important to mention that E-selectin is constitutively expressed on surfaces of venular endothelial cells of bone marrow and skin (McEver, 2015b).

During type II activation of ECs, inflammatory cytokines promote transcription and translation of CAMs to mediate leukocyte transport; of which E-selectin is a major player. E-selectin has several leukocyte binding targets (Figure 1.6).

P-selectin glycoprotein ligand-1 (PSGL-1) is present on all leukocytes (Tu *et al.*, 2002; Kappelmayer and Nagy, 2017a; Tinoco *et al.*, 2017). It is a 120kDa transmembrane mucin-like protein, and is the most characterized selectin ligand (McEver, 2015a; Kappelmayer and Nagy, 2017a). It contains branching sites that permit O- and N- linked glycosylation in its extracellular domain, as well as terminal sites which are further modified post-translation by sulphation as well as sialic acid and fucose carbohydrates (Tinoco *et al.*, 2017) (Figure 1.6). The N terminal lectin domain of selectins recognises and binds to sialylated fucosylated or Sialyl Lewis X or sLex carbohydrates (McEver, 2015a). PSGL-1 binds with selectins at varying affinities (Table 1.1). It typically forms homodimers via disulphide bridges that link the two 120 kDa chains, however this dimerization reduces affinity for P selectin (Ehrhardt, Kneuer and Bakowsky, 2004a). PSGL-1 is also regulated by different degrees and forms of glycosylation (Ehrhardt, Kneuer and Bakowsky, 2004a; Tinoco *et al.*, 2017).

In the absence of PSGL-1, E-selectin also has affinity for other binding partners, such as: E-selectin ligand-1 (ESL-1), CD43, CD44, hematopoietic cell E- and L-selectin ligand (HCELL; a specialized glycoform of CD44), cutaneous lymphocyte-associated antigen (CLA; a distinct glycoform of PSGL-1), L-selectin, β2 integrins, and glycolipids (Barthel *et al.*, 2007a; Kappelmayer and Nagy, 2017b) (Figure 1.6). ESL-1, in addition to PSGL-1, also requires appropriate modifications of N-glycans to bind to E selectin (Zarbock *et al.*, 2011a). Sulfation modifications post-translation does not enhance E-selectin binding unlike P- and L-selectin (McEver et al., 2015).

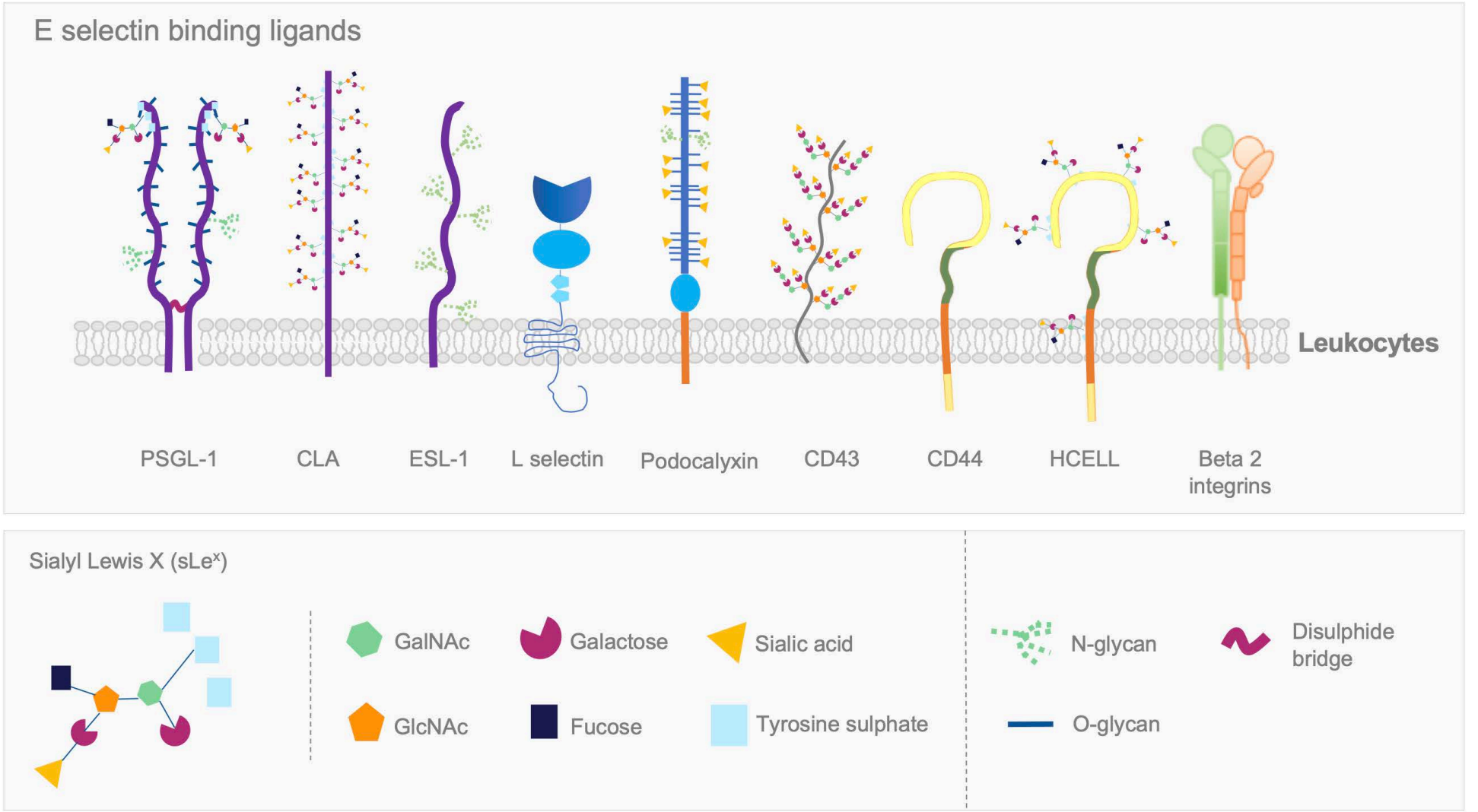

Figure 1.6 ***E-selectin binding ligands.*** *PSGL-1: P-selectin glycoprotein ligand-1; CLA: cutaneous lymphocyte-associate antigen; ESL-1: E-selectin Ligand-1, HCELL: haematopoietic cell E- and L-selectin ligand; GalNAc: N-Acetylgalactosamine.*

Table 1.1 ***Kd (nM) values for PSGL-1 binding with E-, P- and L-selectin****. KD describes the equilibrium dissociation constant. The lower the KD the higher the affinity of the ligand. ND: not determined.*

Selectin	PSGL-1 Kd (nM) (in 150-200mM salt concentration)		Ref
	Monomer	Dimer	
E selectin	ND	1,150 ± 118	(AbuSamra *et al.*, 2015)
P selectin	403	4.1	(Molenaar *et al.*, 2002)
L selectin	47,000	ND	(Klopocki *et al.*, 2008)

1.3.4 The role of leukocytes in vascular inflammation

There are two distinct subsets of leukocytes that coordinate defence; myeloid cells (macrophages and their monocyte precursors; mast cells, dendritic cells, neutrophils, basophils and eosinophils) and lymphoid cells (T-lymphocytes, B-lymphocytes and natural killer (NK) cells) (Roitt *et al.*, 2017).

There is a sophisticated and coordinated interplay between leukocytes and the selectin family that involves chemoattractants, pro-inflammatory cytokines, and integrins. These processes allow the adherence and rolling of leukocytes across the ECs so that they ultimately extravasate and exacerbate the inflammatory response (Ehrhardt, Kneuer and Bakowsky, 2004a).

1.3.5 Leukocyte tethering and rolling

It has been proposed that EC activation initiates a ‘three step area code’ consisting of 1) chemoattractant-receptor 2) selectin-carbohydrate and 3) integrin-Ig ligand interactions. This process mediates leukocyte trafficking from ECs to tissue (Weber, 2003). Chemoattractants bind to G protein coupled receptors (GPCRs) (Figure 1.2), integrins bind to their specific

immunoglobulins (Igs) and selectins bind to their glycoprotein ligands to mediate leukocyte recruitment and rolling (Ehrhardt, Kneuer and Bakowsky, 2004a).

Leukocytes extravasate along and through ECs by paracellular and transcellular migration. The first step of extravasation is tethering; the specific contact of leukocytes with ECs, mediated by the selectin family (Sturtzel, 2017a). Second is the initiation of rolling of leukocytes along the endothelium; this is done by synergistic binding of E-selectin and P-selectin to their glycoprotein ligands presented on leukocytes (Figure 1.6). The rolling process requires rapid formation and breakage of bonds under the high shear blood flow (McEver, 2015b). Rolling enables cells to receive signals that activate integrins, another class of adhesion receptors, which cause the cells to roll slower and to arrest (Zarbock *et al.*, 2011a; McEver, 2015b). PSGL-1-E-selectin interaction causes lymphocyte function associated antigen-1 (LFA-1) activation which itself slows leukocyte rolling velocities by enhancing binding activity of LFA-1 with intracellular adhesion molecule 1 (ICAM-1) (Cappenberg, Kardell and Zarbock, 2022). The binding of ICAM-1 with LFA-1 and vascular cell adhesion molecule 1 (VCAM-1) with very late antigen-4 (VLA-4), induces downstream intracellular signalling that alters cytoskeleton structures, causing fixation and crawling of leukocytes (Sturtzel, 2017a) (Figure 1.7). VCAM-1 binding also induces Rac signalling which induces formation of intracellular gaps via production of reactive oxygen species (ROS) and activation of p38 MAPK, ready for EC diapedesis (van Wetering *et al.*, 2013). Diapedesis is the fifth and final step of the 5 sequential steps and describes the paracellular and/or transcellular movement of leukocytes, aided by the proteins platelet endothelial cell adhesion molecule-1(PECAM-1) and CD99; this process takes around 15-20 minutes (Sturtzel, 2017a) (Figure 1.7). Leukocytes can extravasate through transcellular and paracellular pathways, although *in vitro* studies suggest that the paracellular junction proteins are recruited to podosomes, ring like apertures on the EC surface that aid transmigration through ECs (Pober and Sessa, 2007; Schimmel, Heemskerk and van Buul, 2017).

The initial tethering process, mediated by E- and P-selectin is vital for the vascular immune response to be successful (Sturtzel, 2017a). E-selectin has shown binding to 9 different ligands *in vivo* and *in vitro*; and the presence of these ligands differ in location and quantities on differing types of leukocytes.

.

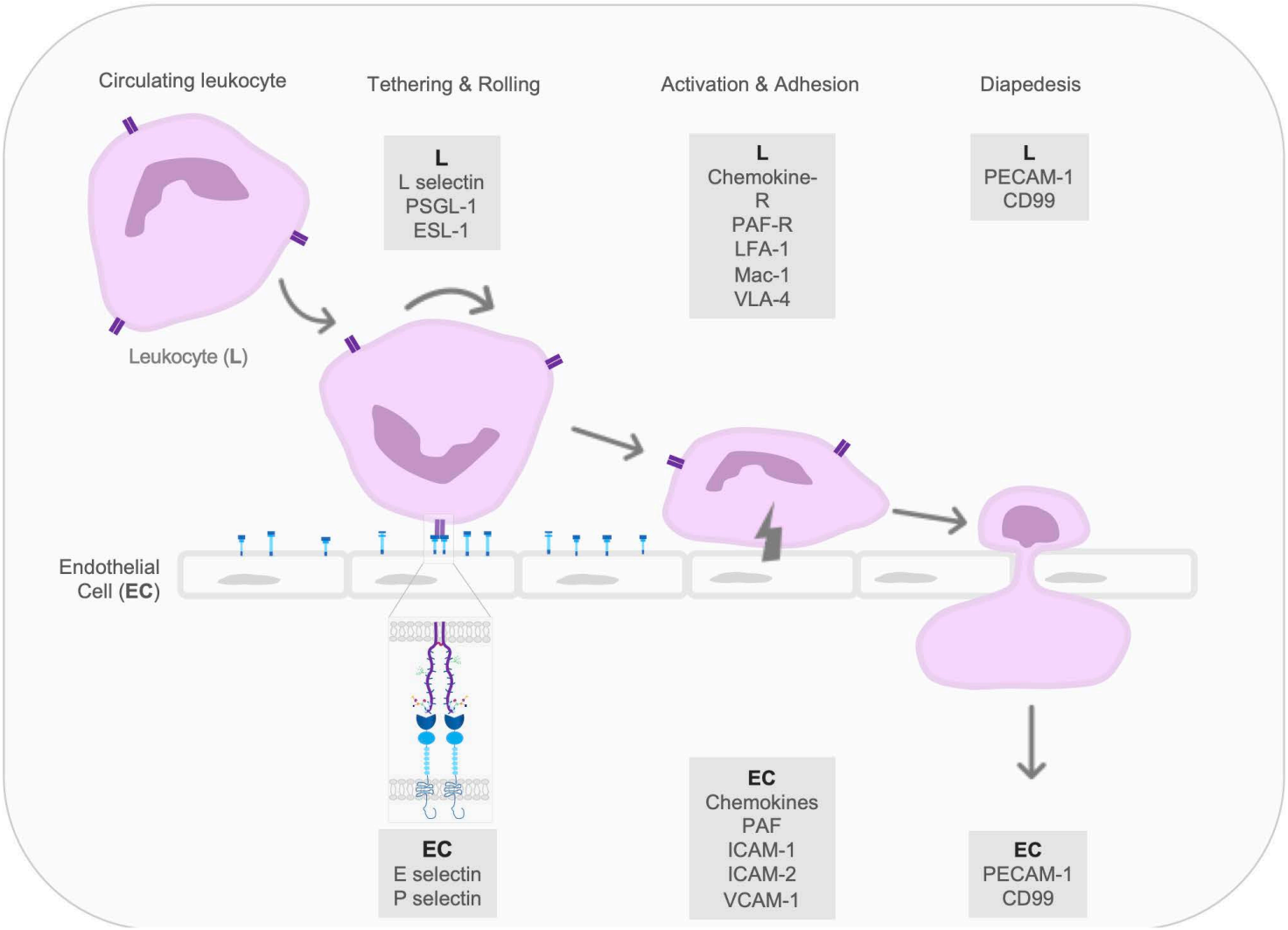

Figure 1.7 Overview of leukocyte extravasation, based on Boehncke, 2004. This figure is oversimplified and not all ligands involved in the process are written. E- and P-selectin establish the first specific but dynamic contacts with leukocytes, via PSGL-1 binding. Leukocytes roll along the endothelium via the synergistic binding of E- and P-selectin with PSGL-1 on Leukocytes. E- and P-selectin also bind to other glycoprotein ligands expressed on leukocytes, however PSGL-1 is the main binding ligand. Leukocytes initiate firm adhesion via binding of intracellular cell adhesion molecules 1 and 2 (ICAM-1 and ICAM-2) with Lymphocyte function-associated antigen-1 (LFA-1) and Vascular cell adhesion molecule-2 (VCAM-2) binding with and very late activation antigen -4 (VLA-4). This induces downstream intracellular signalling that alters cytoskeleton structures causing activation, fixation and crawling of leukocytes. Diapedesis, the process by which leukocytes transmigrate through ECs, is initiated by binding of platelet endothelial cell adhesion molecule-1 (PECAM-1) and CD99.

1.3.6 E-selectin-ligand binding on leukocytes

Human leukocytes present selectin binding ligands to enable the initial tethering and rolling of leukocytes during vascular inflammation (McEver, 2015b). However, the surface topography of each circulating leukocyte as well as the presence of different E-selectin ligands will alter the tethering and rolling efficiency across leukocytes. Neutrophils are the most abundant circulating leukocyte, especially in the first line of host defence. Purified neutrophils have demonstrated a significant increase in adherence to soluble recombinant form of E-selectin in an adhesion assay compared to eosinophils, due to their significant increase in the expression of Sialyl Lewis X (Bochner *et al.*, 1994). Neutrophils also have protruding microvilli which express selectin ligands on the tips of the microvilli which will have better opportunity to reach selectin expressed on the EC surface (Zarbock *et al.*, 2011a; Stadtmann *et al.*, 2013a).

In neutrophils, PSGL-1 and CD43 are expressed on lipid rafts on microvilli and CD44 and L-selectin, concentrated in the valleys between microvilli (Figure 1.8) (Zarbock *et al.*, 2011a). The microvilli have an average length of 0.3 µm (Shao, Ting-Beall and Hochmuth, 1998). When a neutrophil adheres to and rolls on ECs *in vivo*, the shear flow of blood or media imposes a pulling force on PSGL-1-selectin bonds, which are preferably located at the tip of a microvillus (Shao, Ting-Beall and Hochmuth, 1998). Under forces ≤ 34 pN, microvilli can be extended and if the force is > 61pN, a long thin membrane cylinder (a tether) can be formed from it (Shao, Ting-Beall and Hochmuth, 1998). Microvilli extension and tether formation acts like a spring and can decrease the pulling force imposed on the selectin-PSGL-1 binding, therefore prolonging the binding in high physiological shear stress (Shao, Ting-Beall and Hochmuth, 1998). The topography of neutrophils therefore is an advantage for tethering and rolling along endothelium.

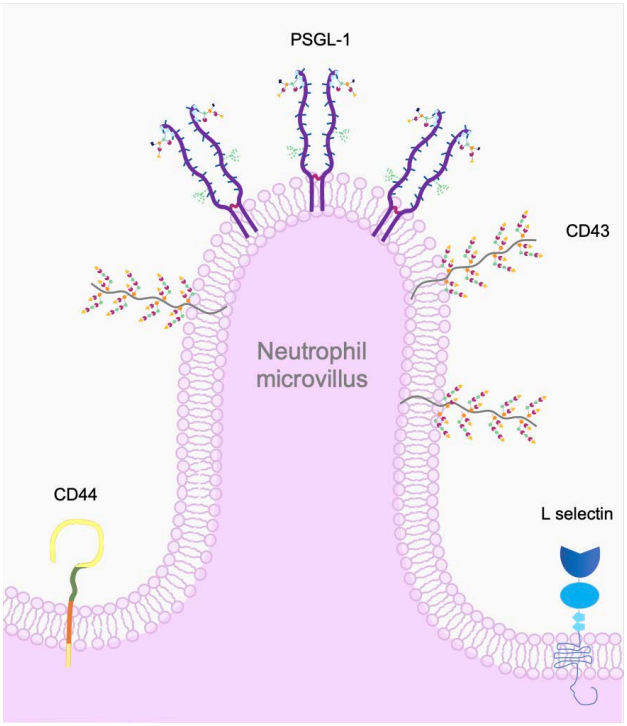

Figure 1.8 Neutrophil microvilli presenting E-selectin ligands. PSGL-1 has been shown to be more concentrated on the tips of microvilli whereas CD43 has been show to be present on microvilli in general and CD44 is seen in between microvilli protrusions.

As well as neutrophils, E selectin has been shown to tether and roll bovine γδ T cells and human αβ T cells, *in vitro* and eosinophils *in vivo* (Jutila *et al.*, 1994; Diacovo *et al.*, 1996; Henriques *et al.*, 1996; Zarbock *et al.*, 2011b).

To support leukocyte rolling, selectins have been shown to have rapid bond association (k_{on}) and dissociation (K_{off}) rate constants and special mechanical properties linking tensile forces and bond dissociation (Dembo *et al.*, 1988; Lawrence and Springer, 1991; Hammer and Apte, 1992). To expand, E-selectin can form 'slip bonds', which last < 1 second and which lifetimes are shortened by forces caused by shear stress < 0.3 dynes/cm^2, and 'catch bonds', which are less intuitive and have lifetimes that are prolonged by increasing force (0.3 – 1.0 dynes/cm^2) (Marshall *et al.*, 2003). This has been proposed to be due to force regulating relative orientations of the lectin and EGF domains, allosterically altering the ligand-binding surface on the lectin domain and thereby altering binding and dissociation rates (McEver and Zhu, 2010; McEver, 2015b). At low shear stresses, leukocytes are seen to roll along endothelium rapidly due to slip bond formation due to the frequent detachment from the endothelium. Higher shear stresses however enable cells to roll slower and more regularly due to stronger catch bonds forming and detachment becoming less frequent (Marshall *et al.*, 2003; Sarangapani *et al.*, 2004; Wayman *et al.*, 2010). However, beyond this 'shear optimum', at shear stresses >1.0 dynes/cm^2 leukocytes start to roll faster and detach more often (Sarangapani *et al.*, 2004; McEver, 2015b).

Another factor affecting binding is the density and the clustering of selectins expressed on the surface of endothelium and the ligands expressed on leukocytes, as well as geometries of rolling cells affected by tensile and compressive forces, which result in altering orientations of selectin-ligand binding (McEver and Zhu, 2010). It has been shown that neutrophils extrude their long membrane tethers at the trailing edge, then launch these slings over the leading edge to form new bonds with endothelium, which mediates slow rolling of leukocytes (Schmidtke and Diamond, 2000; Ramachandran *et al.*, 2004; Sundd *et al.*, 2012; Alwan *et al.*, 2021). Al Alwan et al., 2021, used single molecule imaging and a microfluidic platform to study slow rolling in hematopoietic stem and progenitor cells and a human leukemic progenitor cell line (KG1a) on deposited recombinant human E-selectin coated chamber slides. They found that the formation of tethers, followed by anchoring, detachment and sling formation and lengthening of microvilli achieved slow rolling. In addition, they found that there was rapid diffusion of selectin ligands and spatial clustering at the tethering and anchoring points of the

microvilli, and that motional freedom on the tethers and slings was enhanced by the detachment of the membrane from actin cytoskeleton during formation of tethers. It is proposed that catch-bonds prevent agglutination of circulating leukocytes and leukocyte aggregation during low flow or stasis, e.g. in arterial ischaemia or deep vein thrombosis (DVT) (Yago *et al.*, 2004; McEver, 2015b).

In addition, once E-selectin binds to leukocytes, it has also been proposed to induce leukocyte signalling that modulates leukocyte behaviour via activation of integrins. Integrins are heterodimeric transmembrane cell surface adhesion molecules. There are 18 different α- and 8 different β integrin submits, of which 24 different combinations have been characterised in mammals (Luo, Carman and Springer, 2007). The most common leukocyte integrins are β2-integrins, which consist of a β2-integrin chain (CD18) as well as a variable α-chain which drives ligand specificity (Sun, Hu and Fan, 2021). Such β2-integrins on neutrophils are lymphocyte function-associated antigen-1 (LFA-1, αLβ2, CD11a/CD18) which binds ICAM-1 and Macrophage antigen-1 (Mac-1;αMβ2; CD11b/CD18) which has been shown to bind fibrinogen, fibronectin and complement proteins (Abram and Lowell, 2009; Podolnikova *et al.*, 2015) (see Figure 1.7). This activation occurs when E-selectin (and P-selectin) binds to PSGL-1. Binding induces the phosphorylation and consequential activation of signaling molecules including kinases, adapter proteins and GTPases (Zarbock *et al.*, 2008; Stadtmann *et al.*, 2013b). This induces a cascade of events which lead to conformational changes of LFA-1 from a bent conformation to an extended conformation, which has higher ligand binding affinity and is able to bind to ICAM-1 on endothelium promoting slow-rolling transition (Stadtmann *et al.*, 2011; Cappenberg, Kardell and Zarbock, 2022). The upregulation of β2-integrins decreases rolling velocity and initiates slow rolling (Cappenberg, Kardell and Zarbock, 2022). During slow rolling, there is further neutrophil activation via interaction with inflammatory cytokines and chemokines presented on endothelium, which initiates arrest and adhesion strengthening via stronger neutrophil-endothelial interaction (Campbell *et al.*, 1998; Ley *et al.*, 2007). This then leads to leukocyte diapedesis and leukocytes are delivered to the site of inflammation (see Figure 1.7).

1.4 E-selectin targeting therapies

There are many diseases in which the excessive recruitment of leukocytes is characteristic, including atherosclerosis, atherothrombosis, deep vein thrombosis (DVT) arthritis, psoriasis,

chronic inflammation, chronic obstructive pulmonary disease, stroke, asthma and reperfusion injury (Kerr *et al.*, 2000a; Ohta *et al.*, 2001a; Ulbrich *et al.*, 2006a; Japp *et al.*, 2013a). Moreover, E-selectin knockout (KO) mouse models resulted in amelioration of an array of inflammatory disease phenotypes and cancer metastasis. E-selectin KO, alone and in conjunction with P-selectin KO has been shown to decrease thrombus burden and prevent vein wall fibrosis in thrombosis mouse models, (Myers *et al.*, 2002; Sullivan *et al.*, 2003; Eriksson *et al.*, 2005), reduce adipose tissue damage and lipolysis in an hepatitis mouse model (Rodrigues *et al.*, 2022), reduce allergic inflammation in skin and lung (Jiao *et al.*, 2007), impede inflammatory migration in acute asthma (Banerjee, 2011), delay lesion development and reduce plaque formation in atherosclerosis mouse models (Dong *et al.*, 1998; Collins *et al.*, 2000), as well as reduce cancer metastasis in cancer mouse models for colon and lung cancer (Laferrière *et al.*, 2001; Tremblay, Auger and Huot, 2006; Läubli and Borsig, 2010; Esposito *et al.*, 2019). It is of no surprise that targeting the initial stages of inflammation; i.e. E-selectin expression in vascular endothelial cells, is a desirable area for inhibition, in an attempt to reduce vascular inflammation.

E-selectin is an advantageous target due to its expression in the vicinity of inflammation, infection and cancer. Compared to P-selectin, E-selectin has a substantial increase in cell surface expression in response to TNF alpha (Stocker *et al.*, 2014). E-selectin may therefore be considered a more useful biomarker for inflammation, as it is easier to discriminate expression between inflammatory and non-inflammatory conditions (Ehrhardt, Kneuer and Bakowsky, 2004b). E-selectin has been implicated in many inflammatory diseases, cardiovascular disorders, cancer and metastasis (Barthel *et al.*, 2007b; Aydt, Bock and Wolff, 2010), therefore has been targeted for inhibition by many E-selectin inhibitors.

1.4.1 E-selectin inhibitors, antagonists, antibodies

1.4.1.1 Rivipansel (GMI-1070)

Rivipansel is a synthetic small molecule glycomimetic pan-selectin inhibitor designed to reduce E-, P- and L-selectin interactions with leukocytes, as well as to inhibit leukocyte interaction with red blood cells (RBCs) in order to treat sickle cell anaemia (SCD). Rivipansel was found to inhibit selectin binding *in vitro* and selectin-mediated effects *in vivo* (Chang *et al.*, 2010). Rivipansel was found to reduce leukocyte adhesion and red blood cell (RBC) adhesion to leukocytes as a consequence of E-, P- and L-selectin inhibition (Chang *et al.*, 2010).

During Phase I clinical trials, 15 patients with sickle cell anaemia were given 2 infusions of Rivipansel. The inhibitor was classified as safe for sickle cell anaemia patients, Rivipansel significantly decreased biomarkers of endothelial activation; soluble E-selectin (sE-selectin) soluble P-selectin (sP-selectin) and soluble ICAM (sICAM) as well as biomarkers that represent leukocyte activation (MAC-1 and LFA-1). In a subset of patients there was a suggestion of increased blood flow, which is a sign of positive treatment of sickle cell anaemia patients.

In Phase II clinical trials, 76 SCD patients with vaso-occlusive crises (VOC) were treated with Rivipansel every 12 hours for up to 15 doses in a randomised, placebo control, double blind study (Telen *et al.*, 2015). In this phase II trial, Rivipansel treatment led to no reductions over time to resolve VOC episodes, however there were clinically meaningful reductions in mean and median times to reach VOC resolution of 41 and 63 hours observed in the active treatment group vs the placebo group (Telen *et al.*, 2015). In addition, mean cumulative IV opioid analgesic use, in response to VOC, was reduced by 83% with Rivipansel vs placebo ($P< 0.010$) (Telen *et al.*, 2015). Pfizer have now set out phase III clinical trials for Rivipansel in the treatment of 345 with VOC in hospitalized subjects with SCD. However, an independent study of Rivipansel has shown ineffectiveness over the time from the beginning of depolarization to repolarization of ventricles (the QT interval) in 48 healthy African American subjects compared with placebo (Tammara *et al.*, 2017).

1.4.1.2 Uproleselan (GMI-1271)

Uproleselan is a small molecule E-selectin antagonist, that has been targeted for treatment of deep vein thrombosis (DVT), acute myeloid leukaemia (AML) and multiple myeloma in Phase I –Phase III clinical trials. For DVT treatment, in Phase I clinical trials, the safety and pharmacokinetics of Uproleselan was assessed in a single ascending dose study in healthy subjects (Devata *et al.*, 2020). The E-selectin antagonist was deemed safe, there was no evidence of lower extremity DVT on baseline ultrasound studies (Devata *et al.*, 2020). Phase II clinical trials attempted to treat patients 18 - 75 years old with or without acute isolated calf vein thrombosis, however this trial was terminated due to lack of funding (Devata *et al.*, 2020). For AML treatment, Uproleselan was used to treat AML patients ≥18 years who have relapsed in AML in Phase I, II and III clinical trials; when added to chemotherapy for AML patients, there were promising remission rates and survival outcomes, and reduced rates of mucositis (DeAngelo *et al.*, 2019). However, all the data have not been released and Phase III clinical

trials are still classed as recruiting. Due to the apparent success in AML, Phase I clinical trials have commenced for Multiple Myeloma.

1.4.1.3 CDP850

CDP850 is a humanised monoclonal E selectin antibody therapy, used in a multicentre, randomized, placebo-controlled trial to investigate the clinical efficacy for the treatment of moderate to severe chronic plaque psoriasis (Bhushan *et al.*, 2002). Nine male subjects (age range 25 – 47 years) were given 20 mg/kg of CDP850 intravenously as a single dose and four subjects (three males and one female; age range 23 -50 years) received placebo infusion. Psoriasis area and severity index (PASI) was used to assess the clinical efficacy. The treatment was well tolerated with minimal side effects, and tissue biopsies followed by immunohistochemical analysis showed significant decreases in E selectin compared to placebo ($p<0.01$). This was not, however, accompanied by a significant reduction in neutrophils or lymphocytes in the dermis and therefore was not concluded to possess a therapeutic benefit in the treatment of chronic plaque psoriasis (Bhushan *et al.*, 2002).

Of those that did not pass Phase II clinical trials; Rivipansel showed lack of therapeutic efficacy in an independent Phase II clinical trial for sickle cell anaemia; Uproleselan passed safety assessment in Phase I clinical trials however there has been no published data regarding Phase II trials for DVT and AML patients; Phase I clinical trials for GI-270384X were terminated for an unknown reason and CDP850 concluded no therapeutic efficacy as an anti-inflammatory for psoriasis (Table 1.2).There are many factors that may have affected the efficacy of E-selectin inhibitors in clinical trials. In some cases, there have been difficulties in targeting the initial stage of leukocyte recruitment, due to lack of specificity for targeting E-selectin, or selectins at all, low IC_{50} values and/or short half-lives (Schön, 2005). However, for E-selectin targeting therapeutics which had high target specificity, it is unknown why there is such a low efficacy for the therapeutic. One important factor is that selectins aren't fully understood in their functionality and there may be functional overlap between E-, P- and L- selectin (Schön, 2005). This has been explored in E-, P- and L- selectin knockout mice, where in the case of loss of function of one selectin, another selectin member can compensate in mediating leukocyte tethering and rolling (Jung and Ley, 1999; Collins *et al.*, 2001). Therefore, it will be of key interest to study whether there is any interplay between the selectin family members. This can be explored by investigating whether E selectin interacts and forms complexes with the other selectin family members. In addition, the endogenous expression of E-selectin under

differential cytokine regulation will aid the understanding of what drives E-selectin expression, when E-selectin expression peaks and how it is down-regulated. A model of expression that can also measure E-selectin binding will be extremely useful for future testing of E-selectin therapeutics efficacy in reducing the cytokine induced expression.

Table 1.2 E selectin targeting therapies

Name	Delivery system	Recognition element	Clinical stage	Specifically binds E selectin	Pan-selectin inhibitor / other	Efficacy with reducing inflammatory symptoms	Ref.
Rivipansel (GMI 1070)	n/a	sLea/x mimetic	Phase I	N	Pan-selectin inhibitor	Y	(Wun *et al.*, 2014)
			Phase II	N	Pan-selectin inhibitor	Y	(Telen *et al.*, 2015)
			Discovery/ Preclinical	N	Pan-selectin inhibitor	N	(Tammara *et al.*, 2017)
GI-270384X	n/a	Unknown	Phase I	Y	ICAM-1 AND Esel inhibitor	N	(Clinicaltrial. gov, 2007)
GMI-1271 or Uproleselan **for DVT**	n/a	potent small-molecule E-selectin antagonist,	Phase I	N	E selectin and CXCR4 inhibitor	n/a	(Devata *et al.*, 2020)
			Phase II			Unknown	(Devata *et al.*, 2020)
GMI-1271 or Uproleselan **for AML**	n/a		Phase I				(Clinicaltrial. gov, 2014)
			Phase II				(Clinicaltrial. gov, 2014)
			Phase III (Recruiting)				(Clinicaltrial. gov, 2018)
GMI-1271 or Uproleselan **for Multiple Myeloma**	n/a		Phase I				(Clinicaltrial. gov, 2016)

CDP850	n/a	Humanised E selectin monoclonal antibody	Phase II	Y	N	N	(Bhushan *et al.*, 2002)
n/a	Antibody-coupled liposomes	E selectin antibody	Discovery/ preclinical	Y	N	n/a	(Bendas *et al.*, 1998)
n/a	Antibody-coupled liposomes	E selectin monoclonal antibody	Discovery/ preclinical	Y	N	n/a	(Bendas *et al.*, 1999)
n/a	Antibody-coupled liposomes	E selectin monoclonal antibody	Discovery/ preclinical	Y	N	n/a	(Kessner *et al.*, 2001)
n/a	poly(e-caprolactone) (PCL) polymer microspheres	Humanised E and P selectin monoclonal antibody (HuEP5C7.g2)	Discovery/ preclinical	N	Pan-selectin inhibitor	n/a	(Dickerson *et al.*, 2001)
n/a	Polystyrene nanospheres	Humanised E and P selectin monoclonal antibody (HuEP5C7.g2)	Discovery/ preclinical	N	Pan-selectin inhibitor	n/a	(Blackwell *et al.*, 2001)
n/a	PLA- PEG microspheres	Humanised E selectin monoclonal antibody (68-5H11)	Discovery/ preclinical	Y	N	n/a	(Sakhalkar *et al.*, 2003)
n/a	Liposomes	Murine E selectin monoclonal antibody (H18/7)	Discovery/ preclinical	Y	N	Y	(Spragg *et al.*, 1997a)
n/a	Liposomes	Sialyl Lewis X	Discovery/ preclinical	N	Pan-selectin inhibitor	Y	(Minaguchi *et al.*, 2008)
n/a	PLA nanoparticles	Mannose based Sialyl Lewis X	Discovery/ preclinical	N	Pan-selectin inhibitor	Y	(Banquy *et al.*, 2008)
n/a	HPMA copolymers	Quinic acid (Qa) based analogue of sialyl Lewis X	Discovery/ preclinical	N	Pan-selectin inhibitor	n/a	(Shamay *et al.*, 2009c)

n/a	Lipidic microparticles	E selectin thiolated Qa peptide ligand	Discovery/ preclinical	Y	N	Y	(Myrset *et al.*, 2011)
n/a	Polymeric (PVGL) prodrug	Sialyl Acid	Discovery/ preclinical	Y	N	Y	(Hu *et al.*, 2018a)
n/a	PEG/PEI nanoparticles	E-selectin-targeting (ESTA) multistage vector (MSV)	Discovery/ preclinical	Y	N	Y	(Ma *et al.*, 2016a)
n/a	PLA Nanoparticles	Sialyl Lewis X	discovery/ preclinical	N	Pan-selectin inhibitor	Y	(Jubeli *et al.*, 2012)
n/a	HPMA copolymers	E-selectin binding peptide (Esbp)	Discovery/ preclinical	Y	N	Y	(Tsoref *et al.*, 2018)
n/a	Multistage vector microparticle	ESTA	Discovery/ preclinical	Y	N	Y	(Ma *et al.*, 2016a)
n/a	Peptide	E selectin specific Peptide-Glycosaminoglycan	Discovery/ preclinical	N	Pan-selectin inhibitor	Y	(Wodicka *et al.*, 2019)
n/a	Immunoliposomes	(SATA)-modified mouse anti human E-selectin antibody	Discovery/ preclinical	Y	N	Y	(Gholizadeh *et al.*, 2018a)
n/a	poly n-butyl cyanoacrylate (PBCA)-shelled microbubbles	E selectin specific peptide	Discovery/ preclinical	Y	N	Y	(Spivak *et al.*, 2016)
EL-246	n/a	Humanised E and L selectin monoclonal antibody	Preclinical / discontinued	N	Pan-selectin inhibitor	N	(Carraway *et al.*, 1998)
n/a	Peptide	Sialyl Lewis X	Discovery/ preclinical	N	Pan-selectin inhibitor	N	(Stahn *et al.*, 1998)
n/a	Thioaptamer	ESTA	Discovery/ preclinical	Y	N	Y	(Mann *et al.*, 2010)

n/a	Thioaptamer	ESTA	Discovery/ preclinical	Y	N	Y	(Morita *et al.*, 2016)
n/a	Antibody drug conjugate	E selectin antibody	Discovery/ preclinical	Y	N	Y	(Bhaskar *et al.*, 2003)
n/a	HPMA copolymers	E-selectin binding peptide (Esbp)	Discovery/ preclinical	Y	N	Y	(Shamay *et al.*, 2009a)
n/a	Peptide	Esbp	Discovery/ preclinical	Y	N	Y	(Shamay *et al.*, 2015a)
n/a	Micelle	Sialic Acid	Discovery/ preclinical	N	Pan-selectin inhibitor	Y	(Xu *et al.*, 2019)
ISIS9481	n/a	E selectin specific oligodeoxynucleotide	Discovery/ preclinical	Y	N	Y	(Goldfarb *et al.*, 2010)
GMI-1359	n/a	Small molecule E selectin Inhibitor	Discovery/ preclinical	N	E selectin and CXCR4 inhibitor	Y	(Festuccia *et al.*, 2020)
Compounds 1-4 unknown	n/a	Unknown	Discovery/ preclinical	Y	N	n/a	(Barra *et al.*, 2016a)
GMI-1271 or Uproleselan	n/a	Small molecule E selectin antagonist	Discovery/ preclinical	Y	N	Y	(Culmer *et al.*, 2017)
GMI-1271 or Uproleselan	n/a	Small molecule E selectin antagonist	Discovery/ preclinical	Y	N	Y	(Myers *et al.*, 2019)
EP-5C7	n/a	Humanised P and E selectin monoclonal antibody	Discovery/ Preclinical	N	Pan-selectin inhibitor	Y	(He *et al.*, 1998)
GMI-1070	n/a	Small molecule glycomimetic pan-selectin antagonist	Discovery/ Preclinical	N	Pan-selectin inhibitor	Y	(Chang *et al.*, 2010)
SDA	n/a	E and P Selectin specific DNA Aptamer	Discovery/ Preclinical	N	Pan-selectin inhibitor	Y	(Faryamma nesh *et al.*, 2014)

1.5 Thesis aims

Whilst the inducers of E-selectin in ECs, and the E-selectin-leukocyte interactions have been well established, the differential kinetics of cytokine activation has not been assessed in live cells extensively. In addition, E-selectin membrane association, dimerization and clustering has not been well considered in the context of drug binding, and a model to detect specific E-selectin-drug binding has not been conducted in a live whole cell format. This project therefore aimed to characterise membrane expression of E-selectin induced by specific cytokines, using antibody-based methods as well novel luciferase-based technologies. In addition, the interaction of E-selectin with other membrane bound selectins and receptors, as well as with E-selectin binding peptide (Esbp) is reported, using novel technologies which are used widely to investigate receptor dimerization and receptor-ligand binding.

Chapter 3 aimed to develop an in vitro assay utilising an anti-E-selectin monoclonal antibody in conjunction with fluorescence microscopy and enzyme linked immunosorbent assay (ELISA) to detect varying levels of E-selectin expression in response to inflammatory stimuli in fixed human umbilical vein endothelial cells (HUVECs). In particular, it aimed to characterise the TNF alpha induced response in HUVECs.

Chapter 4 aimed to improve upon the previous system by using CRISPR-Cas9 to append an 11 amino acid NanoLuciferase (NanoLuc) fragment (HiBiT) onto the N-terminus of E-selectin in HUVECs and immortalised (TERT2) HUVECs. This technology aimed to measure E-selectin expression in live cells with high sensitivity over a long period of time (15 hr), to allow conclusions to be drawn about the potency and dynamics of cytokine inducement of E-selectin cell surface.

Chapter 5 aimed to broaden the use of the HiBiT E-selectin CRISPR edited cells to evaluate the ability of an E-selectin binding peptide (Esbp) to induce HiBiT-E-selectin internalisation. Further, a full-length NanoLuc E-selectin cell line was produced in a model cell line (HEK293T cells), with the aim to evaluate E-selectin binding using bioluminescence resonance energy transfer (BRET) in whole cells and in membranes. Nanoluc or SNAP-tag E-/L-/P-selectin constructs were then co-expressed in HEK293Ts with the aim to evaluate dimerization and consequential clustering of selectins using BRET.

Chapter 2 General Materials and Methods

2.1 Cell culture

All cells were passaged using the same sequential steps however there were variations in the media, trypsin concentration and coating of flasks used. Human umbilical vein endothelial cells (HUVECs) and human telomerase reverse transcriptase (hTERT2) immortalised HUVECs were maintained in Medium 200 (M200500, ThermoFisher Scientific, USA) supplemented with 2.2% large vessel endothelial supplement (LVES) (50X, A1460801, ThermoFisher Scientific (Gibco), USA). Human embryonic kidney (HEK) 293T cells and HEK293-Glosensor (HEKG) cells were maintained in Dulbecco's modified Eagle's medium (DMEM) (D6429, Sigma Aldrich, UK) supplemented with 10% foetal calf serum (FCS) (F2242, Sigma Aldrich, UK). All cells were kept in cell culture incubators maintaining an atmosphere of 5% CO_2 / 95% air. Medium 200, DMEM, Trypsin-Ethylenediaminetetraacetic Acid (EDTA) (T4174, Sigma Aldrich, UK) and Phosphate Buffered Saline (PBS) (D8537, Sigma Aldrich, UK) were all brought up to 37°C before passaging of cells to avoid cell stress. All cell culture techniques were carried out in class II laminar flow cell culture hoods.

2.1.1 Passaging cultured cells

Cells were grown in 75cm^2 flasks (T75s) unless otherwise mentioned, until they reached ≥70% confluency. Cells were washed once with 5 – 10ml PBS, before they were trypsinised with Trypsin-EDTA for ≤ 5 min. Trypsin is a protease, which proteolytically cleaves C-terminal lysine and arginine, in order to disrupt focal adhesions anchoring cells to the culture dish. EDTA acts as a chelator for calcium and magnesium divalent cations, which disrupts and weakens cadherin induced cell-cell adhesion. Trypsin-EDTA therefore separates cells from each other as well as from tissue culture plastic. Trypsin-EDTA solution was received as a 10X stock before diluting to 1X or 4X Trypsin-EDTA according to use with HEK293Ts/HEKGs cells or Wildtype/hTERT2 HUVECs. After 2 – 5 min, trypsin was inhibited using DMEM supplemented with 10% FCS. FCS contains natural protease inhibitors, such as α1-antitrypsin, which neutralises trypsin. 10ml of DMEM 10% FCS was added 5min post trypsinisation to prevent damaging of cell surface proteins and trypsin-EDTA induced cell toxicity and the solution was washed along the tissue culture plastic twice to ensure all cells were dislodged and in the suspension. The cells were then centrifuged at 150 xg for 4 min and the supernatant discarded. The cell pellet was resuspended using 2ml of appropriate medium using pipette action. The appropriate volume of cell suspension was then added to a new T75 containing 10ml appropriate medium.

2.1.2 Freeze/thawing cells

'Freezing solution' was made by supplementing foetal calf serum with 10% (w/v) dimethyl sulfoxide (DMSO). The freezing solution was then filter sterilized using a 20ml syringe and a 0.2µm filter. DMSO helps to prevent the formation of ice crystals during the freezing process, subsequently improving cell viability when cells are thawed in the future. Cells were detached from the T75 tissue culture plastic as described before (see *passaging cultured cells*), centrifuged at 150 xg for 4 minutes and supernatant discarded. Cells were resuspended in 2ml freezing solution and 1ml was aliquoted into two separate cryogenic tubes. These tubes were then placed in a cryogenic freezing container (Nalgene® Mr. Frosty, C1562, Sigma Aldrich, UK), filled with isopropanol and placed in a -80°C freezer. The isopropanol filled freezing container allows controlled slow freezing of the cells at a rate of 1°C per minute when placed in the -80°C freezer. For long term storage, the cryogenic tubes were then placed into a vapour phase liquid nitrogen vessel (-196°C) (Isothermal cyrostorage unit with carousel storage system, CBS V-3000ABC). To thaw cells, the cryogenic tubes were taken out of vapour phase liquid nitrogen vessel and allowed to defrost at room temperature which typically took 5 minutes. In a tissue culture hood, 1ml of cells was then added into a T75 flask containing 10ml of the appropriate medium which had been warmed to 37°C. The flask was immediately placed into a 37°C incubator 5% CO_2/ 95% air. The following day, the media was replaced with fresh medium to aid removal of cell debris from cells which did not survive the thawing process. When cells reached ≥70% confluency they were passaged and used for experimentation.

2.1.3 Cell seeding

2.1.3.1 96-well plate cell seeding

All cell types were seeded onto either flat-bottomed black Greiner-96 well plates (Greiner Bio-One 655090), flat bottomed white Greiner-96 well plates (Greiner Bio-one 655089) or flat-bottomed clear polystyrene TC-treated 96-well plate (Corning, USA, 3596) with different plate coating techniques and at different cell seeding densities. In general, when confluency was ≥70%, cell detachment was performed as previously described (see passaging cultured cells) from one T75 flask. The cell pellet was then resuspended in 2ml of appropriate medium and cells were counted using a haemocytometer. 10µl of cell suspension was loaded onto a haemocytometer, and cells were counted within the central 1mm^2 square (the central 1mm^2 area is divided into 25 small squares, each 0.04 mm^2 and each of these is marked into a further

16 tiny squares). Cells were counted 3 times and the average taken from each count was multiplied by 10,000; representing the average amount of cells present in 1ml of media. From this concentration, the volume required to obtain the correct seeding density was calculated and the cells were diluted appropriately using the chosen media. 100µL of cell suspension was then seeded per well using an Eppendorf® Multipette® Plus pipette (Z374563, Sigma Aldrich, UK) and a 10ml Eppendorf combitip (Z762806, Sigma Aldrich, UK). Cell suspension was drawn up and expelled once before seeding to ensure full mixing of cells. Cells were seeded typically 24 hours before experiment to allow adherence.

2.1.3.2 µ-slide 8 well plate cell seeding

HUVECs and TERT2 HUVECs were seeded onto µ-Slide 8 well chambered coverslips (Thistle Scientific, (Ibidi), 80826), with 'ibidiTreat' surface modification. When confluency reached ≥ 70%, cells were lifted off the T75 flask and centrifuged as described previously (see 2.1.1 Passaging cultured cells), and the cell pellet was resuspended in 2ml medium 200. The cells were counted as described above (see 2.1.3.1 96-well plate cell seeding) using a haemocytometer and the appropriate dilutions were carried out for the appropriate seeding densities (ranging from 10,000 – 50,000 cells per well depending on the experiment and cell type.) using 300µL volume of cell suspension per well. Cells were typically seeded 24hr before experiment to allow adherence.

2.1.4 HUVECs

HUVECs are a primary non-immortalized cell line of human origin, derived from endothelium of veins found in the umbilical cord. The HUVECs used in these experiments were isolated from a single donor newborn male, ThermoFisher Scientific (C0035C, LOT# 1606186). HUVECs grow in an adherent monolayer and adopt a so-called cobblestone phenotype.

2.1.4.1 Passaging

HUVECs were defrosted at passage 2 and maintained until passage 6 in T75s. Cells were detached from the T75 tissue culture plastic using trypsin-EDTA and the flask was placed into 37°C incubator to ensure optimal enzymatic activity for ≤5min. Detachment and centrifugation was performed as described before (see 2.1.1 Passaging cultured cells). The cell pellet was resuspended using 2ml medium 200 using pipette action ≤7 times to prevent shear stress of cells. The appropriate volume was then added to a new T75 containing 7 - 10ml medium 200.

HUVECs were not passaged in a ratio greater than 1:10, as HUVECs require cell-cell contact to encourage growth. Media was replaced every 2 – 3 days to improve cell growth.

2.1.4.2 Cell seeding

96-well plates

HUVECs were seeded onto flat bottomed black sided Greiner-96 well plates for widefield imaging, flat bottomed white sided Greiner-96 well plates for luminescence assays and flat bottomed clear polystyrene TC-treated 96-well plates for alkaline phosphatase assays as described previously (see 2.1.3.1 96-well plate cell seeding). The appropriate volumes were then diluted in Medium 200 supplemented with 2.2% LVES to obtain seeding density of 30,000 cells per well. Cells were seeded the day before experiment to allow adherence.

µ-slide 8 well plate

Cells were seeded onto IbidiTreat coated µ-Slide 8 well chambered coverslips for confocal imaging. HUVECs were prepared for plating as described previously (see 2.1.3.2 µ-slide 8 well plate cell seeding) and were seeded at seeding density of 10,000 cells per well using 300µL volume of cell suspension per well. Cells were seeded the day before experiment to allow adherence.

2.1.5 TERT2 HUVECs

Human telomerase reverse transcriptase 2 (hTERT2) immortalised HUVECs were isolated from a single donor newborn female (American Type Culture Collection (ATCC), CRL-4053, LOT# 70023166). Telomerase reverse transcriptase (TERT) is a ribonucleoprotein polymerase which facilitates the addition of telomere repeat TTAGGG. With every cell division, there is decrease in telomerase expression, which causes shortening of telomeres and eventually cell senescence. TERT2 HUVECs were transduced with hTERT, to prevent the diminishing of TERT and prolong the life of HUVEC cell line (Chang *et al.*, 2005).

2.1.5.1 Passaging

hTERT2 HUVECs were grown in 0.1% gelatin coated T75s and split when they reached ≥70% confluency, from passage 2– passage 20. Gelatin solution (G1393, Sigma Aldrich, UK) was received at 2% and diluted to 0.1% with sterile PBS in a class II laminar flow cell culture hood. T75 flasks were incubated with 3ml 0.1% gelatin solution (30min, 37°C) and washed with 5ml PBS before cells were passaged into the flask. TERT2 HUVECs were lifted off of the tissue

culture plastic using 4X Trypsin-EDTA (37°C, ≤5min) and trypsin neutralisation and centrifugation of cells were performed as described previously (see 2.1.1 Passaging cultured cells). 2ml Medium 200 supplemented with 2.2% LVES was used to resuspend the cell pellet and mixed using pipette action ≤10 times to prevent shear stress of cells. The maximum split ratio for hTERT2 HUVECs was 1:10, as hTERT2 HUVECs rely on cell-cell contact to encourage growth. Media was replaced every 2 – 3 days to improve cell growth.

2.1.5.2 Cell seeding

96 well plates

hTERT2 HUVECs were plated onto 0.1% gelatin coated black-sided flat bottomed Greiner 96 well plates for widefield imaging and 0.1% gelatin coated white-sided flat bottomed Greiner 96-well plate for luminescence assays. 0.1% gelatin solution was diluted from 2% gelatin solution as described previously (see 2.1.5.1 Passaging). 50µl per well 0.1% gelatin was incubated in 96 well plates (37°C, 20min) and each well was washed once with 50µl PBS before cell seeding. hTERT2 HUVECs were seeded as described previously (see 2.1.4.2 Cell seeding). Cells were seeded at 30,000 cells per well and left for 24hr in a tissue culture incubator (37°C 5% CO_2) before experimentation.

2.1.6 HEK293Ts & HEKGs

Human embryonic kidney cells were isolated from a single donor female (ATCC Virginia, USA, CRL-3216). HEK293T cells are a highly transfectable variant of HEK293 cells, additionally stably transfected with the SV40 T-antigen. The SV40 T-antigen modification allows competence to replicate vectors carrying the SV40 region of replication, making these cells ideal model cells for overexpression of proteins/receptors of interest, particularly for transient transfection. HEK293 GloSensor (HEKG) cells stably express a cyclic Adenosine Monophosphate (cAMP) Biosensor (E2301, Promega, UK), as a means to measure signalling through cAMP in live cells with luminescence screening (Fan *et al.*, 2008). HEKGs were used for SNAP-tag E-selectin transfection and widefield imaging, as they are also a highly transfectable cell line and often a higher transfection efficiency was observed in HEKGs compared to HEK293Ts. Both HEK293Ts and HEKGs present epithelial morphology and grow in an adherent monolayer.

2.1.6.1 Passaging HEK293Ts and HEKGs

HEK293Ts and HEKGs were passaged as described previously (see 2.1.1 Passaging cultured cells) using 1X Trypsin-EDTA (< 2min at room temperature). The cell pellets for both cell types were resuspended in 2ml DMEM 10% FCS before they were split into T75 containing 10 – 20 ml pre-warmed DMEM 10% FCS. HEK293Ts and HEKGs were typically passaged in 1:10 - 1:20 split ratios, depending on experiment dates. Flasks were typically split 1-2 times a week.

2.1.6.2 Cell seeding

HEK293Ts and HEKGs were seeded onto a poly-D-lysine coated black-sided flat-bottomed Greiner 96 well plates for widefield imaging and poly-D-lysine coated white-sided flat-bottomed Greiner 96-well plate for luminescence assays. Poly-D-lysine hydrobromide (PD) (Sigma Aldrich UK, P6407) was received as a lyophilised powder (5mg) and was resuspended in 1ml sterile PBS before dispensing for communal use into 40µl aliquots. 5mg/ml PD was diluted to 0.1mg/ml in sterile PBS and filter sterilised using a 20ml syringe and a 0.2µm filter. 50µl of PD was incubated per well in 96 well plates for 30min (37°C) and washed with 50µl PBS once before seeding cells. HEK293Ts and HEKGs were seeded at 20,000 cells per well unless otherwise stated as described previously (see 2.1.3.1 96-well plate cell seeding), and left to adhere to the plate for 24hr in a tissue culture incubator (37°C 5% CO_2) before experimentation.

2.2 Microscopy

2.2.1 Confocal microscopy

HUVECs and TERT2 HUVECs plated onto µ-slide 8 well plates were imaged using a Zeiss Laser Scanning Microscope (LSM) 880, fitted with a 40x/1.20 W Corr M27 water-immersion objective (Zeiss, Germany). The refractive index of the µ-slide 8 well plates was calculated by ibidi (1.52) and is close to the refractive index of water (1.33) used as the immersion liquid. The refractive index (RI) describes the extent to which light refracts when passing through the ibidi polymer plate and/or water; having these units matching as close as possible increases the the light rays which will form the final image. An Argon 488 / Diode 405-30 laser was used, at 2% laser power with a pinhole diameter of 1 airy unit (AU). Image acquisition was performed using the proprietary Zeiss software Zen, at 512x512 frame size, with 8 averages, and gains of 850 (for 488nm excitation) and 600 (for 405nm excitation). Images were edited with the addition of scale bars and exported as 8-bit TIFs using Zen 2010 software (Zeiss, Germany).

2.2.2 Widefield microscopy

HUVECs, TERT2 HUVECs, HEK293Ts and HEKGs plated on black sided flat bottomed 96 well plates were all imaged using the MetaXpress IX Micro widefield plate reader (Molecular Devices; 20X air objective) fit with a Xenon lamp. 4',6-diamidino-2-phenylindole (DAPI) and fluorescein isothiocyanate (FITC) filters were used when imaging, and 4 sites per well were acquired. MetaXpress High Content Image Acquisition and Analysis software (version 4) was used to acquire, analyse and save images as TIFs.

2.2.3 Bioluminescent microscopy

HEK293T NanoLuc E-Selectin stable cell lines, as well as genome edited HiBiT E-selectin HUVEC/TERT2 HUVEC cells were imaged for luminescence expression using a live cell bioluminescence imaging system; Olympus Luminoview 200 (LV200, Olympus Lifescience). Before imaging, cells were treated as described in 2.8.4 Bioluminescent imaging. A 512 x 512 image was captured using brightfield (exposure 50 ms, gain 50) and bioluminescence filters (exposure 10s, gain 50) for NanoLuc-Selectin HEK293T cell lines. For CRISPR-Cas9 edited cells, a higher exposure time and gain was used for bioluminescence (exposure 20s, gain 200), as there was much lower endogenous expression in comparison to over-expressed stable cell lines.

2.3 Immunolabeling

Immunolabeling describes the experimental process of antibody–antigen binding to aid detection and localisation of specific proteins within or on the surface a cell. Antibodies are glycoproteins belonging to the immunoglobulin (Ig) superfamily and they bind via their fragment antigen binding (Fab) region, which is specific for a particular antigen. Foreign antigens that enter an organism, are bound by circulating B cells, which consequentially mature and release antibodies against the antigen. This natural immune response is exploited *in vivo* in order to produce monoclonal antibodies for specific proteins and is termed the hybridoma technology. This process involves immunizing an animal with the proper antigen to cause antibody production for an optimal amount of time before sacrificing the animal and isolating B-cells from the spleen. Then, these B-cells are fused to immortal myeloma cells to produce a hybridoma cell line, which constitutively expresses the antibody of interest. This technology allowed the production of the monoclonal anti-E-selectin antibody (produced in a mouse;

Sigma Aldrich, UK, Clone 1.2B6 S9555) used in these experiments. Secondary antibodies target and bind to primary antibodies acting as an indirect detection mechanism. These secondary antibodies should be raised in a different species to the primary antibody but show specificity against the host species of the primary antibody. In these experiments, an Alexa Fluor 488 conjugated chicken anti-mouse secondary antibody (ThermoFisher Scientific, A-21200) and an alkaline phosphatase conjugated goat anti-mouse secondary antibody (Sigma Aldrich, UK A9316) were used to bind against the mouse monoclonal anti-E-selectin antibody and enable detection of endogenous E-selectin in HUVECs and TERT2 HUVECs. Alexa Fluor 488 conjugated secondary antibody enabled detection of E-selectin using widefield and confocal imaging. Alkaline phosphatase conjugated secondary antibodies hydrolyse p-Nitrophenyl Phosphate substrate (pNPP) into p-nitrophenol and inorganic phosphate which results in a yellow substrate. This causes a colorimetric response which can be read using a Dynex MRX plate reader and was indicative of E-selectin expression.

2.3.1 Immuno-fluorescence labelling

After experimentation on HUVECs/TERT2 HUVECs in µ-slide 8 well plates (see 2.7.2 Time course assays), cells were fixed using 3% paraformaldehyde (PFA) diluted in PBS (Sigma Aldrich UK, HT501128) for 20min (RT). PFA reacts with proteins, causing covalent cross-links to form between molecules. In doing so, PFA preserves and stabilises cell morphology, inactivates any cell-degrading proteolytic enzymes, and strengthens the sample of cells to then undergo immuno-fluorescent labelling. Cells can be kept for up to 1 month after fixation. Wells were washed before and after each sequential step three times (5min) using 300µl PBS per well. For primary antibody labelling, cells were blocked using 3% bovine serum albumin (BSA, Sigma Aldrich UK, 03117332001) 1% glycine (Sigma Aldrich UK, G8898) diluted in PBS (30min, RT), followed by 10% chicken serum (CS, Sigma Aldrich UK, C5405) diluted in PBS (30min RT). BSA is commonly used to saturate excess cell surface proteins and therefore reduce the non-specific binding of the anti-E-selectin monoclonal antibody. Glycine (1%) was incubated alongside BSA as it prevents excessive cross-linking produced after PFA fixation. Wells were then incubated with anti-E-selectin monoclonal antibody diluted 1:2000 in 10% CS overnight (4°C). The next day, wells were incubated with Alexa Fluor 488 conjugated chicken anti-mouse secondary antibody diluted 1:500 in 10% CS (1hr, RT). Nuclei were stained using bisBenzimide H33342 trihydrochloride (H33342, Sigma Aldrich UK, B2261) diluted 1:1000 in PBS (20min, RT). Cells were kept in 300µl PBS and plates were wrapped in foil until the plates were imaged.

2.3.2 Alkaline phosphatase labelling

After experimentation, HUVECs in flat bottomed, clear 96 well plates cells were washed, fixed, and blocked as previously described (see 2.3.1 Immuno-fluorescence labelling). Wells were then incubated with mouse monoclonal anti-E-selectin antibody, diluted 1:500 in 10% CS overnight (4°C). The next day, cells were incubated with alkaline phosphatase conjugated goat anti-mouse secondary antibody (1hr, RT), and nuclei were stained as previously described (see 2.3.1 Immuno-fluorescence labelling). After 5 washes with PBS, wells were incubated with 3.7% (w/v) pNPP substrate (Thermofisher Scientific USA, 34045), diluted in 1 litre diethanolamine (DEA) buffer (16.36g NaCl, 102mg $MgCl_2$ 6 H_2O, 100ml DEA, in 1L ddH_2O, pH 9.85) for 20min (RT). The plate was read immediately using the Dynex MRX revelation microplate reader.

2.4 Molecular biology

E-selectin (NM_000450.2), L-selectin (NM_000655.5) and P-selectin (NM_003006.4) mammalian gene expression vectors were designed and ordered from VectorBuilder.com (USA). These constructs were then isolated and ligated into destination vectors containing the appropriate tag (NanoLuciferase (NanoLuc) or SNAP-tag; see Figure 2.1 below, before they were transformed into DH5 alpha *E.coli* to aid the amplification of expression vectors. These NanoLuc/SNAP-tag selectin expression vectors were then extracted from *E.coli* and analysed to verify the DNA fragment size using gel electrophoresis or to verify their sequences using Sanger sequencing. These expression vectors were utilised for mammalian cell transfection and expression of NanoLuc/ SNAP-tag selectin proteins in HEK293Ts and HEKGs. The process of construct isolation, ligation, transformation and analysis is summarised in Figure 2.1 and the techniques used to create these selectin fusions i.e polymerase chain reaction (PCR), agarose gel electrophoresis, DNA purification from PCR product/excised gel bands, DNA concentration quantification and Sanger sequencing are discussed below.

2.4.1 Preparation of Broths and Buffers

Broths were prepared for molecular biology techniques, kept for < 2 months and only used in a sterile environment. Buffers were prepared in advance of experimentation. BSA containing buffers were made up on the day of experiment and not re-used.

Luria Betani (LB) broth

Luria Betani (LB) Broth is nutrient rich growth medium, containing peptides, amino acids and carbohydrates in a low-salt formulation which is commonly used to culture *E. coli*. LB broth powder (L3022, Sigma Aldrich UK) contains NaCl, (5 g/L), Tryptone, (10 g/L) and Yeast Extract (5 g/L) (pH 6.8 – 7.2). LB broth was made up by dissolving 2% w/v LB broth powder (L3022, Sigma Aldrich UK) in ddH_2O and autoclaving the mix until the broth was sufficiently dissolved and sterile. Use of sterile broths was only done in the presence of a Bunsen burner flame to maintain sterile conditions. For ampicillin-resistant LB broth, 0.1% (v/v) ampicillin (A0839, PanReac) was added following autoclaving.

LB broth with agar (LB agar, Lennox, L2897, Sigma Aldrich UK) was utilised for the growth of transformed *E. coli* on agar plates. This formulation of LB broth contained 5 g/L agar, so that the solution solidifies at room temperature and enables spreading of liquid LB broth on a petri dish format. LB agar was dissolved in ddH_2O (3.5% w/v or 35g in 1L) and autoclaved to sterilise the formulation. After sufficient cooling to prevent denaturation of antibiotic, LB agar was supplemented with 50µg/ml ampicillin to aid selective growth of transformed *E. coli*. 10ml Ampicillin LB agar was then poured into a Sterilin™ 90mm petri dish (101VR20, ThermoFisher Scientific UK) and left to cool at RT until the agar solidified. Prepared plates were stored upside down at 4°C until required.

Buffers

Tris-acetate-EDTA (TAE) buffer was used as a running buffer and to prepare agarose gels. This buffer is able to maintain pH 8.3 as well as conduct electricity. TAE buffer was made up as a 50x stock concentration, which was diluted to 1x working solution prior to electrophoresis. The buffer consists of Trizma ® base (40mM), acetic acid (20 mM) and EDTA dihydrate (1 mM).

Hanks Buffered Saline Solution (HBSS) is a commonly used buffer used with live cells, as it maintains pH and osmotic balance. HBSS also contains inorganic salts and carbohydrates that provides energy for cells. HBSS was made up as a 10x stock concentration in 1L ddH_2O, and 10mM D-glucose was added after autoclaving to buffer to prevent denaturation. The 10 x stock was then diluted in double distilled H_2O 10 fold to achieve a 1x HBSS dilution. The resultant 1x HBSS consisted of sodium chloride (145mM) HEPES buffer (10mM), potassium chloride (5mM), sodium pyruvate (2mM), sodium bicarbonate (1.5mM), calcium chloride dihydrate

(1.3mM) and magnesium sulphate heptahydrate (1mM) and D-glucose (10mM) in 1L ddH_2O. The stock was stored at 4°C. Before use on cells, HBSS was typically supplemented with 0.1% BSA and brought up to 37°C.

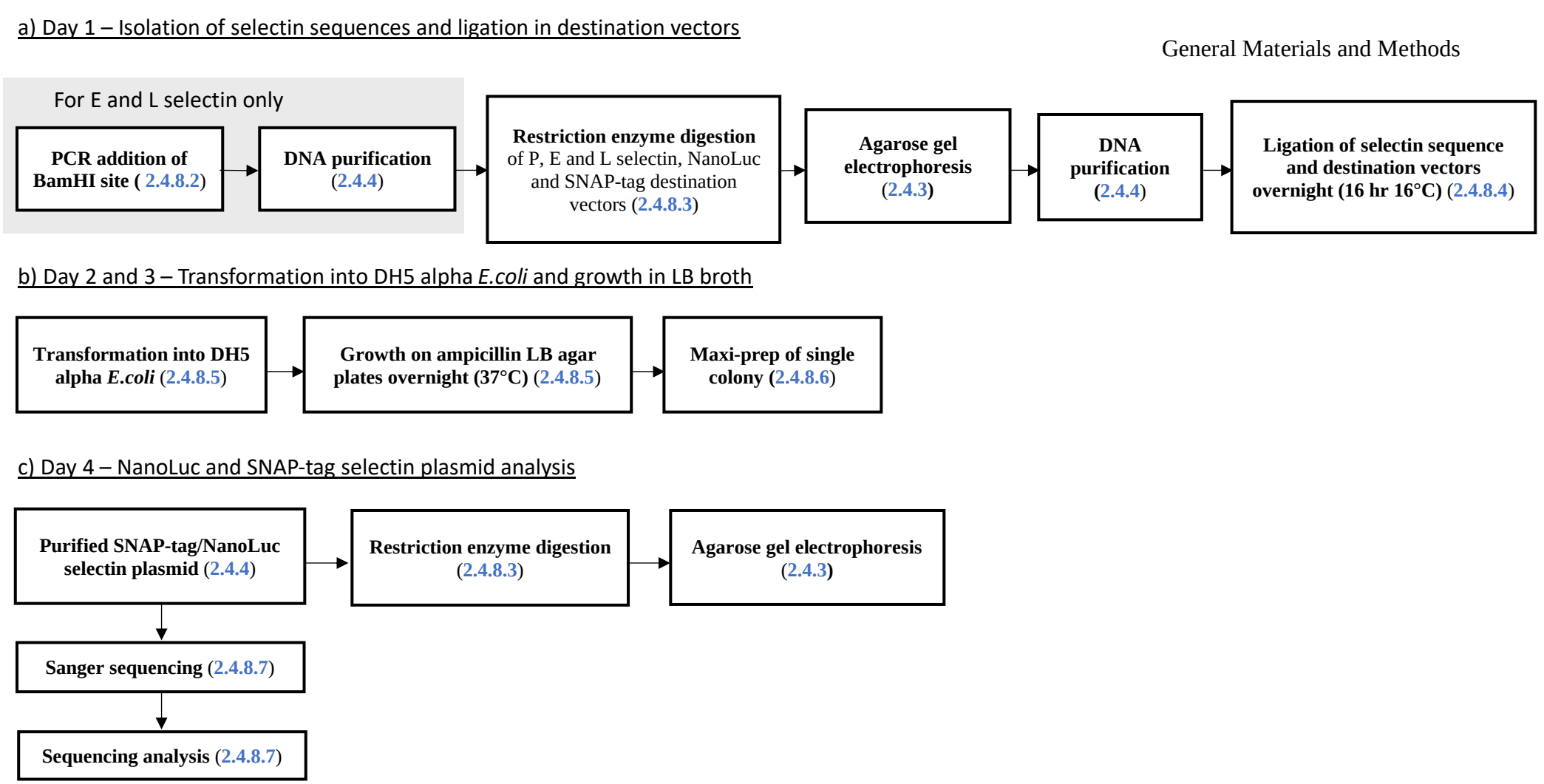

Figure 2.1 Summary of SNAP-tag-selectin and NanoLuc-selectin construct generation using molecular biology techniques. NB see heading numbers in blue indicating sections to find further detail. These steps were undergone after design of and subsequent maxiprep of Selectin vectors received from vectorbuilder.com (see 2.4.7 Design of NanoLuc and SNAP-tag selectin expression vectors). a) Selectin sequences were isolated, and ligated into destination vectors containing SNAP-tag and NanoLuc tags at the N-terminal region. To do this, E and L selectin only were modified for N-terminal addition of BamHI, before the DNA was then purified. The P, E, and L-selectin plasmids were then restriction enzyme digested to isolate each selectin sequence, alongside the destination vectors containing SNAP-tag and NanoLuc This particular combination of restriction enzymes produced sticky ends that aided efficient ligation. These products were then ran on a 1% agarose gel, and the appropriate bands were excised, and DNA purified. Then, the purified selectin insert sequences and destination vectors were ligated together overnight. b) Over the next 2 days, the ligated plasmids were transformed into DH5 alpha E.coli, and grown on an ampicillin positive plate to select for only the successful transformations. A single colony was picked and grown in LB broth to then be maxi-prepped. c) The next day, the maxi-prepped plasmids were verified as containing the SNAP-tag / NanoLuc N-terminal tag, as well as the selectin sequence, using both restriction enzyme digestion and agarose

2.4.2 Polymerase chain reaction (PCR)

Polymerase chain reaction (PCR) utilises a polymerase and single-stranded oligonucleotides (also known as primers) to amplify a specific region of DNA by several orders of magnitude (Garibyan and Avashia, 2013). Primers are designed to be complementary to the regions of interest, in a forward and reverse position. It has been previously identified that the optimal length for primers to act is 18-30 base pairs, with 40-60% guanine/cytosine (GC) content, ensuring the 3' end was a G/C to promote strong binding (termed a 'GC clamp') (Lorenz, 2012). The annealing temperature (Tm) for specific primers was calculated using an online Tm calculator (promega.co.uk). In all PCR reactions, GoTaq® G2 Polymerase (M7841, Promega, UK), a full-length form of *Taq* DNA polymerase was used, which is thermostable enzyme isolated from bacteria that catalyses the synthesis of DNA. Colourless GoTaq reaction buffer (5X) (M792, Promega UK), containing 7.5mM $MgCl_2$ was used in conjunction with GoTaq polymerase, as well as 0.2µM Deoxynucleotide Triphosphates (dNTPs) and the reaction mix was made up to 50µl using ddH_2O. The final concentrations used for each component is detailed in Table 2.1. The PCR reaction mix was added to a 0.2 ml PCR tubes (PK960; Scientific Lab Supplies, UK) and added to the inner wells in the Eppendorf® Mastercycler PCR machine (Eppendorf, Germany). The cycling conditions to obtain maximal amplification of DNA is provided in Table 2.2.

Table 2.1 PCR components, volumes and concentrations. Where dNTP: deoxyribonucleotides, Fwd: Forward, Rev: Reverse.

Component (+ stock concentration)	Final vol	Final Conc.
GoTaq reaction buffer (10x)	10	1 X
dNTPs (10 mM)	1	0.2 µM
Fwd primer (10 µM)	0.5	0.1 µM
Rev primer (10 µM)	0.5	0.1 µM
GoTaq G2 Polymerase (5U/µM)	0.25	1.25 U
Template HUVEC DNA (50 ng/µl)	2 µl	100 ng
H_20	35.75 µl	

Table 2.2 PCR cycling conditions.

**Where X is the appropriate annealing temperature determined by the primers used.*

Temperature	**Time (minutes:seconds)**
95°C	2:00
95°C *Denaturation*	0:30
X°C *Annealing*	1:00
72°C *Extension*	1:00
30 cycles	
72°C *Final extension*	10:0
4°C *Hold*	∞

2.4.3 Agarose gel electrophoresis

Gel electrophoresis is a technique used to separate DNA fragments depending on their size. An electric current is applied through an agarose gel, and the negatively charged DNA moves towards the positive electrode at differing speeds according to their size; i.e. shorter fragments will migrate further than longer fragments. Gels were made by dissolving agarose gel powder (A9539, Sigma Aldrich, UK), in Tris-Acetate-EDTA (TAE) buffer (40mM Trizma® base, 20mM Acetic acid, 1mM EDTA dihydrate in 1L ddH20) by applying heat. Agarose is a polysaccharide extracted from seaweed, which requires heat (87-89°C) to break non-covalent interactions between polymer strands so that it can dissolve into aqueous buffer (Lee *et al.*, 2012). Upon cooling (36-39°C), the non-covalent interactions are re-established and the gel solidifies. The concentration of agarose dissolved depended on the purpose of the experiment. If DNA was to be extracted and isolated from a gel, a 0.5% gel was used as lower temperatures were required to melt gels in DNA purification stage (see 2.4.4 DNA purification) and higher yields were observed. If DNA fragment sizes were checked, a 1% gel was used. If the DNA fragments were close in size and needed a longer, slower process of separation, a higher percentage (3%) gel was used. Final volume of 50ml was used for a small gel set up and for larger, 100ml was used. Once the agarose gel powder had all dissolved, the 50ml/100ml volume was left to cool before adding Ethidium Bromide (4% w/v). Ethidium bromide binds to DNA so that in the presence of UV light, DNA will illuminate and a DNA banding pattern can be visualised. The gel mix was then poured into a gel chamber, a gel comb was used to push out any bubbles and then placed at one end to introduce wells for which DNA could be dispensed.

After the gel solidified (10-20min at RT after pouring), the comb was removed and the gel was inserted into a gel electrophoresis unit (Gel PowerPac Basic, Bio-Rad, UK), containing enough TAE buffer to cover the gel. DNA was mixed with purple gel loading dye (B7024S, New England Biolabs UK) (15% w/v) before the DNA mix was loaded into the wells. This dye contains glycerol to help ensure that the sample easily sinks into the well. A 1 Kbp BenchTop Ladder (G754A, Promega USA) was added alongside samples for size reference. Typically, 12µl final volume of DNA mix was added to the gel. The electrophoresis unit was run at 90V for 30-45 minutes depending on the size of DNA fragments and concentration of gel used. Bands were then visualised using a UV box; a UV transilluminator GVS-30 (Syngene, UK) was used if bands were to be excised and a GeneFlash Gel Documentation System (Syngene, UK) was used to take images of bands to determine DNA fragment size. When DNA bands were excised, they were cut out rapidly using a scalpel to avoid UV damage of DNA before they were transferred into a pre-weighed 1.5ml microcentrifuge tube and the additional weight of the excised band was then calculated.

2.4.4 DNA purification

Following PCR (see 2.4.2 Polymerase chain reaction (PCR)) and/or gel electrophoresis (2.4.3 Agarose gel electrophoresis), DNA was purified using a Wizard® DNA Clean-Up kit (A9282, Promega, USA). This kit aims to remove excess nucleotides and primers from PCR mixes and recovers isolated DNA fragments from agarose gels. It does this by resuspending DNA fragments in the presence of chaotropic salts which free DNA from water. This solution was a guanidine isothiocyanate mix and was termed ‘Membrane Binding Solution’ (MBS). This resuspension was then pipetted onto a silica membrane column, which bound DNA after centrifugation. After wash steps, DNA could then be eluted using water. The specific measures to conduct DNA purification are detailed below.

After excising the gel slice containing the insert DNA, the gel was weighed and 10µl MBS per 10mg of gel slice was added. The mixture was vortexed and heated to 60°C until the gel slice was completely dissolved. For the larger sized E-selectin and P-selectin, DNA fragments were not vortexed, but mixed gently to prevent shearing. Alternatively, an equal volume of Membrane Binding Solution was added to the PCR amplification. The dissolved gel mixture or prepared PCR product was then transferred into a minicolumn assembly which contained a silica membrane column and a collection tube. The minicolumn assembly was centrifuged at 16,000 *xg* for 1 minute and the flowthrough was discarded. The membrane was then washed using 700µl Membrane Wash Solution (MWS) which contained 95% ethanol for 1 min. This

step was then repeated using 500µl MWS (5min). Any residual ethanol was then evaporated by centrifuging the column assembly dry (2min). The minicolumn was then carefully transferred into a sterile 1.5ml microcentrifuge tube, and 30µl pre-warmed (60°C) nuclease-free water was added directly onto the centre of the column and incubated for 5min, before centrifuging (16,000 *xg*) to elute the DNA from the column. This elution step was repeated by pipetting the flowthrough back onto the silica membrane and incubating for 5min, before re-centrifuging the mix. This increased the yield of DNA that was eluted. The DNA was kept at -20°C.

2.4.5 DNA concentration quantification

DNA concentrations were quantified using a microvolume spectrophotometer (DeNovix DS-11 Series). 1µl of sample was pipetted onto the spectrophotometer against a blank (1µl nuclease-free water). The spectrophotometer then measured the absorbance at 260nm, and DNA concentration was calculated in ng/µl. The DNA purity was estimated by calculating the ratio of absorbance at 260nm and at 280nm. Ratios <1.8 suggest contamination due to protein and ratios >2.0 suggest contamination due to RNA.

2.4.6 DNA sequencing

Sanger sequencing was performed by University of Nottingham sequencing facility; Deep Seq, which houses an Illumina MiSeq and NextSeq500 sequencing platforms.

For sequencing whole selectin sequences, primers were designed for every 300bp along each selectin sequence. This was to ensure that there was sufficient overlap of sequenced DNA fragments along selectin sequences. Generally, T7P (5’ TAATACGACTCACTATAGGG 3’) was used to sequence regions flanking the plasmid ORF and therefore could sequence for N-terminal tags such as NanoLuc or SNAP-tag.

During Sanger sequencing, the designed primers bound to their homologous site on the selectin sequence, and a DNA polymerase was used to extend the primer, using fluorescently labelled dideoxynucleotide triphophates (ddNTPs). ddNTPs are nucleotide bases which have had an oxygen removed from their chemical structure, to inhibit the extension of the sequence by polymerase. Therefore, Sanger sequencing results in the formation of extension products of various lengths which had been terminated by ddNTPs at the 3’ end. These extension products are then separated by Capillary Electrophoresis (CE), which like gel electrophoresis (see 2.4.3 Agarose gel electrophoresis), separates DNA fragments due to their size using an electrical current. The DNA fragments were injected into a glass capillary filled with a gel polymer and

a current was applied. Negatively charged DNA fragments then move towards the positive electrode and the speed of migration of DNA fragments is inversely proportional to its size. This induces separation of extension products with a resolution of one base. A laser then excites the dye labelled DNA fragments as they pass through the capillary, and the specific nucleotide is identified due to their fluorescent tag.

The result is a data file revealing the sequence of the DNA in an electropherogram trace file, which was viewed using SnapGene Viewer. The trace file graphically depicted the sequence as a series of coloured peaks corresponding to each nucleotide base. Sequences near the beginning and end of the reaction that showed overlapping peaks were excluded. Sequences were accepted if they displayed individual, sharp and evenly spaced peaks, and were stitched together from the different primers shown in Table 2.6 by identifying the over-lapping regions between each primer.

2.4.7 Design of NanoLuc and SNAP-tag selectin expression vectors

Selectin constructs were designed and ordered from VectorBuilder.com (Figure 2.2). Restriction enzyme sites were mutated out of each selectin sequence (see Table 2.3) at the design stage to prevent cutting of sequences at the wrong sites when incubated with restriction enzymes. All mutations were made so that there was no subsequent change in the amino acid or the function of the overall protein (silent mutations). The resulting sequences were further modified by addition of enzyme sites BamHI (GGATCC) on the N terminus and XhoI (CTCGAG) on the C terminus (Table 2.4). Addition of these enzyme sites enabled restriction enzyme digestion of each selectin sequence in the desired final vector at stage (see 2.4.8.3 Restriction enzyme digestion).

Each expression vector also contained a human cytomegalovirus (CMV) promoter which strongly promotes transcription and translation of the selectin sequence after transfection in mammalian cells (Ma *et al.*, 2012) and an SV40 poly(A) signal after the C-terminal which helps the stability of the mature mRNA and therefore increases efficiency of mRNA translation in mammalian cells (Wildeman, 1988). To enable selection, the expression vectors also contained an ampicillin resistance cassette (Figure 2.2).

*Table 2.3 Silent mutations in P-selectin, E-selectin and L-selectin sequences to silence restriction enzyme sites. See nucleotides in **red** to identify the silent mutations created and the position along the sequence for each enzyme site in brackets (bp).*

Enzyme sites	Original sequence	P-selectin silent mutations	E-selectin silent mutation	L-selectin silent mutations
BamHI	GGATCC	GGAT**T**C *(282bp)*	GG**G**TCC *(1218bp)*	
EcoRI	GAATTC	GAA**C**TC *(1497bp)*	GA**G**TTC *(1350bp)*	
		GA**G**TTC *(1773bp)*		
HindIII	AAGCT	AAGC**G** *(1335bp)*	AA**A**CT *(402bp)*	
			AAG**T**T *(783bp)*	
			AAGC**G** *(1092bp)*	
KpnI	GGTACC	GGTA**T**C *(702bp)*		GG**C**ACC *(657bp)*
		GGTA**T**C *(1410bp)*		
PvuI	CGATCG	CG**T**TCG *(1668bp)*		
SacI	GAGCTC	GA**A**CTC *(612bp)*		
XhoI	CTCGAG	CT**A**GAG *(525bp)*		
XbaI	TCTAGA	TCT**G**GA *(2205bp)*		

Table 2.4 Primers designed for N-terminal addition of BamHI site on E-selectin and L-selectin. See addition of BamHI site (GGATCC) in blue. The Tm (°C) was calculated using SnapGene Viewer.

Selectin		Primer information				
		Sequence	Length (BPs)	%GC	Binding sites (bp)	Calculated Tm (°C)
E-selectin	Forward primer	GAC**GGATCC**TGGTCTTACAACACCTC	26	54	704 - 726	54
	Reverse primer	GCTGGGTCTCGAGTTAAAG	19	53	2474 - 2492	54

L-selectin	Forward primer	GAC**GGATCC**GATTTCCTGGCACATCATG	28	54	770 - 788	54
	Reverse primer	CTGGGTCTCGAGTTAATATGG	21	48	1796 - 1816	54

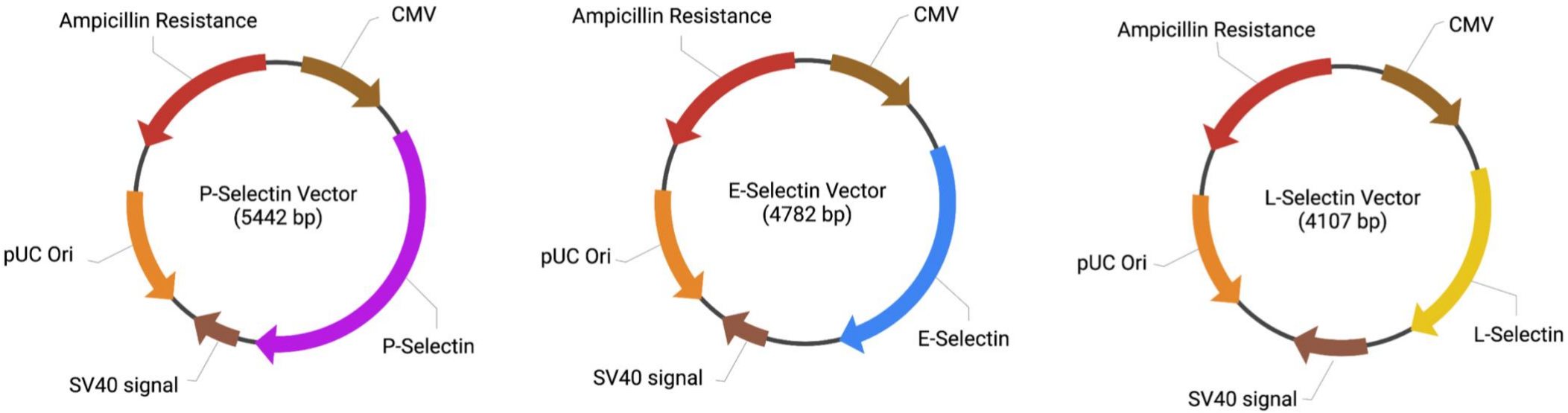

Figure 2.2 P-selectin, E-selectin and L-selectin vector maps ordered from VectorBuilder.com. Each vector contained a human cytomegalovirus (CMV) before the N-terminal, and an SV40 poly(A) signal after the C-terminal. The ampicillin resistance cassette enabled selection of constructs in ampicillin positive agar plates and ampicillin supplemented LB broth solutions. The pUC Ori sequence, also known as the origin of replication, is recognised by a cell's DNA replication proteins, and allows initiation of DNA synthesis.

2.4.8 Generation of NanoLuc and SNAP-tag selectin constructs

2.4.8.1 Maxi-prep of P, E and L selectin expression vectors

Selectin expression vectors were received as a glycerol stock which was kept at -80°C. P, E and L selectin glycerol stocks were grown in 5ml LB broth by scraping frozen glycerol stocks with a yellow pipette tip and dropping the tip into 5ml LB broth containing 5µl Ampicillin. The LB broth solutions were then left to grow in a Stuart SI600 orbital shaker (79520-16, TEquipment) set at 37°C, 225 revolutions per minute (rpm) for 8hr until it reached log phase of growth. The 5ml prep was then poured into 120ml LB broth with 120µl ampicillin and left to grow overnight in the 37°C orbital shaker.

The next day, plasmids were purified using Promega's PureYield™ plasmid Maxi-prep System (A2393, Promega USA). This system is designed to purify large quantities of plasmid DNA using a silica-membrane column, where the *E.coli* DNA is bound and washed with an endotoxin removal wash and Column Wash (salt/ethanol solution) before it is then eluted using nuclease free water, using a vacuum manifold system (Vac-Man; Promega, USA). The wash steps remove any protein, RNA and endotoxin contaminants.

The full volume of grown *E. coli* (120ml) were pelleted at 4,000 xg for 10 minutes at 4°C before they were resuspended in 12mL Resuspension Solution (Promega, USA). The resuspended *E.coli* were then lysed using 12mL Cell Lysis Solution after inverting the tube 5 times and incubating at room temperature (3min). The lysis reaction was neutralized using 12mL Neutralization Solution, the tube was inverted 15 times gently, which produced a flocculant solution with medium-sized clumps. The lysate was then centrifuged at 15,000 xg for 20min at 4°C. Using a column stack and vacuum manifold, the lysate was then drawn through a PureYield™ Clearing Column and PureYield™ Maxi Binding Column using maximum vacuum. To do this, one half of the lysate was added at a time. The Clearing Column was then removed, and 5mL Endotoxin Removal wash was pulled through the column, followed by 20ml Column Wash. The membrane was allowed to dry by leaving the column on maximum vacuum for 5min. The DNA was then eluted from the column by addition of 1ml nuclease free water and the purified DNA was collected in a 1.5ml microcentrifuge tube using the Eluator™ Vacuum Elution Device (A1071, Promega USA). The concentration of DNA was determined by use of the NanoDrop spectrophotometer (see 2.4.5 DNA concentration quantification).

2.4.8.2 Restriction enzyme site addition to E-selectin and L-selectin

Following plasmid amplification and purification above, the selectin sequences were then cut out of the plasmid and purified, to enable ligation into SNAP-tag and NanoLuc containing destination plasmids. These destination plasmids were N-terminal SNAP-tag and NanoLuc Adenosine A_3 receptor containing plasmids obtained from Mark Soave. Before proceeding with E-selectin and L-selectin plasmids however, an additional step was required to add BamHI sequences (GGATCC) in the correct position. Due to an error of not adding the restriction enzyme site after the signal sequence at the design stage, PCR was used to add GGATCC to the N-terminal region of E-selectin and L-selectin (Figure 2.3). Primers were designed with homology arms to the N-terminal region of E/L-selectin and the BamHI sequence on the 5' end and reverse primers were designed for the C-terminus of E-selectin/L-selectin (see Table 2.4). PCR was then performed as described previously (see 2.4.2 Polymerase chain reaction (PCR)) to amplify this region of DNA, flanked with BamHI site. PCR product was then purified as described above (see 2.4.4 DNA purification) and the product was restriction enzyme digested (see 2.4.8.3 Restriction enzyme digestion).

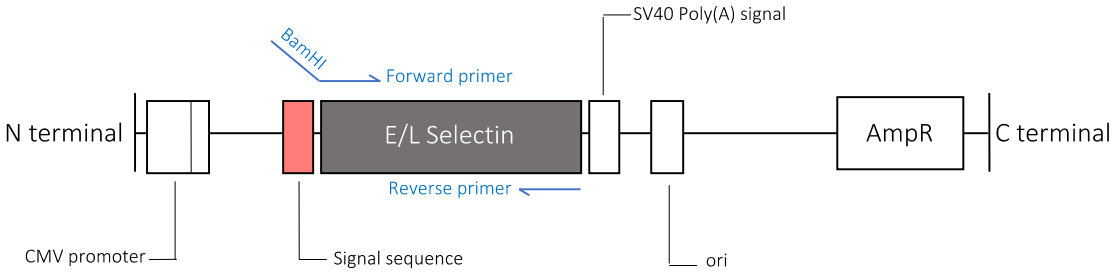

*Figure 2.3 N-terminal addition of BamHI site to E-selectin and L-selectin using primers (see Table 2.4) and PCR. Primers (seen in **blue**) were designed to amplify the selectin sequence and to append a BamHI restriction enzyme site on the N-terminus of E-selectin and L-selectin after it's signal sequence.*

2.4.8.3 Restriction enzyme digestion

Restriction enzymes are endonucleases isolated from bacteria that cleave DNA sequences at specific sequences which are typically 6-8 consecutive bases long (Loenen *et al.*, 2014). After digestion, they produce 'sticky ends', where one strand is overhanging the other to form a short single-stranded segment (typically 4 nucleotides in length) (Figure 2.4). These sticky ends aid the ligation of this fragment DNA into a destination vector. A thermosensitive alkaline phosphatase (TSAP) was also used, to dephosphorylate vector DNA 3' and 5' overhangs to prevent recircularization of plasmids before ligation.

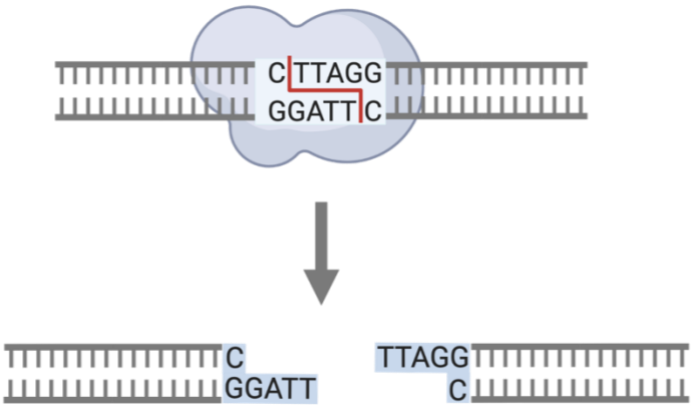

Figure 2.4 Sticky ends produced after restriction enzyme digestion. In this example, a BamHI (GGATTC) targeting restriction enzyme has cut target DNA at this specific site, leaving 'sticky ends' where one strand is overhanging the other. This aids efficient ligation.

The restriction enzymes used to generate these tagged selectin constructs were BamHI (GGATCC) (R6021, Promega USA), XhoI (CTCGAG) (R6161, Promega USA) and KpnI (GGTAC) (R6341, Promega USA). Buffers which optimised the cutting efficiency of restriction enzymes were identified using an online restriction enzyme tool by Promega (www.promega.co.uk/resources/tools/retool/) and used in the restriction enzyme DNA mix (see below Table 2.5).

Table 2.5 Restriction enzyme buffers. Buffers were all bought from Promega, USA, and the buffers were chosen that had maximal % co-activity

Restriction enzyme combination	Promega Buffer used	% co-activity
BamHI and XhoI	Buffer B (R9921, Promega USA)	75
BamHI and KpNI	Multicore (R9991, Promega USA)	75

Selectin expression vectors and destination vectors containing SNAP-tag or NanoLuc were restriction enzyme digested to cut out selectin sequences and to open up vectors for ligation. To do this, 5µg plasmid DNA was incubated with 2µl of BamHI and XhoI at 37°C for 2hr (using a Biometra TRIO Thermoblock, Analytik Jena) for all plasmids. The digests were then incubated with 2µl TSAP (M9910, Promega USA) (20min 37°C), before TSAP was irreversibly inactivated by heating at 74°C (15min). Digested DNA was then run on a 1%

agarose gel as described previously (see 2.4.3 Agarose gel electrophoresis), using a 1kbp DNA ladder to reference DNA sizes. The gel was visualised using a UV box and the bands of appropriate sizes (P-selectin: 2505bp, E-selectin: 1845bp, L-selectin: 1170bp, SNAP-tag destination vector (6000bp): NanoLuc destination vector (6000bp) were rapidly excised to avoid DNA nicking, and DNA was purified and quantified as described previously (see 2.4.4 DNA purification and 2.4.5 DNA concentration quantification).

2.4.8.4 Ligation into destination vectors

Purified E-selectin, P-selectin and L-selectin DNA were ligated into the purified destination vectors containing SNAP-tag or NanoLuc N-terminal tags. Ligation was underwent using T4 DNA ligase (M0202, New England Biolabs (NEB), UK) alongside a 10X T4 ligase buffer (B0202S, NEB, UK). T4 ligase is a ligation enzyme isolated from *E. coli* that were infected with the lytic bacteriophage T4 (Rossi *et al.*, 1997). This ligase catalyzes the formation of phosphodiester bonds with compatible cohesive ends by the joining of 3'-OH and 5'-phosphate groups (Rossi *et al.*, 1997). Ligation was underwent using an insert:vector DNA ratio of 3:1, at a lower temperature to aid stable duplex forming between sticky ends (16°C) overnight (16hr). This was run against a negative control where the vector was incubated with T4 ligase mix in the absence of insert.

To calculate the amount of DNA (ng) to achieve 3:1 insert:vector ratio, an online ligation calculator by New England Biolabs (NEB) was used (https://nebiocalculator.neb.com/#!/ligation). The calculator considered the insert and vector size (kilobases (kb)) using the following equation (see below Equation 1):

Equation

1 Calculation of the required amount of DNA (ng)to achieve 3: 1 *insert: vector ratio*

$$Required\ mass\ insert\ (ng) = \ insert{:}\ vector\ ratio \times \ mass\ of\ vector\ (ng)\ \times \frac{size\ of\ insert\ (kb)}{size\ of\ vector\ (kb)}$$

Once the amount of insert / vector DNA (ng) was calculated, the volume required of isolated DNA was calculated (see below Equation 2):

Equation 2 Calculation of the volume required of DNA for ligation reactions

$$Volume\ DNA\ (\mu l) = \frac{Required\ mass\ DNA\ (ng)}{Concentration\ of\ DNA\ (ng/\mu l)}$$

Ligation reactions were prepared over ice, in 0.5ml microcentrifuge tubes. The applicable volumes of vector and insert to achieve a 3:1 ratio were mixed with 1µl T4 ligase buffer and 0.5µl T4 ligase, and made up to 10µl with ddH_2O. The ligation mix was then incubated at 16°C (16hr) using a Biometra TRIO heat block. The next morning, the T4 ligase was heat inactivated at 65°C (10 min), then cooled to room temperature before transforming into DH5 alpha cells.

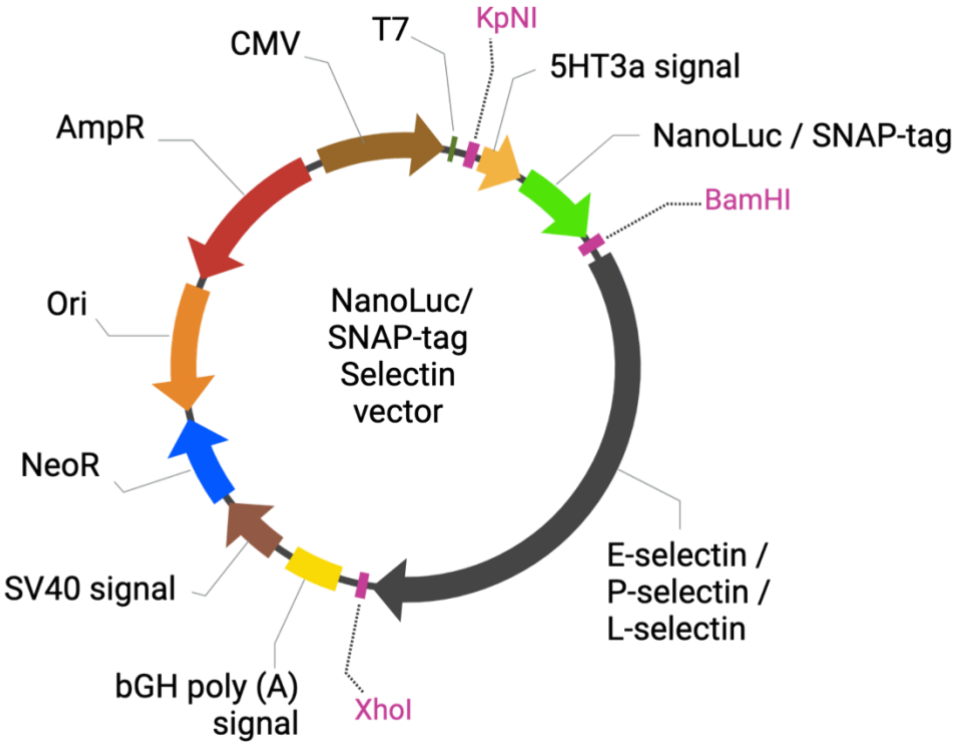

*Figure 2.5 Vector map for NanoLuc and SNAP-tag selectin constructs. E-selectin, P-selectin and L-selectin sequences were ligated into a NanoLuc/SNAP-tag containing destination vector. The destination vector contained a 5-hydroxytryptamine 3a (5HT3a) signal peptide, a NanoLuciferase (NanoLuc) or SNAP-tag N-terminal tag, the appropriate selectin sequence, a bovine growth hormone poly adenylation (bGH) signal, SV40 signal and human cytomegalovirus (CMV) promoters, Ampicillin resistance (AmpR) and Neomycin resistance (NeoR), an origin of replication (Ori), and a T7 promoter. Just before the 5HT3a signal and around the selectin sequence, restriction enzyme sites (seen in **purple**) were present, which aided the selectin construct analysis and verification.*

2.4.8.5 Transformation into DH5 alpha

Ligation mixes were transformed into Subcloning efficiency™ DH5α Competent Cells (18265017, ThermoFisher Scientific UK). DH5α Competent Cells are engineered *E. coli* cells

which have been mutated at recA1 and endA1 to increase the insert stability of plasmids and therefore maximise transformation efficiency of plasmids and the yield of maxipreps (Hanahan, Jessee and Bloom, 1991; Chan *et al.*, 2013).

To undergo transformation, 2µl of the ligation mix was gently mixed with 25µl of DH5α cells and incubated over ice for 30min. After incubation, the ligation-DH5α mix was heat shocked at 42°C for 30 seconds using a heat block and then immediately mixed with 250µl LB broth. The mix was then placed in an orbital shaker set at 225 rpm (37°C) for 1hr. This step aided growth of the transformed bacteria. 250µl of the mix was then spread onto an ampicillin agar plate (see 2.4.1 Preparation of Broths and Buffers) using a plastic L shaped spreader. After addition of 250µl transformed bacteria, the plates were left for 20min before they were inverted and incubated at 37°C overnight. In the presence of ampicillin, only the transformed DH5α cells containing vectors with ampicillin resistance survived. The ligation control where only destination vector was in the ligation mix (see 2.4.8.4 Ligation into destination vectors) was also spread on the agar plate as a negative control.

2.4.8.6 Maxiprep of SNAP-tag/NanoLuc DNA constructs

The next day, observed colonies on each agar plate were picked using a yellow pipette tip, making sure that as little agar was taken up in the tip and targeting only a single colony. A single, isolated colony was picked to minimise the chance of an untransformed/mutated transformed DH5α population contaminating another successfully transformed DH5α population and this affecting downstream transfection experiments. The colony was then dropped into 5ml LB broth containing 5µl ampicillin and grown for 8hr in an orbital shaker (37°C, 79520-16, TEquipment) set at 225 rpm. This 5ml ligated plasmid DH5α mix was then maxiprepped as described previously (see 2.4.8.1 Maxi-prep of P, E and L selectin expression vectors) and the concentration was quantified as described previously (see 2.4.5 DNA concentration quantification).

2.4.8.7 Verification of SNAP-tag and NanoLuc Constructs

To verify that the ligation of selectin sequence into the NanoLuc and SNAP-tag vectors were successful, the maxiprepped SNAP-tag and NanoLuc -selectin DNA (see 2.4.8.1 Maxi-prep of P, E and L selectin expression vectors) was analysed using restriction enzyme digestion and gel electrophoresis, as well as Sanger Sequencing. Due to the restriction enzyme site positions seen in Figure 2.5, the successful ligation would produce a fragment of specific size (depending

on the insert isolated) upon digestion with KpnI and BamHI due to cutting out SNAP-tag/NanoLuc, and a larger E/P/L-selectin fragment due to digestion with BamHI and XhoI (sizes P-selectin: 2505bp, E-selectin: 1845bp, L-selectin: 1170bp). The ligated SNAP-tag/NanoLuc selectin plasmids were digested with either KpNI + BamHI with Multicore buffer or BamHI + XhoI with Buffer B as described previously (see 2.4.8.3 Restriction enzyme digestion). The digestions were then separated on a 1% agarose gel for 45 min at 90 V as described previously (see 2.4.3 Agarose gel electrophoresis). Where a successful ligation was observed, the DNA plasmid was then sequenced by DeepSeq in University of Nottingham (see 2.4.6 DNA sequencing) using primers designed every 300bp along the selectin sequence (see Table 2.6). The resultant sequences was stitched together, and blasted against NanoLuc/SNAP-tag sequence as well as the appropriate selectin sequence using NCBI blast (https://blast.ncbi.nlm.nih.gov/Blast.cgi?PROGRAM=blastn&PAGE_TYPE=BlastSearch&LINK_LOC=blasthome).

Table 2.6 Primers designed for Sanger sequencing for verification of P-selectin, E-selectin and L-selectin. Primers were designed to anneal every 300bp along the length of each Selectin sequence. Primers were ensured to have a glycine cytosine (GC) content of >40%, and annealing temperature (Tm) (°C) within 1°C of each other. All primers were designed, and Tm calculated using SnapGene Viewer.

Selectin		Primer				
		Sequence	Length (BPs)	%GC	Binding sites	Calculated Tm (°C)
P-selectin	Primer 1	gacatgggtgggaaccaaaaaggc	24	54	309 - 332	62
	Primer 2	caacacgtgctcatgaactgcag	23	52	625 - 647	62
	Primer 3	ccatggactgtgttcatccgctcac	25	56	1007 - 1031	63
	Primer 4	ccccttcggtgcctttaggtatcag	25	56	1395 - 1419	62
	Primer 5	ctcttgtgacaacggctttaagctgg	26	50	1806 - 1831	63
	Primer 6	ccattgtctggagggccagttac	23	57	2202 - 2204	62
E-selectin	Primer 1	gctccaggtgaacccaacaataggc	25	56	298 -322	63
	Primer 2	aactaatgggagcccagagccttc	24	54	836 -859	62
	Primer 3	cgaagggtttggtgaggtgtgc	22	59	1316 - 1337	62

	Primer 4	gtgtgcaagttcgcctgtcc	20	60	1549 - 1568	62
L-selectin	Primer 1	ccggaagataggaggaatatggacgtg	27	52	318 - 344	62
	Primer 2	cagctcacagtgtgccttcagc	22	59	702 - 723	63
	Primer 3	ggctggcaaggagattaaaaaaaggc	26	46	1103 - 1128	62

2.5 Transfection of SNAP-tag and NanoLuc selectin expression vectors

Recombinant cell lines were generated, and transient transfections performed in HEK293Ts and HEKGs using the NanoLuc and SNAP-tag selectin plasmids. Transfection describes the introduction of DNA into cells, so that it is transcribed and translated and the protein of interest in expressed (Jacobsen, Calvin and Lobenhofer, 2009). The transfected DNA has potential to either be transiently expressed for a limited period of time (see 2.5.1 Transient transfections), or integrated into the genome of the host cell to produce what is called a stable cell line (see 2.5.2 NanoLuc E-selectin stable cell line generation). FuGENE® HD Transfection Reagent (E2311, Promega USA) was utilised as a transfection reagent. FuGENE is a lipid-based transfection reagent, which is able to encapsulate hydrophilic DNA. The FuGENE encapsulated DNA can then permeate the hydrophobic cell membranes of a variety of cell types with high efficiency (Jacobsen, Calvin and Lobenhofer, 2009). Opti-MEM™ reduced serum medium (31985062, Gibco™, ThermoFisher Scientific UK) is a modification of Eagles Minimum Essential Medium (MEM) which has been buffered with HEPEs and sodium bicarbonate and supplemented with hypoxanthine, thymidine, sodium pyruvate, L-glutamine, trace elements, and growth factors. Opti-MEM™ was used as a recombinant DNA and FuGENE diluent as it allowed reduced serum conditions which optimises the transfection procedure (Rashid and Coombs, 2019). In all transfections, a 3:1 FuGENE:DNA ratio was used as recommended (promega.com).

2.5.1 Transient transfections

Transient transfection using FuGENE allows DNA to bypass the cell membrane and enter the cell cytoplasm. Here, the plasmid is transcribed into mRNA and this mRNA is translated into the protein of interest. NanoLuc and SNAP-tag selectin vector DNA were transiently transfected into HEK293Ts and/or HEKGs for imaging (see 2.11 Un-labelled E-selectin binding peptide internalisation assays), and NanoBRET binding experiments (see 2.9 E-selectin interactions with endothelial cell receptors and 2.10 Fluorescent E-selectin binding peptide NanoBRET assays).

HEK293Ts or HEKGs were plated onto PD coated 96 well plates (see 2.1.6.2 Cell seeding) at 20,000 cells/well. The next day, when cells reached 50-60% confluency, they were transfected with the appropriate NanoLuc/SNAP-tag plasmid DNA at a FuGENE:DNA ratio of 3:1. In a sterile 1.5ml tube, all plasmid DNA was diluted to 100ng/µl using Opti-MEM, and the appropriate volume to achieve 100ng addition per well was added to another sterile tube, containing 0.3µl per 100ng plasmid DNA to achieve the 3:1 FuGENE:DNA ratio. The DNA amounts differed for saturation assays (see 2.9 E-selectin interactions with endothelial cell receptors). This transfection mix was mixed using pipette action 10 times, before the tube was centrifuged to ensure that all of the mix was out of the tube lid. The FuGENE was allowed to encapsulate the plasmid DNA for 10 minutes at room temperature, before 5µl per well was added to each well using an Eppendorf® Multipette® Plus pipette. Cells were then incubated at 37°C 5% CO2 for 24 hours before experimenting.

2.5.2 NanoLuc E-selectin stable cell line generation

A stable cell line is a homogenous population of cells, stably expressing a transfected gene insert. NanoLuc E-selectin, L-selectin and P-selectin stable cell lines were generated for use in peptide binding experiments (see 2.10 Fluorescent E-selectin binding peptide NanoBRET assays). HEK293Ts were passaged into a T25 flask (see 2.1.6.1 Passaging HEK293Ts and HEKGs), and when they reached 60% confluency they were transfected using FuGENE HD transfection reagent. To do this, 8.8µg NanoLuc E-selectin, NanoLuc L-selectin or NanoLuc P-selectin DNA was incubated with 26µl FuGENE diluted in Opti-MEM (making up a total volume of 400µl) mixed using pipette action and incubated for 10min (RT). The total volume (400µl) was then added to the T25 flask and incubated for 24hr (37°C, 5% CO_2). Then, to isolate and propagate individual clones of transfected cells, G418 antibiotic (Geneticin, Invitrogen) was used to select for only cells successfully transfected with the Neomycin resistant NanoLuc plasmids. An un-transfected T25 flask of HEK293Ts was grown and treated with G418 alongside stably transfected cell lines as a negative control. G418 is an aminoglycoside antibiotic produced by Micromonospora rhodorangea bacterium which inhibits protein synthesis, and therefore causes cell death, via binding to eukaryotic ribosomes (Eustice and Wilhelm, 1984). The negative control T25 HEK293Ts will therefore all die in the presence of G418 and the transfected HEK293Ts should not be affected. G418 was diluted to 1mg/ml in 10ml 10% FCS/DMEM, before this selective medium was added to each T25. Selective medium was replenished every 3-4 days for the next 14 days, until cell death plateaued. Then, the selective medium was replaced with 0.1mg/ml G418 for a further week.

By this stage, the negative control cells should have all died and all cells that remained in the transfections were NanoLuc E/L/P-selectin expressing populations. These cells were then screened for luminescence (see 2.9 E-selectin interactions with endothelial cell receptors), after which G418 was no longer necessary. E-selectin, L-selectin and P-selectin stable cell lines were then bulked up, and frozen down for further use (see 2.1.2 Freeze/thawing cells).

2.5.3 NanoLuc E-selectin membrane preparations

NanoLuc E-selectin membrane preparations were made from the NanoLuc E-selectin stable cell line produced (see 2.5.2 NanoLuc E-selectin stable cell line generation) for use in peptide binding experiments (see 2.10 Fluorescent E-selectin binding peptide NanoBRET assays). This process involves isolating the stably NanoLuc E-selectin expressing outer membranes from the rest of the cell components (soluble proteins, nuclear material, other internal membranes and organelles) by disrupting the cells and separating components using differential centrifugation. NanoLuc E-selectin stable HEK293T cell lines were grown in T175 flasks containing 10% FCS/DMEM until they reached 90% confluency. The media was then removed, and the cells were washed once with 10ml PBS and 20ml PBS was then added. The cells were then lifted off of the flask by using a cell scraper, and the 20ml suspension was added to a 50ml falcon tube before the cells were centrifuged at 400 x g for 12 minutes (4°C) (T580R Eppendorf, Germany). The supernatant was removed and the isolated cells were then resuspended in 10ml PBS, and homogenised (10x 3 s bursts, 15,000 rpm) using an electronic handheld IKA T10 Ultra Turrax homogeniser. The cell mix was then subject to further centrifugations to isolate the membranes from the other cell components; 1,500 x g (20min) (4°C) (T580R Eppendorf, Germany), then 50,000 xg (30min, 4°C) (3K30 Sigma, UK). The resultant cell pellet contained only membranes and was resuspended in 1ml PBS. This resuspension then underwent a further homogenisation step using a borosilicate glass tissue grinder (1-7725T-1, Corning®), where the sample was added into the cylindrical portion of the mortar and the pestle was rotated downward 15 times. The concentration was then determined using a bicinchoninic acid assay (Pierce™ BCA Protein Assay, ThermoFisher Scientific,UK), and the resuspension was diluted to 1mg/ml using PBS. This process was repeated for 4 more T175s containing NanoLuc E-selectin HEK293Ts, to ensure an n of 5 was conducted using 5 different membrane preparations. Membrane preparations were aliquoted and stored at -20°C.

2.6 CRISPR-Cas9 genomic editing

Clustered regularly interspaced palindromic repeats (CRISPR)-Cas9 is a genome editing technique which utilises bacterial CRISPR-Cas systems that functions in adaptive immune systems to protect against viral infection (Robb, 2019).

The ribonucleoprotein (RNP) delivery technique was utilised in both HUVECs and TERT2 HUVECs to add a HiBiT tag to the N-terminus of E-selectin. This was necessary to perform the NanoLuc Binary Technology (NanoBiT) experiments (see 2.8 HiBiT E-selectin Luminescence assays). All CRISPR reagents were ordered from Integrated DNA Technologies (IDT, USA).

2.6.1 Design of CRISPR RNA and repair templates

CRISPR RNA (crRNA) is one constituent of the guideRNA complex (gRNA) and is responsible for directing gene insertion to the target of interest (in this case E-selectin). crRNA was designed to be homologous to the N-terminal region of interest on the N terminus of E-selectin (CGTGGAGGTGTTGTAAGACC) after it's signal sequence (TGCTTCTCATTAAAGAGAGTGGAGCC). The sequences were designed using the CRISPOR program design tool (http://crispor.tefor.net), by inputting this N-terminal section of E-selectin genomic sequence (found on University of California Santa Cruz (UCSC) using the latest upload; Dec.2013(GRCh38/hg38 human assembly) into the software (Concordet and Haeussler, 2018). Potential guide sequences for protospacer adjacent motif (PAM) regions were listed and the highest predicted efficiency sequence and location was selected. Cas9 protein requires a PAM site (specifically NGG for Cas9, where 'N' is any nucleotide base) to serve as a binding signal for Cas9.

The repair template was designed to contain the desired HiBiT sequence (GTGAGCGGCTGGCGGCTGTTCAAGAAGATTAGC), with a Glycine-Serine-Serine-Glycine (GSSG) linker (GGGAGTTCTGGC), containing left and right homology arms (71 base pairs in length) on either side to aid the insertion of the HiBiT-GSSG sequence (2.7b). The HiBiT insertion disrupted the PAM site (GGA), thus preventing recutting of edited DNA by residual Cas9 (2.7a).

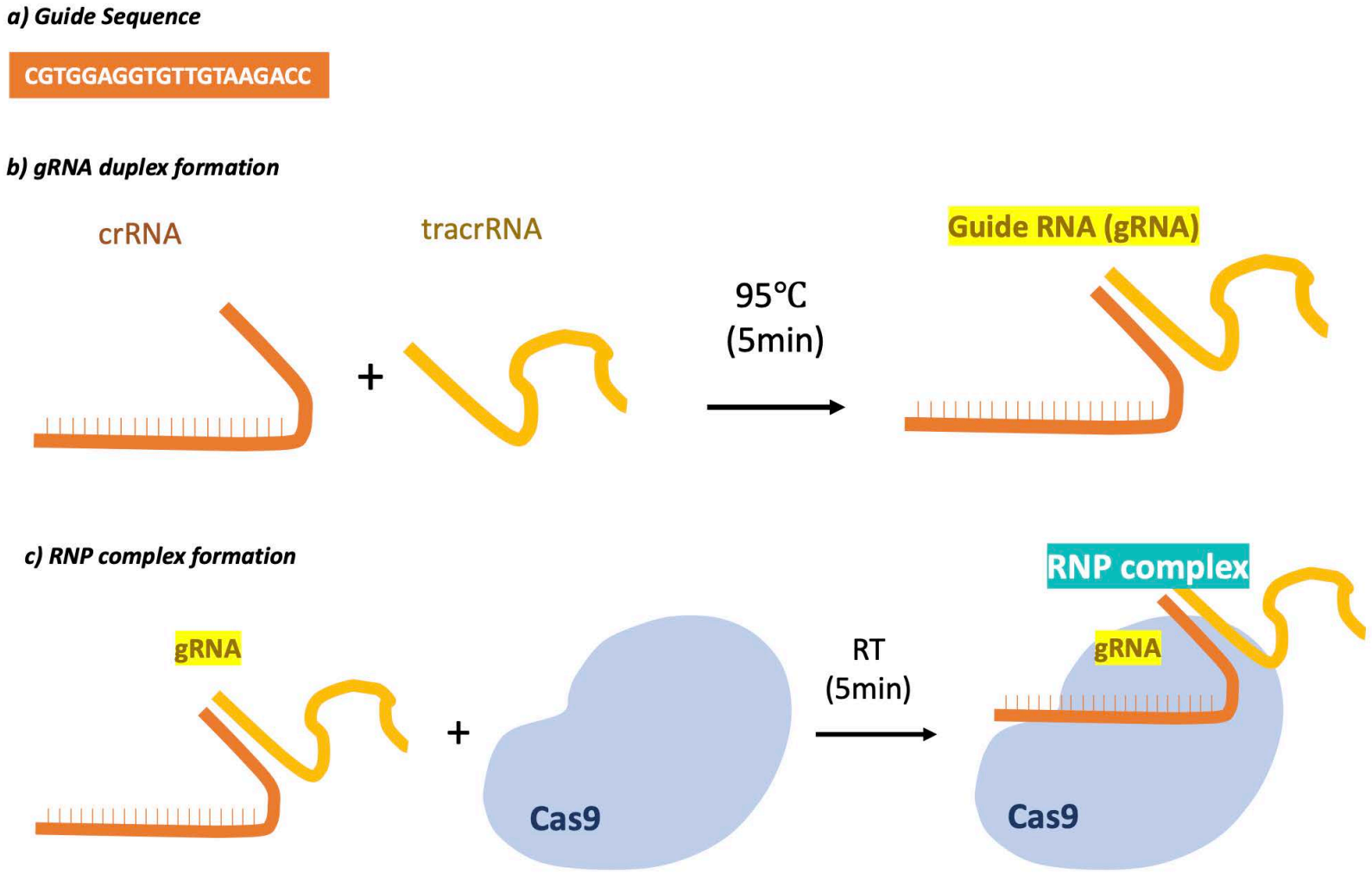

Figure 2.6 RNP complex formation. a) the guide sequence was designed to be homologous to the N-terminal region of E-selectin, at the location of the HiBiT insert and was 20bp long. b) to form the guide RNA (gRNA) duplex, CRISPR RNA (crRNA) and trans-activating CRISPR RNA (tracr RNA) were annealed together (95°C, 5min), before the mix was left to cool (15min, RT). c) Then the ribonucleoprotein (RNP) complex was formed by incubating equal parts of gRNA and purified Cas9 protein (RT, 5min).

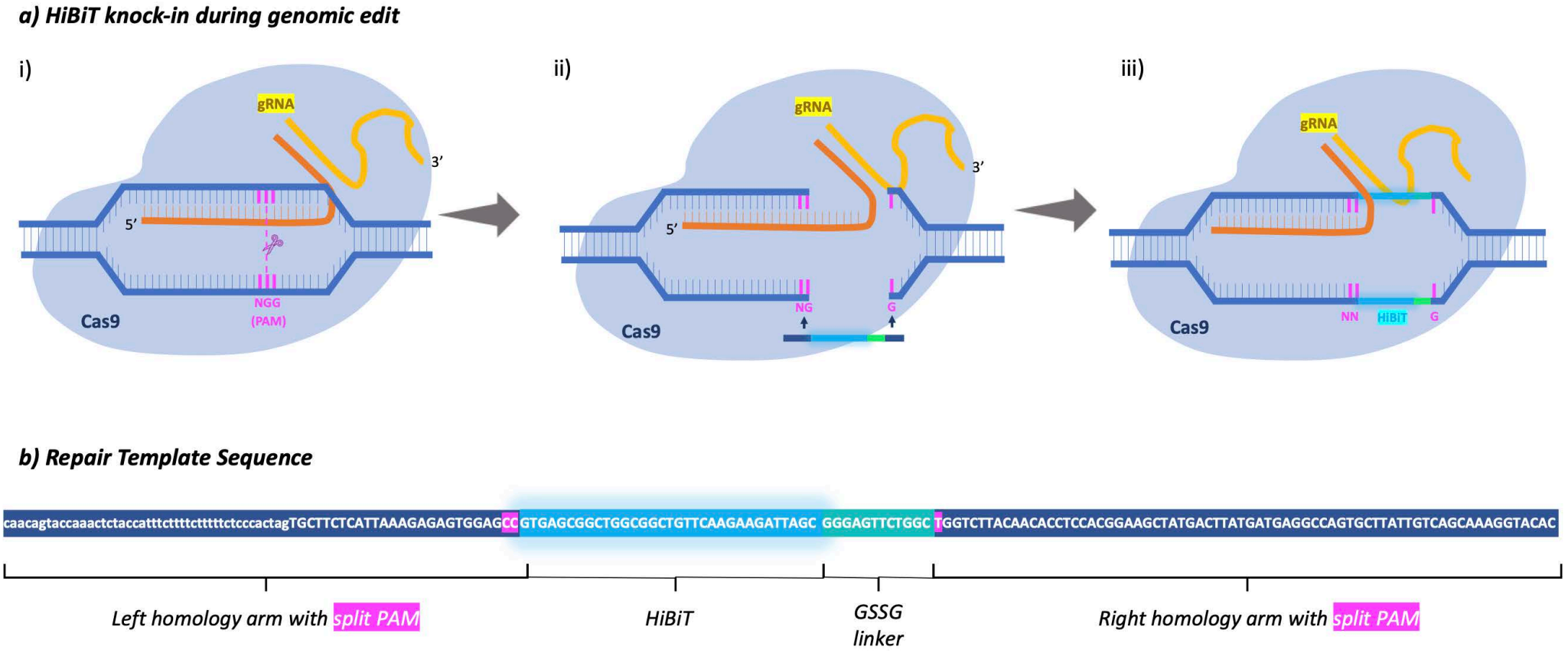

Figure 2.7 The HiBiT-GSSG knock-in was designed to be inserted in-between the Cas9 PAM site to prevent re-cutting by residual Cas9. a) This schematic describes the process of CRISPR-Cas9 gene editing within cells and helps explain the rational for preventing re-cutting and re-editing at this specific PAM site. i) The RNP complex seeks out and only binds to the PAM site (NGG shown in pink). Upon binding to the PAM site, the target DNA region unwinds and the base pairing between the gRNA and the target strand of the DNA is initiated. Then the RNA-DNA hybrid (R-loop) is extended and DNA cleavage is activated at the PAM site. ii) and iii) in the presence of the repair template, the homology arms around the cleaved DNA aid the insertion and repair of the N-terminal region with this HiBiT plus linker edit (shown in light blue and light green respectively). Lower case lettering indicates intron regions with upper case lettering indicating exon regions.

2.6.2 RNP complex formation

The ribonucleoprotein (RNP) complex describes the complex formed between guide RNA (gRNA) and the Cas9 protein (Robb, 2019). First, crRNA (Figure 2.6a) and transactivating CRISPR RNA (Alt-R® cas9 tracrRNA, 1072533, IDT USA) were annealed together by incubating at a 1:1 ratio at 95℃ (5min), to form the gRNA duplex (Figure 2.6b). The reaction was left to cool for 15min before addition of purified Alt-R® S.p. Cas9 nuclease V3 (1081059, IDT USA) (at a 2:1 ratio (guideRNA:Cas9; to achieve a 1500nM gRNA:750nM Cas9 final concentration in the electroporation cuvette) for 5min (RT) (Figure 2.6c).

2.6.3 Testing for SNPs in the PAM region and Cas9 cutting efficiency at its target region

The genomic DNA from HUVECs of the target region for editing was screened for single nucleotide polymorphisms (SNPs) that may have affected CRISPR-Cas9 mediated gene editing. The cutting efficiency of the RNP complex (see 2.6.2 RNP complex formation) was also tested before proceeding to edit HUVECs and TERT2 HUVECs.

WT HUVECs were grown in a T75, trypsinised and centrifuged to form a cell pellet as described previously (2.1.5.1 Passaging). Genomic DNA was then extracted, using an E.Z.N.A Tissue DNA Kit (D3396-01; Omega Bio-tek, USA). Primers were designed around the N-terminal region of E-selectin (Table 2.7) to amplify this 370bp region using polymerase chain reaction (PCR) (see Figure 2.8) (see 2.4.2 Polymerase chain reaction (PCR)). 100ng of DNA was then added to a mix containing forward and reverse primers (0.1µM) dNTPs (0.2µM), GoTaq reaction buffer (1X final concentration) and GoTaq G2 Polymerase (1.25U) and was made up to final volume 50 µl using ddH_2O on ice. The 50µl reaction was mixed in a PCR tube and centrifuged. This process was performed for 5 x 50 µl PCR reactions in parallel. The reaction mixes were placed in an Eppendorf® Mastercycler PCR machine (Eppendorf, Germany) and the PCR was run using an annealing temperature appropriate for the forward and reverse primers (60℃); additional cycling conditions are detailed in Table 2.2. The 5 PCR mixes were then pooled and run on a 3% agarose gel (see 2.4.3 Agarose gel electrophoresis) at 90V for 45 minutes. The band for this amplified region of DNA was visualized using a UV box, quickly excised using a scalpel and gel purified using Promega's Wizard® SV Gel and PCR Clean-up System (see 2.4.4 DNA purification). The concentration of DNA was determined using a NanoDrop spectrophotometer (see 2.4.5 DNA concentration

quantification). This N-terminal region of DNA was then sequenced (see 2.4.6 DNA sequencing) and the sequence was blasted against the published genomic E-selectin cDNA sequence (NM_000450.2) using NCBI BLAST and checked for SNPs.

Table 2.7 Primers for analysis of N-terminal 370bp region of E-selectin. Primers were designed on SnapGene Viewer, and ordered from Sigma Aldrich (UK) and kept at -20°C.

Forward primer	GAGCCCAGTTCTTGGCTTCT
Reverse primer	TCTGGGCCATGTCACAAACA

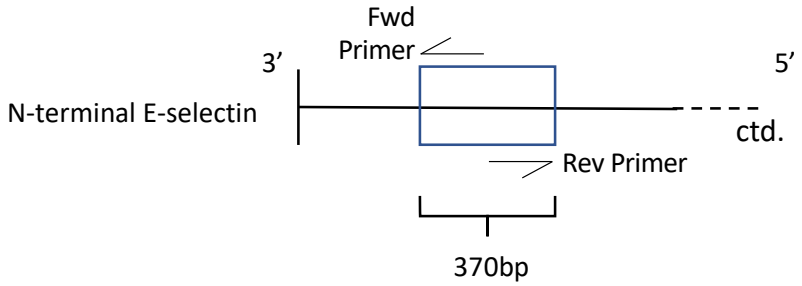

Figure 2.8 Amplification of 370bp region of N-terminal E-selectin using forward (Fwd) and reverse (Rev) primers seen in Table 2.7. Once this region was amplified, the PCR product underwent PCR clean-up, and was then analysed as described in 2.6.3 Testing for SNPs in the PAM region and Cas9 cutting efficiency at its target region and 2.6.8 Verification of homozygous edit.

A larger N-terminal region around the PAM site for E-selectin was PCR amplified using primers which amplified an 873bp region (Table 2.8). These primers were designed such that cutting at the PAM site by Cas9 would produce one longer and one shorter segment of DNA (337bp and 536bp) that could be separated and visualized using gel electrophoresis (Figure 2.9). The 873bp region of DNA was PCR amplified as described above and the PCR mix was then purified (see 2.4.4 DNA purification).

The RNP complex of CRISPR RNA, tracr RNA and Cas9 was formed (see 2.6.2 RNP complex formation). Then, 10x Cas9 nuclease reaction buffer (200µM HEPEs, 1M NaCl, 50mM MgCl2, 1mM EDTA) was adjusted to pH 8.5 and filter sterilized using a 0.2µm filter. 1µl of 10x Cas9 nuclease reaction buffer was incubated with 100nM RNP complex, 20nM of the isolated and purified TERT2 HUVEC DNA and made up to a final volume of 10µl with nuclease free water in a PCR tube (RT). A negative control was run in parallel where there was no RNP complex added. All reactions were done in duplicate so that they could be pooled

together and seen with better clarity on the agarose gel. The mixes were incubated at 37°C for 60 min using the Eppendorf Mastercycler PCR machine, after which, 1µl of proteinase K (20mg/ml) was added to all reactions and incubated at 56°C (10 min, Eppendorf Mastercycler PCR machine). The duplicate reactions were pooled together before 2µl of gel loading buffer was added, and they were loaded against a 100bp ladder on a 1% agarose gel at 90V for 45min (see 2.4.3 Agarose gel electrophoresis). The resultant bands were imaged using a UV box fixed with a camera.

Table 2.8 Primers for Cas9 cutting analysis.

Forward primer	CCTCATACAGTGCTTCTTGGTGC
Reverse primer	TCTTGCCCACATTCACACAAAACA

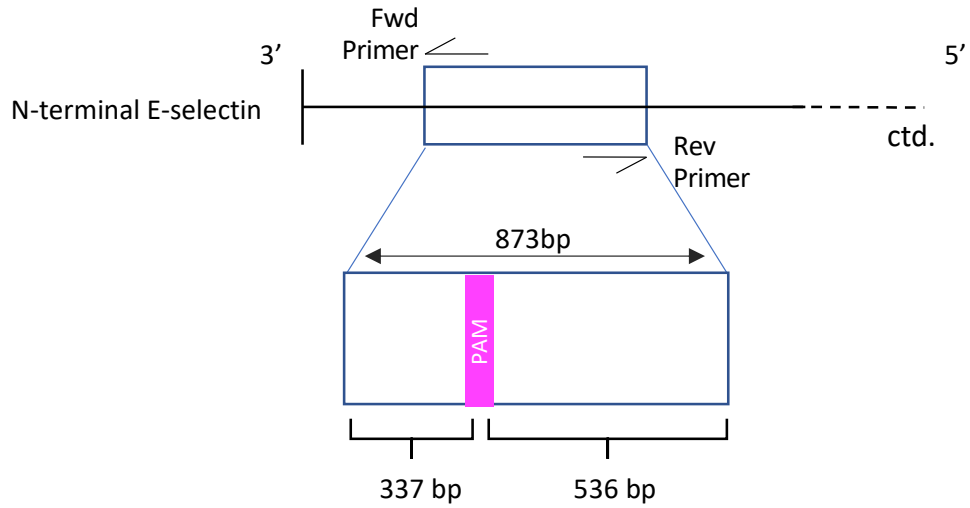

Figure 2.9 The 873 bp region of N-terminal E-selectin DNA was PCR amplified and purified. This region of DNA was then incubated with the RNP complex. Upon cutting at the PAM region (seen in pink), two fragments will be produced (337bp and 536bp in size) which will be observed on an agarose gel. The cutting efficiency of RNP complex is therefore analysed by the presence and strength of the bands on the agarose gel.

2.6.4 Electroporation of RNP complex and repair template into wildtype/TERT2 HUVECs

The RNP complex was annealed as described previously (see 2.6.2 RNP complex formation). Then, 4µl of repair template ((100µM) custom designed and sourced from IDT USA) and 4 µl Electroporation Enhancer (1075916, IDT USA), was added to the RNP complex mix, and incubated for 5 min (RT) forming the 'CRISPR mix'. Alt-R® Cas9 Electroporation Enhancer is a single-stranded DNA oligonucleotide functioning as a Cas9 DNA carrier, improving the delivery of the RNP complex during transfection. HUVECs and TERT2 HUVECs were trypsinised, pelleted and counted as described previously (2.1.4.1 Passaging and 2.1.4.2 Cell seeding). 500,000 cells were then pelleted using a centrifuge. The supernatant was carefully aspirated and the pellet was resuspended in 100 µl Ingenio electroporation solution (MIR 50114; Mirus Bioscience, UK). The resuspended cells were then mixed gently but thoroughly with the CRISPR mix, and the cell-CRISPR mix was then transferred into an electroporation cuvette gently to avoid generating bubbles, using an Ingenio plastic cell dropper (MIR50125, Mirus Bioscience). HUVECs or TERT2 HUVECs were then electroporated using a Nucleofector 3b Device electroporator (Lonza AMAXA; HUVEC – human A-034 programme). Electroporation of cells induces a brief electric field across each cell, leading to polarisation of the plasma membrane. This causes reversible loss of plasma membrane integrity and consequential formation of pores which are large enough to allow diffusion of DNA into the cell. Optimised combinations of field strength (Volts (V) /cm), time constant (determined by resistance and capacitance in the complete circuit) and electroporation buffer composition is required for this process to not induce irreversible damage to the plasma membrane. The Amaxa nucleofector system (Lonza) have optimized the electroporation parameters for HUVECs and have available an old protocol (U-001) and a new protocol (A-034), which differed in electroporation parameters which are not reported. IDT also provide an electroporation buffer, termed electroporation solution and an electroporation enhancer which is a single-stranded DNA oligonucleotide computationally designed to be non-homologous to human genome and functions as a carrier DNA. Cells were then taken up from the cuvette and resuspended in warmed Medium 200, at the appropriate volume to achieve the desired seeding density. Cells were seeded into 0.1% gelatin coated Greiner white-sided 96 well plates to grow until they reached 70-80% confluency.

2.6.5 Generation of HiBiT E-selectin mixed population cell line

500,000 TERT2 HUVECs were electroporated with CRISPR mix (see 2.6.4 Electroporation of RNP complex and repair template into wildtype/TERT2 HUVECs). This cell population was then resuspended in warmed Medium 200 supplemented with 2.2% LVES and grown in a 25cm^2 tissue culture flask (T25) which had been pre-coated with 0.1% gelatin (20min, 37°C). Media was replaced every 2 days to aid growth of HiBiT E-selectin mixed population (mx) TERT2 HUVECs . When cells reached 70-80% confluency, cells were transferred into a T75 flask as described previously (see 2.1.4.1 Passaging). HiBiT E-selectin (mx) TERT2 HUVECs were then bulked up and frozen down for further use (see 2.1.2 Freeze/thawing cells).

2.6.6 Generation of HiBiT E-selectin clonal cell line

To generate a clonal HiBiT E-selectin TERT2 HUVEC cell line, HiBiT E-selectin (mx) TERT2 HUVECs were single cell seeded into a 0.1% gelatin coated 96 well plate. This was achieved by counting the cell population, and initially diluting this suspension to give a density of 10,000 cells per ml. Cells were then further diluted to give a density of 20 cells per ml. Cells were seeded as 200µl cell suspension per well and left to grow over the course of 3-4 weeks. Each well was visually checked for single colonies. This helped to assess whether clones were grown from a single cell before screening the whole plate. Media was replaced to aid the growth of cells and minimise the effect of any well evaporation.

2.6.7 Screening for HiBiT Clonal TERT2 HUVECs

When the single seeded TERT2 HUVECs (mx) had grown to >60% confluency in a 96 well plate, cells were lifted off each well by addition of 50µl 4X Trypsin (< 5min 37°C) using a multichannel pipette (3125000010, Eppendorf Germany). Trypsinisation was ended by addition of 100µl Medium 200 per well using a multichannel pipette, and half of the volume was then reseeded in the same well plate position onto a new, 0.1% gelatin coated white-sided Greiner 96 well plate. The rest of the original cells were left in the plate to adhere and regrow, for further use. Media was replaced the following day after cells had adhered in both 96 well plates to promote cell growth.

When the reseeded cells for screening grew up to >70% confluency, every well was incubated with 1nM TNF alpha diluted in Medium 200 supplemented with 2.2% LVES (6hr, 37°C 5% CO2). Purified LgBiT protein (N3030, Promega USA) was added (1:400 final dilution in well, 37C, 20min) and Furimazine substrate (N1110, Promega USA) was added (1:400 final dilution in well, 5min) before an opaque plate back was added (Perkin Elmer and luminescence measured using a PHERAstar FS plate reader (BMG LabTech) using filters to measure

NanoLuc emissions at 450 nm (30nm bandpass). 'Hit' wells were defined as wells producing luminescence units of >100,000. 'Hit' wells were then identified in the corresponding original 96 well plate. These wells were then trypsinised and the whole population was re-seeded into a 0.1% gelatin coated 24 well plate. When cells grew up to >80% confluency in a 24 well plate, the whole cell population was trypsinised as described previously and reseeded into a T25. When cell confluency reached >70% in the T25, cells were trypsinised using 1ml 4X trypsin and were transferred into a T75 flask. Clonal cell lines were then bulked up, and frozen down for further use (see 2.1.2 Freeze/thawing cells).

2.6.8 Verification of homozygous edit

To test whether one allele (heterozygous) or both alleles (homozygous) of the E-Selectin gene had been edited with the HiBiT tag, PCR and gel electrophoresis techniques were used. First, the same primers used in '2.6.3 Testing for SNPs in the PAM region and Cas9 cutting efficiency at its target region' were used to amplify the 370 bp N-terminal region of E-selectin. If the HiBiT edit had been successful, a 45bp addition (HiBiT + GSSG linker) in length would be visible on an agarose gel compared to WT unedited DNA. If the edit was heterozygous, two bands would be observed, indicative of a population of unedited (370bp) and edited (415bp) DNA. If the edit was homozygous, only one band would be observed on the agarose gel (415bp).

The HiBiT E-selectin clone DNA and wildtype TERT2 HUVEC DNA were isolated using the E.Z.N.A Tissue DNA Kit, and the N-terminal region of E-selectin was amplified using PCR as described before (see 2.6.3 Testing for SNPs in the PAM region and Cas9 cutting efficiency at its target region). Both wildtype and edited PCR mixes then underwent a PCR clean up (see 2.4.4 DNA purification), before they were ran on a 4% agarose gel at 90 V for 1 hour (see 2.4.3 Agarose gel electrophoresis) using a 100bp DNA ladder for reference (N3231S, New England BioLabs UK). The bands were then visualized using a a UV transilluminator GVS-30 (Syngene, UK)

2.7 Antibody labelling assays

To determine, visualise and quantify E-selectin expression in HUVECs and TERT2 HUVECs, cells were antibody-labelled using a monoclonal E-selectin antibody and the appropriate secondary antibody conjugated to either AlexaFluor 488 or alkaline phosphatase (see 2.3.1

Immuno-fluorescence labelling and 2.3.2 Alkaline phosphatase labelling). The effect that cytokine stimulation for increasing periods of time (0-8hr) and at increasing concentrations has on E-selectin cell membrane expression was assessed using these antibody labelling methods. The assays conducted prior to E-selectin antibody labelling and visualisation/quantification are described below.

2.7.1 Concentration response experiments.

TNFα, Histamine and $VEGF_{165}$a concentration responses were conducted to assess the potency of these cytokines to stimulate cell surface expression of E-selectin in HUVECs and TERT2 HUVECs. Human Tumour Necrosis Factor-α (TNFα) (H8916-10UG, Sigma Aldrich UK), was received as a lyophilised powder and resuspended in ddH_2O to 0.1mg/ml (5790nM equivalent). Recombinant Human $VEGF_{165}$ Protein (with carrier) (depicted as '$VEGF_{165}$a' 293-VE-050, R&D systems, USA), recombinant Human VEGF $_{165}$b Protein (with carrier) (3045-VE-025, R&D systems, USA) and recombinant Human VEGF 121 (aa 207-327) Protein (with carrier) (4644-VS-010, R&D systems, USA) were all received as a lyophilised powder and resuspended to 1µM in sterile PBS ($VEGF_{165}$a and $VEGF_{165}$b) or sterile 4mM HCl in ddH_2O ($VEGF_{165}$b). Histamine dihydrochloride (H7250, Sigma Aldrich UK) was dissolved in ddH_2O to 1mM.

The antibody alkaline phosphatase labelling (see 2.3.2 Alkaline phosphatase labelling) was used to quantify E-selectin expression in HUVECs. HUVECs were plated onto flat bottomed clear polystyrene TC-treated 96-well plates (Corning, USA, 3596) as described previously (see 2.1.4.2 Cell seeding) at 30,000 cells per well in Medium 200 supplemented with 2.2% LVES. The next day when HUVECs reached 70-80% confluency, wells were incubated with E-selectin inducing cytokines. For TNF alpha, 7 different concentrations were diluted at 10x the desired well concentration (0.1nM for 0.01nM well concentration, 0.4nM for 0.04nM well concentration, 1nM for 0.1nM well concentration, 3nM for 0.3nM well concentration, 5nM for 0.5nM well concentration, 7nM for 0.7nM well concentration and 10nM for 1nM well concentration) in medium 200 (2.2% LVES), and wells were incubated with 5µl of each concentration in 45µl medium 200 for 6hr (37°C, 5% CO_2). For $VEGF_{165}$a, $VEGF_{165}$b and VEGF121, a single concentration was used (100nM), by addition of 5µl neat stock to 45µl medium 200 in the well and incubated for 6hr (37°C, 5% CO_2). For Histamine stimulation, 100nM addition was achieved by making up 1000nM dilution in medium 200 and adding 5µl to 45µl medium 200 in the well (6hr, 37°C, 5% CO_2). For co-stimulation experiments, 5µl of each TNF alpha concentration was incubated with 5µl of $VEGF_{165}$a / Histamine dilutions in

40µl medium 200 in the well (6hr, 37°C, 5% CO_2). After 6hr, each well was washed once with PBS before cells were fixed, blocked and antibody labelled with monoclonal E-selectin antibody and alkaline phosphatase secondary antibody as described previously (see 2.3.2 Alkaline phosphatase labelling). The E-selectin expression, quantified as optical density (O.D.) values, was then inputted and analysed in Prism 9 software.

2.7.2 Time course assays

Reverse time course assays were conducted on HUVECs and TERT2 HUVECs in response to 1nM TNF alpha, 100nM $VEGF_{165}$a and 100nM Histamine.

For alkaline phosphatase quantification, HUVECs / TERT2 HUVECs were seeded at 30,000 cells/well in clear 96 well plates 24 hr prior to experimentation as described previously (see 2.7.1 Concentration response). For confocal imaging experiments, HUVECs were seeded onto Ibidi µ-slide 8 well plates at 10,000 cells per well as described previously (see 2.1.4.2 Cell seeding). The next day, 10x desired well concentrations of TNF alpha (10nM), Histamine (1000nM) and $VEGF_{165}$a (1000nM) were diluted using Medium 200. All appropriate wells were replaced with 45µl (96 well plate format) or 270µl (ibidi µ-slide 8 well plate format) medium 200 (2.2.% LVES) and 5µl (96 well plate format) or 30µl (ibidi µ-slide 8 well plate format) of each E-selectin stimulant was added to each appropriate well at the appropriate time. TNF alpha, Histamine or $VEGF_{165}$a were added at time point 0hr and then after 2hr, 4hr, 7hr and 7.5hr (37°C, 5% CO_2) and cells were fixed at 8hr time point using 3% PFA/PBS (20min, RT). This reverse time course experiment achieved incubation times with stimulants for 30min, 1hr, 4hr, 6hr and 8hr. 96 well plates were alkaline phosphatase labelled and the E-selectin expression was quantified as described previously (see 2.3.2 Alkaline phosphatase labelling and 2.8.2 Concentration response assays). Ibidi µ-slide 8 well plates were AlexaFluor 488 labelled as described previously (see 2.3.1 Immuno-fluorescence labelling) and imaged using the LSM 880F confocal microscope (see Confocal microscopy).

2.8 HiBiT E-selectin Luminescence assays

Cell lines which were genetically modified to tag E-selectin with HiBiT all underwent concentration responses and kinetic screens in response to different inflammatory cytokines. The cell surface expression of HiBiT-E-selectin was then quantified using NanoLuc binary technology (NanoBiT), and an imidazopyrazinone substrate (Furimazine or Endurazine) and

resultant luminescence was read using a PHERAstar FS plate reader or a bioluminescent widefield microscope (LV200).

2.8.1 NanoBiT

NanoLuciferase binary technology (NanoBiT) describes a system which detects the re-complementation of 2 fragments of the novel luciferase NanoLuciferase (NanoLuc) (Figure 2.10a). NanoLuc is a 19.1kDa luciferase enzyme, isolated from the deep-sea shrimp *Oplophorus Gracilirostris* (Hall *et al.*, 2012). Compared to Renilla luciferase (Rluc) and Firefly luciferase (Fluc), NanoLuc displays 150-fold brighter luminescence on a per mole basis, is 20nm blue-shifted, has a 20% narrower spectrum relative to Rluc and is smaller in size (Rluc: 36kDa, Fluc: 61 kDa) (Hall *et al.*, 2012; England, Ehlerding and Cai, 2016). Promega have been able to split NanoLuc into a 1.1kDa high affinity fragment (termed HiBiT) and a complementary larger fragment (termed LgBiT; 17.6kDa) (Dixon *et al.*, 2016). LgBiT is cell impermeable therefore will only re-complement with surface-expressed HiBiT E-selectin. Upon re-complementation, in the presence of a furimazine substrate, luminescence is produced. Furimazine is oxidized by the NanoLuc luciferase, producing the products Furimamide, carbon dioxide and luminescence (Figure 2.11). CRISPR-Cas9 genomic engineering was used to append HiBiT to the N terminus of endogenously expressed E-Selectin in HUVECs and TERT2 HUVECs (see 2.6 CRISPR-Cas9 genomic editing), and NanoBiT enabled detection of cell surface expression. For end point reads of HiBiT E-selectin expression (see 2.8.2 Concentration response assays and 2.8.4 Bioluminescent imaging), HUVECs and TERT2 HUVECs were washed once with PBS after experimentation, and then incubated with purified LgBiT protein (N3030, Promega USA) diluted 1:400 in 0.1% BSA HBSS for 20min (37°C). Furimazine was then added (1:400 in 0.1% BSA HBSS) (5min, RT). For 96 well plates, an adhesive plate back seal was adhered to the bottom of the plate to minimise any loss of signal, and the plate was read on the FS PHERAstar plate reader (BMG LabTech), using filters measuring luminescent emissions at 450nm (30nm bandpass). For bioluminescent imaging, a plate back was not used and the plate was imaged using an LV200 widefield microscope (see 2.2.3 Bioluminescent microscopy).

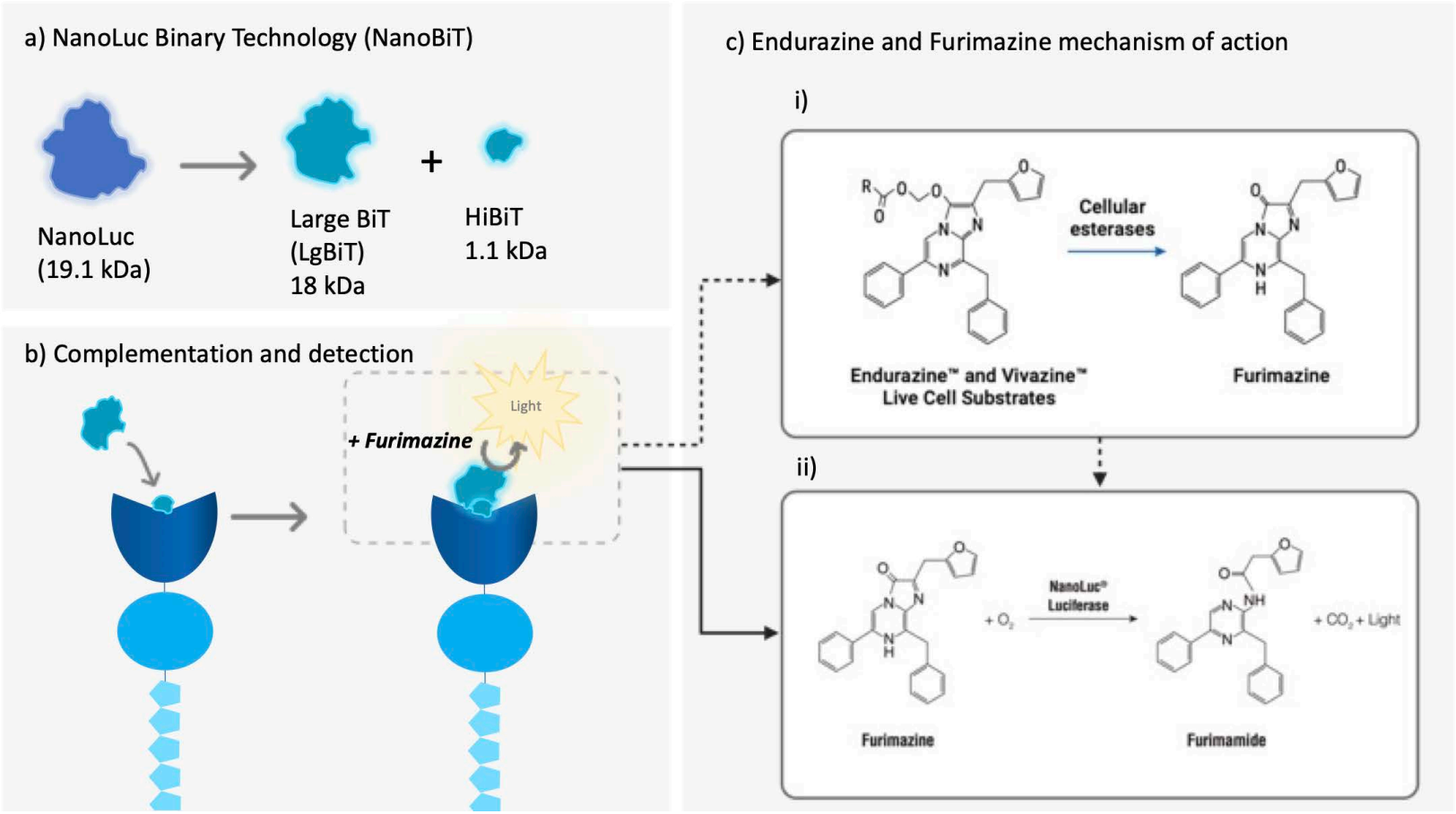

Figure 2.10 NanoBiT technology was utilised to detect E-selectin surface expression. a) *NanoLuc was split into the high affinity HiBiT (1.1kDa) fragment and the larger (18 kDa) LgBiT fragment. b) The HiBiT tag appended to N-terminal E-selectin re-complements with LgBiT. In the presence of furimazine, luminescence is produced which can be quantified on an PHERAstar plate reader. c)i) For kinetics experiments, Endurazine was used as a substrate. Endurazine releases furimazine in the presence of cellular esterases, therefore a prolonged and constant supply of Furimazine is available for living cells. This image was sourced from Promega.com* (Promega Corporation., 2018)(27). *c)ii) Oxidation of Furimazine by NanoLuc produces luminescence. In the presence of NanoLuciferase (NanoLuc) Furimazine is converted to Furimamide with by-products of CO_2 and light, which is detected using a PHERAstar plate reader. This image was sourced from Promega.com* (Promega Corporation, 2018a)

2.8.2 Concentration response assays

Concentration responses for TNF alpha, lipopolysaccharide (LPS) (Isolated from *E.coli* O55:B5, L2880 Sigma Aldrich UK), interleukin-1 alpha (IL-1 alpha, I2778, Sigma Aldrich UK) and interleukin-1 beta (IL-1 beta, SRP3083 Sigma Aldrich UK) were conducted in genome edited HUVECs and TERT2 HUVECs (see 2.6.4 Electroporation of RNP complex and repair template into wildtype/TERT2 HUVECs , 2.6.5 Generation of HiBiT E-selectin mixed population cell line and 2.6.6 Generation of HiBiT E-selectin clonal cell line). LPS, IL-1 alpha and IL-1 beta were all received as lyophilised powders and reconstituted in either ddH_2O (LPS and IL-1 beta) or 0.1% BSA PBS (IL-1 alpha) to 1mM stock concentrations and kept at -20°C.

All genome edited HUVECs/TERT2 HUVECs were seeded onto 0.1% gelatin coated white-sided 96 well plates as described previously (see 2.1.4.2 Cell seeding). For edited WT HUVECs, cells were seeded at 20,000 cells per well due to the limited supply of cells in each electroporation. For genome edited TERT2 HUVECs (mixed population and clonal cell lines), cells were seeded at 30,000 cells per well. All experimentation occurred when cells reached 80% confluency in each well. On the day of experimentation, TNF alpha (concentration range (nM): 0.05, 0.50, 1.0), LPS (concentration range (nM): 5.0, 30, 50), IL-1 alpha and IL-1 beta (concentration range (nM): 50, 200, 500) were diluted to their appropriate concentrations in Medium 200 supplemented with 2.2% LVES. The TNF alpha concentration range was based on previous E-selectin stimulation studies using ranges 1 – 20 ng/ml (0.006 – 1.2 nM) TNF alpha, which exhibited a significant and detectable increase in E-selectin expression (Wong and Dorovini-Zis, 1996; Read *et al.*, 1997; Rahman *et al.*, 1998; Stocker *et al.*, 2000). Genome edited WT HUVECs, TERT2 HUVECs (mx) and clonal TERT2 HUVECs were incubated with the appropriate concentrations of TNF alpha, LPS, IL-1 alpha and IL-1 beta for 6 hours (37°C, 5% CO_2). NanoBiT complementation was then conducted by addition of LgBiT (1:400) (20 min, 37°C) and furimazine substrate (1:400), and the plates were read with an opaque plate back added and using an FS PHERAstar plate reader as described previously (see 2.8.1 NanoBiT).

2.8.3 Kinetics screen

A kinetic screen of HiBiT E-selectin expression across the course of 15 hours was conducted using Endurazine™ substrate (N2570, Promega USA) and Opti-MEM™ (31985062,

ThermoFisher Scientific UK) in response to cytokines TNF alpha, LPS, IL-1 alpha, IL-1 beta, Histamine and $VEGF_{165}a$.

Endurazine is a protected form of furimazine in which there is an addition of an R group (see Figure 2.11ci) which 'cages' the furimazine from being oxidised by NanoLuc. This R group is cleaved only in the presence of cellular esterases, producing a steady release of bioavailable Furimazine in live cells (Dale *et al.*, 2019). NanoBiT luciferase then oxidises Furimazine and luminescence is produced as described previously (Figure 2.10cii).

For kinetic screening, clonal HiBiT E-selectin TERT2 HUVECs were used (see 2.6.6 Generation of HiBiT E-selectin clonal cell line). Cells were seeded onto 0.1% gelatin coated white-sided 96 well plate (see 2.1.5.2 Cell seeding) at 30,000 cells/well in the evening and experimented on the following evening. On the day of experimentation, all appropriate wells were replaced with Opti-MEM, supplemented with Endurazine (1:100), and LgBiT (1:400). Wells were included where there was no addition of LgBiT (LgBiT control wells) to test for LgBiT depletion. 50µl PBS was then added to all other wells to aid with humidity control across the plate. TNF alpha (1nM), Histamine (100nM), $VEGF_{165}a$ (100nM), LPS (50nM), IL-1 alpha (500nM) and IL-1 beta (500nM) were then added into the appropriate wells in triplicate. An Empore™ Sealing Tape (66881-U, Sigma Aldrich) was adhered to the top of the plate to prevent evaporation of buffer from the wells throughout the 15hr kinetic screen, and a plate back was adhered to the bottom of the plate. The plate was then immediately put into the FS PHERAstar plate reader, set at 37°C to read luminescence at 450nm (30nm bandpass, gain 3600) every 10 minutes for 15 hours. The next day, LgBiT (1:400) was added to the LgBiT control wells, and luminescence output was compared to vehicle wells (where there was no cytokine addition, 1:100 Endurazine and 1:400 LgBiT, (incubated for 15 hr 37°C)) by addition of 10^{-9} nM purified HiBiT protein (N3010, Promega USA) (5min, 37°C). All data was exported onto an Excel spreadsheet and analysed using Prism 9 software.

2.8.4 Bioluminescent imaging

Bioluminescent images of NanoLuc-selectin constructs in HEK293Ts, and HiBiT E-selectin in HUVECs and TERT2 HUVECs were acquired using a bioluminescent LV200 widefield microscope (2.2.3 Bioluminescent microscopy). All cell types were plated onto a Cellvis 4-chamber 35mm dish (NC0832919, Fisher Scientific, UK), at 100,000 cells per quadrant overnight (37°C, 5% CO_2). For NanoLuc selectin constructs, the NanoLuc selectin fusions

were constitutively expressed, and no stimulation was required. When cells reached 80% confluency, luminescence was imaged after the addition of Furimazine (1:400 well concentration). In contrast, HiBiT E-selectin endogenous expression was induced by 1nM TNF alpha (6hr, 37°C 5% CO_2) in the applicable endothelial cell line. NanoBiT complementation was then induced after addition of LgBiT and Furimazine was added as described previously (2.8.1 NanoBiT).

2.9 E-selectin interactions with endothelial cell receptors

To investigate the interactions of E-selectin with the other selectin family members (L-selectin and P-selectin), as well as other vascular disease relevant endothelial cell receptors (VEGFR2 and NRP-1), Bioluminescence Resonance Energy Transfer (BRET) was used. BRET occurs between a bioluminescent donor (in this case we used NanoLuc; therefore NanoBRET was utilised) and a fluorescent acceptor, when their proximity is ≤ 10 nm apart (Woo, Hong and Dinesh-Kumar, 2017) (Figure 2.11c/d). Within this proximity, resonance energy from the bioluminescent donor is transferred to a fluorescent acceptor, causing the fluorophore to excite. Therefore, binding can be studied between NanoLuc and fluorophore tagged proteins using this technique, as the numeric ratio of excited fluorescence intensity : luminescence (the BRET ratio) increases, this is indicative of increased binding between tagged proteins. The dynamics of the BRET ratio can be used to spot non-specific BRET interactions, as non-specific BRET will increase linearly with increasing acceptor concentrations, however specific binding induces a progressive increase in the BRET signal in a hyperbolic manner, until there is complete saturation of all donors with acceptor molecules (Borroto-Escuela, Dasiel O. MarcFlajolet Agnati, Greengard and Fuxe, 2013).

Here, a fixed amount of donor cDNA (NanoLuc-fusion proteins) was co-transfected with increasing concentrations of acceptor cDNA (SNAP-tag-fusion proteins), in order to study specific binding between E-selectin and selectin family members, as well as VEGFR2 and NRP-1.

2.9.1 NanoBRET between E-selectin and selectin family

The formation of heterodimers and homodimers with E-selectin and selectin family members was studied using NanoBRET. A fixed concentration of NanoLuc E-selectin (10ng), as well as increasing concentrations of SNAP-tag selectin constructs (0 – 100ng) were co-transfected in HEK293Ts, using FuGENE® HD reagent (E2311, Promega USA), and Opti-MEM. A positive

and negative control was included alongside each experiment on the same plate, whereby the known homodimer formation of Neuropilin-1 (NRP-1) was used as a positive control, and the absence of interaction between E-selectin and the G protein-coupled receptor (GPCR) Adenosine-A_3 (A3) receptor was used as a negative control. A total concentration of 100 ng DNA was transfected in each scenario, and this was achieved by the addition of pcDNA3.1 (Zeo) plasmids (an empty vector containing no receptor sequence) alongside the lower concentrations of acceptor and donor DNA. After transfection, SNAP-tag selectin constructs were fluorescently labelled using a SNAP-Surface® 488 (S9124S, New England Biolabs UK) ligand. SNAP-tag is 20kDa mutant of a DNA repair protein; O^6-alkylguanine-DNA alkyltransferase which has the ability to rapidly react with fluorescent benzylguanine (BG) derivatives leading to irreversible covalent binding of the SNAP-tag with the synthetic probe (Cole, 2013) (Figure 2.11b).

HEK293Ts were plated onto Poly-D-lysine coated white-sided Greiner 96 well plates (see 2.1.6.2 Cell seeding), at 20,000 cells/well. The next day, when confluency reached 60%, HEK293Ts were co-transfected with NanoLuc and SNAP-tag cDNA fusions. The different concentrations of DNA were diluted into microcentrifuge tubes using Opti-MEM before addition to wells. First, 10 ng NanoLuc E-selectin plasmid was added to all wells, before addition of 0 ng, 5 ng, 10 ng, 20 ng, 40 ng, 60 ng, 80 ng or 100 ng SNAP-tag E-selectin/SNAP-tag L-selectin/ SNAP-tag P-selectin plasmid DNA. To achieve a constant DNA concentration of 100 ng within each tube, pcDNA3.1 (Zeo) was added at concentrations 100 ng (where there was no addition of SNAP-tag selectin DNA), 95 ng, 90 ng, 80 ng, 60 ng, 40 ng, 20 ng and 0 ng. FuGENE was then added to achieve a FuGENE:DNA ratio of 3:1 (see 2.5.1 Transient transfections), and the DNA mixture was mixed 15 times using pipette action, and left for 10 minutes (RT) to allow encapsulation of DNA by FuGENE. The same concentrations were made up in parallel with the negative control; donor NanoLuc E-selectin and acceptor SNAP-tag A3, and the positive control; donor NanoLuc NRP-1 and acceptor SNAP-tag NRP-1. Then, 5µl of each DNA mix was added to each well in triplicate in the 96 well plate and left for at least 16 hr to allow transfection of plasmids (37°C, 5% CO_2). The next day, the SNAP-tag-fusion receptors were labelled with SNAP-Surface® 488 (S9124S, New England Biolabs UK). SNAP-surface 488 was diluted to 0.5 µM in 0.1% BSA DMEM, and wells were incubated with 100µl per well for 30 min (37°C 5% CO_2). Wells were then washed 3 times with 100µl/well 0.1% BSA HBSS, and fluorescence intensity (to monitor the expression of SNAP-tagged proteins) was measured using PHERAstar FS plate reader following excitation at 485 nm and emission monitored at 520 nm. Wells were then incubated with Furimazine substrate (1:400

final concentration in well) for 5 min (RT), and the luminescence signals at 475 nm and 535nm (535 nm, 30 nm bandpass) were measured using the PHERAstar FS plate reader, for 3 cycles. The data was then exported onto an excel file, and the BRET ratio was calculated by dividing the luminescence at 535nm by the luminescence at 475nm in each well from the second cycle of data.

2.9.2 NanoBRET between E-selectin and VEGFR2/NRP-1

NanoBRET interactions were studied between NanoLuc E-selectin and Halo-tag VEGFR2 / SNAP-tag NRP-1 (see 2.9.1 NanoBRET between E-selectin and selectin family). HaloTag ® (Promega, USA) is a 33 kDa sequence that irreversibly forms covalent bonds with chloroalkane moieties. Here, VEGFR2 N-terminally tagged with HaloTag were labelled using a cell impermeable Alexa Fluor 488 HaloTag ligand (0.5 µM, 30 min, 37°C 5% CO_2; G1002; Promega Corporation, USA) to measure cell surface expression and interactions with NanoLuc E-selectin via NanoBRET. A constant amount of NanoLuc E-selectin (10ng) was co-transfected with 0 – 100ng of either Halo-tag VEGFR2 or SNAP-tag NRP-1, utilising pcDNA3.1 (zeo) vector as an empty vector to achieve 100ng per tube, as described previously (see 2.9.1 NanoBRET between E-selectin and selectin family).

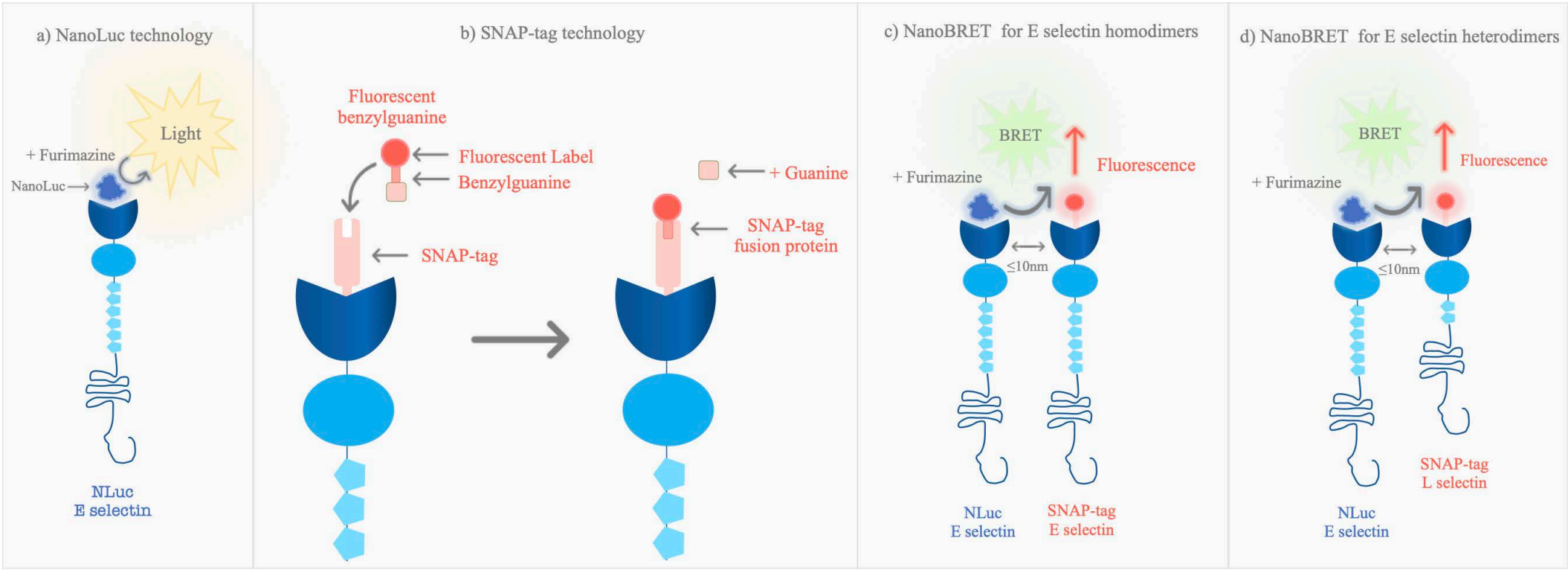

Figure 2.11 The use of NanoLuc and SNAP-tag technologies to study selectin interactions. a) Furimazine oxidises NanoLuciferase producing energy in the form of photons. b) The addition of a fluorescent benzyl guanine leads to covalent binding of the the probe with SNAP-tag-selectin complexes. c) Investigation of E selectin homodimers using NanoBRET d) Investigation of E selectin heterodimers using NanoBRET. If NanoLuc E selectin and fluorescently labelled SNAP-tag-selectin are ≤10nm apart, resonance energy is transferred between NanoLuc and the fluorophore, causing excitation of the fluorophore. The subsequent emissions of both luminescence and fluorescence can be detected as a ratio; so named the BRET ratio. The BRET ratio is indicative of formation of either homodimers or heterodimers of E selectin with the selectin family.

2.10 Fluorescent E-selectin binding peptide NanoBRET assays

E-selectin binding peptide (Esbp; primary sequence DITWDQLWDLMK) was designed and ordered from ThermoFisher Scientific (UK) appended with 2 different Alexa Fluor fluorophore tags (Figure 2.12). This peptide was discovered amongst a range of lectin binding clones, via screening phage display peptide libraries against receptors (Martens *et al.*, 1995; Yu *et al.*, 2009). It was stipulated that Esbp bound specifically to E-selectin and not P-selectin or L-selectin, inhibited HL-60 cell adhesion to immobilised E-selectin and reduced neutrophil rolling on LPS-stimulated HUVECs (Martens *et al.*, 1995; Shamay *et al.*, 2009b). Two different fluorophores with and without a linker were ordered; an AlexaFluor633-Esbp and an AlexaFluor488-Esbp with a GGGG linker. In theory, the fluorescent conjugation would enable quantification of peptide binding to NanoLuc-tagged E-selectin via NanoBRET (see 2.9.1 NanoBRET between E-selectin and selectin family for more information on NanoBRET). Like with receptor dimerization experiments (see 2.9.1 and 2.9.2), saturable binding would be observed with an increased concentration of fluorescent-peptide addition if there was specific binding, which would be displaced by a high concentration of unlabelled peptide. Saturation experiments were therefore conducted with these fluorescent peptides with an increasing concentration of fluorescent peptide concentration, alone and in the presence of 10µM unlabelled Esbp to investigate the binding properties of AF633/AF488-Esbp. NanoLuc E-selectin stable cell line (see 2.5.2 NanoLuc E-selectin stable cell line generation) and NanoLuc E-selectin membranes (see 2.5.3 NanoLuc E-selectin membrane preparations) were used for these NanoBRET experiments. The peptide was further investigated for binding to NanoLuc L-selectin and NanoLuc P-selectin using the stable cell lines generated. Peptides arrived as a lyophilised powder (unlabelled: clear, labelled: blue), and were reconstituted in 50% dimethyl sulfoxide (DMSO)/ddH_2O to achieve a concentration of 1 mM.

Unlabelled ***Esbp***	[NH2]**DITWDQLWDLMK**[COOH]
Alexa Fluor 633 - ***Esbp***	[NH2]C**AF633DITWDQLWDLMK**[COOH]
Alexa Fluor 488 - ***Esbp***	[NH2]**AF488CGGGGDITWDQLWDLMK**[COOH]

Figure 2.12 Esbp sequences ordered from ThermoFisher Scientific (UK). Two tags were experimented with (Alexa Fluor 633 and Alexa Fluor 488) for NanoBRET interactions with NanoLuc E-selectin. Where D: Aspartic acid (asp), I: Isoleucine (Ile), T: Threonine (The), W: Tryptophan (Trp), Q: Glutamine (Gln), L: Leucine (Leu), M: Methionine (Met), K: Lysine (Lys), C: Cysteine (Cys).

2.10.1 Saturation assays in NanoLuc E-selectin stable cell line

The NanoLuc E-selectin stable cell line (see 2.5.2 NanoLuc E-selectin stable cell line generation) was plated onto a PD coated white-sided greiner 96-well plate at 30,000 cells/well and incubated for 24 hr (37°C 5% CO_2). The next day, media was replaced with warm 0.1% BSA/HBSS (see 2.4.1 Preparation of Broths and Buffers). Concentrations for 15.6 nM 31.3 nM 62.5 nM 125 nM 250nM 500nM 1000 nM, 2000 nM well addition of AF633 / AF488 conjugated Esbp were diluted in 0.1% BSA/ HBSS in 0.5 ml microcentrifuge tubes, as well as 10µM unlabelled Esbp. Fluorescent-peptide concentrations were then added in triplicate in the presence / absence of 10µM Esbp, and the plate was wrapped in foil and incubated for 1 hr (37°C). Furimazine was then added (1:400 final well dilution) (5 min, RT), before the plate was read for dual luminescence a fluorescence (appropriate for AF633 and AF488) using the PHERAstar FS plate reader. The BRET ratio was calculated by dividing fluorescence intensity by luminescence, and all data was analysed in Prism 9 software.

2.10.2 Saturation assays with altering BSA concentrations

As no binding was seen with AF633 Esbp, a higher BSA concentration was used to test whether this higher concentration was required to keep fluorescent Esbp in solution. NanoLuc E-selectin stable cell line was plated onto 96 well plate was described previously (see 2.10.1 Saturation assays in NanoLuc E-selectin stable cell line). The next day, preparations of BSA/ HBSS (0%, 0.1% and 1%) were warmed to 37°C before experimentation. These solutions were then used to dilute 5 nM, 50 nM 500 nM 1000 nM AF633 Esbp, and addition in the absence / presence of unlabelled Esbp

(10µM) was conducted as described previously (2.10.1 Saturation assays in NanoLuc E-selectin stable cell line). The plate was read after addition of Furimazine (1:400, 5 min RT) using the PHERAstar FS plate reader.

2.10.3 Saturation assays with NanoLuc P-selectin and L-selectin stable cell lines

Saturation assays were also conducted in NanoLuc P-selectin and NanoLuc L-selectin stable cells lines created previously (see 2.5.2 NanoLuc E-selectin stable cell line generation). This was to test whether Esbp bound to other selectin family members. NanoLuc P-selectin, NanoLuc L-selectin and NanoLuc E-selectin stable cell lines were plated onto the same PD coated white sided 96 well plate as described previously (see 2.1.6.2 Cell seeding) at seeding density 30,000 cells/well. The next day, wells were treated with AF633 Esbp at the same range and in the same conditions as described previously (see 2.10.1 Saturation assays in NanoLuc E-selectin stable cell line), before the plate was read using a PHERAstar plate reader, after addition of Furimazine substrate (1:400, 5min RT).

2.10.4 Saturation assays conducted in membranes

Saturation assays utilising AF488-Esbp were conducted in NanoLuc E-selectin membranes (see 2.5.2 NanoLuc E-selectin stable cell line generation). Protein concentration of the membranes was deduced using a Pierce™ bicinchoninic acid (BCA) protein assay kit (23227, ThermoFisher Scientific UK), and absorbance was measured using a Dynex MRX plate reader. Membrane preparations were stored at -20°C.

The effect of membrane concentration, and saponin concentration on NanoBRET between NanoLuc E-selectin and AF488-Esbp was investigated. Saponin prevents vesicle formation of membranes. It does this by interacting with membrane cholesterol and forming holes in the membrane (Jacob, Favre and Bensa, 1991). 0.1% BSA/HBSS and 0.1% BSA, 0.25% Saponin/HBSS were prepared and incubated at 37°C before experimentation. 1 µg, 2 µg, 5 µg and 10 µg NanoLuc E-selectin membranes diluted in either buffer, were added to a white sided 96 well plate and incubated for 20 min (37°C). 200nM of AF488-Esbp was then added to appropriate wells in each different membrane concentration, with and without saponin and compared to vehicle. Wells were then incubated with Furimazine (1:400, 5 min RT) and the plate was read using a PHERAstar plate reader.

Saturation assays were performed using 2µg addition of membranes in a white-sided 96 well plate, with and without 0.25% saponin in 0.1% BSA HBSS buffer. Vehicle, 3.1 nM, 6.3 nM, 12.5 nM, 25 nM, 50 nM, 100 nM and 200 nM were diluted in either buffer, before each concentration was added in triplicate in the absence / presence of 10µM unlabelled Esbp. The plate was then incubated with Furimazine (1:400), and was read using a PHERAstar plate reader.

2.11 Un-labelled E-selectin binding peptide internalisation assays

Due to no saturable binding being observed with fluorescently labelled Esbp, the hypothesis that the fluorophore was affecting E-selectin binding was explored. To do this, the effect of addition of unlabelled Esbp was investigated in transiently transfected SNAP-tag E-selectin HEKGs, as well as in CRISP-Cas9 edited HiBiT E-selectin clonal TERT2 HUVEC cell lines.

2.11.1 SNAP-tag E-selectin internalisation assay

First, HEKGs were plated onto a PD coated black-sided 96 well plate at 20,000 cells/well (see 2.1.6.2 Cell seeding). The next day, HEKGs were transiently transfected with 100 ng SNAP-tag E-selectin as described previously using FuGENE HD reagent for 24 hours (37°C 5% CO_2) (see 2.5.1 Transient transfections). The next day, SNAP-tag E-selectin was labelled using SNAP-surface 488 diluted to 0.5 µM in 0.1% BSA/DMEM and incubated for 30 min (37°C 5% CO_2). Wells were then washed three times with 0.1% BSA/HBSS. 100nM Esbp diluted in 0.1% BSA/HBSS was added to wells in a reverse time course manner to achieve 60 min, 30 min, 15 min and 5 min incubation. At time point 0, all wells were fixed using 3% PFA/PBS (20 min, RT). Wells were then washed with PBS 3 times, before nuclei were labelled using H33342 (1:1000 in PBS) for 20 min (RT). Wells were washed with PBS a further 3 times before the plate was read using an IX micro widefield plate reader (see Widefield microscopy).

2.11.2 HiBiT E-selectin internalisation assay

To investigate Esbp induced internalisation of HiBiT E-selectin, a reverse time course was performed where Esbp was incubated with HiBiT E-selectin clonal TERT2 HUVECs for 60 min, 30 min and 5 min and the change in luminescence due to surface HiBiT E-selectin expression was assessed.

The clonal HiBiT E-selectin TERT2 HUVEC cell line was plated onto a white-sided 96 well plate at 30,000 cells/well as described previously (see 2.1.5.2 Cell seeding). The next day, wells were replaced with 0.1% BSA/HBSS, and incubated with 100nM Esbp diluted in 0.1% BSA/HBSS for 60 min, 30 min and 5 min, and compared to vehicle. After the final time point, wells were incubated with Furimazine (1:400 dilution), and the plate was read for luminescence using a PHERAstar plate reader.

2.12 Data analysis

2.12.1 Software

All images acquired from IX micro widefield microscope were collected using MetaXpress 2.0 software (Molecular Devices, USA), and images acquired from 880F confocal microscope were collected using Zen 2010 software (Zeiss, Germany). These images were edited either using Zen (black edition) software (Zeiss, Germany) or ImageJ Fiji software (National Institutes of Health). To view, edit and design plasmids, as well as designing primers, SnapGene Viewer 2.8.1 (GSL Biotech, USA) was used. To align sequences, Nucleotide BLAST® was used online (blast.ncbi.nlm.nih.gov/Blast) (NCBI, NIH, Bethesda, USA). For design of CRISPR-Cas9 guide RNA and targeting PAM sequence, an online program was use (using PAM for 20bp-NGG- Sp Cas9, SpCas9-HF1, eSpCas9 1.1) (Tefor infrastructure, 5.0, USA) via the website crispor.tefor.net.

To quantify E-selectin internalisation in HEK293Ts, image analysis algorithms for multiwavelength cell scoring on MetaXpress software (Molecular Devices, USA) were used which detected and counted nuclei (with a mask 5 – 20 µm in diameter and a threshold above background of 100 grey levels) and intracellular regions of high intensity FITC fluorescence as ‘granules’ were detected on a per cell basis (2 – 20µm in diameter, intensity above background: 50 grey levels, assigned to nuclei per field).

2.12.2 Statistics

All quantified data is expressed as a mean ± standard error from the mean (SEM) and presented and analysed using GraphPad Prism software version 9.4.1. (GraphPad Software, LLC). A statistical difference was defined if calculated p value <0.05, and details for the statistical tests

taken and resultant *p* values were reported in figures, tables or in the appropriate results section. For parametric data, independent sample t-tests or a one-way or two-way ANOVA was used with Tukey post-hoc tests for multiple comparisons.

Chapter 3 Investigating cytokine-induced upregulation of E-selectin expression in endothelial cells

3.1 Introduction

For the past 30 years, E-selectin expression on ECs in response to inflammatory stimuli has been increasingly understood due to the development and improvement of E-selectin detection assays (summarised in Table 3.1). Bevilacqua *et al.,* (1987) discovered E-selectin and designated it endothelial leukocyte adhesion molecule 1 (ELAM-1); they were the first to develop the anti-E-selectin monoclonal antibodies H18/7 and H4/18 (Table 3.1). These antibodies were able to inhibit selectin mediated neutrophil adhesion in human leukemia-60 (HL-60) cells and inhibit polymorphonuclear (PMN) leukocyte adhesion (Bevialacqua *et al.,* 1989). Since then, several antibodies have been made against activated EC membrane proteins and this represents an effective way to detect selectin expression in response to inflammatory stimuli. With these antibodies, a comparison of the location of selectins within the cell, stimulants for selectin synthesis and expression, and the dynamics of selectin expression can be evaluated between the selectin family members and other cell adhesion molecules in an inflammatory environment.

As summarised in Table 3.1, the majority of previous studies have used anti-E-selectin antibodies developed to assess expression of E-selectin in a range of endothelial cells. These uses have included Immunoprecipitation to isolate and concentrate E-selectin that had been expressed in response to TNF alpha / IL-1 beta in HUVECs. Antibody labelling for E-selectin and probing with a Sepharose-4b coupled secondary antibody, enabled immobilisation of antibody-E-selectin complexes, which were detected on an SDS page revealing 115 kDa and 97 kDa E-selectin variants. E-selectin antibodies were also used for detection of protein upregulation via enzyme-linked immunosorbent assays (ELISA), utilising peroxidase / alkaline phosphatase conjugated secondary antibodies and an appropriate substrate to measure colorimetric response indicative of E-selectin expression. In addition, antibody auroprobe (gold particles) have been used with anti-E-selectin antibodies to aid imaging experiments, and fluorescein isothiocyanate (FITC) / Phycoerythrin (PE) conjugated antibodies used for flow cytometry analysis. In many cases, E-selectin mRNA was measured using northern blot analysis and appropriately labelled E-selectin probes for E-selectin hybridisation. When these probes were labelled with radioactive phosphorus [^{32}P] this was termed an RNase protection assay (RPA). Northern blot analysis allows the study of RNA expression within a sample by separating RNA samples by size and using a hybridisation

probe complementary to part or the entire sequence. For example, a 1.35 kb human E-selectin [^{32}P] labelled fragment and a [^{32}P] labelled full length E-selectin cDNA probe was used to analyse the mRNA expression. All of these antibody-dependent methods were successful in observing the presence of E-selectin, however it is important to note that all were indirect measures of E-selectin expression, and there was lack of spatial resolution of E-selectin localisation and temporal dynamics of expression.

Through these investigations (detailed in Table 3.1), E-selectin expression is known to be mediated by inflammatory cytokines that are produced and released from activated leukocytes (TNF α, IL-1 α, IL-1 β and histamine) as well as endotoxins such as lipopolysaccharide; derived from the outer membrane of gram-negative bacteria. E-selectin expression can also be induced by growth factors. Vascular endothelial growth factor (VEGF) has been shown to induce E-selectin expression before (Kim *et al.*, 2001, 2003). In these instances, 20 ng/ml VEGF induced E-selectin mRNA expression at low levels in a time dependent manner that peaked at 6 hr in HUVECs. This group further investigated the mechanism of upregulation via the nuclear factor-kappa beta (NF-kB) pathway, as they found that E-selectin mRNA expression was decreased by inhibitors for phospholipase C, NG-kB and protein kinase C. Further studies found that VEGF dose dependently upregulated E-selectin (0 – 20 ng/ml) and was inhibited by adrenomedullin which affected the leukocyte adhesiveness due to reduced E-selectin expression (Kim et al., 2003).

Table 3.1 ***Methodology for detecting E-selectin expression in endothelial cells.*** *Where RPA=RNase protection assay, ELISA = enzyme linked immunoassay, ELAM-1 = endothelial leukocyte adhesion molecule, TNF = tumour necrosis factor, LPS = lipopolysaccharide, IL-1 = interleukin-1, mAb = monoclonal antibody, VEGF = vascular endothelial growth factor, NF-kB = nuclear factor kappa-light-chain-enhancer of activated B cells, PI = Phosphoinositide, HUVECs = human umbilical chord endothelial cells, COS = fibroblast-like cell line derived from monkey kidney tissue, HBMECs = human brain microvascular endothelial cells, HPAECs = human pulmonary artery endothelial cells, PAECs = porcine aortic endothelial cells, MVECs = microvascular endothelial cells.*

Main findings	Method for evaluating E-selectin expression								Cell type	Antibody used	Inducers of E-selectin expression found	Reference
	Immuno-precipitation	Leukocyte adhesion assay	Northern blot analysis	Western blot analysis	RPA	Immuno-cytochemistry	ELISA	Flow cytometry				
Discovery of ELAM-1 (E-selectin)	✓	✓							HUVECs	H18/7 and H4/18 monoclonal antibody	TNF alpha and IL-1 beta	Bevilacqua et al., 1987
Transfection of isolated E-selectin into COS cells enabled the analysis of expression, and sequencing of E-selectin	✓	✓	✓						COS cells and HUVECs	H18/7 and H4/18 monoclonal antibody	TNF alpha and IL-1 beta	Bevialacqua et al., 1989
Histamine enhanced the TNF alpha induced E-selectin expression							✓		Vascular endothelial cells	KM973 anti-E-selectin antibody	Histamine and TNF alpha	Miki et al., 1996
LPS, TNF alpha and IL-1 beta mediate E-selectin expression						✓	✓		HBMECs	Mouse anti-E-selectin antibody 3B7	LPS, TNF alpha and IL-1 beta	Wong and Dorovini-Zis, 1996
TNF alpha activates NF-kB and JNK/p38 to induce E-selectin transcription	✓			✓					HUVECs	N/A	TNF alpha	Read et al., 1997
E-selectin expression is due to TNF alpha activation of NF-kB pathway and ROS production			✓			✓		✓	HPAECs	N/A	TNF alpha	Rahman et al., 1998
E-selectin was induced by LPS over 5 hr. mAb against E-selectin induced a rise in Ca2+ levels and rearrangment of cytoskeleton		✓					✓		HUVECs	Anti–E-selectin mAb CBL180 (Cymbus Bioscience Ltd)	LPS	Lorenzon et al., 1998
E-selectin is differentially regulated compared to P-selectin by TNF alpha and IL-4.		✓	✓					✓	PAECs	Anti-E-selectin Ab 1.2B6	TNF alpha	Stocker et al., 1999
IL-1 alpha induced E-selectin expression in >700 x more sites /µm2.								✓	Human Lung MVECs	IgG1 mAb anti- E-selectin, PE conju-gated	IL-1 alpha	Levin et al., 2001
VEGF165a can stimulate E-selectin expression via NF-kB activation, with PI 3'-kinase-mediated suppression		✓			✓				HUVECs	N/A	VEGF165a	Kim et al., 2001
Adrenomedullin inhibited VEGF165a induced E-selectin expression		✓			✓				HUVECs	N/A	VEGF165a	Kim et al., 2003

The cytokines bind to their receptors presented on endothelial cells (TNF alpha with the TNF-receptor (TNFR), IL-1 alpha with the IL receptor-1 (ILR1), histamine with the Histamine-1 receptor (H1R), LPS with the toll-like receptor-4 (TLR4) and VEGF with the VEGF receptor 2 (VEGFR2)), which then cause E-selectin to be transcriptionally upregulated via the nuclear factor kappa beta (NF-κB) pathway (summarised in Figure 3.1). NF-κB represents a family of inducible transcription factors which regulate genes involved in a cell's inflammatory response (Liu *et al.*, 2017). In the case of E-selectin regulation, the transcription factors involved are NF-κB1 (also named p50) and RelA (also named p65). This p50p65 heterodimer is maintained in the cytoplasm by association with IκBα. The inflammatory mediators TNF alpha, IL-1 alpha, LPS, Histamine and $VEGF_{165}$a all bind to their receptors, and upon doing so generate intracellular signals which ultimately phosphorylate IκBα, targeting IκBα for degradation by ubiquitin (McEver, 1997; Read *et al.*, 1997). VEGF has been proposed to induce this degradation *via* a different primary pathway, in which binding to VEGFR2 induces activation of the PLCγ-sphingosine kinase-PKC cascade which in turn activates the p50p65 heterodimer (Kim *et al.*, 2001) (Figure 3.1). TNF alpha has also been proposed to induce ubiquitination of the IκBα-p50p65 heterotrimer via signalling through the mitogen-activated protein (MAP) kinase pathway, through MAP kinase kinase kinase (MKKK 3,4 and 6) (Read *et al.*, 1997) (Figure 3.1). This pathway also induces activation of JNK and p38 MAP kinases, which phosphorylate c-JUN and ATF-2 respectively which are constitutively present within the nucleus (McEver, 1997; Read *et al.*, 1997). Therefore, the translocation of p50p65 heterodimer, and activation of c-JUN and ATF-2, promote the binding of these transcription factors to the E-selectin promoter region, which induces E-selectin transcription. The binding of p50p65 and c-JUN-ATF2 heterodimers at multiple sites on HMGI(Y) protein, bends the DNA to facilitate the formation of a higher order complex which is necessary for transcriptional activation.

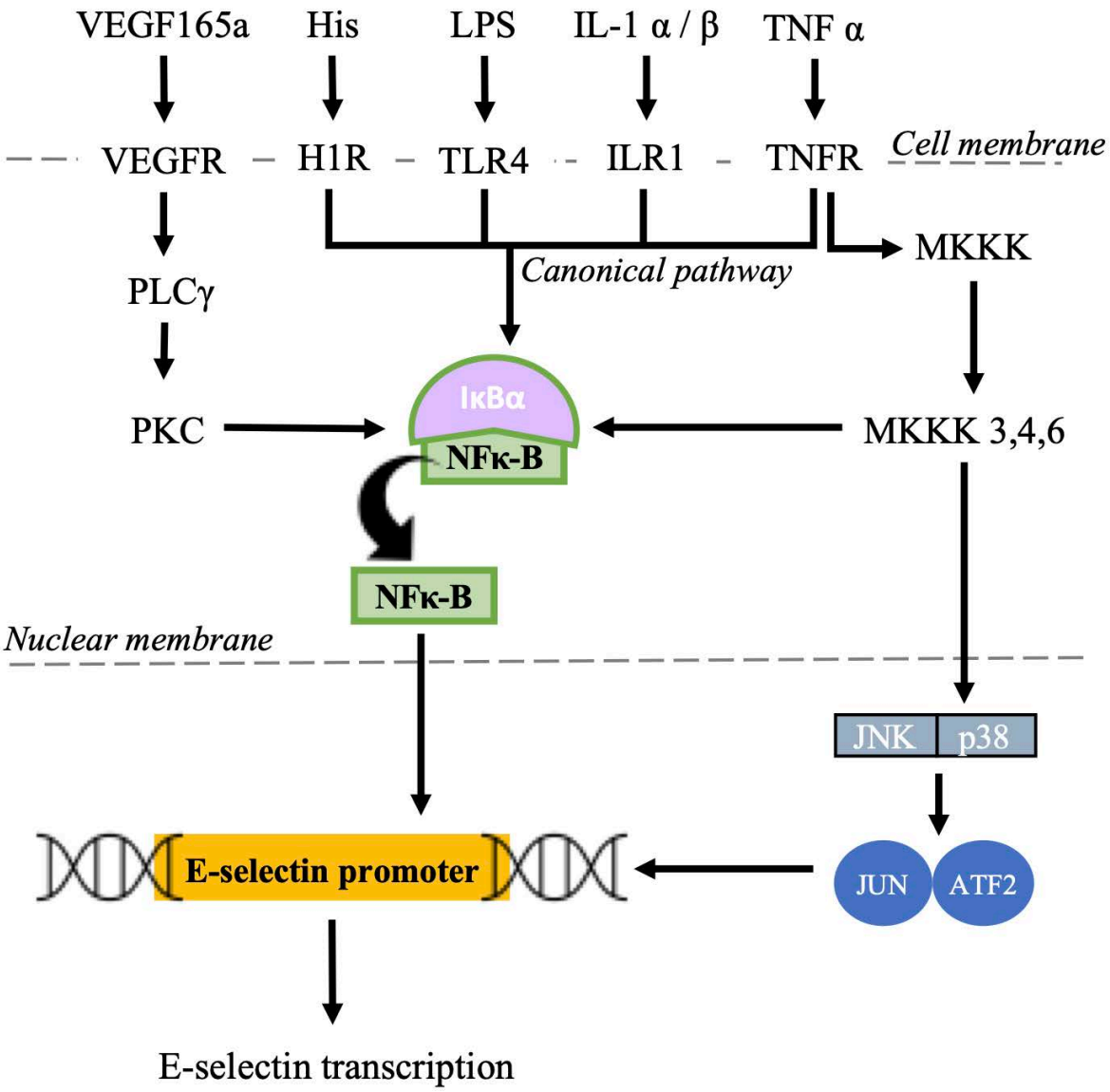

Figure 3.1 ***A simplified view of the proposed transcriptional regulation of E-selectin by VEGF$_{165}$a, Histamine (His), LPS, IL-1 α / β or TNF α according to Read et al., 1997, Wyble et al., 1997, McEver, 1997 and Kim et al., 2001.*** *All stimulants have the potential to activate the nuclear factor kappa beta (NFκ-B) pathway. This pathway entails the ubiquitination of the Inhibitor of Kappa Light Chain Gene Enhancer (IκBα, shown in pink), which releases NFκ-B so that it can translocate to the nucleus and associate with the E-selectin promoter region. Here, E-selectin transcription is activated. VEGF$_{165}$a has been postulated to induce NFκ-B activation through the PLC γ-sphingosine kinase-PKC cascade, whereby PKC activates NFκ-B. TNF alpha, as well as activating NFκ-B in the canonical pathway, also activates MAP kinase kinase kinases (MKKK) and MAP kinase kinase (MKK 3,4 and 6). This leads to activation of JNK and p38 MAP kinases, which phosphorylate c-JUN and ATF2 which activates transcription of E-selectin. The MAP kinase pathway can also activate NF-κB.*

In contrast, P-selectin expression is induced at a faster rate due to its storage system in WPBs, and some cytokines selectively induced P-selectin but not E-selectin expression (for example, interferon gamma (IFN-y), thrombin and Interleukin-4 (IL-4)) (Table 3.2). Interestingly, IL-4 increased TNF alpha induced P-selectin expression but decreased TNF alpha induced E-selectin expression, suggesting that a shift of the relative densities of the two selectins towards P-selectin, is favourable in some inflammatory environments suggesting context dependent changes in expression (Stocker *et al.*, 2000). Despite the differential kinetics and expression, both selectins are induced by inflammatory mediators in a time and concentration dependent manner in endothelial cells (Bevilacqua *et al.*, 1987; Bevialacqua *et al.*, 1989; Lorenzon *et al.*, 1998; Stocker *et al.*, 2000).

Table 3.2 Known stimulants for E-selectin and P-selectin expression in endothelial cells

	E-selectin	P-selectin
TNF alpha	✓	✓
IL-1 alpha	✓	✓
IL-1 beta	✓	✓
LPS	✓	✓
Histamine	✓	✓
IFN-y		✓
VEGF165a	✓	✓
Thrombin		✓
IL-4		✓

There have been reports of basal levels of expression of both E and P selectins observed when using some of the anti-selectin antibodies, irrespective of inflammatory stimulus used. For example, basal levels of expression have been observed with P-selectin but not E-selectin in porcine aortic endothelial cells (Stocker *et al.*, 2000), however this is not a consistent observation as data from human brain microvascular endothelial cells has suggested that a basal level of E-selectin expression could only be seen in a few cells in the field of view using immunocytochemistry (Wong and Dorovini-Zis, 1996).

Understanding the endogenous regulation of E-selectin expression in an inflammatory environment is the first step towards creating a representative model of E-selectin expression. This chapter therefore aims to optimise an *in vitro* model of E-selectin expression to compare and contrast to previous studies detecting expression.

3.2 Results

3.2.1 Antibody labelling optimisation for E-selectin and P-selectin

Optimization experiments were conducted to determine the best environment and coating for culture of HUVECs in ibidi 8-well assay plates. HUVECs did not grow well in the gelatin coated flask, and almost all HUVECs lifted off of the surface of the uncoated glass 8-well plate. Among the top 3 (Collagen IV, Ibidi Treat and Poly-D-lysine) Ibidi treat had the best confluency of HUVECs compared to Poly-L-lysine or Collagen IV (Figure 3.2). Alkaline phosphatase (AP) experiments were optimized after testing different dilutions of the AP secondary antibody in HUVECs stimulated with 1 nM TNF alpha. The appropriate dilution was concluded to be 1:100 diluted in 10% goat serum as this provided the greatest degree of optical density unit increase compared to the vehicle treated cells (Figure 3.3).

There were no non-specific secondary antibody effects with any of the control conditions and HUVECs were easily detected in widefield and confocal images with nuclear staining (Figure 3.4). Non-stimulated wells revealed that there was basal expression of P-selectin in a few cells in the field of view, contrary to E-selectin which was completely reliant on TNF alpha stimulation for expression (Figure 3.4). In widefield images, an increase in the number of cells expressing P-selectin can be qualitatively assessed after TNF alpha stimulation; however, this was not calculated as a significant increase from basal when quantified using multi-wavelength cell scoring and comparing the percentage of cells that were positive for Alexa Fluor 488, indicative of selectin expression (Two-way ANOVA, $p = 0.9734$). In contrast, E-selectin expression was only visible in images following 2 hr TNF alpha stimulation. Only a few cells in the field of view expressed E-selectin at this time point and concentration of TNF alpha, however it was still calculated as a significant increase in expression compared to basal (**$P<0.01$) (Figure 3.4). When comparing P vs E-selectin TNF alpha concentration response, there was no significant difference quantified ($p=0.6709$) but when comparing basal levels (vehicle) P-selectin had significantly higher expression levels (* $P<0.05$).

Figure 3.2 ***Ibidi treat coating produced the best HUVEC adherence and confluency after plating 6000 cells/well for 24 hr (37°C, 5% CO2).*** *Images depict µ-slide 8 well plates with different coatings; Collagen IV, Ibidi treat, Poly-l-lysine and Gelatin, as well as an uncoated glass 8 well plate were used to assess HUVEC adherence post seeding*

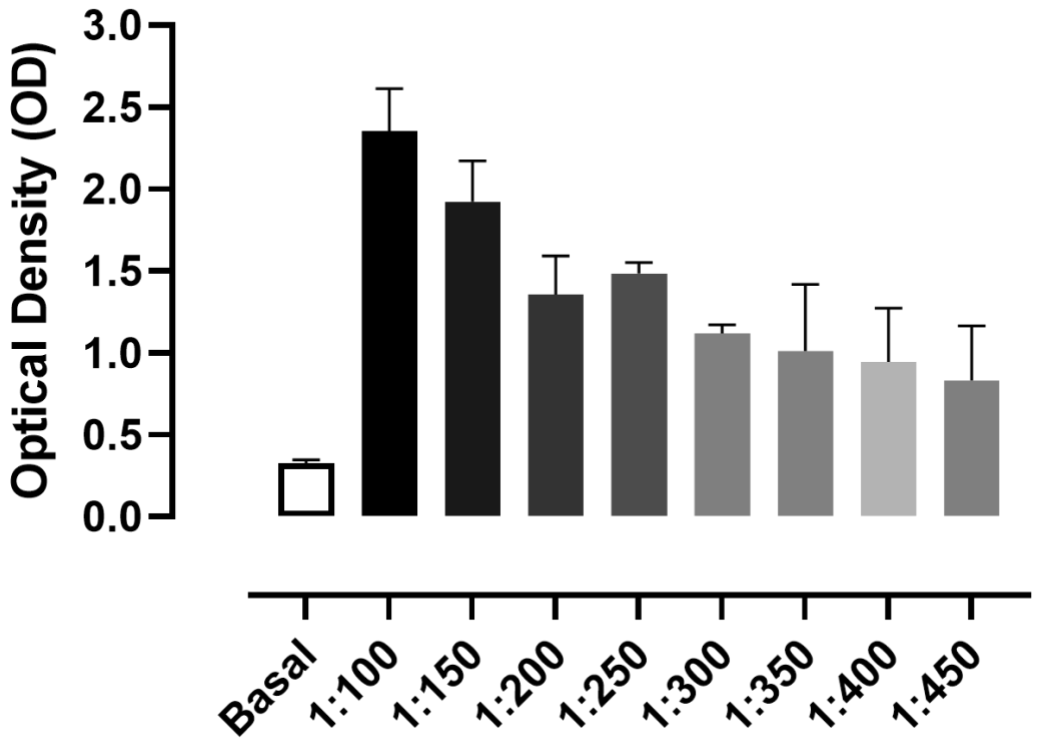

Figure 3.3 ***Alkaline phosphatase secondary antibody dilution assay. The secondary antibody was diluted to seven different dilutions in order to decipher the optimal concentration to use in E-selectin ELISA assays.*** *A trend of increasing Optical Density (OD) units was found with increasing concentrations of Alkaline Phosphatase secondary antibody concentration. (N=2 error bars= SD).*

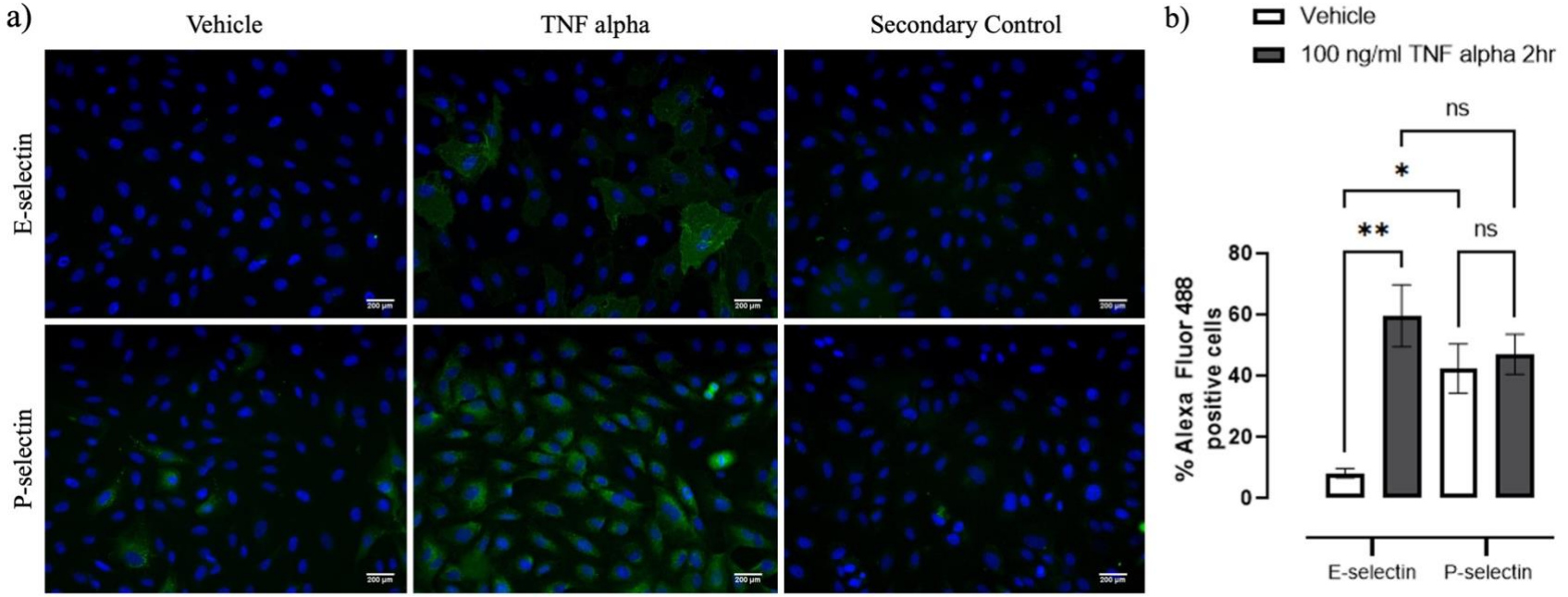

Figure 3.4 ***P-selectin displayed significant basal expression in comparison to E-selectin.*** *a) IX micro widefield images of vehicle, TNF alpha stimulated (2 hr, 100 ng/ml 37°C 5% CO2), and secondary control wells. Scale bar = 200 µm, blue signal is H33342 stained nuclei and green signal is either Alexa Fluor 488 labelled E-selectin or P-selectin. P-selectin expression can be seen in un-stimulated cells (vehicle) indicating that there is basal expression. b) IX micro images were quantified using multiwavelength cell scoring (MWCS); TNF alpha stimulated E-selectin expression was significantly increased compared to basal (two-way ANOVA with post-Hoc Tukeys multiple comparisons test **p < 0.01), in contrast to P-selectin expression which had high basal expression that was not significantly different from TNF treated HUVECs (p = 0.2077). N=3, where error bars = SEM. c) statistical differences (* = p <0.05, ** = p <0.01 and ns = not significant p >0.05)*

3.2.2 TNF alpha concentration and time course assay development

A time course of TNF alpha induced E-selectin expression was then conducted using a higher resolution confocal microscope (LSM 880 confocal microscope). These experiments revealed that cells began to express E-selectin visibly after 1 hr of stimulation; this expression increased in a time dependent manner which peaked at the 6 - 8 hr time point (Figure 3.5). It was evident within the images that most, but not every cell, was expressing E-selectin after TNF alpha stimulation, and that for the cells expressing E-selectin it was hard to define membrane expression. Often, a ring of higher intensity E-selectin expression was seen around the nucleus which faded and increased in intensity again at the outer cell membrane (Figure 3.6). Also throughout all images representing endogenous expression of E-selectin, many small punctate regions within the cell were observed.

To quantify E-selectin expression, AP was used as a secondary antibody. Different dilutions of the AP secondary were examined in 1 nM TNF alpha stimulated or vehicle HUVECs, and the appropriate dilution was concluded to be 1:100 in 10% goat serum as this provided the greatest degree of optical density unit increase compared to the vehicle treated cells (Figure 3.3). Subsequently, in alkaline phosphatase quantified data, a significant increase in optical density units (> 2.0) was observed in HUVECs after incubation with 2 nM TNF alpha compared to vehicle (unpaired t-test, ****P<0.0001) (Figure 3.7a). A concentration response experiment determined that the EC_{50} for TNF alpha was 0.0155 nM ± 0.00283 (Figure 3.7b). A time course experiment was also conducted and, similar to the confocal images, expression of E-selectin peaked at the 6 – 8 hr time point (Figure 3.5). When the time course response was conducted with a 10-fold lower concentration (0.1 nM), E-selectin expression decreased significantly after 8 hr compared to 6 hr.

The coefficient of variation (CV) was calculated for each concentration response and time point by dividing the population standard deviation by the population mean, illustrating the reproducibility of the response in these experiments. The average CV for TNF alpha concentration response was 16%, half the calculated CV for time course response (37%). Therefore, the repeatability between experiments for TNF alpha response was high.

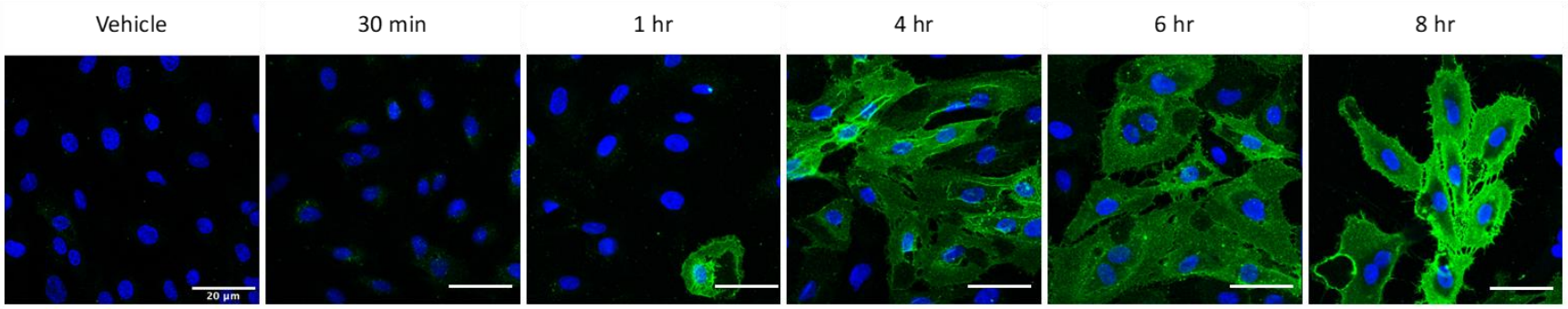

Figure 3.5. ***TNF alpha time course response for E-selectin expression in HUVECs.*** *Confocal images of HUVECs stimulated with 1 nM TNF alpha for 0 – 8 hr (37°C 5% CO2). Blue represents H33342 stained nuclei and green signal represents Alexa Fluor 488 labelled E-selectin. Scale bar = 20µm.*

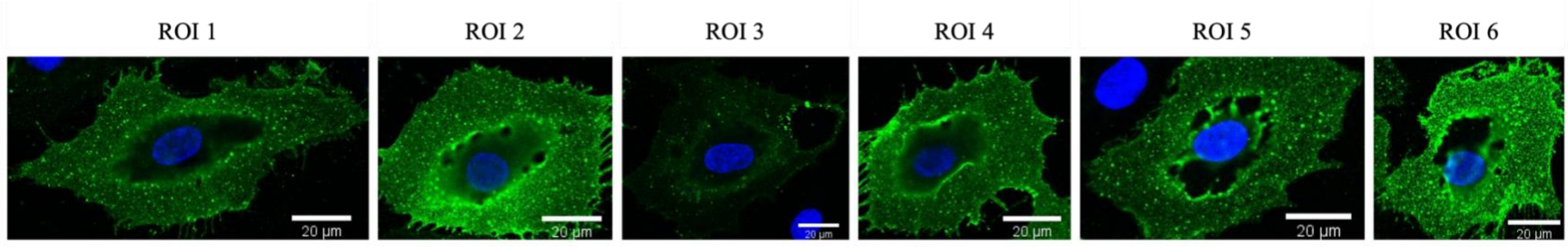

Figure 3.6 ***Regions of interest (ROIs) taken of TNF alpha stimulated HUVECs which presented the same expression patterns.*** *HUVECs were stimulated for 6 hr (1 nM, 37°C 5% CO2), blue signal represents H33342 labelled nuclei, green signal represents E-selectin labelled with anti-E-selectin monoclonal antibody and Alexa Fluor 488 conjugated secondary antibody. Scale bar = 20µm.*

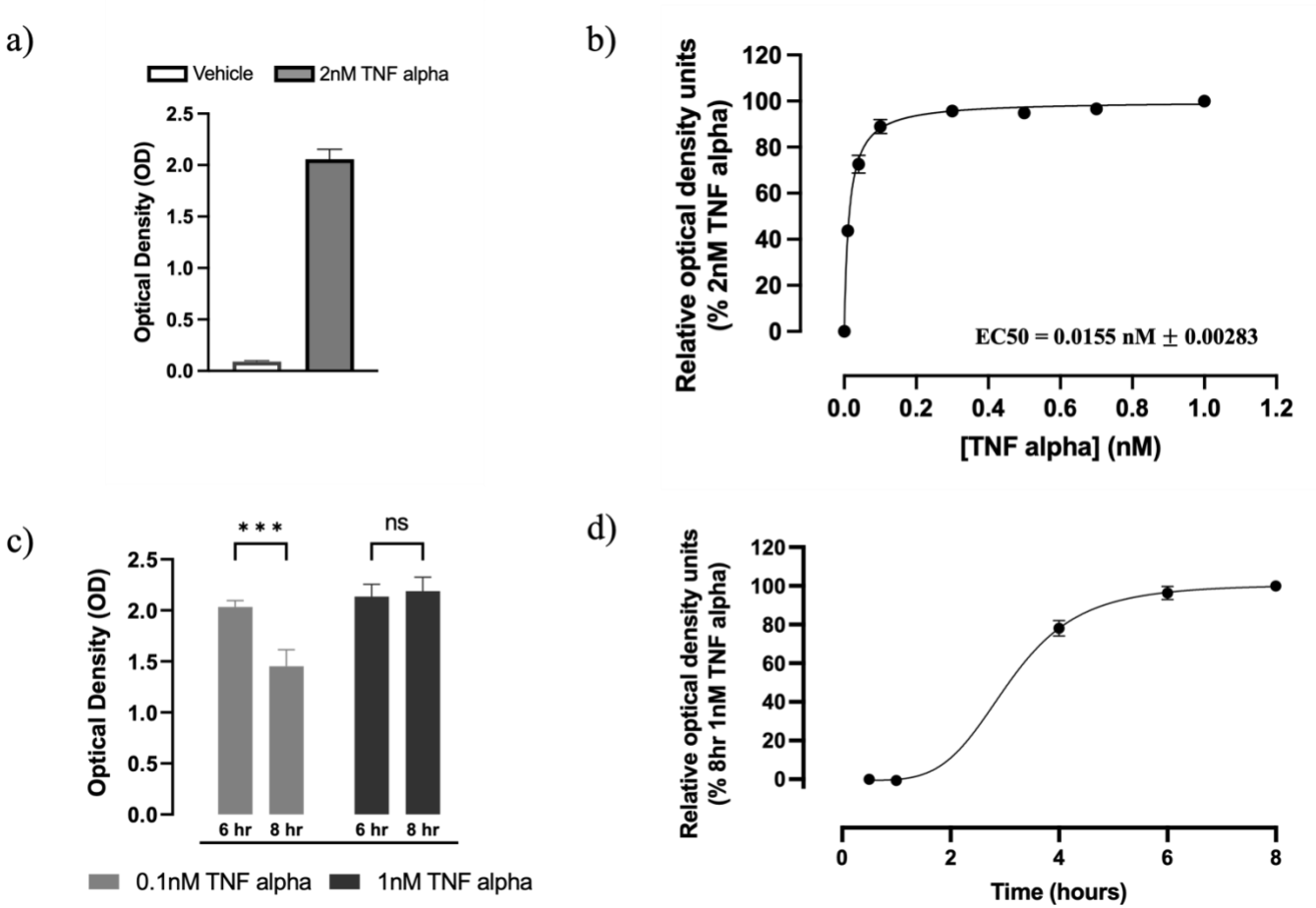

Figure 3.7 ***Quantification of E-selectin expression using alkaline phosphatase secondary antibody and p-nitrophenol phosphate (pNPP) substrate****. a) A significant increase in optical density values was observed after stimulation with TNF alpha (unpaired t-test ****p<0.0001 (t=20.15, df=28)) (2 nM, 6 hr, 37°C 5% CO2), and b) a concentration response of TNF alpha (0 – 1 nM) stimulation; EC_{50} = 0.016 nM ± 0.003 (SEM) (n=5) c) There was a significant decrease in expression observed (two--way ANOVA, post-hoc Tukey's multiple comparisons test ***p = 0.0002) from 6 – 8 hr stimulation with concentration 0.1 nM TNF alpha but not for 1 nM TNF alpha. d) TNF alpha stimulated HUVECs 0 – 8hr displayed a similar time course response as is seen in confocal images.*

3.2.3 VEGF165a and Histamine inducement of E-selectin expression

Other inflammatory mediators were then investigated for their ability to induce E-selectin expression in HUVECs, including histamine (100 nM), $VEGF_{165}a$ (100 nM) and another isoform of VEGF-A which is anti-angiogenic ($VEGF_{165}b$ (100 nM)). The higher concentrations of $VEGF_{165}a$ and histamine were required to observe a significant E-selectin response. Histamine and $VEGF_{165}a$ induced E-selectin expression after 8 hrs of incubation; shown in confocal images and in AP quantification (Figure 3.5 and Figure 3.7, respectively). Expression was notably lower than TNF alpha induced expression and visibly less intense in confocal images with cells that did express E-selectin due to $VEGF_{165}a$ or histamine stimulation sparse in the field of view. The expression pattern of E-selectin did seem comparable to that seen following TNF alpha stimulation, with punctate regions of E-selectin observed in positive cells and a brighter region of staining round the nucleus. Notably, with both histamine and $VEGF_{165}a$ stimulation, a number of cells expressing E-selectin appeared to be undergoing replication (Figure 3.10). Alkaline phosphatase quantification was able to pick up on the lower expression levels due to histamine and $VEGF_{165}a$ (mean OD values after 6 hr stimulation were 0.292 for histamine and 0.135 for $VEGF_{165}a$) (Figure 3.9). Time course stimulation experiments revealed that, like when stimulating with TNF alpha, E-selectin expression peaked at the 6 – 8 hr time point when induced with histamine or $VEGF_{165}a$ (Figure 3.9).

Interestingly, TNF alpha induced E-selectin expression in HUVECs could be significantly increased by 28.3% when co-stimulated with 100 nM histamine (**$p < 0.001$) or 21.8% when co-stimulated with $VEGF_{165}a$ ($p < 0.05$) (Figure 3.11). However, the activity of $VEGF_{165}a$ was not replicated when stimulating with another VEGF-A isoform ($VEGF_{165}b$). $VEGF_{165}b$ did not significantly increase E-selectin expression alone, or when used in co-stimulation with 1 nM TNF alpha for 6 hr of incubation (37°C 5% CO_2) (Figure 3.12).

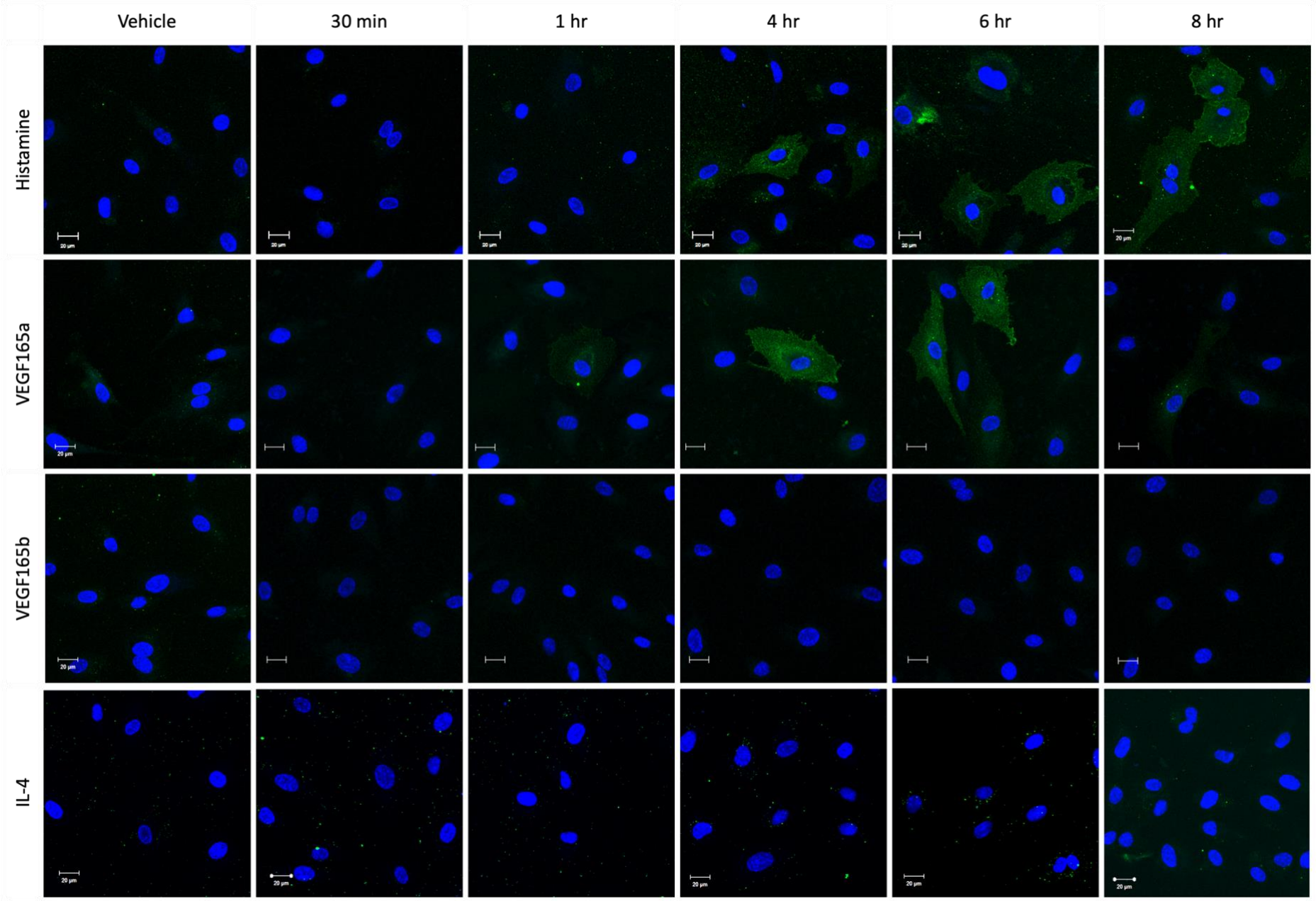
Vehicle
30 min
1 hr
4 hr
6 hr
8 hr
Histamine
VEGF165a
VEGF165b
IL-4

Figure 3.8 Histamine, $VEGF_{165}a$, $VEGF_{165}b$ or IL-4 time course for E-selectin expression in HUVECs. Confocal images of HUVECs stimulated with 100 nM histamine, 100 nM $VEGF_{165}a$, 100 nM $VEGF_{165}b$ or 100 ng/ml IL-4 for 0 – 8 hr (37°C 5% CO2). Blue represents H33342 stained nuclei and green signal represents Alexa Fluor 488 labelled E-selectin. Scale bar = 20µm, n=5. E-selectin expression was relatively low compared to Figure 2 (TNF alpha stimulated E-selectin expression), however like TNF alpha induced expression, fluorescence intensities (indicative of E-selectin expression) were brighter and present in more cells in the field of view over time due to histamine and $VEGF_{165}a$ stimulation. The VEGF splice variant $_{165}b$ however, like IL-4, did not induce E-selectin expression at any time point 0 – 8 hr

.

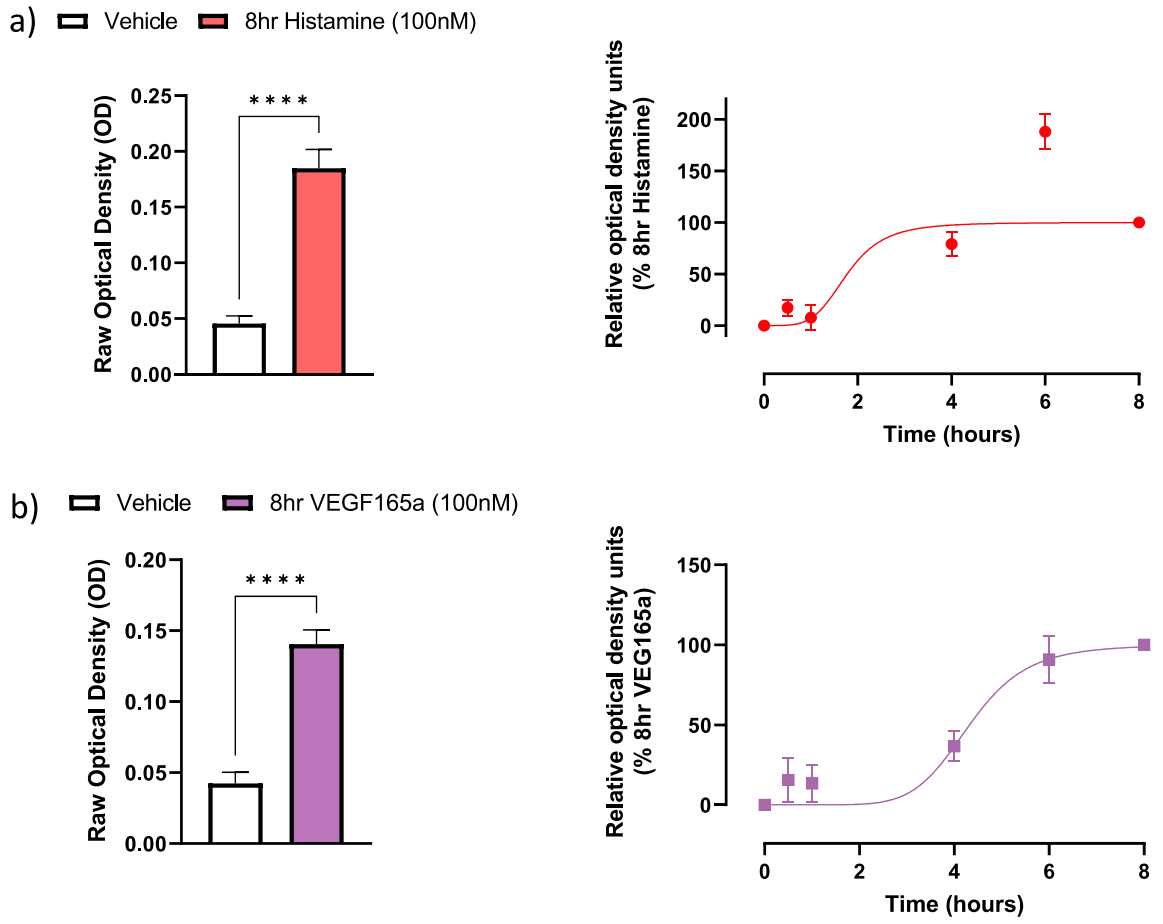

Figure 3.9 ***Alkaline phosphatase detection of Histamine or VEGF$_{165}$a induced E-selectin expression over 8 hr.*** *a) Histamine significantly increased E-selectin expression compared to vehicle (unpaired t-test ****p<0.0001), and peaked E-selectin expression at 6 hr in HUVECs. b) VEGF$_{165}$a induced E-selectin expression (unpaired t-test ****p<0.0001) compared to vehicle which peaked at 6 hrs. n = 5 error bars = SEM*

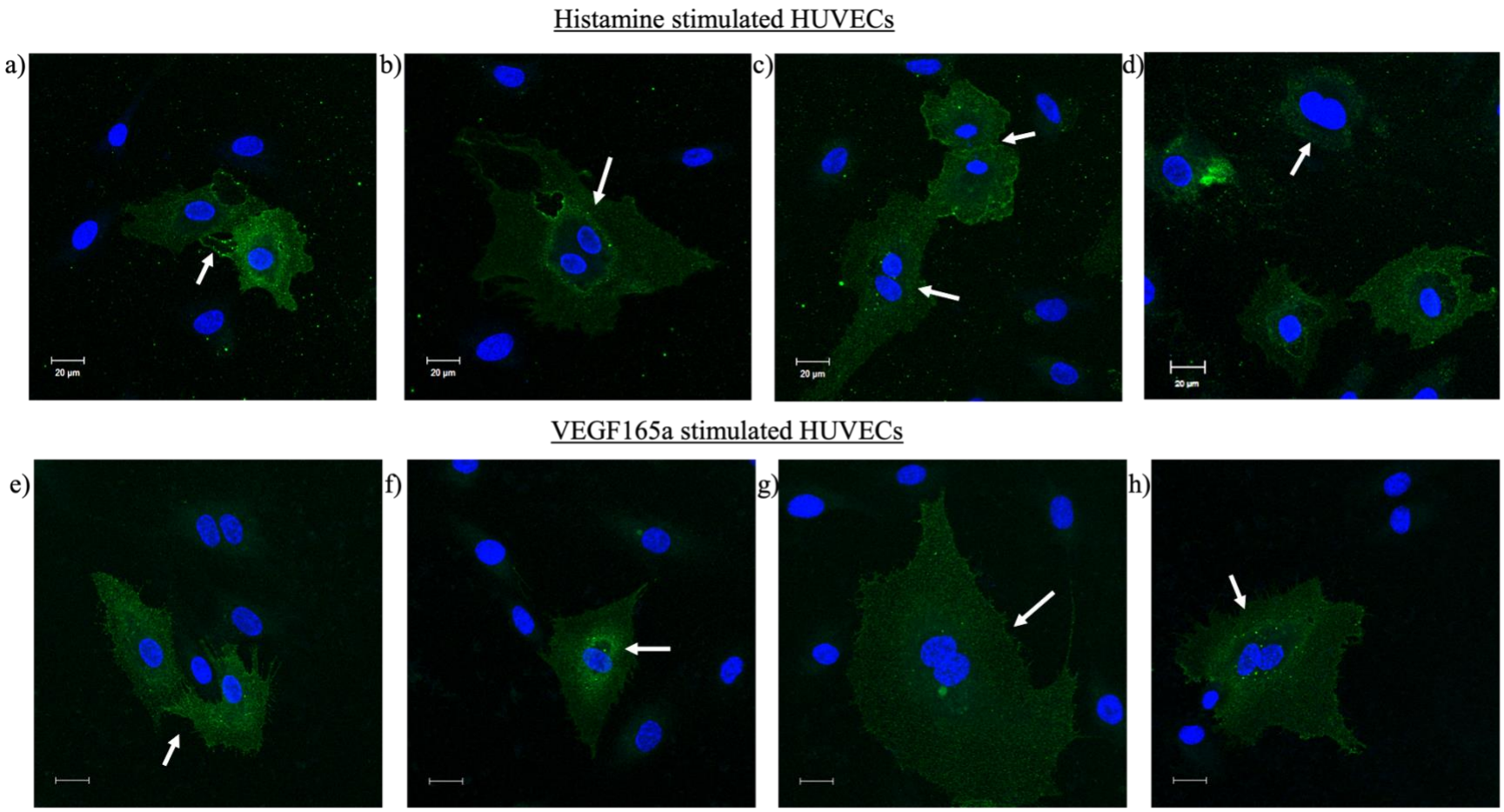

Figure 3.10 ***In Histamine and VEGF$_{165}$a treated HUVECs, a number of cells which were expressing E-selectin were undergoing replication.*** *These images were selected from the library of histamine induced expression after 6 hr (a and b) and 8 hr (c and d), and VEGF$_{165}$a induced expression after 4 hr (e) 6 hr (f) and 8 hr (g and h) (100 nM, 37°C 5% CO2). See white arrows for cells which have already undergone/are undergoing replication that are also expressing E-selectin. Scale bars represent 20 µm. Blue signal is H33342 labelled nuclei and the green signal represents Alexa Fluor 488 labelled E-selectin.*

.

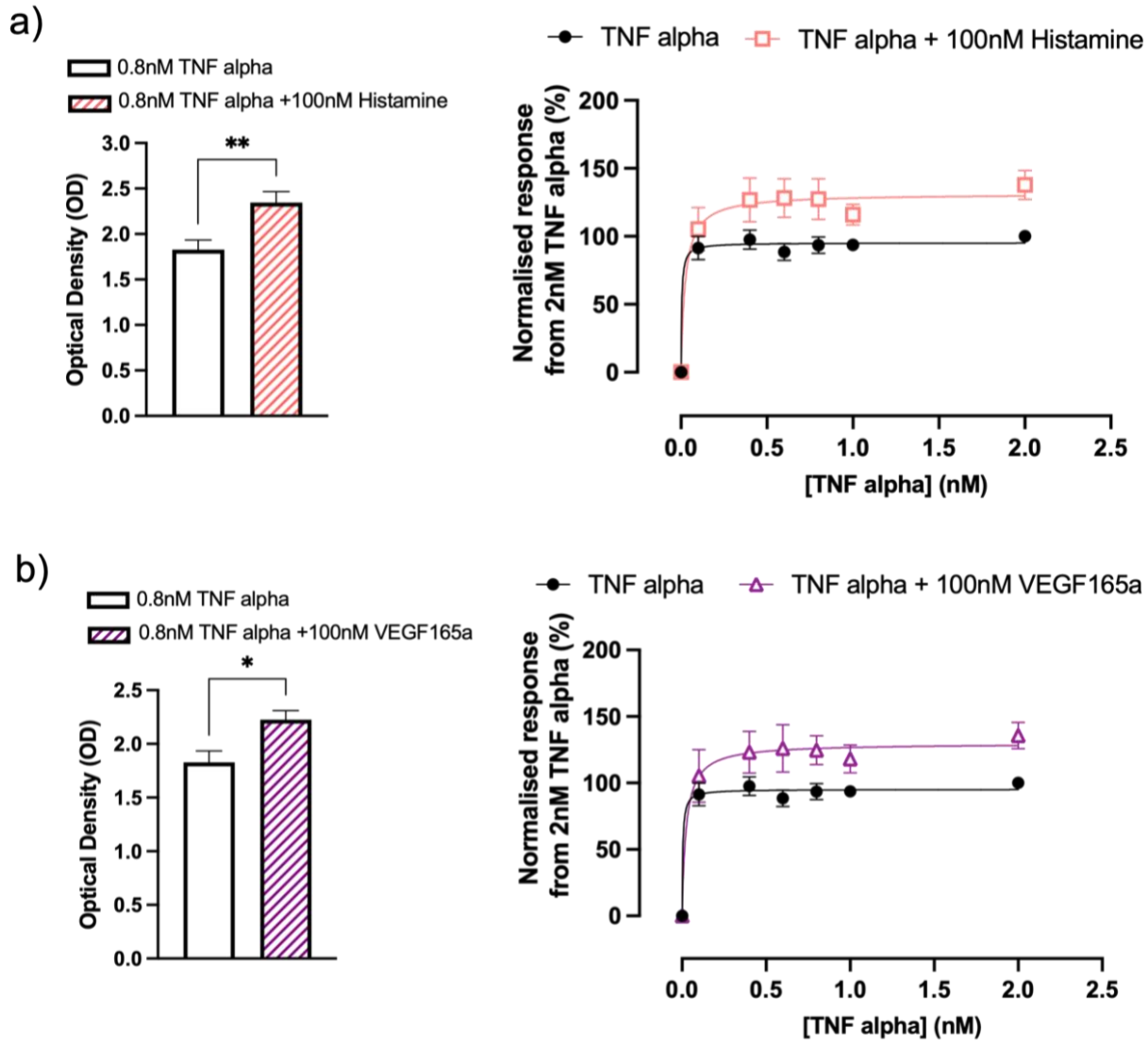

Figure 3.11 Histamine and VEGF$_{165}$a enhanced TNF alpha induced E-selectin expression in HUVECs. *a) 100 nM Histamine significantly increased TNF alpha induced E-selectin expression (un-paired t-test p <0.001) at TNF alpha concentrations >0.5 nM. b) 100 nM VEGF$_{165}$a significantly increased TNF alpha induced E-selectin expression (unpaired t-test p <0.05), at concentrations > 0.6 nM TNF alpha. n = 5 error bars = SEM.*

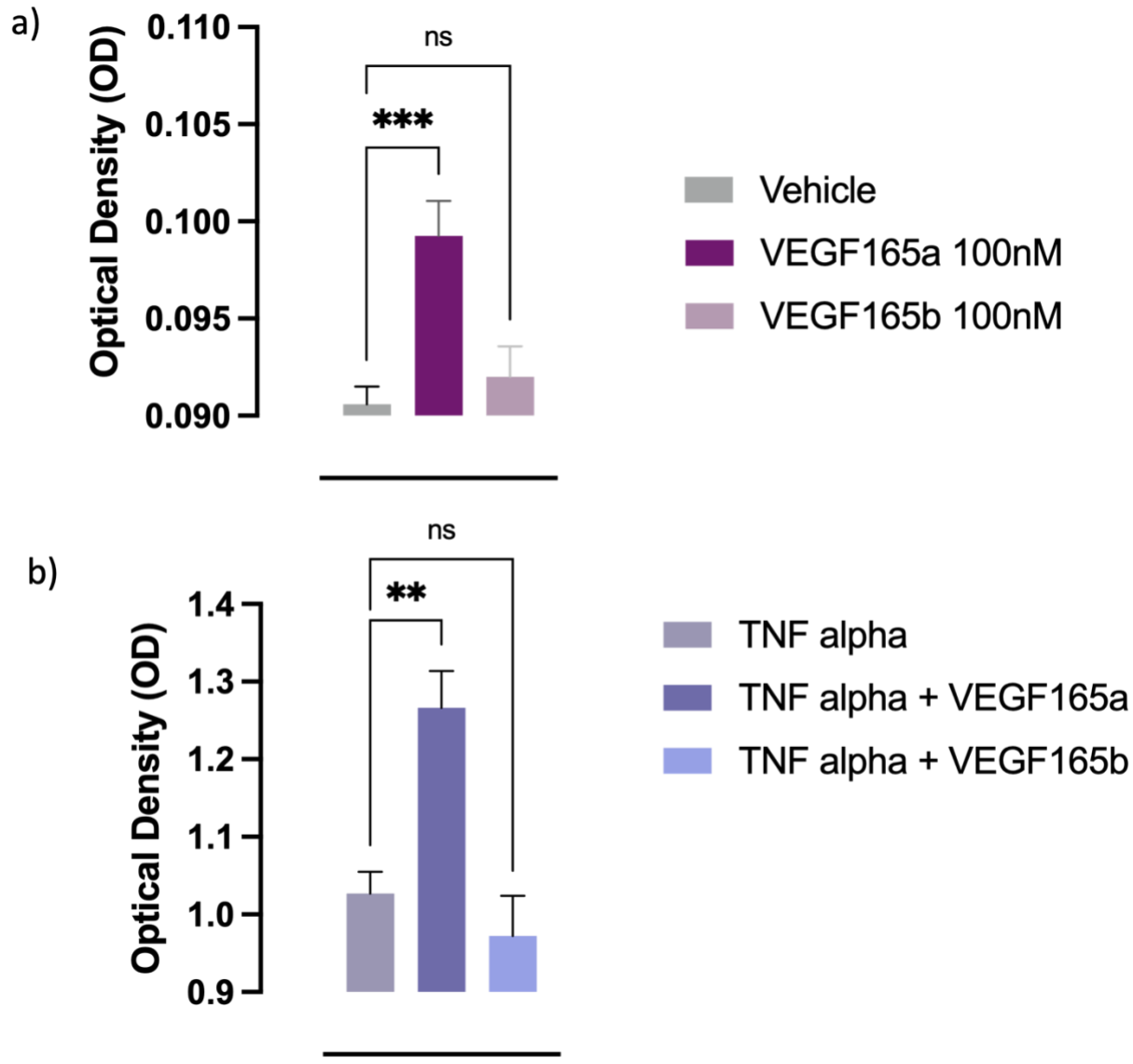

Figure 3.12 ***Only the VEGF$_{165}$a isoform, and not VEGF$_{165}$b, stimulates E-selectin expression in HUVECs****. a) 100 nM VEGF$_{165}$a significantly induced E-selectin expression (One-way ANOVA ***p= 0.0005) in HUVECs however this was not seen with 100 nM VEGF$_{165}$b. b) VEGF$_{165}$a significantly enhanced the TNF alpha induced E-selectin expression (One-way ANOVA **p= 0.0026) and there was no significant difference seen with addition of 100 nM VEGF$_{165}$b. n=3, error bars= SEM.*

3.3 Discussion

This chapter explored inflammatory cytokine and growth factor inducement of E-selectin expression in HUVECs using antibody labelling techniques in fixed cells. We were able to visualise and quantify E-selectin expression over time after incubation with varying concentrations of TNF alpha, Histamine, IL-4 and two VEGF-A splice variants $VEGF_{165}a$ and $VEGF_{165}b$.

TNF alpha was demonstrated to be a potent E-selectin stimulant (EC_{50} = 0.0155 nM); even the lowest concentration (0.01nM) produced a 10-fold increase in expression. Peak expression was seen after 6-8 hr stimulation (1 nM) and a 68-fold increase in expression was observed from basal compared to peak expression. Confocal imaging revealed that intense expression was displayed at this time point, where most cells were expressing E-selectin. Interestingly, not every cell expressed E-selectin even after 8 hr stimulation. In addition, the expression pattern of E-selectin in response to TNF alpha did not look like it was exclusively membrane associated. Punctate regions of expression within the cell suggests that E-selectin was labelled within the cell, due to permeabilization of HUVECs occurring at some point within the experiments. This could have occurred due to the following; TNF alpha has been previously shown to induce endothelial cell barrier dysfunction and result in enhanced permeability of the cell membrane in rat lung microvascular endothelial cells, mouse renal endothelial cells, human glomerular endothelial cells and HUVECs (Friedl *et al.*, 2002; Sawant *et al.*, 2013; Xu *et al.*, 2015). This has been proposed to occur due the presence of tissue factor (also termed factor III or CD142), which is a protein present in endothelial cells responsible for initiating blood coagulation (Friedl *et al.*, 2002). Friedl *et al.*, (2002) found that endothelial cell monolayer permeability increased significantly in a time dependent manner after 0 – 3 hr incubation with 1µg/ml TNF alpha in HUVECs. This data brings scepticism to whether what is measured is membrane bound E-selectin only. The same expression patterns of E-selectin were seen after $VEGF_{165}a$ and histamine incubation, although at a much lower fluorescence intensity. $VEGF_{165}a$ and histamine have also been implicated in increasing vascular permeability, therefore this could explain this pattern (Qin *et al.*, 2013; Ourradi *et al.*, 2017; Moya-García *et al.*, 2021). Another reason for why E-selectin is not evidently on the outer most perimeter of each cell and therefore the membrane, is that HUVECs lie flatter than other cells

and therefore imaging one cross section in the Z position is more difficult. The resultant image would therefore not be from one plane in the Z position but a merge of several planes which could result in misleading localisations of labelled E-selectin. Knowing where E-selectin is labelled is important as the function of E-selectin begins after it has reached the plasma membrane, so that it can interact with and subsequently deliver leukocytes to areas of inflammation. Therefore, it is extremely valuable when considering the therapeutic potential of targeting E-selectin, to know whether it is largely expressed on the cell surface or whether it is within the cytoplasm (and whether this population has functional relevance). Previously, mRNA expression was used to define surface expressed E-selectin (Bevialacqua *et al.*, 1989; Read *et al.*, 1997; Rahman *et al.*, 1998; Stocker *et al.*, 2000), however this won't have guaranteed membrane expression only. For future studies, a membrane stain such as CellMask™ Plasma membrane stain could be used so that co-localisation of E-selectin with the membrane could be confidently determined using microscopy. Alternatively, co-labelling with antibodies selective for known endosomal markers (for example Rab5 for early endosomes, LAMP-1 for lysosomes) would also be advantageous to investigate if the pattern of staining I have observed for E-selectin here is not an imaging artefact.

The journey of E-selectin expression after TNF alpha stimulation has been described as an upregulation in transcription, followed by an increase in surface protein expression over the course of 6 hr until levels decrease back to baseline by 24 hr (Wyble *et al.*, 1997). This data has corroborated that in the first 6 hr of stimulation with TNF alpha, an increase in expression is detected, however we found that a decrease in TNF alpha induced E-selectin is dependent on concentration. We found that in 0.1 nM TNF alpha stimulated HUVECs, this downregulation was observed but levels remained high in HUVECs when stimulated with a 10-fold greater concentration.

Lower levels of TNF alpha have been used previously (10 pg/ml or 0.6 pM) (Wyble *et al.*, 1997), which have been suggested to better compare to physiological levels (30.5 ± 1.0 pg/ml or 1.8 pM ± 0.06 pM) (Wyble *et al.*, 1996). In cases of inflammatory disease and sepsis, serum TNF alpha levels increase significantly and have been shown to correlate to severity of disease (Popa *et al.*, 2007; Bradley, 2008; Kany, Vollrath and Relja, 2019). For example, in cases of congenital heart failure, Parkinsons disease and Graves disease, the serum TNF levels more than double, and in cases of psoriasis and sepsis, TNF alpha levels increase to more than 10x the control levels (Noori

et al., 2017; Zhu *et al.*, 2020; El-Kattan *et al.*, 2022; Kurtovic and Halilovic, 2022). The concentrations used therefore are more indicative of levels in inflammatory disease states.

Compared to TNF alpha, $VEGF_{165}$a and histamine required a concentration 100-fold higher to provide a significant upregulation in E-selectin from basal. A 4.9-fold and 6.1-fold increase in E-selectin expression was observed due to 100 nM $VEGF_{165}$a and 100 nM histamine respectively and peak optical density values were 14-fold lower for $VEGF_{165}$a (0.206) and 10.4-fold lower for histamine (0.279) compared to TNF alpha (2.886). This was reflected in confocal imaging, where only a few cells in the field of view expressed E-selectin in response to $VEGF_{165}$a and histamine and in these instances, the expression was comparably low. This is in agreement with studies which have compared histamine and $VEGF_{165}$a induced E-selectin expression with TNF alpha in vascular endothelial cells (Miki *et al.*, 1996; Stannard *et al.*, 2007). However, E-selectin expression peaked 2 hours later than what was found in other studies, in which E-selectin expression saturated after 4 hours in HBMECs (Wong and Dorovini-Zis, 1996; Stocker *et al.*, 2000). This discrepancy in the data could be explained by the fact that different endothelial cell types were used. Galley et al., (1999) compared E-selectin expression in three different endothelial cell lines; HUVECs, a spontaneously transformed ECV304 cell line and the hybrid cell line EA.hy926. They found that TNF alpha induced E-selectin expression was 100 fold lower in ECV304 and EA.hy926 cell lines and that mRNA expression was undetectable in comparison to HUVECs. The results could be due to different culture conditions, or represent the functional heterogeneity of endothelial cells from different vascular beds. A lot of previous studies also experimented with HUVECs, however due to differences in HUVEC donors, there would have been subsequent physiologic variability of individual umbilical cords. One major difference to consider is the sex of the donor. Although the effect of sex differences from HUVEC donors has not been explored in the context of E-selectin expression, differences have been observed for GPCR expression, pro-angiogenic responses, cell proliferation, migration and viability (Addis *et al.*, 2014; Boscaro *et al.*, 2020). In all cases, female donors exhibited higher GPCR expression and responsiveness to pro-angiogenic factors compared to male donors, which was hypothesised to be due to the hormone microenvironment and sex-specific factors (Boscaro *et al.*, 2020).

Studies that examine whether VEGF can mediate E-selectin expression are less common; only 2 other reports have noted a correlation in *in vitro* experiments, and there were contradicting findings

from Stannard et al., (2007), who found that VEGF stimulation alone did not induce E-selectin expression. Kim et al (2001) and (2003) found that E-selectin mRNA and protein expression was upregulated by VEGF in HUVECs through NF-kB activation, as it was significantly suppressed by a VEGFR2 (F1k-1/KDR) inhibitor, and inhibitors of PLC NF-kb, sphingosine kinase and PKC but not by inhibitors for MEK 1/2 or NOS. They found that E-selectin mRNA was upregulated after 2hr – 4hr stimulation (20 ng/ml), and a reduction of expression was seen after 4hr. $VEGF_{xxx}a$ isoforms are considered pro-angiogenic growth factors however different isoforms exist which exhibit anti-angiogenic activity as well ($VEGF_{xxx}b$). This could explain the discrepancy between results as the isoforms used were not defined. This chapter reports that the pro-angiogenic isoform $VEGF_{165}a$ but not the anti-angiogenic isoform $VEGF_{165}b$, induced E-selectin expression.

A large proportion of $VEGF_{165}a$ stimulated cells which displayed E-selectin expression were undergoing replication. Previous studies have associated E-selectin expression with G_0/G_1 cell cycle phase after stimulating cells with growth factors. Jianying Luo, Paranya and Bischoff (1999), found that there was a linear correlation of E-selectin levels with the percentage of endothelial cells in G_0/G_1 after stimulation with basic fibroblast growth factor. They also found that E-selectin expression was 5x higher in proliferating cells in comparison to confluent Human dermal microvascular endothelial cells (HDMECs) (Jianying Luo, Paranya and Bischoff, 1999).

Histamine also induced E-selectin expression in a time dependent manner and was comparable in expression dynamics to $VEGF_{165}a$. Like $VEGF_{165}a$, only a few cells in the field of view were expressing E-selectin, notably a large proportion were undergoing replication, and at comparably lower levels to TNF alpha. It has been documented that Histamine induced leukocyte recruitment has primarily been due to rapid P-selectin expression (McEver *et al.*, 1989; Miki *et al.*, 1996), less so E-selectin expression. This notion is relevant with respect to the present findings, as histamine induced E-selectin expression was low even after 8 hours of stimulation.

Histamine and $VEGF_{165}a$ were also both found to significantly increase the TNF alpha induced E-selectin expression (see Figure 3.11). Stannard *et al.*, (2007) found that this dual action explained the excessive E-selectin mediated accumulation of macrophages in atherosclerotic plaques, and Miki et al., (1996) used this finding to highlight E-selectin's role in allergy. This proposed synergy

of $VEGF_{165}$a and histamine with TNF alpha could suggest that E-selectin is expressed in inflamed environments that also require neovascularisation, such as in cancer, rheumatoid arthritis and atherosclerosis.

3.4 Conclusions

In conclusion, the antibody labelling procedures used in this chapter were necessary to evaluate E-selectin expression in fixed HUVECs, and a concentration and time dependent regulation of E-selectin expression was observed for TNF alpha. Histamine and $VEGF_{165}$a also induce E-selectin expression at lower levels, and both increased the TNF alpha induced response. This implicates the important role E-selectin plays in vascular inflammation and angiogenesis. However, the monoclonal antibody labelling procedure potentially induced unwanted HUVEC permeabilization, and didn't guarantee exclusive membrane labelling and subsequent quantification. Future experiments are needed to dynamically investigate and quantify E-selectin expression in response to inflammatory mediators that can guarantee membrane expression only and with increased temporal sensitivity. This can be done in live endothelial cells using luciferase based technologies.

Chapter 4 Using CRISPR-Cas9 in conjunction with NanoBiT to develop a HiBiT E-selectin assay system in live human endothelial cells

4.1 Introduction

As previously described, it is possible to measure the upregulation of E-selectin in response to TNF alpha, IL-1 alpha/beta, LPS, histamine and VEGF stimulation using monoclonal / polyclonal antibody labelling. However, it is difficult to determine membrane only expression using such methods, in addition to it lacking real information on the dynamics of cell surface translocation. For these methods, cells must be fixed which risks permeabilization artefacts, the process of immunolabelling and imaging is laborious and there is a missed opportunity to evaluate expression in live cells. This chapter focused on developing an *in vitro* assay for detection of cell surface E-selectin expression that could replicate the WT HUVEC response quantified in Chapter 3, in live cells. For this reason, CRISPR-Cas9 was used in conjunction with NanoLuc binary technology (NanoBiT) in HUVECs and TERT2 immortalised HUVECs to develop a method that could overcome the limitations of detection using antibody labelling.

The CRISPR-Cas9 system was first discovered as an adaptive immune system in bacteria and archaea, to protect from invading viral or plasmid nucleic acid infection by introducing double strand breaks (DSBs) into invading plasmids and phages (Doudna and Charpentier, 2014). Furthermore, it was found that this mechanism could be exploited in scientific research to introduce point mutations, deletions or insertions at specific points within the genome. The complex mechanisms underlying CRISPR-Cas9 can be reduced in practice to the use of an endonuclease, one of which is a CRISPR-associated protein Cas9, utilising a guide sequence within an RNA duplex (tracrRNA:crisprRNA) to form base pairs with DNA target sequences. Once this complex is bound, Cas9 can introduce a site-specific DSB in the DNA sequence. This binding and consequential DNA DSB is reliant on the presence of a protospacer adjacent motif (PAM) sequence, which for Cas9 is NGG (where N is any nucleotide base). The inherent mechanism of genomic DNA repair is then exploited in the cell, as in the presence of an appropriate repair template, that is designed to have homology to either end of the DSB, an insertion can be made at this specific site via homology-dependent repair. This ability to introduce site-specific insertions into DNA is extremely useful in order to specifically introduce tags onto proteins of interest in order to track their endogenous trafficking, expression, secretion, signalling, binding and internalisation. Because of this, CRISPR genome editing systems are one of the most robust platforms in basic biomedical research in addition to having many potential therapeutic applications.

The tag of choice used to follow the cell surface expression of E-selectin was HiBiT; a component of a split NanoLuc enzyme that is used in the NanoLuc Binary Technology (NanoBiT) system (Dixon *et al.*, 2016). NanoBiT is a technology developed by Promega Corporation (USA), who were able to split the NanoLuciferase enzyme into a large fragment (LgBiT, 19 kDa) and a small fragment (HiBiT, 1.1 kDa). Upon re-complementation of these fragments, full length NanoLuc induces the substrate Furimazine to luminesce, which can be detected via luminescence imaging or using a luminometer, such as the BMG LabTech PHERAstar FS plate reader. As the purified LgBiT fragment is cell impermeable, HiBiT/LgBiT recomplementation is exclusively localised to the cell surface. Therefore, production of luminescence is indicative of cell surface expression of endogenously expressed HiBiT tagged E-selectin on the surface of living HUVECs.

Previously, HiBiT has been appended to proteins or receptors of interest using molecular biology techniques and detection with purified LgBiT has been used in over expression systems in HEK293Ts. Here, investigation of membrane protein or receptor expression, internalisation, GPCR effector recruitment, protein/receptor conformational changes and receptor signalling was achieved (Oh-hashi *et al.*, 2017; Inoue *et al.*, 2019; Leroy *et al.*, 2019; Soave, Heukers, *et al.*, 2020; Soave, Kellam, *et al.*, 2020; White *et al.*, 2020; Peach *et al.*, 2021; Dijon, Nesheva and Holliday, 2022; Kozielewics and Schulte, 2022; Luís *et al.*, 2022; O'Neill and Knaus, 2022; Reyes-Alcaraz *et al.*, 2022). In addition, the NanoBiT system has been coupled with a third fluorescently tagged protein to allow NanoBRET studies to continue investigation of drug binding, and drug induced changes at a molecular complex that has been defined using NanoBiT (HiBiT and LgBiT show minimal luminescence when expressed alone). White *et al.*, (2020) utilised CRISPR-Cas9 to append HiBiT onto the N-terminus of endogenously expressed CXCR4 in order to investigate cell surface expression as well as drug induced receptor conformational changes. They delivered the CRISPR reagents via plasmid transfection to HEK293 cells; here, a puromycin resistant Cas9 expression construct (pSpCas9(BB)-2A-Puro (PX459 V2)) was incorporated with guide RNA sequence targeting the N-terminal region of interest. A HiBiT repair template with a GSSG linker was synthesised as a single stranded oligo DNA nucleotide (ssODN). These CRISPR components were then transfected into HEK293 cells using a liposome transfection reagent, and edited cells were selected for using puromycin and the consequential HiBiT-CXCR4 clone expanded. This clone was able to investigate cell surface expression, conformational changes and internalization of CXCR4 using NanoBiT

complementation technology and measuring luminescence output with a PHERAstar plate reader (White et al., 2020).

The methods of delivery for CRISPR reagents remain to either deliver via lipofection or via electroporation. Implementing CRISPR-Cas9 gene editing can be done by delivering Cas9 DNA to the cell as either a Cas9 expression plasmid (or lentiviral Cas9), delivering Cas9 mRNA, or utilising a Cas9 stable cell line. The same goes for CRISPR gRNA delivery which can be delivered via an expression plasmid (or lentiviral sgRNA), or by an *in vitro* transcribed (IVT) sgRNA. In addition, one can also use synthetic Double stranded DNA fragments called gBlocks® which drive expression of sgRNA (Jin and Marquardt, 2020). The most efficient delivery however has been found to be using a purifed Cas9 protein, crRNA/tracrRNA complex termed the RNP complex (Liang *et al.*, 2015). This method is the Alt-R™ CRISPR-Cas9 System ribonucleoprotein (RNP) delivery system which has been developed by Integrated DNA Technologies (IDT, USA). This system out-performed native CRISPR RNA, IVT sgRNA induced expression, as well as plasmid expression when it came to editing efficiency of cells (Liang *et al.*, 2015) and is particularly advantageous for substantially increasing editing in primary cells such as HUVECs. After RNP complex delivery to cells, the Cas9 degrades after 48 – 72 hours, in contrast to plasmid delivery of Cas9 / guide RNA complex, where it took 24 hr to see the transcribed and translated Cas9 protein, and there was prolonged expression and presence of Cas9 for over 72 hr (Liang *et al.*, 2015). The short time span and rapid degradation of Cas9 via RNP delivery system is advantageous as there is less chance of prolonged Cas9 exposure risking increased off-target cutting. Off target effects can occur even when the gRNA is not completely homologous to the off-target region; similarity of sequence with certain amounts of mismatches can still cause targeting of RNP, leading to Cas9 induced DSB formation and consequential site mutations being formed after native non-homologous end-joining (NHEJ) repair pathways. In addition, for RNP delivery, there is no need to wait for the transcription and translation of Cas9 making this method the fastest experimentally. It has also been argued that plasmids may cause cytotoxicity, and some transfection reagents (e.g. lipids) used for plasmid transfection are themselves toxic to cells (Kurata *et al.*, 2018; Chen, Alphonse and Liu, 2020).

HUVECs are notoriously hard to transfect using liposome based reagents (eg. FuGENE, lipofectamine) as they are more susceptible to cytotoxicity of transfection reagents, they have been shown to degrade exogenous nucleic acids in the cytoplasm, have a limited lifespan, and

have a relatively low proliferation rate (Hunt *et al.*, 2010). Electroporation of HUVECs has been shown to produce comparatively higher transfection efficiencies and lower cytotoxicity (Ear *et al.*, 2001).

This chapter explored the inducement of HiBiT E-selectin in live, CRISPR edited HUVECs and TERT2 HUVECs by a range of inflammatory cytokines. The appendage of HiBiT onto the N terminus of E-selectin using CRISPR-Cas9 gene editing allows real-time quantification of endogenously expressed E-selectin plasma membrane translocation. The addition of the complementary membrane impermeable LgBiT fragment would guarantee membrane only expression is quantified.

4.2 Results

4.2.1 Optimization of CRISPR-Cas9 edit in WT HUVECs

Before CRISPR-Cas9 gene editing of cells, a targeted N-terminal region (370 bp) of E-selectin designed using the genomic DNA sequence, was PCR amplified and Sanger sequenced to confirm the lack of SNPs in the PAM site. This was a crucial step before editing cells as the Cas9 nuclease seeks out this PAM site where it cleaves the DNA; any polymorphisms within this site would result in no genomic editing. The resultant sequenced electropherogram trace file was blasted against the E-selectin gDNA sequence found online (NG_012124.1) (see Figure 4.1) and the two N-terminal regions were homologous. Therefore, there were no SNPs found in this specific PAM site (CCT / GGA) (see Figure 4.1a).

Secondly, the cutting efficiency of the RNP complex formed from the Cas9, TRACR-RNA and CRISPR-RNA was checked via an *in vitro* Cas-9 cleavage assay. Two bands representing 337 bp and 536 bp fragments due to Cas-9 cutting at PAM site were seen clearly in comparison to no RNP complex control (Figure 4.1b), indicating a high cutting efficiency and validity to move on to edit whole cells. Finally, the electroporation efficiency was compared between an Old HUVEC electroporation setting (U-001) and a New HUVEC setting (A-034) for use with Lonza's Nucleofector 3b Device electroporator. These two programmes differ in their electrical parameters for electroporation (specific details are not disclosed by Lonza). HiBiT E-selectin expression following TNF alpha stimulation (1 nM, 6hr 37°C 5% CO2) was higher after electroporation with the new programme; A-034 (n=2) (see Figure 4.1c).

These optimisation experiments revealed the chosen PAM site for editing was not mutated, the cutting efficiency of the designed RNP complex was sufficient and the electroporation efficiency was highest using A-034 setting.

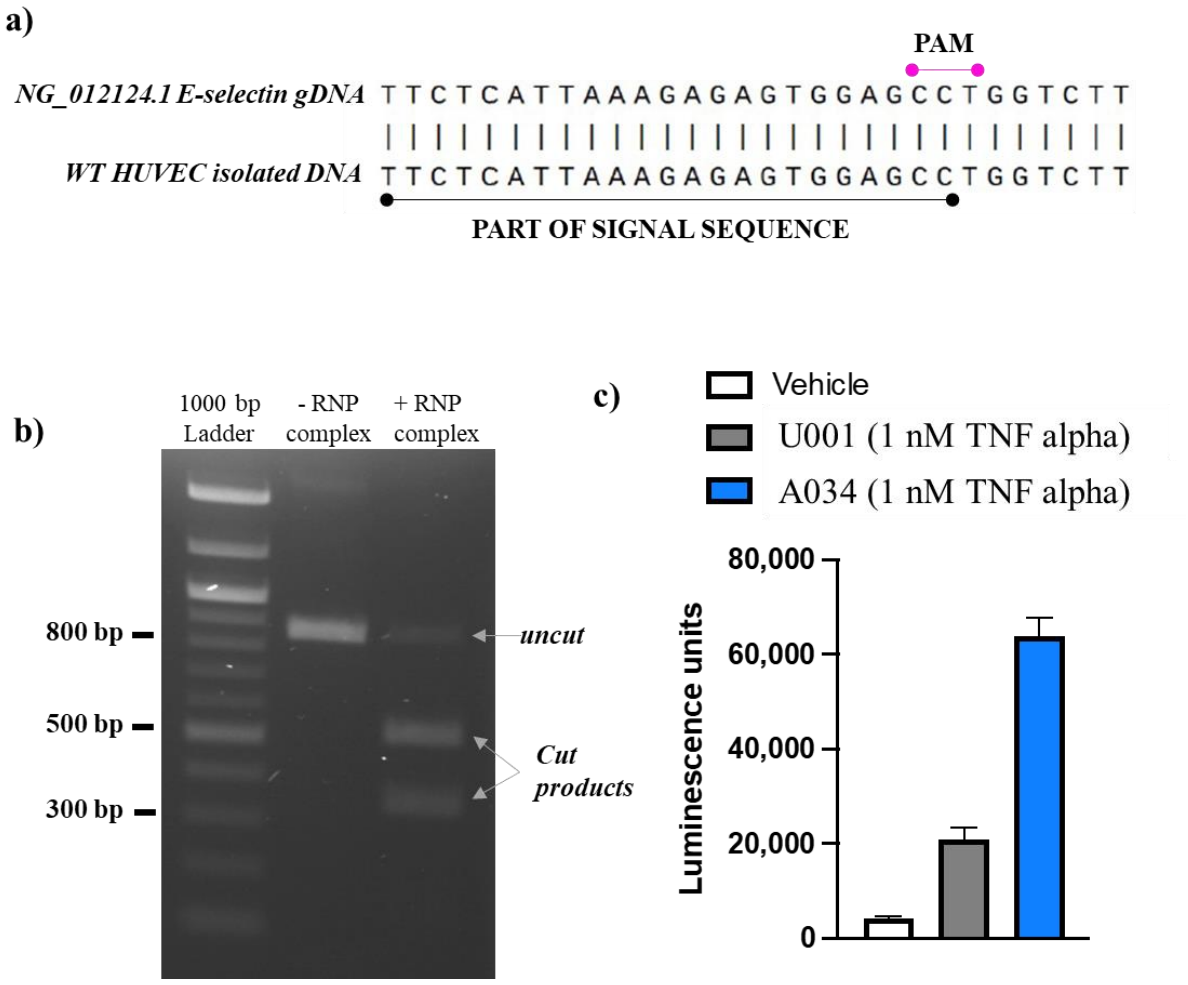

Figure 4.1 ***CRISPR-Cas9 protocol optimization revealed that there were a) no SNPs in the desired PAM site of E-Selectin where editing would ideally occur , b) and confirmed that the RNP complex cut at the PAM site efficiently and that c) the new electroporation setting (A-034) gave the highest luminescence output (n=2) indicative of higher electroporation efficiency****. a) Wildtype HUVEC genomic DNA was isolated and a 370 bp portion of N-terminal E-selectin DNA was PCR amplified. The PCR product was purified and Sanger sequenced (DEEPSEQ, University of Nottingham). The E-selectin gDNA (NG_012124.1) was then blasted against the sequenced portion of DNA and the two were homologous and no SNPs could be identified within the PAM site (CCT). b) The isolated WT HUVEC DNA was then PCR amplified generating an 873 bp fragment. The DNA band was purified and incubated with RNP complex to produce two distinct bands at 337 bp and 536 bp. Only a faint band of uncut DNA remained suggesting a high cutting efficiency, compared to no RNP-complex negative control. c) WT HUVECs were then CRISPR edited using the designed guide and repair templates using a new (A-034) and old (U-001) Lonza electroporation settings. Edited WT HUVECs were stimulated with 1 nM TNF alpha (37°C, 5% CO_2). The new setting produced a >3 times higher luminescence output, indicative of a higher electroporation efficiency (n=2).*

4.2.2 Production of mixed population HiBiT E-selectin cells (WT and TERT2 HUVECs)

WT HUVECs that were CRISPR-Cas9 gene edited produced a visible luminescent signal in a select few cells after stimulation with TNF alpha (1 nM 37°C 5% CO_2) in three out of five repeat experiments (Figure 4.4). Edited WT HUVECs were imaged for luminescence after NanoBiT complementation and addition of furimazine substrate and representative images from each repeat are displayed in Figure 4.4. Not every cell showed sufficient expression of HiBiT E-selectin that was able to be visualised using the LV200 widefield luminescent microscope, and not every experimental repeat produced enough cells that reached this luminescence threshold. Therefore, high variance in HiBiT editing efficiency and/or electroporation efficiency between repeats was observed. Despite this, luminescence above background was always detectable using the PHERAstar FS plate reader between experimental repeats (Figure 4.5), with differential concentration responses for TNF alpha, LPS, IL-1 alpha and IL-1 beta (Figure 4.5) after 6 hr stimulation (37°C 5% CO_2) observed. Here it was found that TNF alpha was the most potent stimulant for E-selectin expression (EC_{50} = 0.0569 nM) followed by LPS (EC50 = 10.001 nM) and IL-1 alpha/beta (EC_{50} values 41.043 nM and 48.255 nM respectively).

Due to the small passage window for WT HUVECs (Liao *et al.*, 2014) (editing was only done with HUVECs P2 - P6), TERT2 immortalised HUVEC cells (TERT2 HUVECs) were used in parallel CRISPR-Cas9 experiments. TERT2 HUVECs express E-selectin with comparable levels to WT HUVECs but have an experimental advantage that they can be used to at least passage 18. Peak expression of E-selectin after 6 hr stimulation with TNF alpha was observed in TERT2 HUVECs (1 nM 37°C 5% CO_2) (Figure 4.2), and expression was also detected in response to LPS, IL-1 alpha and IL-1 beta stimulation (Figure 4.3). A mixed population HiBiT E-selectin cell line was produced (TERT2 HUVEC (mx)). E-selectin expression induced by 1 nM TNF alpha (37°C 5% CO_2) was too low in luminescence intensity to detect via LV200 imaging and was visually comparable to vehicle (Figure 4.6). However, as for WT HUVECs, the PHERAstar FS plate reader was able to detect an increase in luminescence output after TNF alpha stimulation in TERT2 HUVECs (1 nM, 37°C 5% CO_2, mean maximal luminescence = 42, 260 LU) and a comparable TNF alpha concentration response to that determined for WT edited HUVECs (n=5, EC_{50} =0.104 nM).

Both edited WT HUVECs and TERT2 HUVECs were antibody labelled for CD31, an endothelial cell marker to assess whether phenotype was maintained after CRISPR-Cas9 editing. Both cell lines were still positive for CD31 expression with and without genome editing (Figure 4.7).

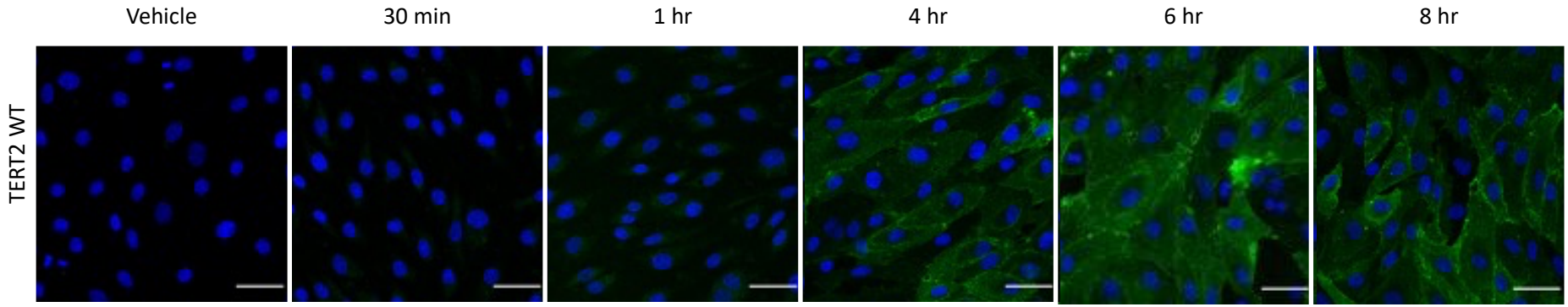

Figure 4.2 ***The TERT2 HUVEC TNF alpha time course response was similar to that seen in WT HUVECs.*** *WT TERT2 HUVECs were treated with 1 nM TNF alpha (0 - 8 hr, 37℃ 5% CO2) and immunolabelled using a anti-E-selectin monoclonal antibody (as used in Chapter 3). E-selectin was expressed after 4 – 8 hr. Where blue signal = H33342 stained nuclei and green signal = Alexa Fluor 488 secondary antibody labelled E-selectin. Scale bar = 50 µm.*

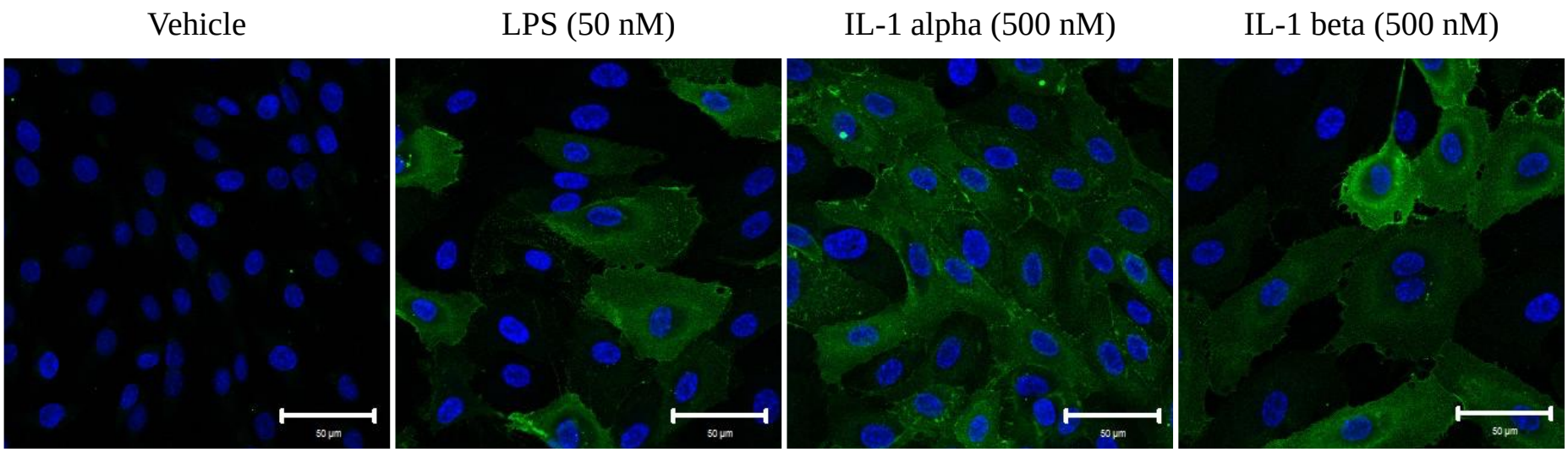

Figure 4.3 ***WT TERT2 HUVECs responded to LPS, IL-1 alpha and IL-1 beta stimulation.*** *WT TERT2 HUVECs were treated with 50 nM LPS, 500 nM IL- alpha and 500 nM IL-1 beta (6 hr, 37°C 5% CO2) and immunolabelled using a anti-E-selectin monoclonal antibody (as used in Chapter 3). E-selectin expression (green signal) was observed in all conditions, however notably IL-1 alpha induced expression in a greater number of cells in the field of view in comparison to IL-1 beta and LPS. Where blue signal = H33342 stained nuclei and green signal = Alexa Fluor 488 secondary antibody labelled E-selectin. Scale bar = 50 µm.*

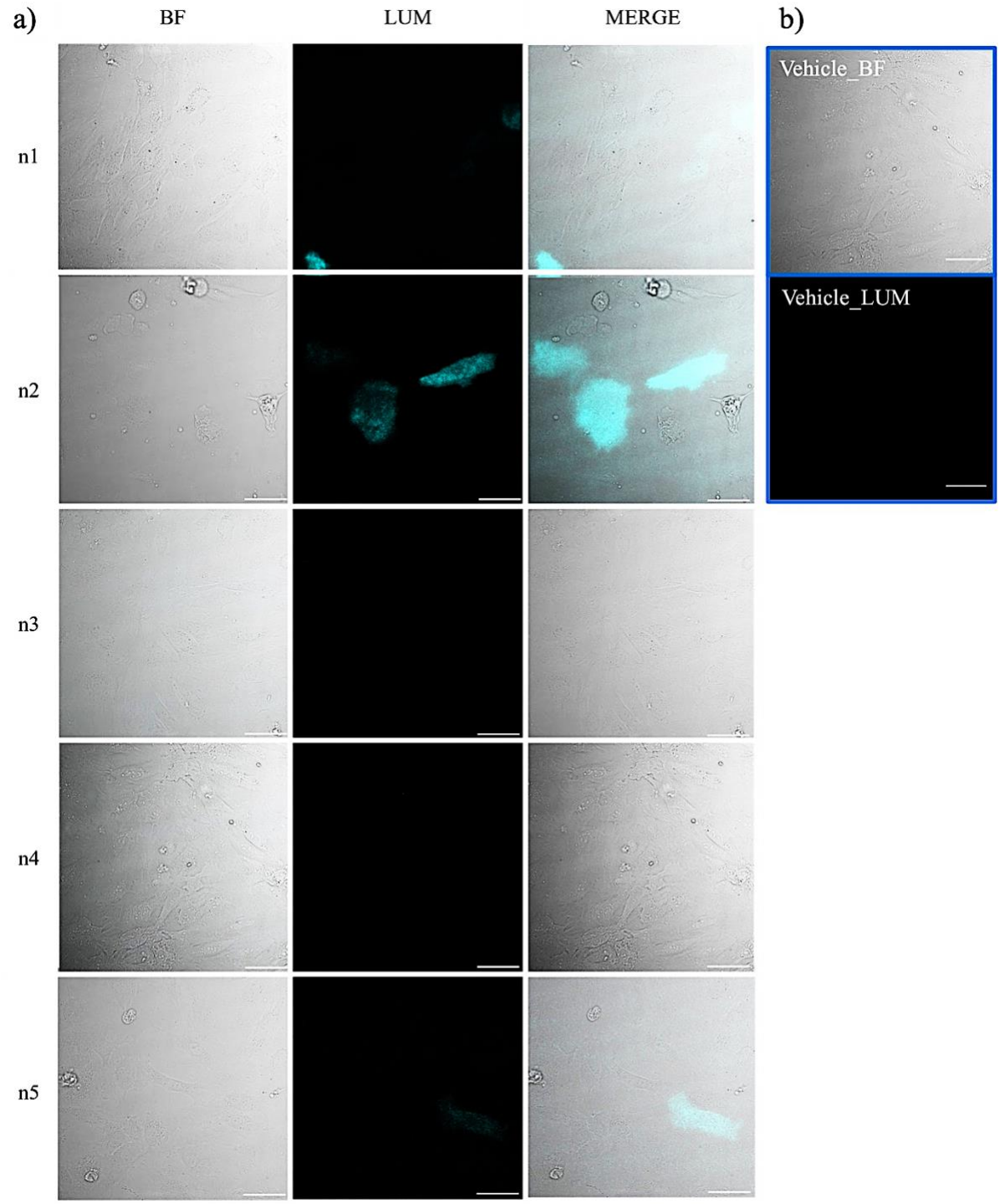

Figure 4.4 ***CRISPR-Cas9 edited WT HUVECs had differential electroporation and editing efficiencies between repeats****. a) Representative images from each repeat are presented under n1 – 5. Edited HUVECs were plated onto Cellvis 4-chamber 35mm dish and stimulated with 1 nM TNF alpha alpha (37°C, 5% CO_2), before addition of LgBiT and Furimazine. b) Vehicle BF and LUM images displayed no detectable luminescence. Images were acquired using a bioluminescence LV200 widefield microscope and edited using FIJI imageJ. Where BF = brightfield, LUM= luminescence and MERGE = overlay. scalebar = 50µm. Only a few cells in the field of view (≤ 3) were found to be expressing HiBiT E-selectin visible using LV200 microscope. N=3 and n=4 gave no visible output of HiBiT E-selectin luminescence signal.*

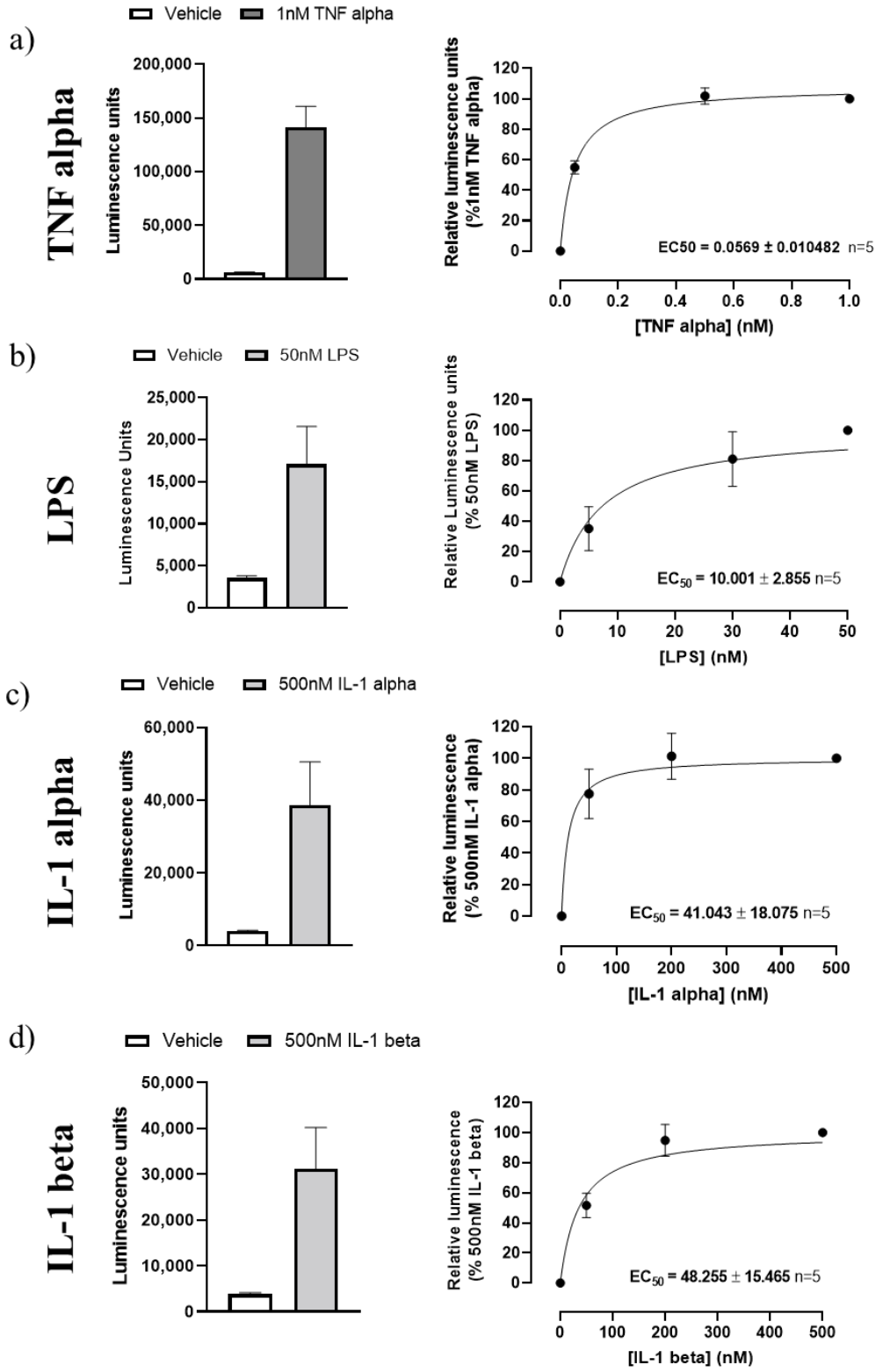

Figure 4.5 ***NanoBiT allowed determination of HiBiT tagged endogenous E-selectin expression in response to TNF alpha, LPS, IL-1 alpha and IL-1 beta. on WT HUVECs*** *a) TNF alpha was the most potent stimulant of E-selectin expression, with luminescence units > 8 fold higher compared to b) LPS, > 4-fold higher than seen due to c) IL-1 alpha and d) IL-1 beta stimulation. The cytokines listed in order of potency were TNF alpha (EC_{50} 0.0569 ± 0.0105), LPS (EC_{50} 10.001 ± 2.855), IL-1 alpha (EC_{50} 41.043 ± 18.075) and finally IL-1 beta (EC_{50} 48.255 ± 15.465) (n=5). Error bars = SEM*

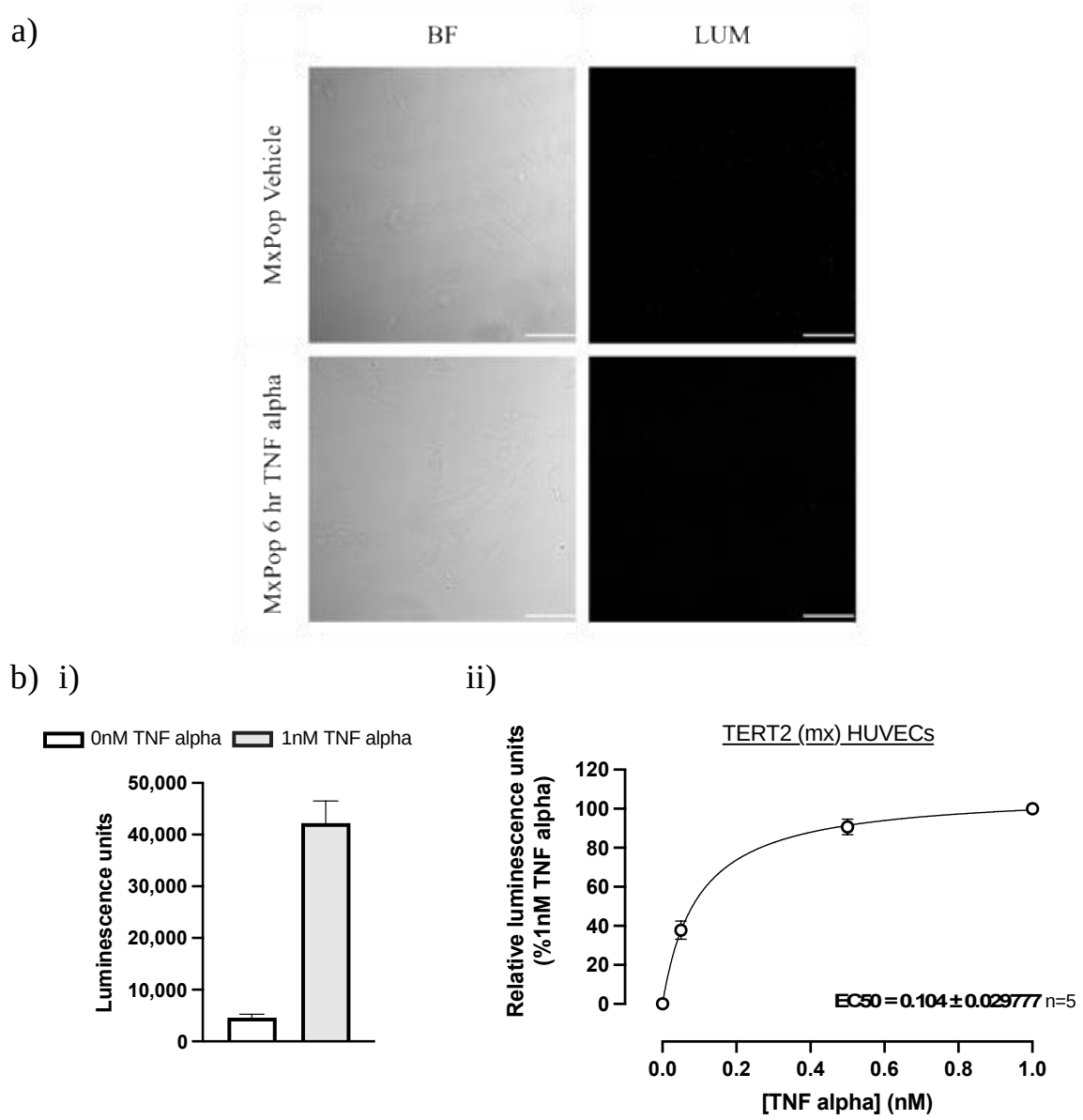

Figure 4.6 ***The LV200 widefield microscope could not detect HiBiT E-selectin expression in mixed population edited TERT2 HUVECs (MxPop), however luminescence was detected using the PHERAstar platereader.*** *a) Representative luminescence images showed no difference between vehicle and TNF alpha stimulated edited TERT2 HUVECs. Where BF = Brightfield and LUM = Luminescence. b) i) luminescence was increased from basal peaking at 42,260 luminescence units measured using a BMG Pherastar FS. ii) a concentration response for 0 – 1 nM TNF alpha was conducted and an EC_{50} value of 0.104 nM ± 0.030 was calculated from n=5 (Error bars = SEM).*

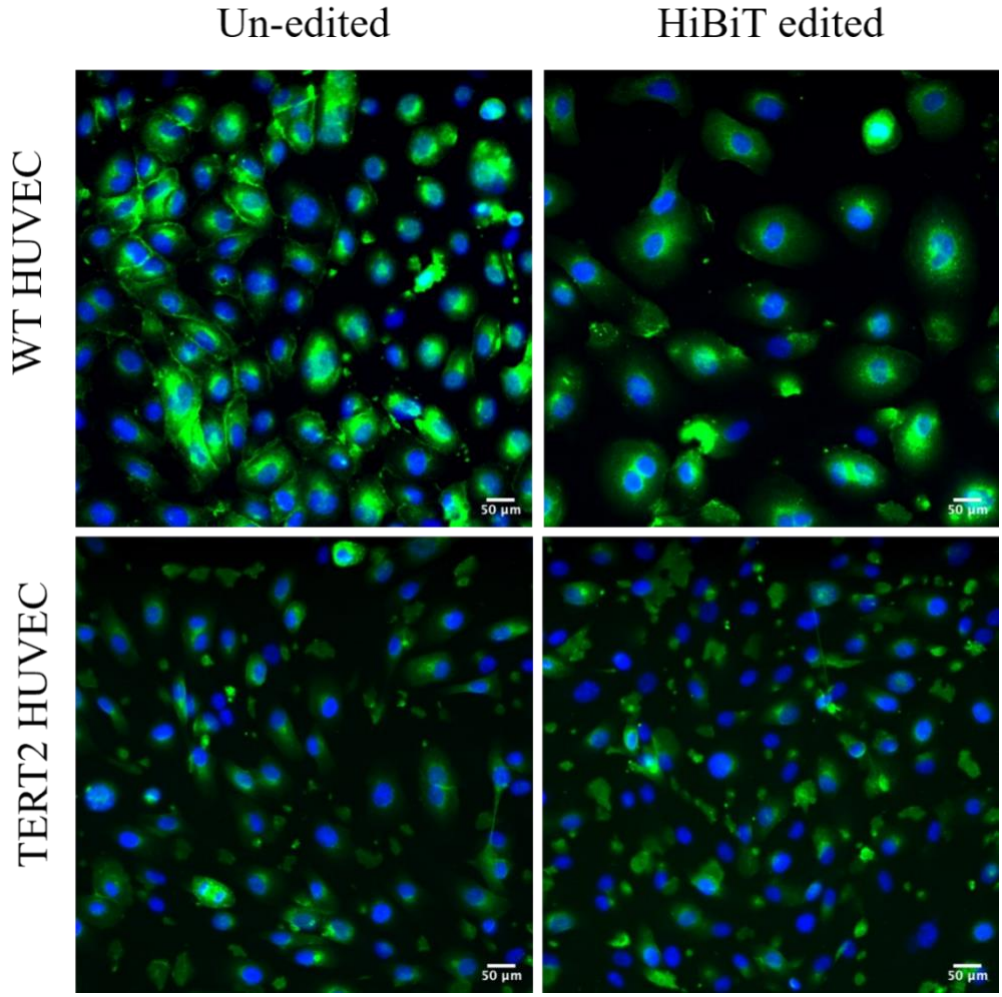

Figure 4.7 ***The genome editing of WT HUVECs and WT TERT2 HUVECs did not affect endothelial cell phenotype.*** *WT HUVECs and TERT2 HUVECs were labelled for CD31 expression using an anti-CD31 primary antibody and Alexa Fluor-488 secondary antibody. CD31 expression was compared for HiBiT edited or unedited cells. Blue signal = H33342 labelled nuclei and green signal = CD31. Scale bar = 50µm. Images were taken using an IX micro widefield microscope and are representative of n=3.*

4.2.3 Production HiBiT E-selectin TERT2 clone

Edited TERT2 HUVECs (mx) were dilution cloned and wells which contained only one colony (via visual examination) were screened for luminescence output after TNF alpha stimulation (1 nM, 6 hr, 37°C 5% CO_2) (Figure 4.8a). It was found that the wells, B4, H3 and C8 produced the highest luminescence output (mean LU = 332,768 LU, 617,535 LU and 1,235,737 LU respectively). The clones were then screened again using TNF alpha concentration response courses to analyse differential E-selectin expression. Clone C8 had the lowest EC_{50} value (0.0604 nM) and the highest luminescence output which was 2-fold or 4-fold higher than B4 or H3 respectively (Figure 4.8b-d). The EC_{50} values were also 4-fold and 10-fold higher in H3 and B4 respectively compared to C8, suggesting that clone C8 was more sensitive to TNF alpha stimulation and the most comparable to the edited WT HUVEC TNF alpha response (WT HUVEC TNF alpha EC_{50}: 0.0569 nM). Clone C8 was then analysed for HiBiT insertion using PCR, electrophoresis and Sanger sequencing (Figure 4.9). After amplification of the edited DNA region (370 bp) using PCR, a +45 bp addition was visualised in Clone C8 compared to wildtype; indicative of the HiBiT-GSSG insertion (Figure 4.9b). Furthermore, only one band was observed, evidencing that both alleles were edited for HiBiT and the clone C8 was homozygous for HiBiT insertion. The same experimental procedure indicated a heterozygous edit for 'B4' as two bands were observed representing the absence and presence of HiBiT edition (Figure 4.9a) per allele. The N-terminal region for clone C8 was Sanger sequenced, and the +45 bp HiBiT-GSSG sequence (GTGAGCGGCTGGCGGCTGTTCAAGAAGATTAGC – GGGAGTTCTGGC) was detected in clone C8 but absent in WT HUVEC genomic DNA (Figure 4.9c). This edit did not affect the HUVEC phenotype, as both early and late passage clone C8 TERT2 HUVECs stained positively for CD31 expression (Figure 4.10).

Unexpectedly, this HiBiT addition into clone C8 disrupted anti-E-selectin antibody binding, potentially due to the HiBiT location disrupting/sterically hindering the antibody epitope or due to HiBiT induced conformational change of E-selectin occluding access of the antibody. This is speculated as the anti-E-selectin antibody was unable to bind to clone C8, after TNF alpha stimulation (Figure 4.11) but was able to bind to unedited E-selectin in WT TERT2 HUVECs (Figure 4.2). Clone C8 was labelled with an anti-HiBiT antibody in the same TNF alpha conditions (0 -8 hr TNF alpha stimulation, 1 nM 37°C 5% CO_2) and HiBiT E-selectin was labelled successfully (Figure 4.11).

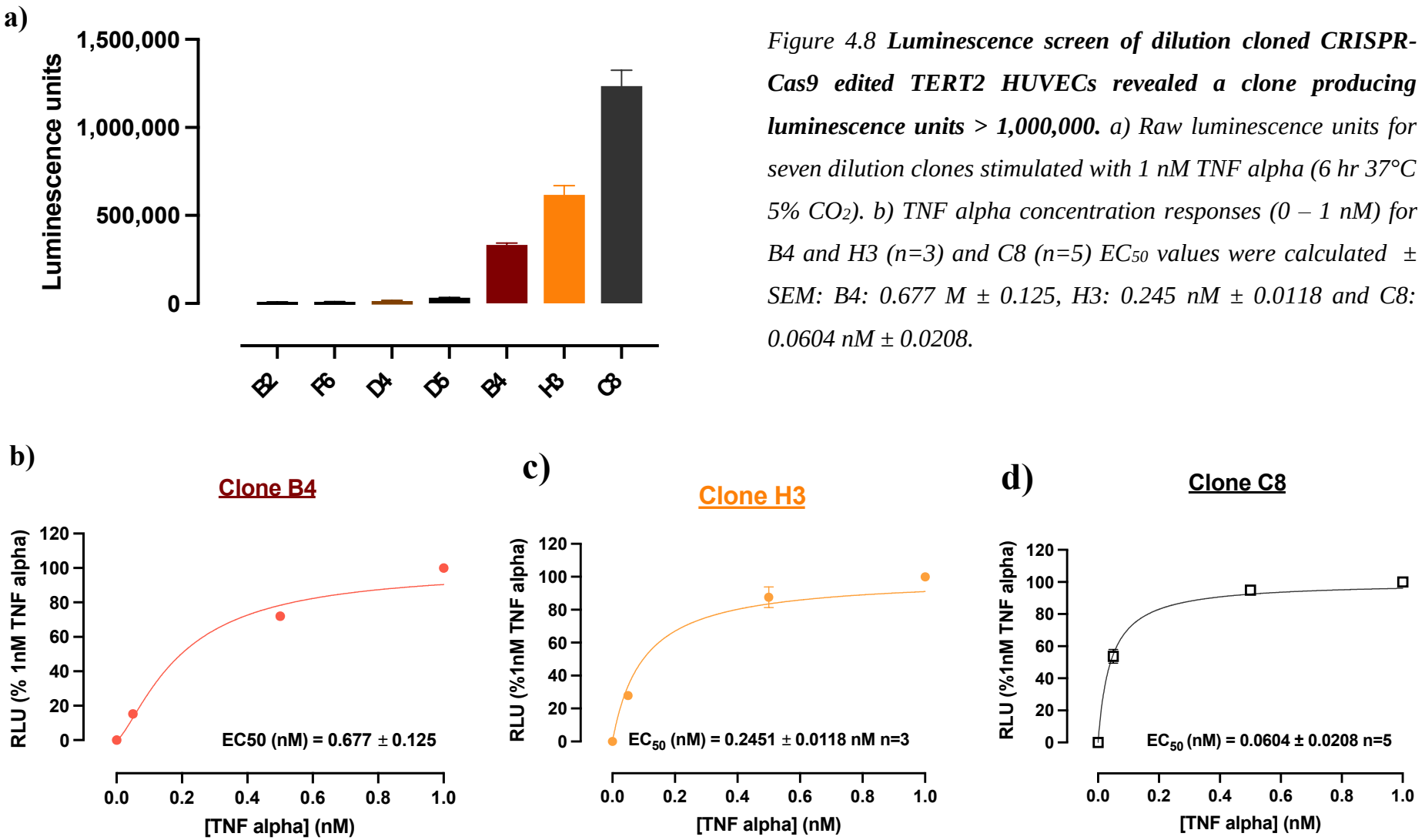

Figure 4.8 ***Luminescence screen of dilution cloned CRISPR-Cas9 edited TERT2 HUVECs revealed a clone producing luminescence units > 1,000,000.*** *a) Raw luminescence units for seven dilution clones stimulated with 1 nM TNF alpha (6 hr 37°C 5% CO_2). b) TNF alpha concentration responses (0 – 1 nM) for B4 and H3 (n=3) and C8 (n=5) EC_{50} values were calculated ± SEM: B4: 0.677 M ± 0.125, H3: 0.245 nM ± 0.0118 and C8: 0.0604 nM ± 0.0208.*

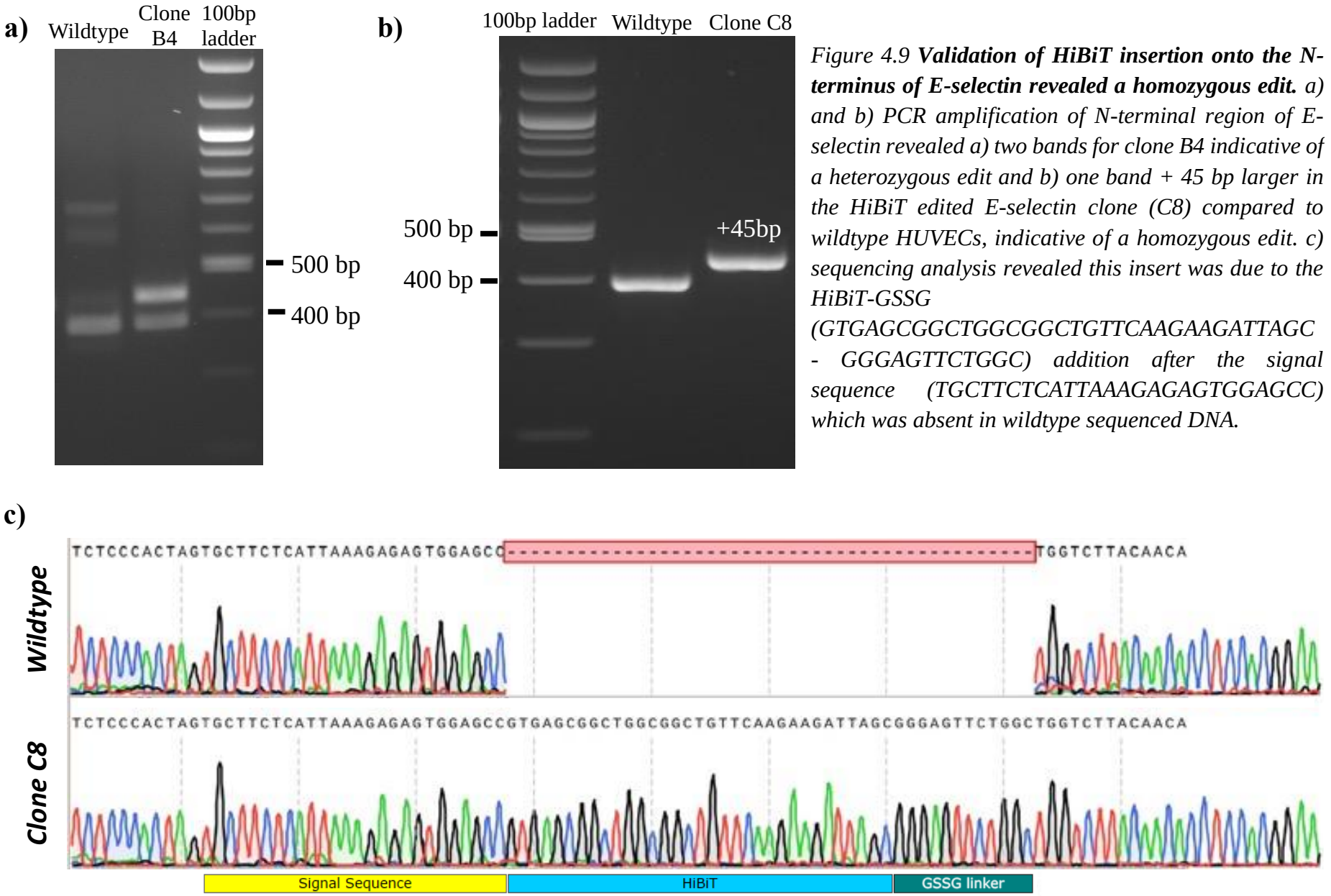

Figure 4.9 ***Validation of HiBiT insertion onto the N-terminus of E-selectin revealed a homozygous edit.*** *a) and b) PCR amplification of N-terminal region of E-selectin revealed a) two bands for clone B4 indicative of a heterozygous edit and b) one band + 45 bp larger in the HiBiT edited E-selectin clone (C8) compared to wildtype HUVECs, indicative of a homozygous edit. c) sequencing analysis revealed this insert was due to the HiBiT-GSSG (GTGAGCGGCTGGCGGCTGTTCAAGAAGATTAGC - GGGAGTTCTGGC) addition after the signal sequence (TGCTTCTCATTAAAGAGAGTGGAGCC) which was absent in wildtype sequenced DNA.*

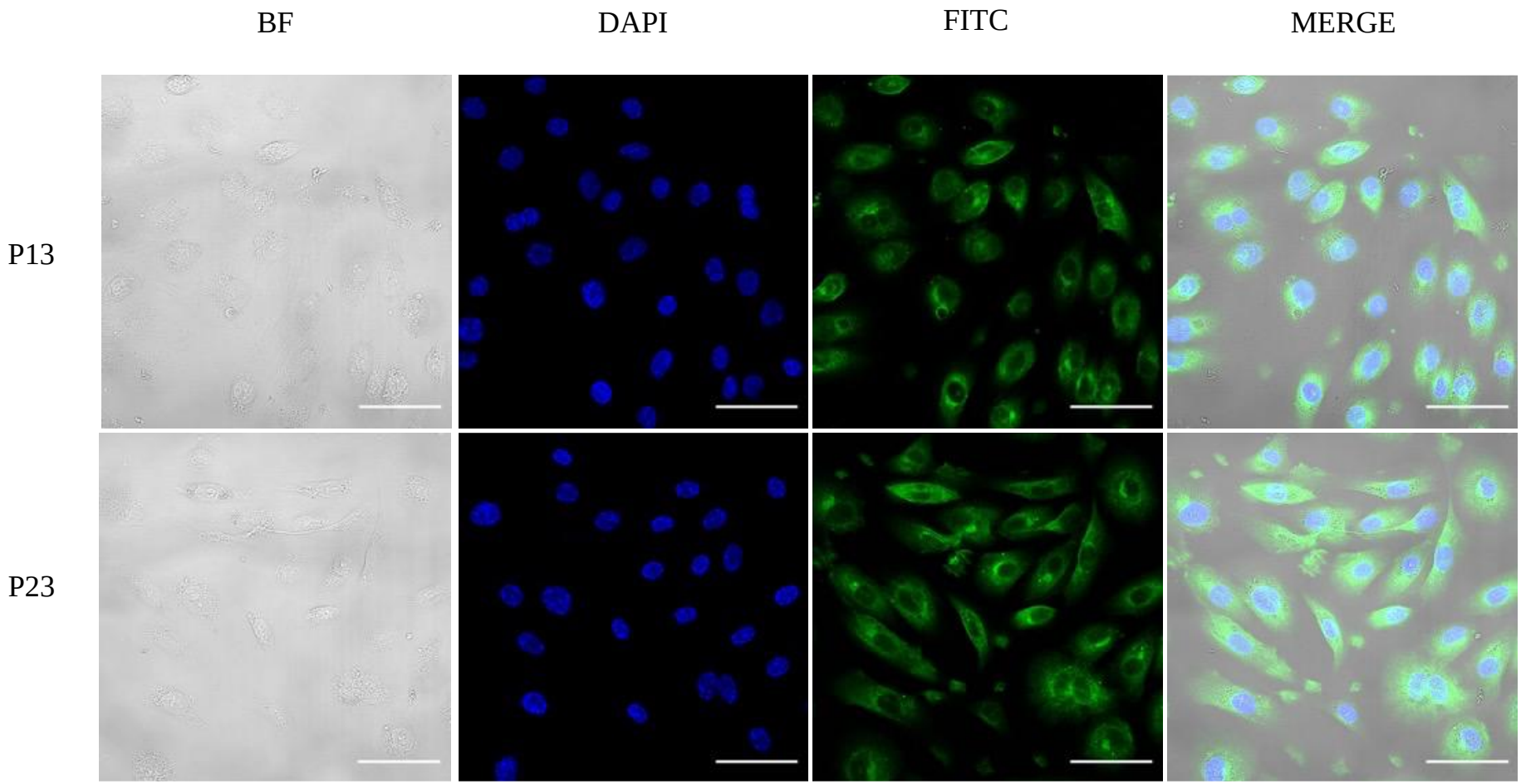

Figure 4.10 ***Clone C8 did not lose endothelial cell phenotype at either early or late passage.*** *Clone C8 was immunolabelled using an anti-CD31 primary antibody and secondary antibody conjugated to Alexa Fluor 488 (green signal), and nuclei labelled with H33342 (blue signal). Images are representative of an n=5. Early passages were P13, P15 and P16 and late passages were P23, P25 and P26. The images used in this figure are early passage = P13 and late passage = P23. Scale bar = 50 µm.*

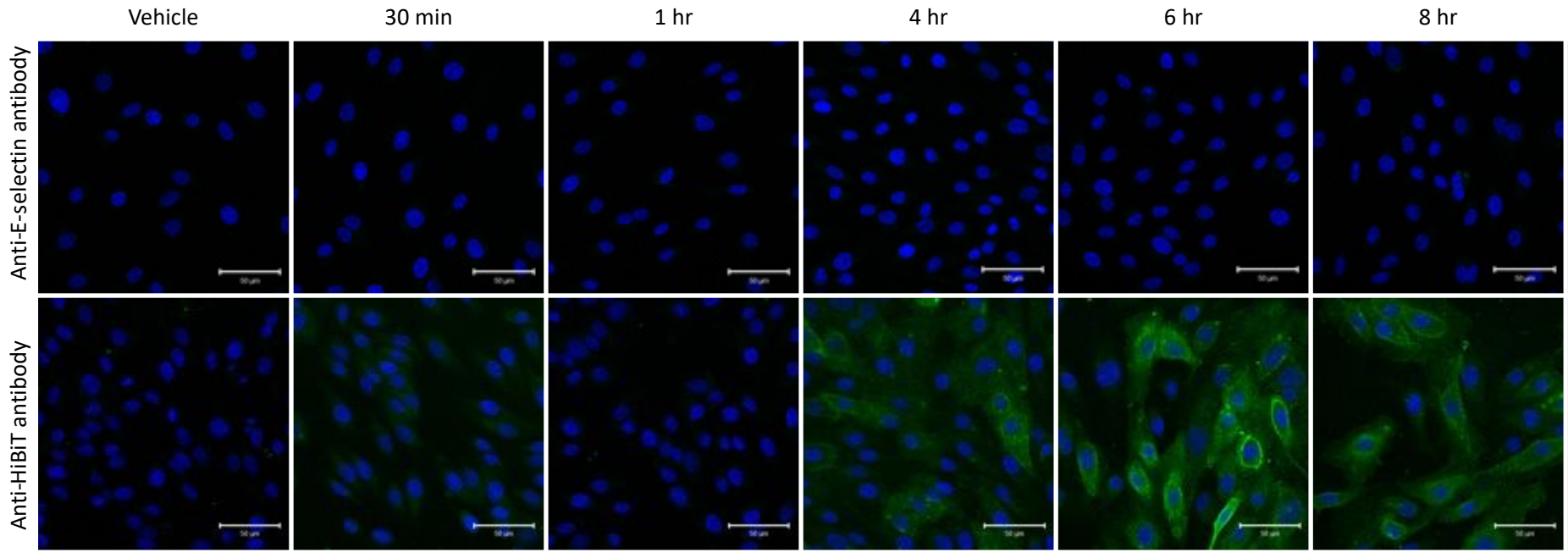

Figure 4.11 ***The anti-E-selectin primary antibody was unable to bind to HiBiT E-selectin.*** *Clone C8 was stimulated with TNF alpha (1 nM 37°C 5% CO_2) for 0 – 8 hr. Wells were then immunolabelled using either anti-E-selectin or anti-HiBiT primary antibody. No HiBiT E-selectin binding was found in clone C8 after immunolabelling with anti-E-selectin antibody, but a HiBiT E-selectin response was monitored using the anti-HiBiT primary antibody. Here, the HiBiT E-selectin expression response is similar to what was seen for WT HUVECs and WT TERT2 HUVECs responding to TNF alpha time course. Confocal images display E-selectin in green (Alexa Fluor 488) and nuclei in blue (DAPI). Scalebar = 50µm.*

4.2.4 Clone C8 inflammatory cytokine concentration response

Clone C8 revealed that like in WT HUVECs, TNF alpha was the most potent stimulant for E-selectin membrane expression, followed by LPS and IL-1 alpha and beta (Figure 4.13). The reproducibility between repeats and the similarity to the wildtype HUVEC cell line (WT (mx)) and the mixed population TERT2 HUVEC cell line (TERT2 (mx)) response, were analysed for clone C8. This was crucial to test whether the genome edit, especially in the clone, had off-target effects for the signalling of E-selectin expression.

Firstly, LV200 imaging revealed a dramatic increase in the intensity of luminescence per cell and the number of cells expressing HiBiT E-selectin in clone C8, compared to that seen in edited WT HUVEC or TERT2 HUVEC mixed populations (Figure 4.12). Quantified maximal luminescence units (LU) due to 1 nM TNF alpha stimulation (6 hr, 37°C 5% CO_2) were 6-fold higher compared to WT HUVECs (mx population), and 17-fold higher compared to TERT2 (mx population). Moreover, the assay window compared to vehicle for clone C8 was 8-fold higher than that for WT or TERT2 HUVECs mixed populations. Fold increase from vehicle was x52, x54 and x426 for WT (mx), TERT2 (mx) and clone C8 respectively. Finally, the coefficient of variation (CV) was calculated for each TNF alpha concentration response (0.05 nM, 0.5 nM and 1.0 nM) between repeat experiments in each cell line. The CV was calculated by dividing the population standard deviation by the population mean, thereby acting as a measure of the precision and repeatability of each assay for each cell line. The average CV for clone C8 was significantly lower compared to the other edited HUVECs (18.6% for clone C8 compared to 53.1% and 39.1% for WT (mx) and TERT2 (mx)) (see Table 4.1). From these comparisons, C8 gave the most sensitive and replicable HiBiT-E-selectin expression that was detectable via LV200 luminescence imaging and luminometer quantification.

The potencies of LPS, IL-1 alpha and IL-1 beta were compared between the WT (mx) and clone C8 in respect to stimulation of E-selectin expression. IL-1 alpha and IL-1 beta concentration responses in clone C8 were comparable to that of wildtype HUVEC mixed edited populations (mx), (EC_{50} values were 41 nM and 48 nM respectively in WT (mx) compared to 33 nM and 31 nM respectively in Clone C8), however this was not observed for LPS induced E-selectin expression, where the EC_{50} value was >3.5-fold more potent in clone C8 compared to edited WT HUVEC mixed population cells (C8= 2.802, WT= 10.001; see Table 4.1).

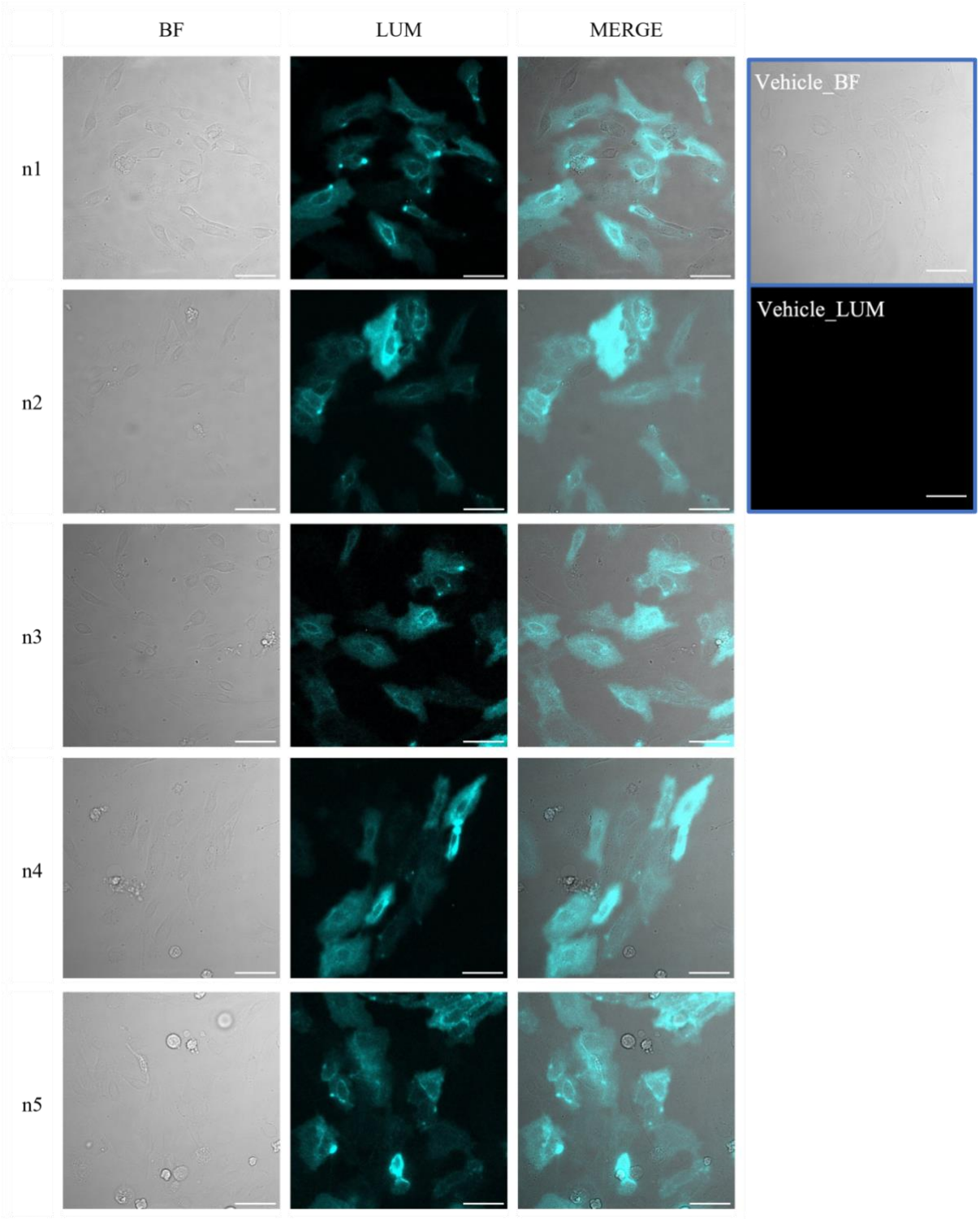

Figure 4.12 ***C8 TERT2 HUVEC clonal cells visibly expressed HiBiT E-selectin in response to 1 nM TNF alpha (6 hr 37°C 5% CO_2).*** *5 representative images from each n number are displayed. Luminescence due to cell surface expression of recomplemented LgBiT-HiBiT E-selectin was visualized (cyan blue). Vehicle wells displayed no luminescence. Where BF= brightfield, LUM = luminescence and MERGE = merged images. Scale bar = 50 µm*

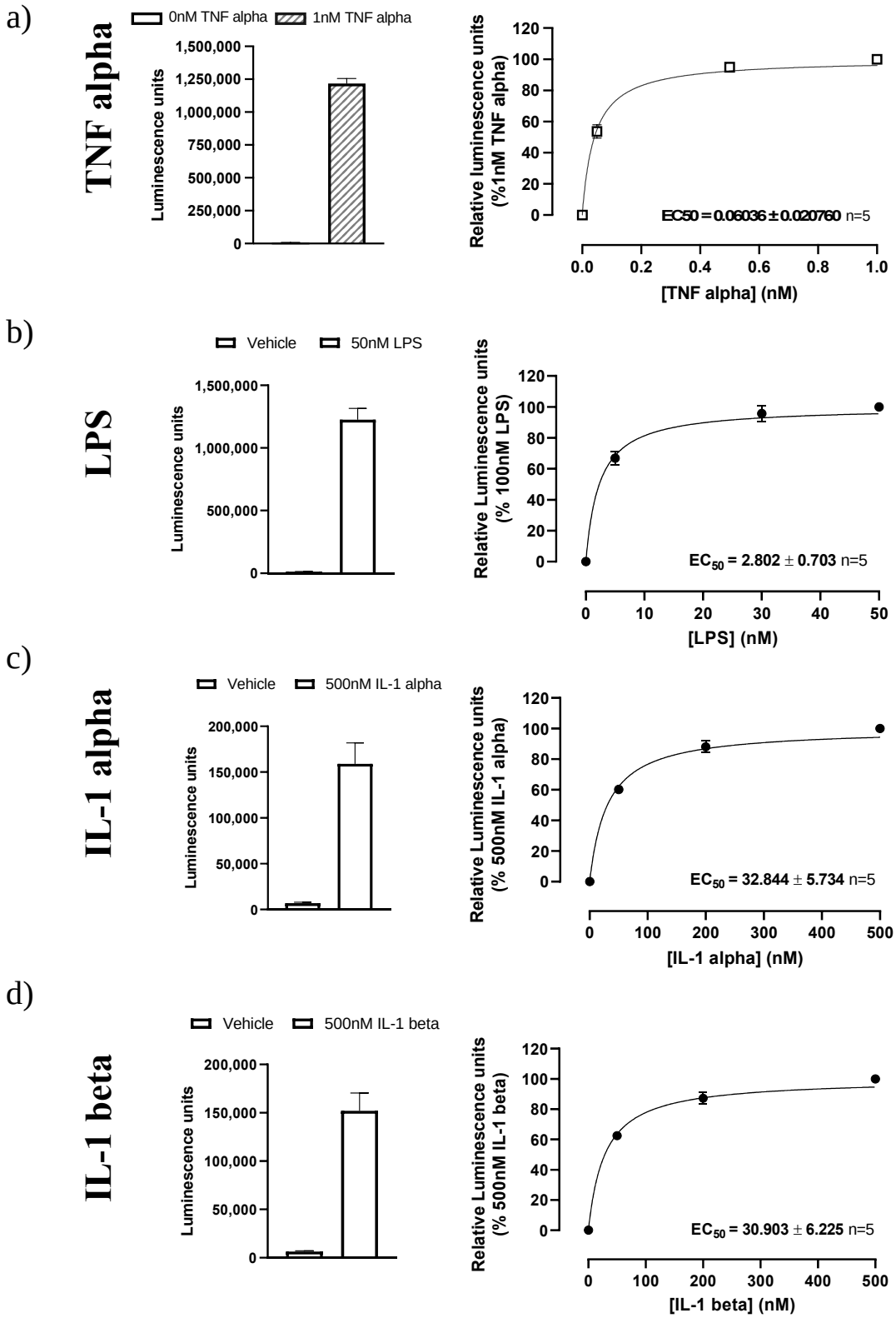

Figure 4.13 ***Like in WT edited cells, concentration response curves revealed that a) TNF alpha was the most potent inducer of E-selectin cell surface expression in comparison to b) LPS, c) IL-1 alpha and d) IL-1 beta.*** *C8 TERT2 HUVECs passage <P15 were stimulated with a) 0 – 1 nM TNF alpha, b) 0 – 50 nM LPS, c) 0 – 500 nM IL-1 alpha or d) IL-1 beta (6 hr 37°C 5% CO_2). Luminescence units were almost 10-fold higher for TNF alpha and LPS in comparison to the interleukins at maximum concentrations, and TNF alpha was > 45 fold more potent than LPS and > 500 fold more potent than IL-1 alpha or beta. Where EC_{50} = concentration in nM ± SEM.*

Table 4.1 ***The difference in EC50 and mean coefficient of variation values between WT (mx) and Clone C8***

	LPS		IL-1 alpha		IL-1 beta	
	EC_{50} (nM)	Mean coefficient of variation	EC_{50} (nM)	Mean coefficient of variation	EC_{50} (nM)	Mean coefficient of variation
WT (mx)	10.001	**61.54%**	41.043	**98.01%**	48.255	**100.14%**
Clone C8	2.802	**41.04%**	32.844	**53.27%**	30.903	**51.52%**
Fold difference	↓ 3.57	↓ 1.50	↓ 1.25	↓1.84	↓1.56	↓1.94

Table 4.2 ***In clone C8 ≥P20, the IL-1 alpha and IL-1 beta potency halved, and the LPS potency almost doubled.***

	LPS		IL-1 alpha		IL-1 beta	
	EC_{50} (nM)	*± SEM*	*EC_{50} (nM)*	*± SEM*	*EC_{50} (nM)*	*± SEM*
Clone C8 >P20	1.4936	0.361	79.58	25.03	74.82	28.94
Clone C8 P12 - P15	2.802	0.703	32.844	5.734	30.903	6.225
Fold difference	↑ 1.88	↑ 1.95	↓ 2.42	↓ 4.37	↓ 2.42	↓ 4.65

In addition, the maximal raw luminescence output detected, and ergo the expression of E-selectin induced by TNF alpha, LPS, IL-1 alpha/beta was dependent on passage number for the TERT2 HUVEC clone C8. By passage 24, the maximal luminescence output in response to the same concentration of cytokine decreased significantly ($p<0.05$ / $p<0.01$) (Figure 4.14) compared to an earlier passage. The maximal luminescence output observed at Passage 12 compared to minimum (passages 20-24) revealed decreases in luminescence units by 11-fold (TNF alpha), 30-fold (LPS), 68-fold (IL-1 alpha) and 48-fold (IL-1 beta) (Figure 4.14b). This effectively made the IL-1 alpha and IL-1 beta induced E-selectin expression 2-fold less potent however interestingly doubled the potency for LPS (Table 4.2). For this reason, passages < P15 were used in C8 experiments.

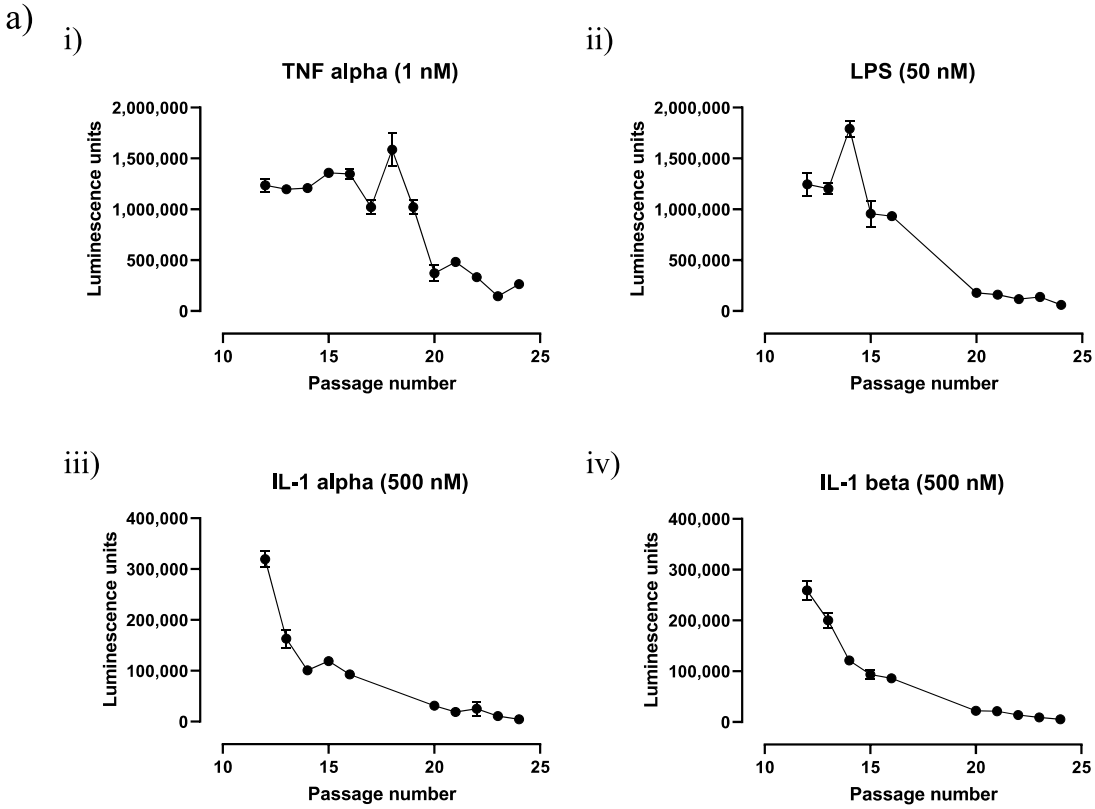

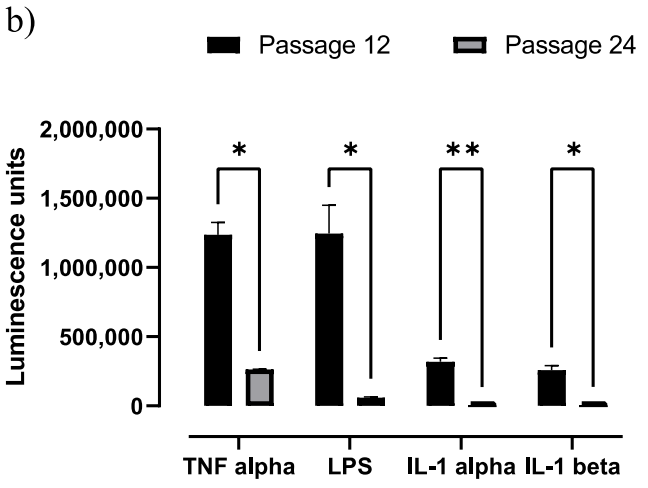

c)

	Max LU	Min LU	Fold decrease
TNF alpha	1,586,526	145,629	**11**
LPS	1,791,249	59,463	**30**
IL-1 alpha	319,599	4667	**68**
IL-1 beta	258,975	5396	**48**

Figure 4.14 ***The maximum raw luminescence units (LU) for TNF alpha, LPS, IL-1 alpha/beta was dependent on passage number.*** *a) The raw LU were isolated from each passage after stimulation with maximal concentrations of i) TNF alpha, ii) LPS, iii) IL-1 alpha, iv) IL-1 beta (6 hr 37°C 5% CO_2). b) In all cases, luminescence output was reduced significantly when comparing passage 12 to passage 24 (One-way ANOVA with post-hoc Tukey's multiple comparisons test * p <0.05 ,** p <0.01) c) Fold decrease in raw luminescence values in LU was greatest for IL-1 alpha and IL-1 beta.*

The homozygous HiBiT addition found in the TERT2 HUVEC C8 clone allowed the detection of E-selectin expression at low levels that could not be detected in the mixed population edits for either wildtype or TERT2 HUVECs. Figure 4.15 and Figure 4.16 revealed that only clone C8 detected a significant increase in luminescence units due to $VEGF_{165}a$ or histamine stimulation. This indicates how important it is for every cell to be edited to enable detection of E-selectin expression at low levels, where only a few cells are expressing E-selectin. This clone was also able to show that consistent to antibody studies, $VEGF_{165}a$ or histamine were able to increase the TNF alpha induced increase in E-selectin expression by 15% and 27% respectively ($p<0.05$) (Figure 4.17).

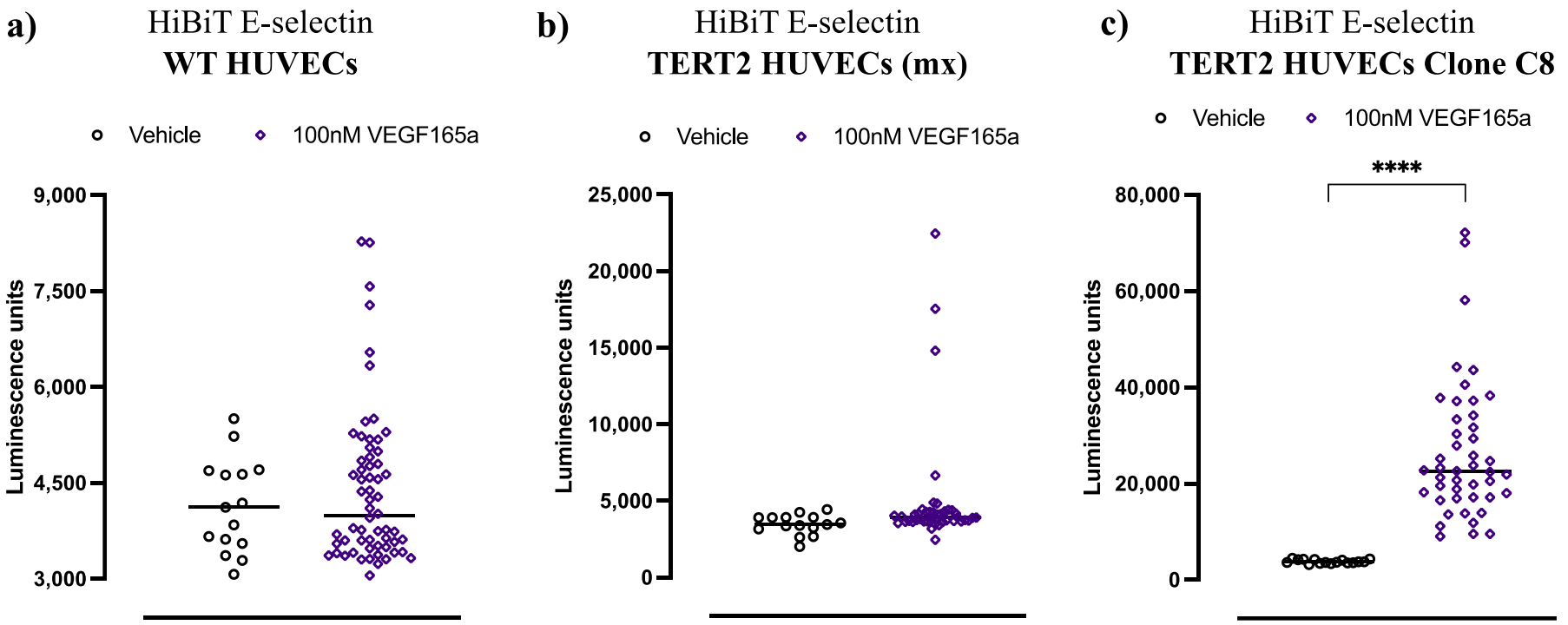

Figure 4.15 ***Only Clone C8 showcased significantly increased HiBiT E-expression in response to VEGF165a (100 nM, 37°C 5% CO_2).*** *Where each point represents a replicate well. a) Mixed population edited WT HUVECs and b) mixed population edited TERT2 HUVECs were unable to detect a significant increase in E-selectin expression in response to $VEGF_{165}$a stimulation c) HiBiT E-Selectin cell surface expression was detected in TERT2 HUVEC Clone C8 following $VEGF_{165}$a stimulation, and a significant increase from vehicle was calculated (unpaired t-test, **** p = <0.0001)*

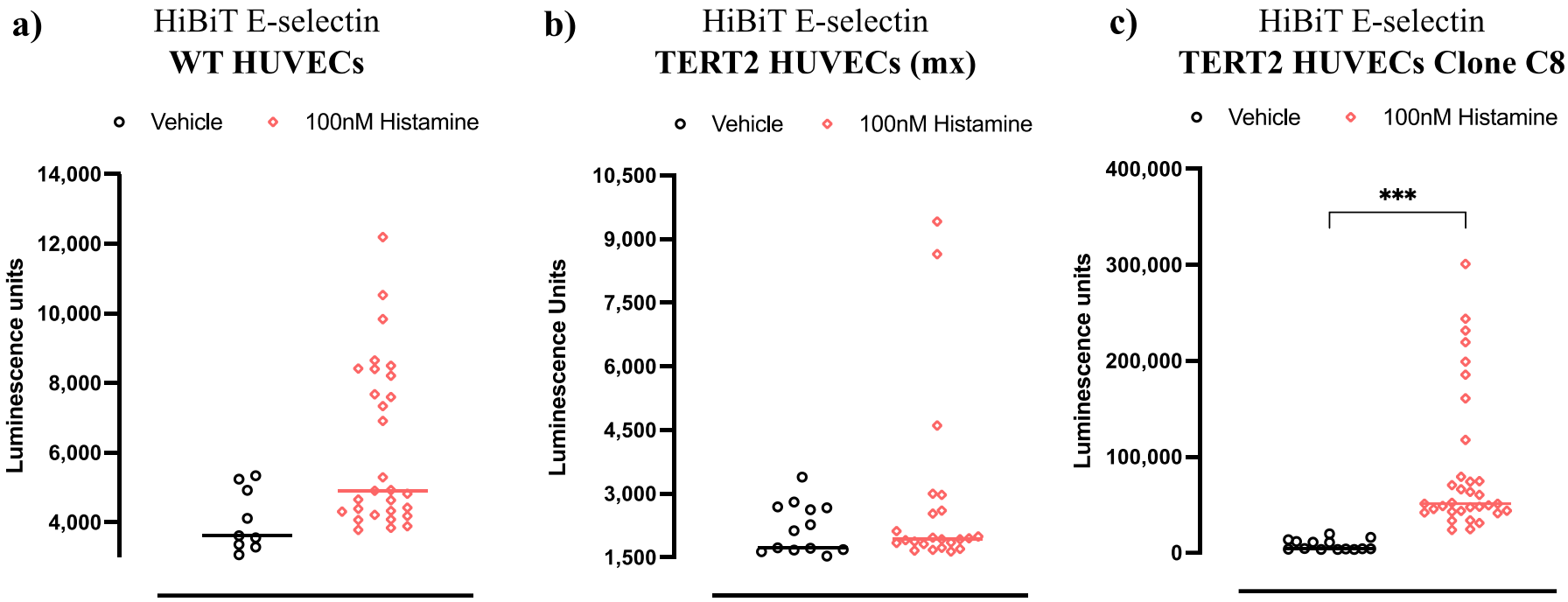

Figure 4.16 ***Only Clone C8 showcased significantly increased HiBiT E-expression in response to Histamine (100 nM, 37°C 5% CO_2).*** *Where each point represents a replicate well. a) Mixed population edited WT HUVECs and b) mixed population edited TERT2 HUVECs were unable to detect a significant increase in E-selectin expression under the same conditions, although some repeats found a significant response (12 repeats >6000 luminescence units in WT HUVECs and 3 repeats >4500 luminescence units in TERT2 HUVECs).c) Clone C8 was able to detect a significant increase in E-selectin expression (Unpaired t-test *** p = 0.0003)*

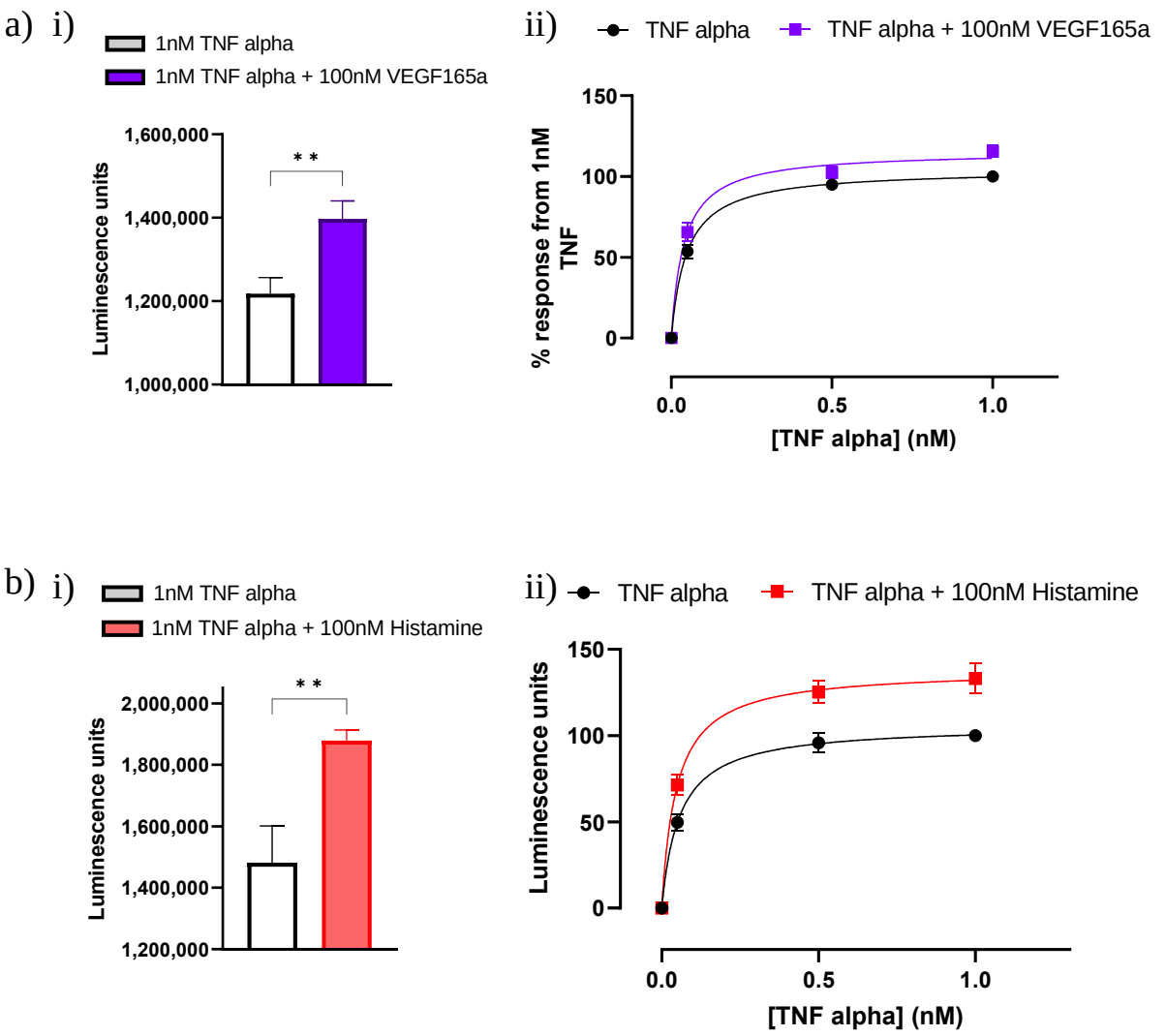

Figure 4.17 ***a) VEGF$_{165}$a and b) Histamine significantly enhanced the TNF alpha induced E-selectin expression in Clone C8.*** ***c)*** *VEGF$_{165}$a induced a 15% increase in expression (unpaired t-test **p = 0.0044) and histamine induced a 27% increase in expression compared to TNF alpha stimulation alone (unpaired t-test **p = 0.0034) (n=5, error bars = SEM).*

c)

	% Increase in luminescence (Co-stimulated with 1 nM TNF alpha)
Histamine	27
VEGF165a	15

4.2.5 Clone C8 inflammatory cytokine 15 hr kinetic screen

A 15 hr kinetic screen of cytokine induced E-selectin expression was optimised in clone C8 using TNF alpha (1 nM), and Opti-MEM supplemented with Endurazine substrate and LgBiT (Figure 4.18). Firstly, the presence of cell culture serum (2.2% LVES) in the buffer reduced the luminescence output significantly (Figure 4.18ai). LgBiT depletion was also not observed over the course of 15 hr as suspected; addition of LgBiT for 15 hr / 20 min and addition of 10^{-9} nM purified HiBiT in both conditions produced no significant difference in luminescence output (Figure 4.18ai/ii) in both serum and serum-free conditions. Finally, it was concluded that a higher concentration of Endurazine was required, as prolonged expression was seen at higher concentrations (dilution 1:100) but not concentrations 5x lower (dilution 1:500) where expression decreased after 8 hr stimulation (Figure 4.18b). After optimization of Endurazine and serum concentrations, a TNF alpha induced response was performed in the absence of serum (Figure 4.19). Like in previous optimization, there was no LgBiT depletion observed with this higher concentration of Endurazine used, and like in concentration response experiments, a significant increase in luminescence output was observed after 8 hr stimulation with 1 nM TNF alpha (LU: 630,000, $p<0.0001$) (Figure 4.19a/b). Data were normalised to 6 hr stimulation, and the kinetics revealed that E-selectin was expressed maximally over the course of 15 hr (Figure 4.19c)

Kinetics assays for effects of LPS, IL-1 alpha/beta, $VEGF_{165}a$, and histamine stimulation were then determined using this assay set up (Figure 4.20 and Figure 4.21). Stimulation with LPS resulted in the second largest increase in HiBiT E-selectin cell surface appearance (after TNF alpha; Maximal LU: 112,890), followed by IL-1 alpha (Maximal LU: 47,528), IL-1 beta (Maximal LU: 26,524) $VEGF_{165}a$ (Maximal LU: 7314) and finally histamine (Maximal LU: 3704). In all cases a decrease in E-selectin expression was observed after a 6 - 8 hr time point by 50% - 70% for LPS, IL-1 alpha/beta and Histamine and 36% for $VEGF_{165}a$ (Figure 4.20 and Figure 4.21d). Surprisingly, an increase in E-selectin expression was also observed in vehicle (see Figure 4.21aii/bii and Figure 4.22). Investigation of endpoint concentration response vehicle LU found that vehicle wells averaged 8485 LU (TNF alpha), 5852 LU (LPS), 4526 LU (IL-1 alpha) and 4954 LU (IL-1 beta) (Figure 4.22a). However, the LU correlated with the decreasing luminescence output from the wells directly below each vehicle well. Specifically in response to 0.05 nM TNF alpha, 1 nM LPS, and 13 nM IL-1 alpha / IL-1 beta, suggesting that the LU in vehicle could be due to bleedthrough luminescence from ligand

treated wells. However, when vehicle wells were placed on the opposite end of the 96 well plate in kinetics experiments, cytokine-independent expression of E-selectin was still observed with mean LU of 2130 at 8 hr (n=5) (Figure 4.22b). E-selectin expression peaked at 8 hr and produced prolonged expression for 15 hr. Despite this, the lower levels of $VEGF_{165}a$ and histamine induced E-selectin expression were still significantly higher than in vehicle treated wells (8 hr, $P < 0.05$ and 0001 respectively) (Figure 4.21ai/bi).

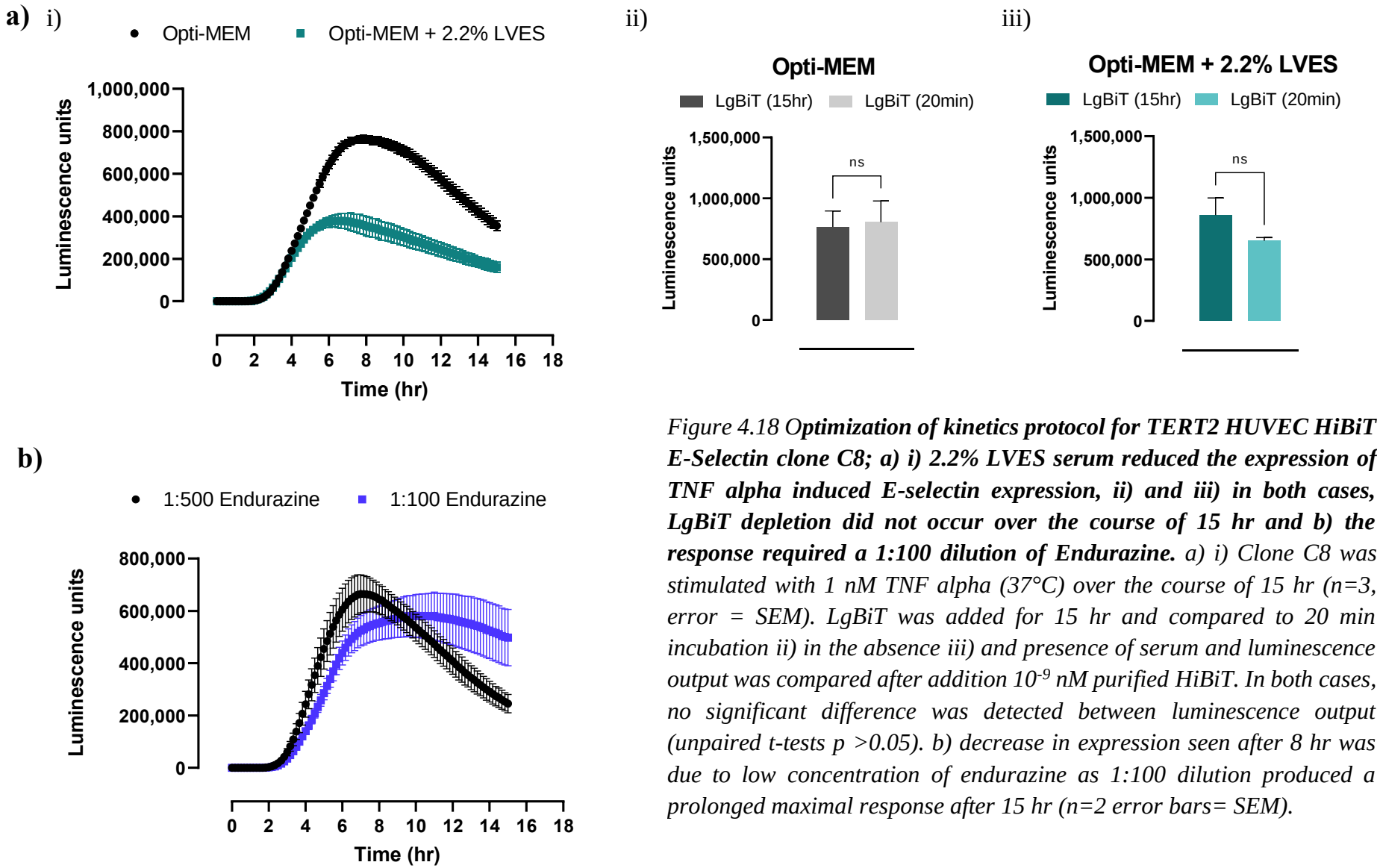

Figure 4.18 ***Optimization of kinetics protocol for TERT2 HUVEC HiBiT E-Selectin clone C8; a) i) 2.2% LVES serum reduced the expression of TNF alpha induced E-selectin expression, ii) and iii) in both cases, LgBiT depletion did not occur over the course of 15 hr and b) the response required a 1:100 dilution of Endurazine.*** *a) i) Clone C8 was stimulated with 1 nM TNF alpha (37°C) over the course of 15 hr (n=3, error = SEM). LgBiT was added for 15 hr and compared to 20 min incubation ii) in the absence iii) and presence of serum and luminescence output was compared after addition 10^{-9} nM purified HiBiT. In both cases, no significant difference was detected between luminescence output (unpaired t-tests p >0.05). b) decrease in expression seen after 8 hr was due to low concentration of endurazine as 1:100 dilution produced a prolonged maximal response after 15 hr (n=2 error bars= SEM).*

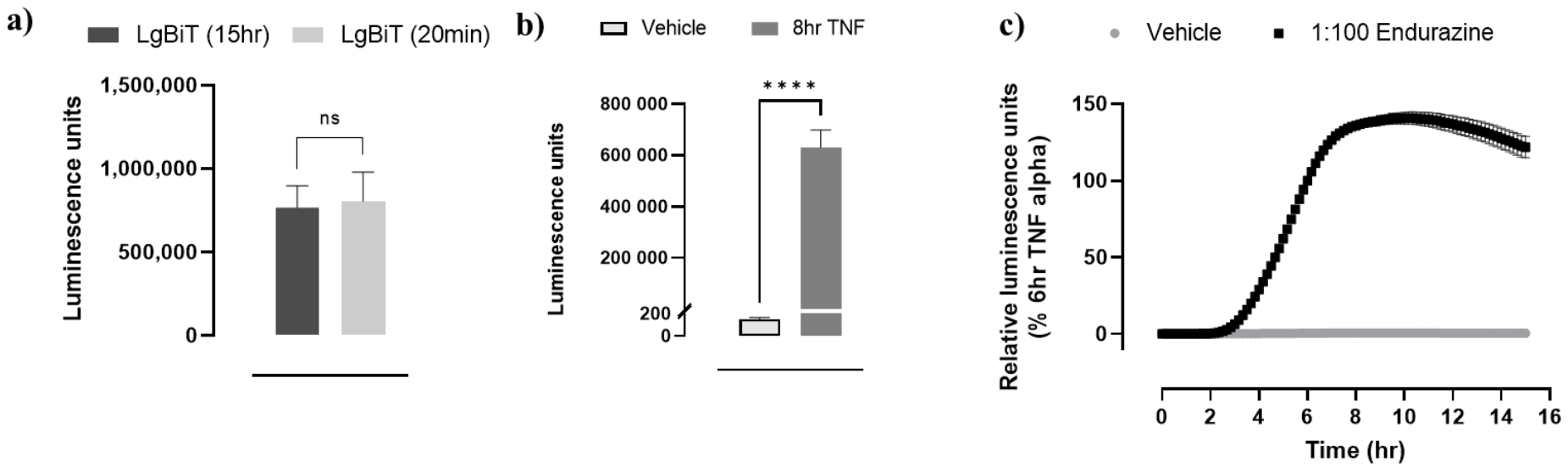

Figure 4.19 ***A kinetic screen of TNF alpha induced E-selectin expression revealed prolonged maximal expression over the course of 15 hr.*** *a) a significant increase in expression of E-selectin was seen after 8 hr (luminescence units 630,000 LU, ****p<0.0001 unpaired t-test). b) E-selectin expression peaked at 8 hr and prolonged maximal expression for 15 hr (37°C, 1:100 Endurazine, n=5 error bars=SEM). c) LgBiT depletion did not occur as no significant difference in luminescence unit output was observed between addition for 15 hr and 20 min after incubation with 10^{-9} nM purified HiBiT.*

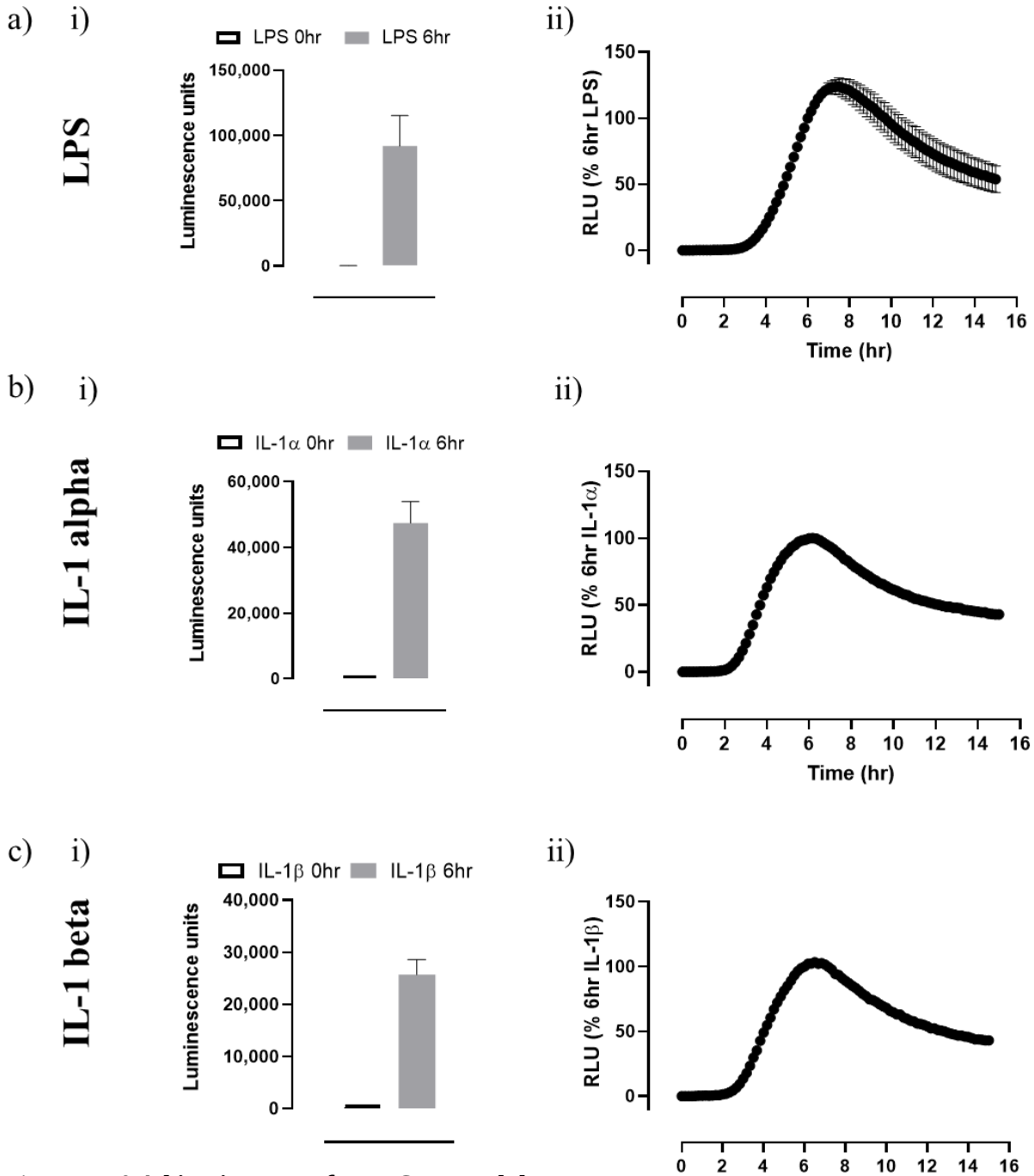

Figure 4.20 ***A kinetic screen for LPS, IL-1 alpha / beta revealed that all ligands induced HiBiT E-selectin expression that reduced by >50% after 15 hr stimulation compared to peak expression at 6 – 8 hr.*** *i) (all) an increase in luminescence units was observed after 6 hr incubation (37°C) with a) LPS, b) IL-1 alpha and c) IL-1 beta. ii) (all) kinetics over 15 hr was performed (37°C), expression peaked at 6 – 8 hr time point. d) expression reduced after 15 hr by 69% for LPS, and 57% for both IL-1 alpha and IL-1 beta.*

d)

	% Reduction in mean luminescer (6 hr vs 15 hr)
LPS	69
IL-1 alpha	57
IL-1 beta	57

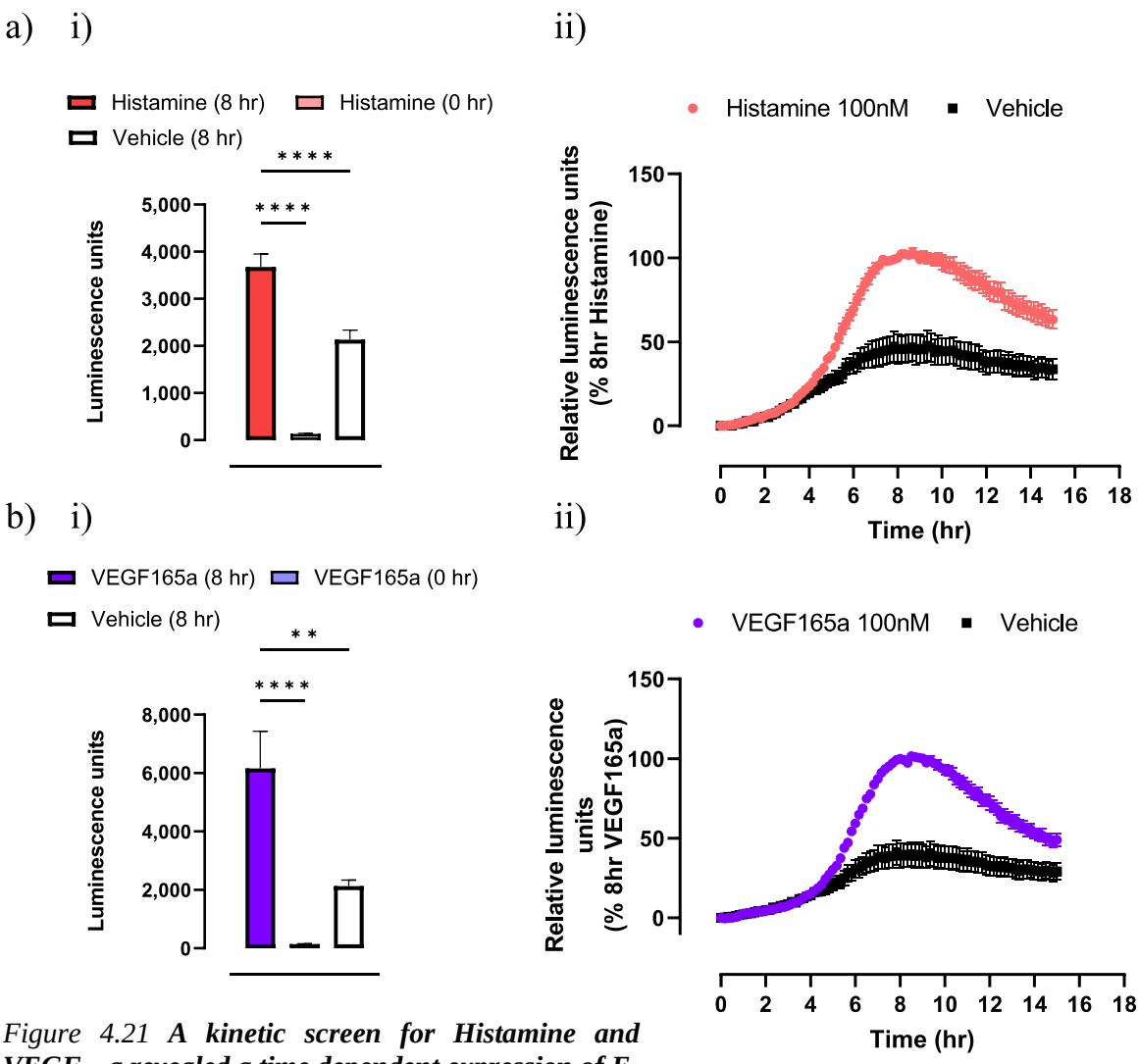

Figure 4.21 ***A kinetic screen for Histamine and VEGF$_{165}$a revealed a time dependent expression of E-selectin peaking at 8 hr.*** *a) i) and b) i) both histamine and VEGF$_{165}$a induced a significantly increased expression after 8 hr of stimulation compared to basal levels (0 hr) and compared to vehicle (8 hr) (one-way ANOVA with post-hoc Tukey's multiple comparisons test ** $p < 0.05$ and **** $p < 0.0001$). a) ii) and b) ii), both kinetic screens reveal peak of expression at 8 hr which c) reduced by 59% for histamine and 36% for VEGF$_{165}$a induced expression after 15 hr of stimulation.*

c)

	% reduction in luminescence (6 hr vs 15 hr)
Histamine	59
VEGF165a	36

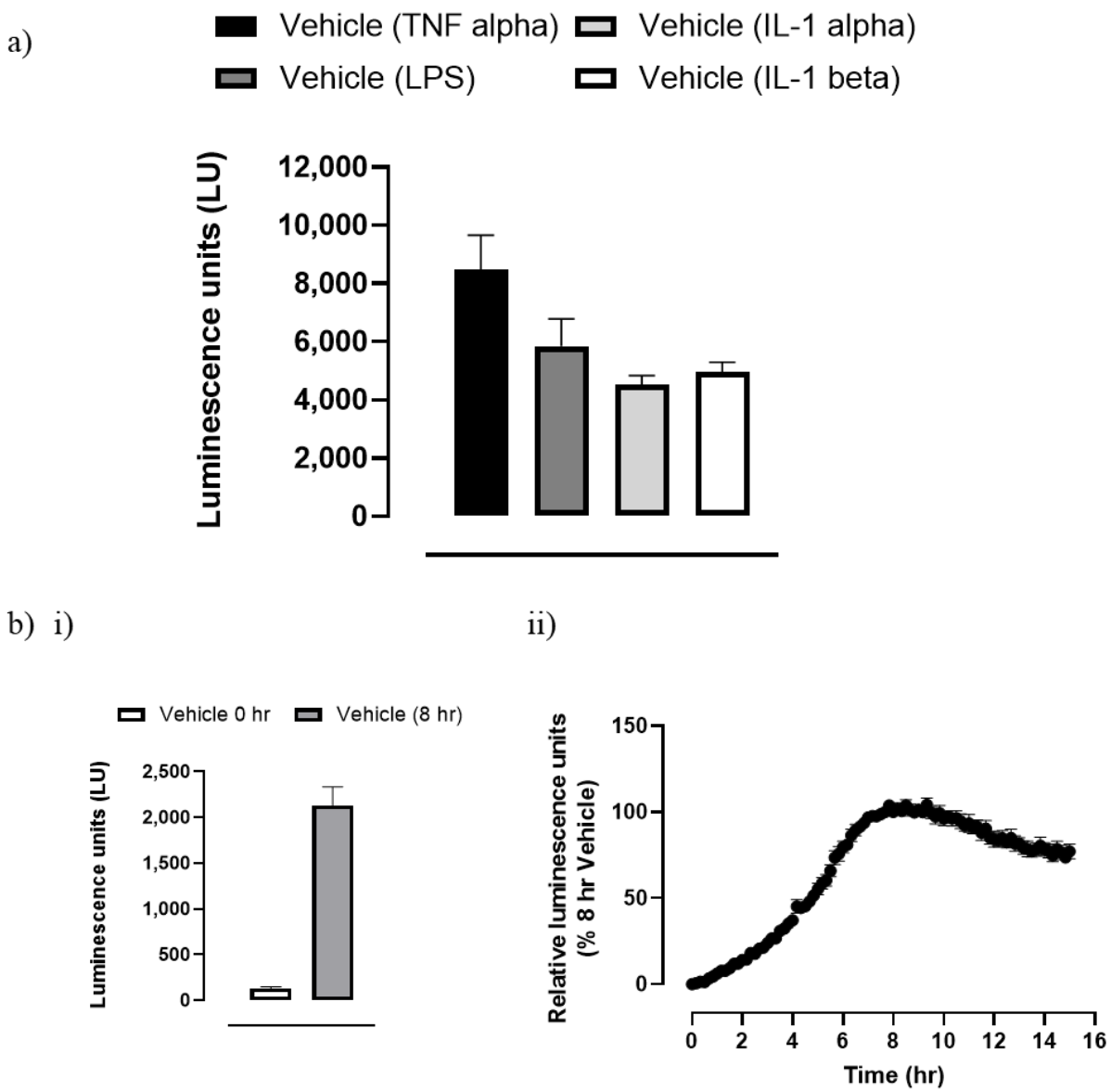

Figure 4.22 ***Cytokine independent expression of E-selectin was observed in TERT2 HUVEC HiBiT E-selectin clone C8 cells****. A) luminescence output detected in vehicle wells in concentration response studies for TNF alpha, LPS, IL-1 alpha and IL-1 beta. b) i) and ii) When normalized to 8 hr vehicle LU, E-selectin expression was detected peaking at 8 hr and remained relatively high for 15 hr from kinetics experiments data.*

The clone C8 kinetics response was compared to alkaline phosphatase quantified TNF alpha time course response from Chapter 3. This comparison revealed that the Clone C8 curve shifted to the right in the TNF alpha time course response (Figure 4.23). This was indicative of a more latent E-selectin expression in HiBiT E-selectin edited TERT2 HUVECs in comparison to unedited WT HUVECs, and in un-tagged E-selectin in comparison to HiBiT tagged E-selectin. As previously discussed, the addition of the HiBiT tag may have potentially interfered with the ability of the monoclonal anti E-selectin antibody to recognise or access its epitope (Figure 4.11). The HiBiT addition may have potentially affected E-selectin kinetics (Figure 4.23), therefore future experiments could look at comparing alternative PAM sites to modify the location of the N-terminal insertions site for HiBiT on E-selectin. Figure 4.24 describes the PAM sites available within this N-terminal region, and crispor.tefor.net resultant calculated MIT and cutting frequency determination (CFD) specificity scores.

a)

	TNF alpha EC_{50} (nM)
WT HUVEC *untagged E-selectin (Chapter 3)*	0.0155
Clone C8 TERT2 HUVEC *HiBiT tagged E-selectin (Chapter 4)*	0.0604

b)

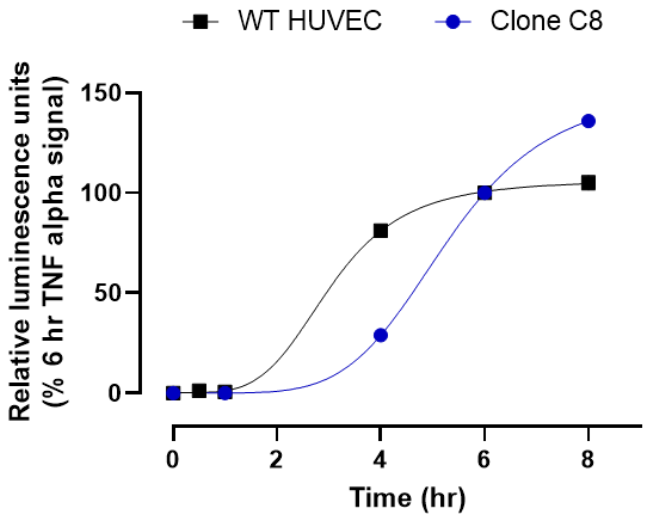

Figure 4.23 ***E-selectin expression in unedited WT HUVECs was more potently induced by TNF alpha and the time course curve for cell surface translocation was delayed for HiBiT-edited-E-selectin in TERT2 HUVEC clone C8.*** *Where unedited E-selectin in WT HUVECs was labelled using an anti-E-selectin antibody and alkaline phosphatase conjugated secondary antibody (see Chapter 3) and HiBiT E-selectin was measured using NanoBiT luminescence assay. a) Comparison of EC_{50} values revealed that TNF alpha was 3.9-fold more potent in inducing E-Selectin cell surface expression in unedited WT HUVECs compared to edited TERT2 HUVEC HiBiT E-Selectin clone C8 b) moreover, the time course of expression in clone C8 had shifted to the right, indicative of later onset of E-selectin cell surface appearance. E-selectin expression however continued to rise at a higher % from 6 hr response in clone C8. Data was normalised to 6 hr TNF alpha response in luminescence units for Clone C8 and optical density units for WT HUVECs. Error bars are present but cannot be seen; error = SEM, n=5.*

a)

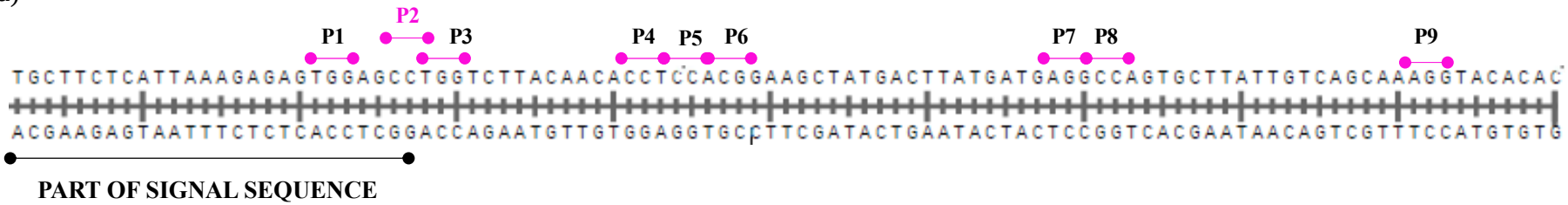

b)

PAM site	PAM sequence	MIT specificity score	CFD specificity score
P1	TGG	67	78
P2	**CCT**	**88**	**94**
P3	TGG	66	84
P4	CCT	90	94
P5	CCA	87	91
P6	CGG	74	86
P7	AGG	77	84
P8	CCA	80	90
P9	AGG	78	86

Figure 4.24 ***Future possible PAM sites to target for HiBiT insertion.*** *PAM = protospacer adjacent motif which is targeted by the Cas9 protein during CRISPR-Cas-9 editing. For Cas9, this sequence must be NGG / NCC (where N = any nucleotide base). crispor.tefor.net was used to find PAM sites in the N-terminal region of E-selectin after the signal sequence, and PAM sites with MIT / CFD specificity score > 60 were selected. A high score is reflective of low off-target effects in the genome, ranging from 0 -100. This is determined by measuring the uniqueness of a guide in the genome using the formula from the MIT CRISPR website or cutting frequency determination (CFD) calculated by MIT. a) location of PAM (P) sites 1-9 along the N-terminus of E-selectin after the signal sequence; each pink line indicates the location of the PAM site. P2, in pink writing is the PAM site used for CRISPR editing in this thesis. b) the listed PAMs 1 -9 and their PAM sequences, as well as MIT and CFD specificity scores calculated by crispor.tefor.net.*

4.3 Discussion

The HiBiT insert and NanoLuc Binary Technology was able to successfully detect E-selectin expression on the surface of WT or TERT2 HUVECs in response to an array of inflammatory cytokines. The potencies of these inflammatory mediators in respect to inducing E-selectin expression could be determined and were relatively comparable to those determined for WT HUVECs in an alkaline phosphatase assay. This experimental approach also allowed the kinetics of E-selectin cell surface expression to be determined with greater temporal sensitivity than able to be performed using antibody labelling. Electroporation of HUVECs and CRISPR-Cas9 gene editing did not affect the endothelial cell phenotype, as evidenced by CD31 antibody labelling.

The use of NanoBiT technology allowed the cell surface expression of E-selectin to be successfully tracked in live cells in real time. In respect to the ligands investigated here, a rank order of potency was observed for TNF alpha, LPS, IL-1 alpha and IL-1 beta respectively. The successful generation of a TERT2 HUVEC clone (Clone C8) homozygous for HiBiT insertion allowed increased sensitivity of E-selectin detection and prolonged kinetic screens.

15 hr kinetic screens conducted in live HUVECs revealed that TNF alpha induced the maximal and longest duration of expression of E-selectin. In contrast LPS, IL-1 alpha, IL-1 beta, $VEGF_{165}$a or histamine were able to induce E-selectin cell surface expression (peak time ~ 6 - 8hr) however compared to TNF alpha, maximal expression decreased by half after 6 - 8 hr. The reason for these decreases in E-selectin levels over time with these mediators could be two-fold; proteolytic cleavage of E-selectin, or E-selectin internalisation. E-selectin internalisation has been visualised before after 4 hr IL-1 treatment in HUVECs, where it was co-localised with lysosomal-associated membrane protein 1 (LAMP-1) in lysosomes, and after 18 hr stimulation only trace amounts were detected within the cell, suggesting E-selectin degradation (Subramaniam, Koedam and Wagner, 1993). Soluble E-selectin (sE-selectin) has been detected in activated endothelial cell systems, one hypothesis for the formation of sE-selectin is that it is separately transcribed, another it that there is alternative gene splicing of E-selectin and a third is that it is formed due to cleavage and release of the extracellular portion of membrane bound E-selectin (Leeuwenberg *et al.*, 1992; Wyble *et al.*, 1997). This hypothesis is supported by the size of sE-selectin (94 kDa) correlating to the size it would be if full-length E-selectin (115 kDa) had been cleaved at the point of membrane insertion (Leeuwenberg *et al.*, 1992). It has also been proposed that ‘cleaved’ sE-selectin may serve a function in binding and

inhibiting E-selectin ligands on leukocytes to inhibit further leukocyte adhesion (Wyble *et al.*, 1997). Future experimentation could look at an even longer time-span of E-selectin kinetics; The long acting Endurazine substrate has been demonstrated to last up to 70 hr (Promega Corporation, 2018b). Therefore, it could be feasible to double the time course used to follow E-selectin expression for longer and investigate downregulation that should eventually occur following TNF alpha stimulation. Knowing that LgBiT depletion is not a limiting factor for at least a 15 hr incubation, makes this feasible approach for future observations.

TERT2 HUVEC HiBiT E-selectin Clone C8 had a large dynamic assay window and was extremely sensitive to ligand treatment; a 426-fold increase in luminescence units compared to vehicle with maximal expression (1 nM TNF alpha) was observed. In comparison, mixed population edited WT HUVECs (from now on termed WT (mx)) produced a 54-fold increase and mixed population edited TERT2 HUVECs (from now on termed TERT2 (mx)) showed a 52-fold increase compared to vehicle. This window was still sufficient for detecting an increase in expression due for TNF alpha, LPS, IL-1 alpha and IL-1 beta treatment, however it was not sufficient for detecting low levels of expression due to $VEGF_{165}a$ or histamine. TERT2 HUVEC HiBiT E-selectin Clone C8 was the only cell line able to detect this increase in expression. Previous antibody labelling studies have shown that not every cell expressed E-selectin after stimulation with $VEGF_{165}a$ or histamine (100 nM, 6 hr 37°C 5% CO_2) and expression was low in comparison to TNF alpha (see 3.2 Results). Because of this seemingly random selection of expressing cells, multiple variables of transfection efficiency and editing efficiency would have decreased the chance of picking up this low expression of E-selectin in mixed population cell lines. This is reflected in the data; for both histamine and $VEGF_{165}a$ experiments, only 10 – 40% of WT (mx), and 7 – 13% of TERT2 cells (mx) generated by repeat electroporations/CRISPR editing experiments showed significantly increased expression compared to vehicle. However, there was consistently significant increases in LU for clone C8 after stimulation with histamine or $VEGF_{165}a$ ($p<0.001$) between experimental replicates. It's worth noting however, that there was still a large range of luminescence output between experiments using 100 nM $VEGF_{165}a$ (9000 – 72,000 LU) or 100 nM histamine (24,000 – 300,000 LU). As this is a clonal population, this variability in luminescence output was not due to differences in electroporation or CRISPR-Cas9 editing efficiency but instead was likely to be a reflection on cell passage number (see Figure 4.14) and cell seeding density variations.

The coefficient of variation was double in WT HUVECs (mx) compared to TERT2 HUVEC HiBiT E-selectin clone C8, reflecting variation between repeat experiments, most likely due to differential electroporation or editing efficiency for the WT HUVECs. Another variable for WT HUVECs (mx) was that the cell seeding density was not always constant. The Lonza electroporation programme A-034, although shown to be more efficient, often caused cell clumping. These clumps were not always possible to resuspend completely in Medium 200 before cell seeding, which sometimes affected the seeding density and therefore the total luminescence output for each repeat. The advantage of the TERT2 HUVEC HiBiT E-selectin clonal population is that it can be continually passaged whilst retaining high HiBiT expression and repeat electroporations of HUVECs are not required to deliver the CRISPR components to the cell before each experiment, therefore the effect of electroporation on cell health is not a factor.

The kinetics data from Figure 4.22 also shed light on a surprising finding that there was cytokine-independent expression of E-selectin in vehicle conditions in clone C8. E-selectin expression has been measured before in the absence of cytokines, and was dependent on plate coating material (gelatin, fibronectin, collagen or fibrinogen increased basal E-selectin whereas poly-L-lysine did not), cell seeding density (the intensity and duration of expression was inversely proportional to cell density) and was mediated by the cell junctional protein platelet/endothelial cell adhesion molecule-1 (PECAM-1, which inhibited E-selectin expression) (Litwin *et al.*, 1997). However, in a study assessing the impact of HUVEC cell density on E-selectin expression, not only was there no basal expression, at low or high seeding density, but after TNF alpha stimulation the inverse relationship was concluded where E-selectin mRNA expression was higher in the confluent monolayer compared to a sparse monolayer (Hamada, Osaka and Yoshida, 2014). Testing cytokine-independent E-selectin expression with differential 96-well coating, at different seeding densities could shed light on whether either were inducing E-selectin expression particularly in vehicle conditions. However, this expression was extremely low in comparison to the TNF alpha, LPS, IL-1 alpha or IL-1 beta signal and could have occurred due to TERT2 HUVEC cell stress resulting from lack of CO_2 control, or the fact that OptiMEM contained lower levels of serum compared to Medium 200 + 2.2% LVES.

Maximal luminescence decreased according to passage number in TERT2 HUVEC HiBiT E-selectin clone C8 with stimulants TNF alpha, LPS, IL-1 alpha or IL-1 beta (Figure 4.14).

Firstly, it was suspected that the TERT2 HUVECs were losing their endothelial cell phenotype and differentiating into fibroblasts, as after visual inspection HUVECs seemed to be more elongated and less round (see Figure 4.10). However, both early (p13) and late (p23) passage cells stained positively for CD31, an endothelial cell marker. Future experimentation could also look at staining for fibroblast cell markers such as vimentin or alpha smooth muscle actin. The late passage TERT2 HUVEC HiBiT E-selectin clone C8 may also be becoming less responsive to inflammatory stimuli, as IL-1 alpha and IL-1 beta responses showed decreased potency in respect to stimulating E-selectin expression with later cell passages.

Lack of antibody binding to HiBiT-E-selectin in TERT2 HUVEC HiBiT E-selectin clone C8 was an unexpected finding. One possibility is that the antibody epitope overlaps at the exact region of HiBiT addition on the N-terminus of E-selectin. This is supported by the anti-E-selectin antibody being able to bind to un-tagged E-selectin in WT TERT2 HUVECs (unedited) after stimulation with TNF alpha, LPS, IL-1 alpha or IL-1 beta. Another possibility is that the HiBiT addition is causing a change in folding of the N terminus of E-selectin, meaning that the epitope is no longer accessible for binding by the antibody. This could cause problems for an *in vitro* assay to detect drug binding as more than one binding site could have been made inaccessible on the N-terminal region. However, this is unlikely, as the HiBiT sequence only caused an 11 amino acid addition. To investigate further, it would have been informative to characterise by X-ray crystallography HiBiT-E-selectin and untagged E-selectin protein structures to determine if any conformational changes have occurred. Alternatively, several other PAM sites on the N-terminus of E-selectin could be targeted for HiBiT addition and the effect of antibody binding could be assessed. Such PAM sites are described in Figure 4.24, location of HiBiT addition could be compared with sites P1 - P9. CRISPR reagents are relatively expensive particularly to do this many edits and is therefore likely to be cost prohibitive. Alternatively molecular biology techniques could be used to append HiBiT to E-selectin at differing N-terminal regions using either Gibson assembly or restriction ligation approaches. Over-expression of such HiBiT-E-selectin constructs in a model cell line such as HEK293Ts, and antibody labelling could shed light on whether altering insertion site resolves the issue of lack of anti E-selectin binding observed in the TERT2 HUVEC HiBiT E-selectin clone C8. In addition, a different mAb which binds a different epitope can be used to see if the problem remains.

It is also important to be aware that the RNP complex used for HiBiT addition, could have introduced off-target cleavage and subsequent downstream effects on edited cells. If the RNP complex bound to any other region of DNA than was intended, it would cause a double strand break (DSB) in an off-target region of DNA and consequential non-specific genetic modifications, consisting of unintended point mutations, deletions, insertions, inversions and/or translocations (Zhang *et al.*, 2015). The targeting specificity is tightly controlled by the 20-nucleotide guide sequence and the presence of the PAM sequence, however off-target cleavage has still been seen with even 3 – 5 base pair mismatches in the PAM-distal region of the gRNA sequence (Zhang *et al.*, 2015). Studies have shown that the 3' end of the guide sequence adjacent to the PAM site was also critical for Cas9 binding, R-loop formation and activation of Cas9 nuclease activity (Jinek *et al.*, 2014; Nishimasu *et al.*, 2014). Here, crispor.tefor.net was used to find the best guide RNA sequence and PAM site optimal for N terminal HiBiT insertion (Haeussler *et al.*, 2016; Concordet and Haeussler, 2018). When predicting off-target cutting, crispor searches the whole genome and allows up to four mismatches for the CRISPR-RNA/PAM sequence. The likelihood of off-targeting was minimised by targeting a PAM site and designing a guide sequence calculated to have the most uniqueness within the genome using formulas from cutting frequency determination (CFD) score and using the MIT specificity score. The specificity scores for the PAM site and guide used were MIT: 88/100 and CFD: 94/100 indicating low off-target effects within the genome. Therefore, we had confidence that the likelihood of off-target DSB was very low. To further detect and investigate whether there was any off target DSBs however, we could have tested predicted off-target sites by using primers designed for these sites with PCR, coupled with Sanger sequencing analysis, knowing that this approach will not amplify off-target hits.

In addition, the HiBiT insert could have affected the E-selectin kinetics. TNF alpha was almost 4-fold less potent (0.0604 nM compared to 0.0155 nM) at stimulating HiBiT E-selectin cell surface expression in TERT2 HUVECs and the time course curve of maximal expression was delayed in comparison to un-edited E-selectin expression in WT HUVECs as measured using alkaline phosphatase readouts (Figure 4.23). However, it would have been more prudent to test the un-tagged E-selectin kinetics in the same cell line (TERT2 HUVECs) using alkaline phosphatase labelling to test whether this discrepancy was due to the cell type or HiBiT addition. This difference may also have been seen due to secondary antibody amplification of E-selectin expression, as more than one fluorescent secondary antibody can bind to anti-E-selectin monoclonal antibody. In comparison, the NanoBiT technology is a more direct method of detection as recomplimentation of LgBiT to HiBiT occurs at a 1:1 ratio. The immortalisation

of the TERT2 HUVEC cell line could also have additionally affected the inflammatory response; an almost 4-fold less potent LPS response was observed in TERT2 HUVEC HiBiT E-selectin clone C8 compared to WT HUVECs (mx). Nevertheless, the rank order of potency for inflammatory mediators used between cell lines remained constant.

4.4 Conclusion

To conclude, a homozygous HiBiT E-selectin clone was produced in TERT2 HUVECs (Clone C8), which enabled highly sensitive detection of E-selectin expression, comparable to WT HUVEC response. TNF alpha was found to be the most potent stimulant for E-selectin expression, which induced prolonged maximal cell surface expression for 15 hr. LPS, IL-1 alpha/beta, $VEGF_{165}$a and histamine all exhibited reduced E-selectin expression after 8 hr. In addition, this clone was the only CRISPR edited cell line able to detect low levels of expression due to $VEGF_{165}$a and histamine, and detected cytokine-independent E-selectin expression over the course of 15 hr.

Chapter 5 Utilising NanoBiT and NanoBRET to investigate E-selectin membrane interactions

5.1 Introduction

E-selectin targeting therapeutics have been developed using technologies ranging from antibodies, peptides and glycomimetics such as sialyl Lewis x (sLe^x). Specific drug binding has been measured previously with recombinant E-selectin coated plates by using fluorescent-conjugations of these therapeutics and quantifying fluorescence intensity in the absence and presence of unlabelled versions of the therapeutic (Kawano *et al.*, 2011; Gholizadeh *et al.*, 2018b; Hu *et al.*, 2018b). In addition, internalisation of E-selectin targeting therapeutics in endothelial cell lines has been quantified for fluorescently labelled therapeutics using flow cytometry (Gholizadeh *et al.*, 2018b; Hu *et al.*, 2018b). The physicochemical process of fluorescence quenching (lowered fluorescence intensity) due to fluorescent-ligand binding has also been exploited to detect E-selectin binding for multiple compounds (Barra *et al.*, 2016b). Another popular route has been to measure the ability of the therapeutic to inhibit selectin-mediated leukocyte adhesion to endothelial cells (Shamay *et al.*, 2009b).

Most of these methods have been successful in detecting E-selectin binding in a clean, but far-removed and indirect format from the complexity of whole cells. Binding to immobilised recombinant E-selectin, by no means guarantees the same binding when the drug is administered to cells, due to the myriad of mechanisms existing to regulate membrane permeability, internalisation, exportation and trafficking (Kiseleva et a., 2018). In addition to these innate barrier defence systems affecting drug interactions, the cell membrane organisation of E-selectins could further complicate binding characteristics of these drugs. For example, it has been documented that the leukocyte ligand-E-selectin binding, and consequential tethering and rolling behaviours have been mediated by the specific site densities of E-selectin on the membrane. It was found that low-site densities encouraged rapid and short-lived tethering events, whereas high site densities resulted in long-lived binding that resulted in continuously rolling of leukocytes. This was due to the formation of new bonds at the leading edge being balanced by the dissociation of existing bonds at the rear edge of the contact area (Li *et al.*, 2015). Site densities of E-selectin expression has been reported to range from 100 - 1000 molecules/μm^2, dependent on the cytokine that has stimulated the expression and the concentration and duration of stimulation (Levin, Ting-Beall and Hochmuth, 2001). The spatial organisation and density of E-selectins hasn't been studied in the context of resultant increase or decrease in drug binding events. This spatial organisation would be heavily influenced by interactions between endothelial cell expressed E- and P-selectin, as well as other endothelial

cell receptors expressed (eg. vascular endothelial growth factor receptor 2 (VEGFR2), Neuropilin1). Knowing if these interactions exist could help contribute towards understanding the bigger picture of selectin membrane organisation and influence and inspire drug design. E-selectin targeting therapeutics could, for example, be designed in a dimeric or multimeric fashion to match the dimeric or multimeric organisation of E-selectin on the cell membrane to facilitate greater blockade of leukocyte binding.

Novel methods have been utilised that can measure both drug:protein and protein:protein interactions in whole cells. One method to investigate these interactions has utilised the physical phenomenon of BRET (described in 2.10 Fluorescent E-selectin binding peptide NanoBRET assays). This method can be easily incorporated into investigating binding in whole cells, by transfecting or editing proteins tagged with a bioluminescent donor and measuring binding of a fluorescent conjugated therapeutic. In this chapter, we utilised BRET to investigate the binding of fluorescently conjugated E-selectin binding peptide (Esbp) to NanoLuc tagged E-selectin in HEK293T cells.

Esbp was discovered after screening a library of recombinant peptides which had sequence similarity for 4 amino acids, Tryptophan (W), Leucine (L), and Methionine (M), with specific placement: 'xxx-**W**-xx-**LW**-xx-**M**-x' where 'x' was any amino acid (Martens *et al.*, 1995). This high-throughput screening was conducted by addition of radio-labelled peptide on immobilised E-selectin, and non-specific binding was deduced by preincubating immobilised E-selectin with 10 µM unlabelled Esbp. They also tested the ability of unlabelled peptides to block [^{3}H] thymidine labelled HL-60 cell adhesion to immobilised E-selectin. For this, the extracellular portion of E-selectin cDNA was amplified using PCR, before ligation in frame with a PI-glycan (PIG) linkage signal sequence in a mammalian expression vector. After transfection of E-selectin with C-terminal PIG into CHO cells, E-selectin was labelled using PIG-linked monoclonal antibody (mAb179, which binds to the C-terminal PIG sequence). The brightest cells were then sorted using fluorescence-activated cell sorting (FACS), and from these cells, the soluble extracellular domain of E-selectin was cleaved from the cell surface using phosphoinositol-dependent phospholipase C (PLC). The PI-PLC harvested E-selectin was then immobilised on a mAb179-coated microtiter well for experimentation. In addition, they tested the ability for unlabelled peptides to inhibit calcein labelled HL-60 cell adhesion in IL-1 stimulated HUVECs and TNF alpha stimulated mouse brain endothelial cells. Using these assays, they found that the peptide sequence DIT**W**DQ**LW**DL**M**K (termed AF10166, which

was later termed Esbp) had the highest affinity for E-selectin (the IC_{50} for inhibition of HL-60 cell adhesion 4.0 nM). A series of truncation experiments revealed that this high affinity was dependent on the most N-terminal aspartic acid (D) and Isoleucine (I); where reductions in affinity were 220-fold and with the C-terminal lysine (K) which when truncated, decreased binding affinity by 120-fold. Further truncation resulted in absolute inhibition of E-selectin binding. In addition, they found that Esbp bound specifically to E-selectin, but not P- or L-selectin. The core sequence of Esbp (glutamine (Gln / Q), Leucine (Leu / L), Tryptophan (Trp / Q) Aspartic acid (Asp / D) shown in bold: DITWD-**QLWD**-LMK) was later discovered to be identical to the first four residues of the mature PSGL-1 sequence which binds to the selectin family. Later, Esbp was tested for its ability to bind E-selectin in the context of inhibiting E-selectin mediated cancer metastasis (Shamay *et al.*, 2009b, 2015b). Here, binding was deduced by measuring inhibition of HL-60 cell binding to recombinant E-selectin coated 96-well plates. This experiment wasn't fluorescent-tag-dependent, as HL-60 cell counts were determined simply by lysing bound HL-60 cells and quantifying myeloperoxidases that were released, using *o*-phenylenediamine as a substrate. In addition, a fluorescent version of the Esbp was incubated with monolayers of TNF alpha activated brain microvascular endothelial (cEND) cells and confocal microscopy, as well as flow cytometry concluded that Esbp bound to E-selectin.

This chapter aimed to produce an improved model for Esbp-E-selectin binding, by investigating binding in native and non-native live whole cells, therefore considering innate barrier defence mechanisms and internalisation. Highly sensitive and novel luciferase technologies NanoBiT and NanoBRET in conjunction with fluorescently conjugated Esbp were used to investigate binding and E-selectin internalisation. The NanoBRET technology was used to investigate further interactions that E-selectin exhibits with members of the selectin family, as well as vascular disease relevant endothelial cell receptors VEGFR2 and Neuropilin-1 (NRP-1). E-selectin binding with other receptors could help with understanding E-selectin membrane organisation and leukocyte binding. Here, NanoLuc-E-selectin and SNAP-tag or Halotag appended versions of the selectin family, VEGFR2 or NRP-1 were used in HEK293Ts to investigate binding using NanoBRET.

5.2 Results

5.2.1 Production of NanoLuc and SNAP-tag selectin constructs

SNAP-tag and NanoLuc E-/P-/L-selectin sequences were all verified using Sanger sequencing, gel electrophoresis, fluorescence and bioluminescence imaging analysis (see figures 5.1 – 5.8). First, all sequences showcased sharp, individual and evenly spaced peaks, which aligned with the sequences designed on SnapGENE viewer. In addition, restriction enzyme digestion with KpnI (K) and BamHI (B) successfully cut out N-terminal SNAP-tag and NanoLuc tags (639 bp) found in all cases after agarose gel electrophoresis. In conjunction, restriction enzyme digestion with B and XhoI (X) resulted in isolation of E-selectin (1845 bp), P-selectin (2505 bp) and L-selectin (1170 bp). Verification of construct formation was further confirmed after transfection of constructs resulted in surface expression of AF488-SNAP surface labelled SNAP-tag P-/E-/L-selectin (Figure 5.4). Although, transfection efficiency was markedly low in these cells. In addition bioluminescence imaging of NanoLuc E-/P-/L-selectin stable cell lines revealed bright expression in every cell, with similar luminescence intensity between cell lines (NanoLuc E-selectin: 505,449 LU, NanoLuc P-selectin: 609,260 LU and NanoLuc L-selectin: 569,383 LU) with an average of >155-fold increase in luminescence units from vehicle (un-transfected HEK293Ts) (Figure 5.8).

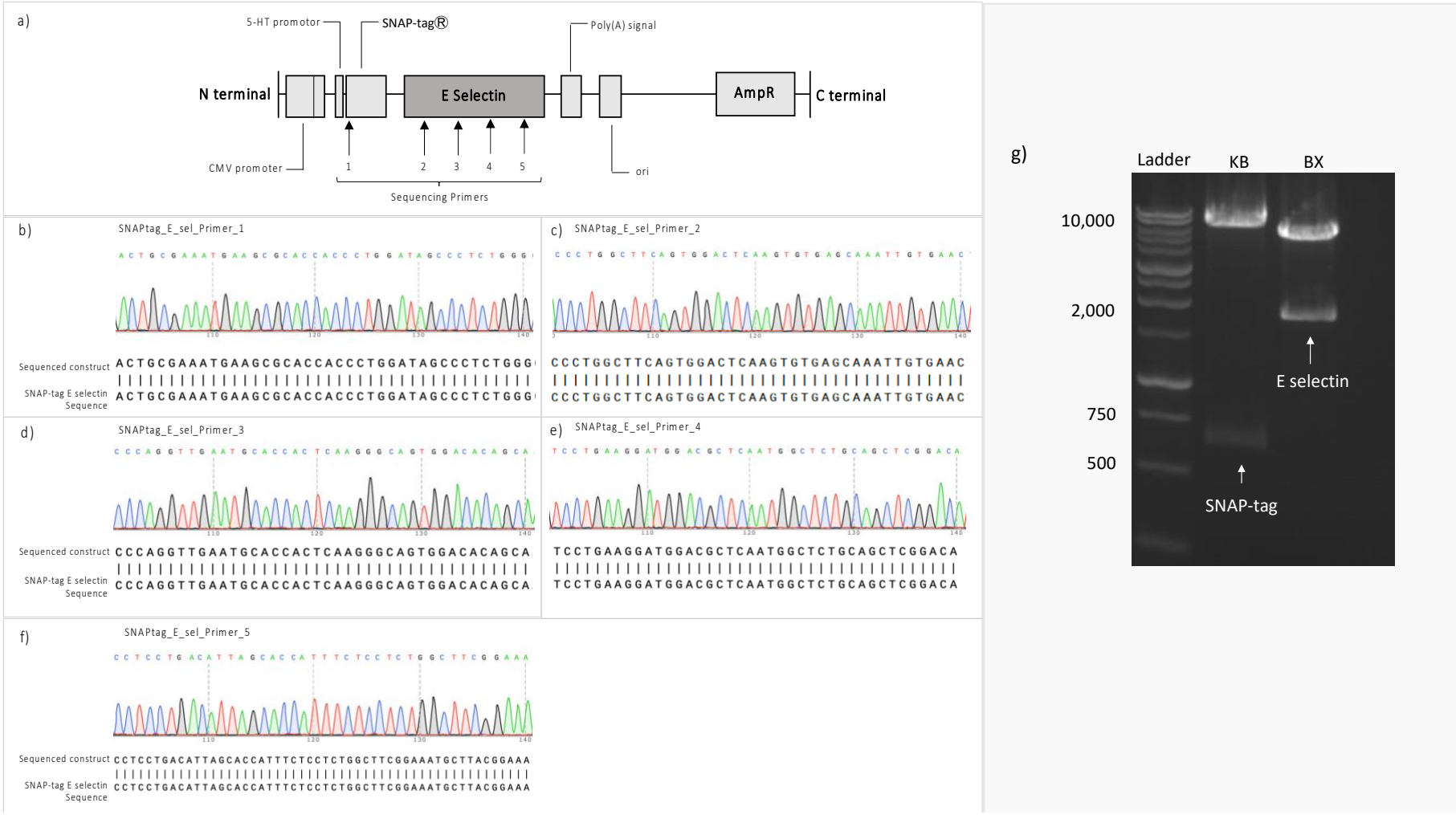

Figure 5.1 ***Sanger sequencing and restriction enzyme digestion verification for the SNAP-tag E selectin construct.*** *a) Structure of SNAP-tag E-selectin and localization for where primers 1-5 are complementary to the SNAP-tag E-selectin sequence. b) c) d) e) and f) A 40bp snapshot of sanger sequencing results for each primer; showcasing individual, sharp and evenly spaced peaks which aligned with known sequence. g) Restriction enzyme incubation with KpNI (K) and BamHI (B) resulted in isolation of the SNAP-tag sequence, in addition incubation with B + XhoI (X) resulted in restriction enzyme cutting and isolation of the E-selectin sequence for the SNAP-tag E-selectin construct.*

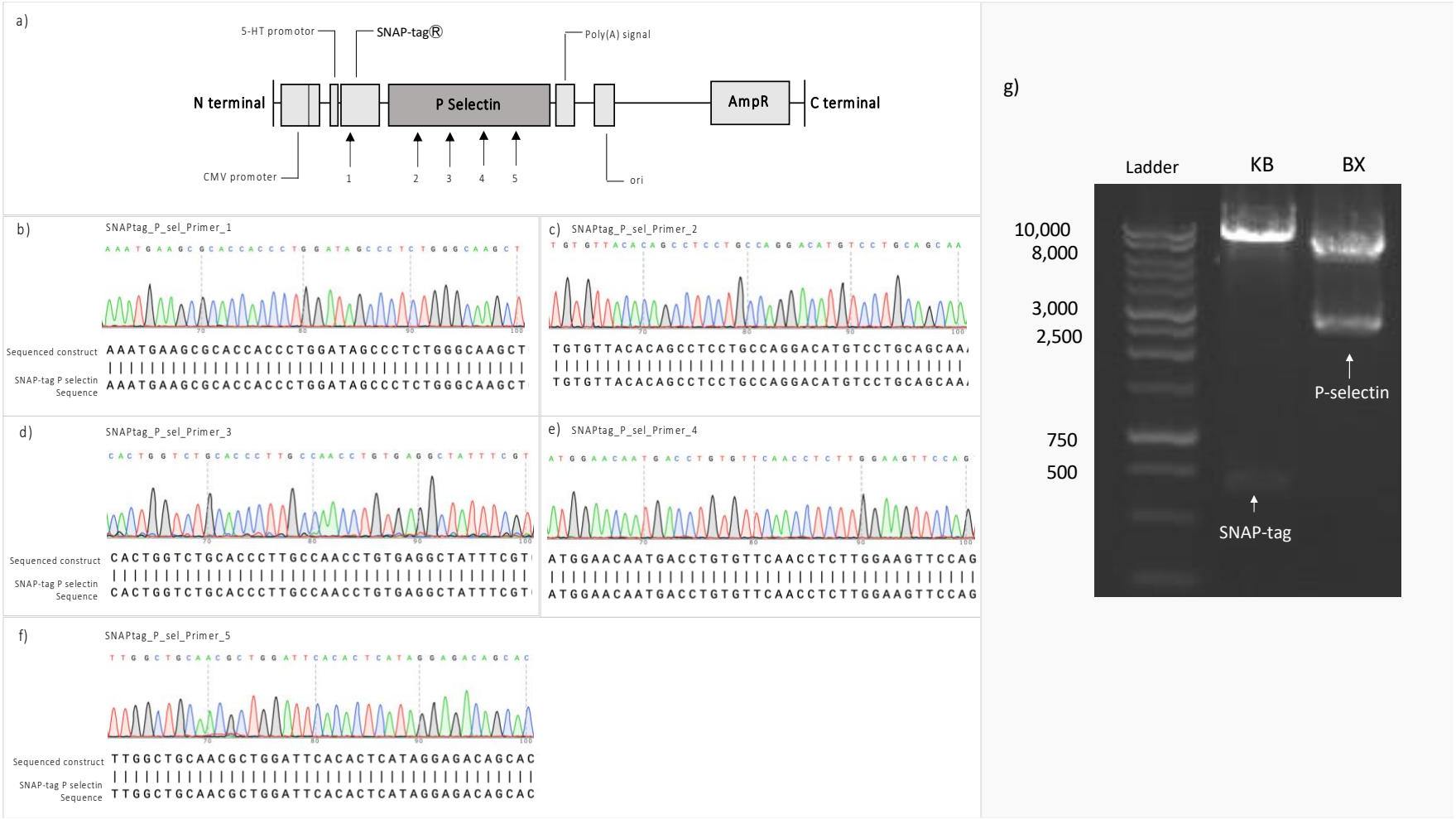

Figure 5.2 ***Sanger sequencing and restriction enzyme digestion verification for the SNAP-tag P-selectin construct.*** *a) Structure of SNAP-tag P-selectin and localization for where primers 1-5 are complementary to the SNAP-tag P-selectin sequence. b) c) d) e) and f) A 40bp snapshot of sanger sequencing results for each primer; showcasing individual, sharp and evenly spaced peaks which aligned with known sequence. G) Restriction enzyme incubation with KpNI (K) and BamHI (B) resulted in isolation of the SNAP-tag sequence, in addition incubation with B + XhoI (X) resulted in restriction enzyme cutting and isolation of the P-selectin sequence for the SNAP-tag P-selectin construct.*

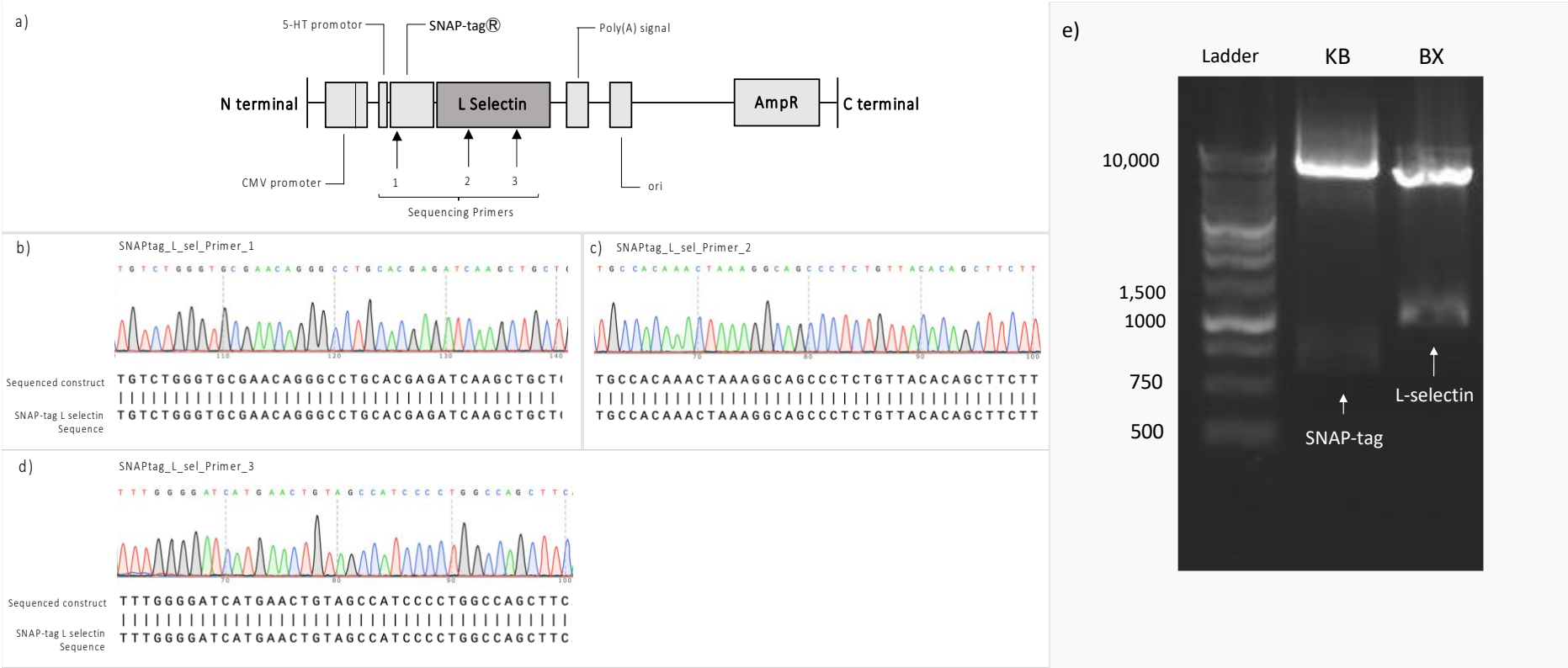

Figure 5.3 ***Sanger sequencing and restriction enzyme digestion verification for the SNAP-tag L-selectin construct.*** *a) Structure of SNAP-tag L-selectin and localization for where primers 1-3 are complementary to the SNAP-tag P-selectin sequence. b) c) and d) A 40bp snapshot of sanger sequencing results for each primer; showcasing individual, sharp and evenly spaced peaks which aligned with known sequence. e) Restriction enzyme incubation with KpNI (K) and BamHI (B) resulted in isolation of the SNAP-tag sequence, in addition incubation with B + XhoI (X) resulted in restriction enzyme cutting and isolation of the L-selectin sequence for the SNAP-tag L-selectin construct.*

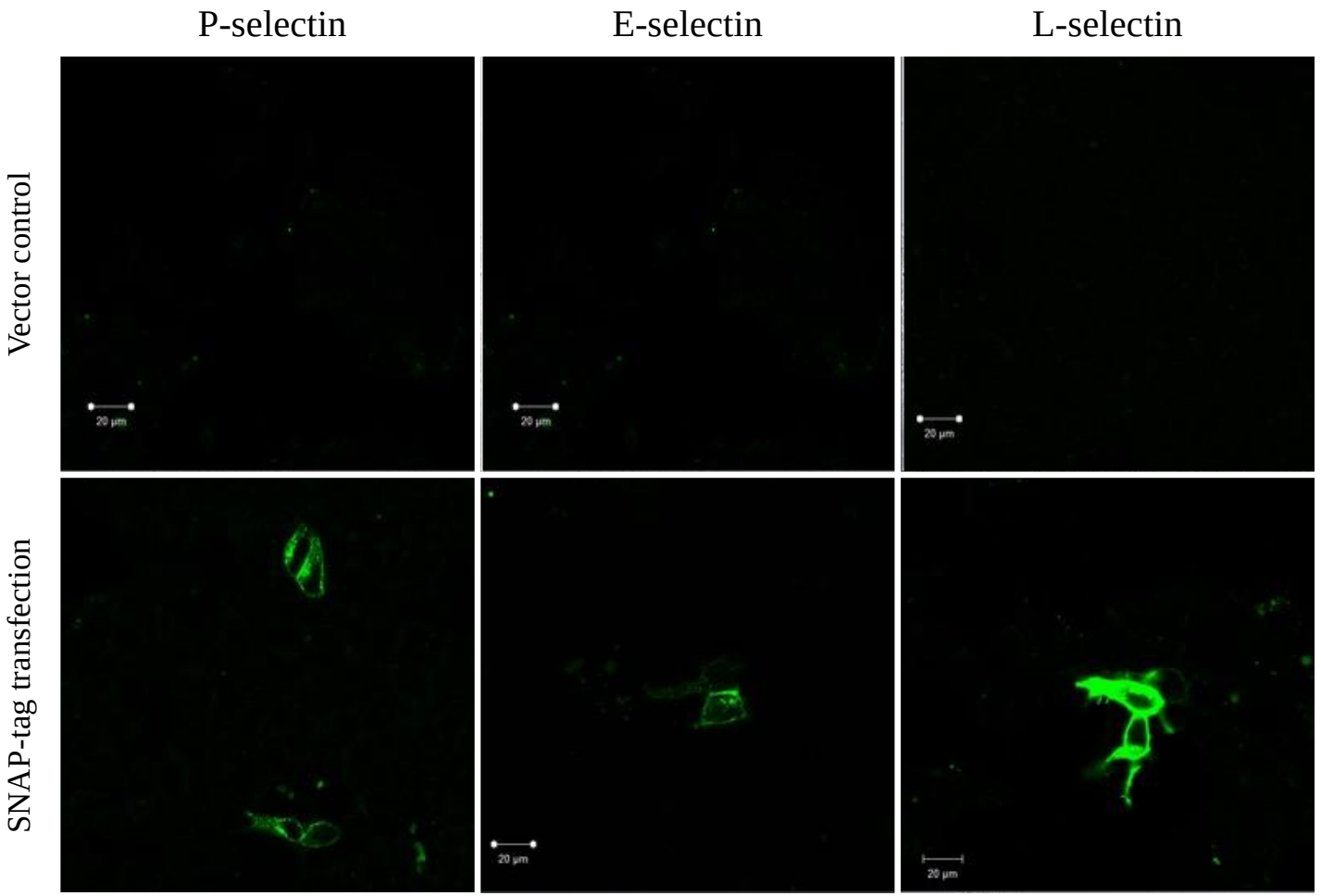

Figure 5.4 ***Transfected SNAP-tag selectin constructs resulted in membrane expression.*** *200 ng of SNAP-tag P-/E-/L- selectin or pcDNA3.1 (Zeo) plasmid (vector control) was transfected into HEKGs using FuGENE HD liposome reagent, 24 hr before cells were labelled with membrane impermeant SNAP surface 488 substrate. Low transfection efficiency was observed. Cells were imaged using 880F confocal microscope. Scale bar = 20 µm.*

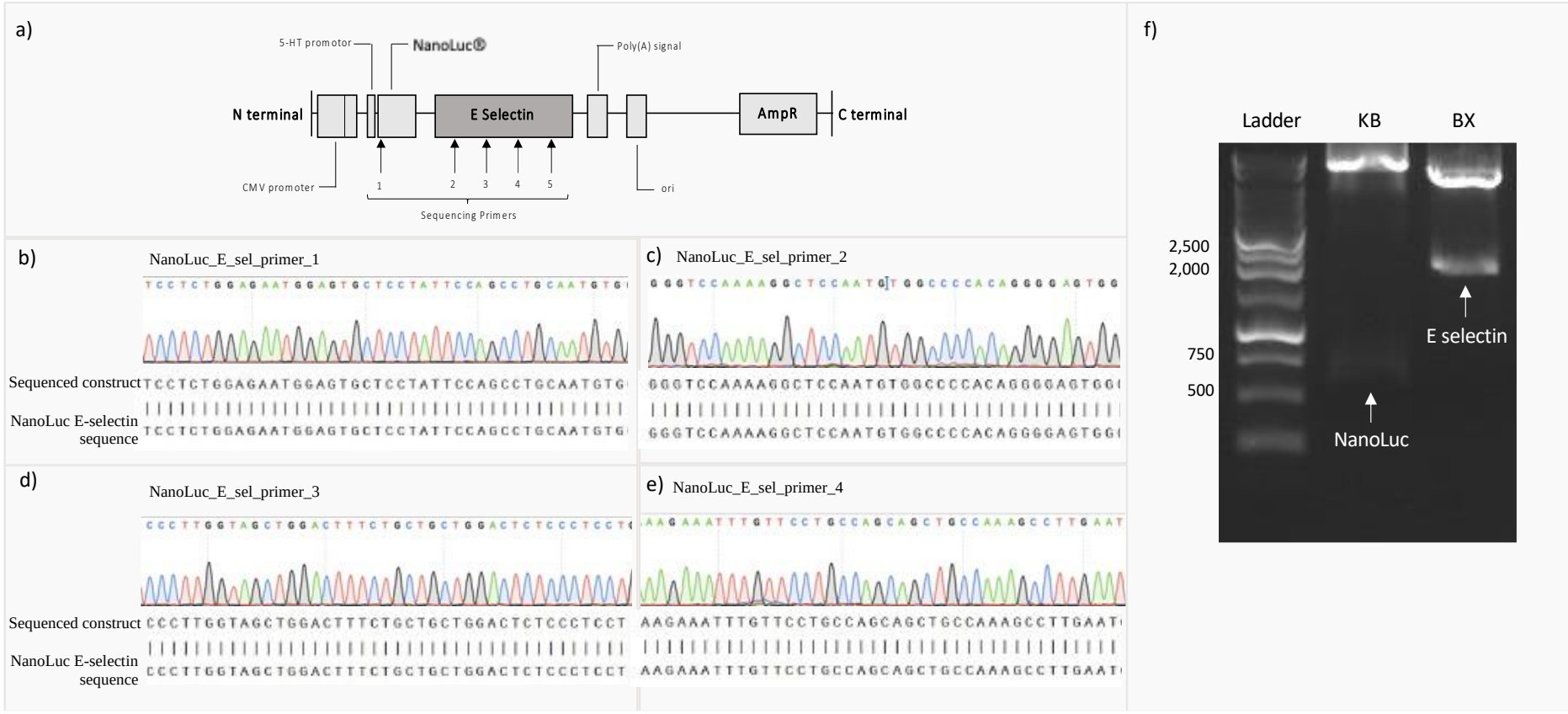

Figure 5.5 ***Sanger sequencing and restriction enzyme digestion verification for the NanoLuc E-selectin construct.*** *a) Structure of SNAP-tag E-selectin and localization for where primers 1-4 are complementary to the SNAP-tag E-selectin sequence. b) c) d) and e) A 40bp snapshot of sanger sequencing results for each primer; showcasing individual, sharp and evenly spaced peaks which aligned with known sequence. e) Restriction enzyme incubation with KpNI (K) and BamHI (B) resulted in isolation of the NanoLuc sequence, in addition incubation with B + XhoI (X) resulted in restriction enzyme cutting and isolation of the E-selectin sequence for the NanoLuc E-selectin construct.*

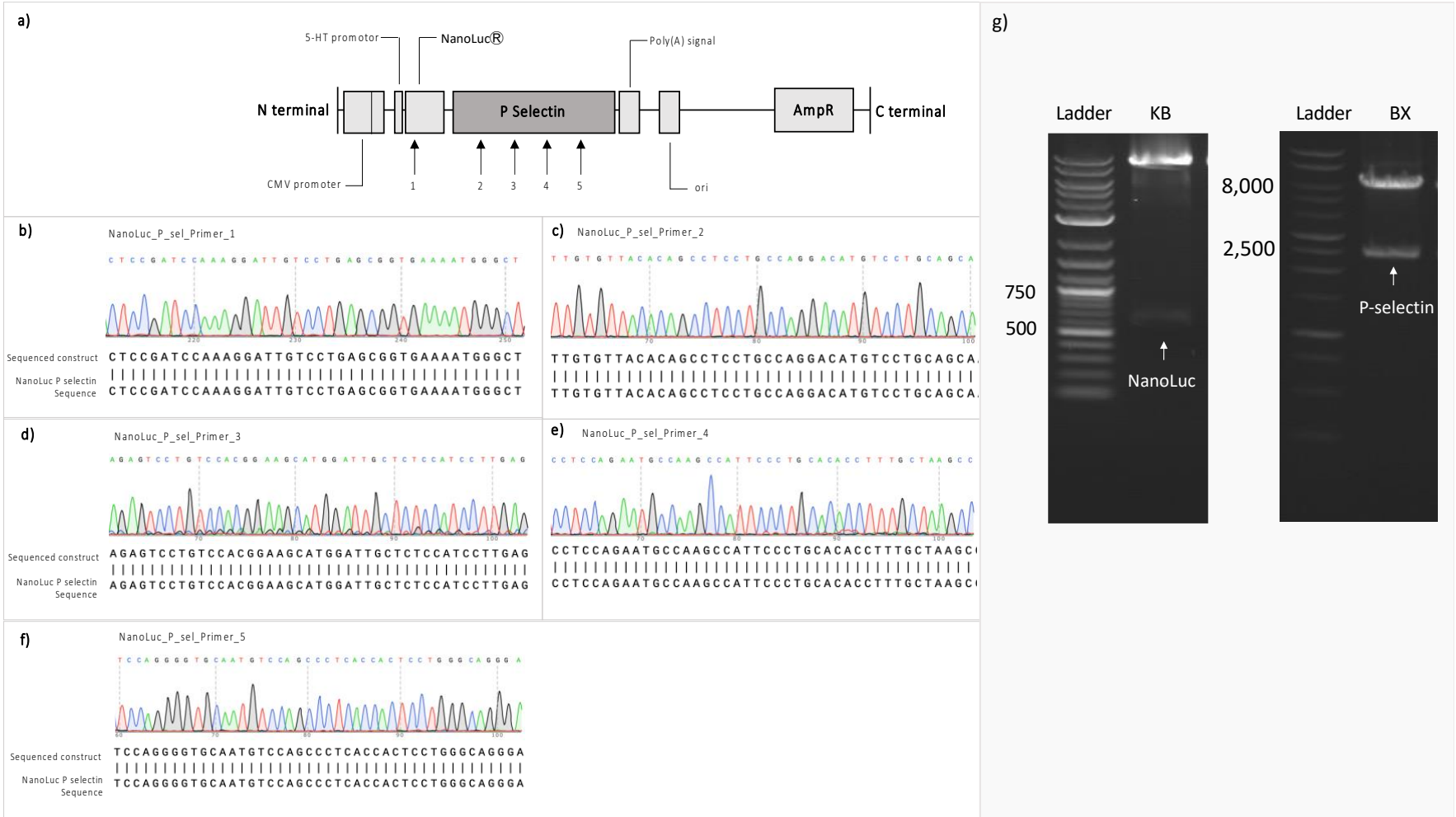

Figure 5.6 ***Sanger sequencing and restriction enzyme digestion verification for the NanoLuc P-selectin construct.*** *a) Structure of SNAP-tag P-selectin and localization for where primers 1-5 are complementary to the SNAP-tag P-selectin sequence. b) c) d) e) and f) A 40bp snapshot of sanger sequencing results for each primer; showcasing individual, sharp and evenly spaced peaks which aligned with known sequence. g) Restriction enzyme incubation with KpNI (K) and BamHI (B) resulted in isolation of the NanoLuc sequence, in addition incubation with B + XhoI (X) resulted in restriction enzyme cutting and isolation of the P-selectin sequence for the NanoLuc P-selectin construct.*

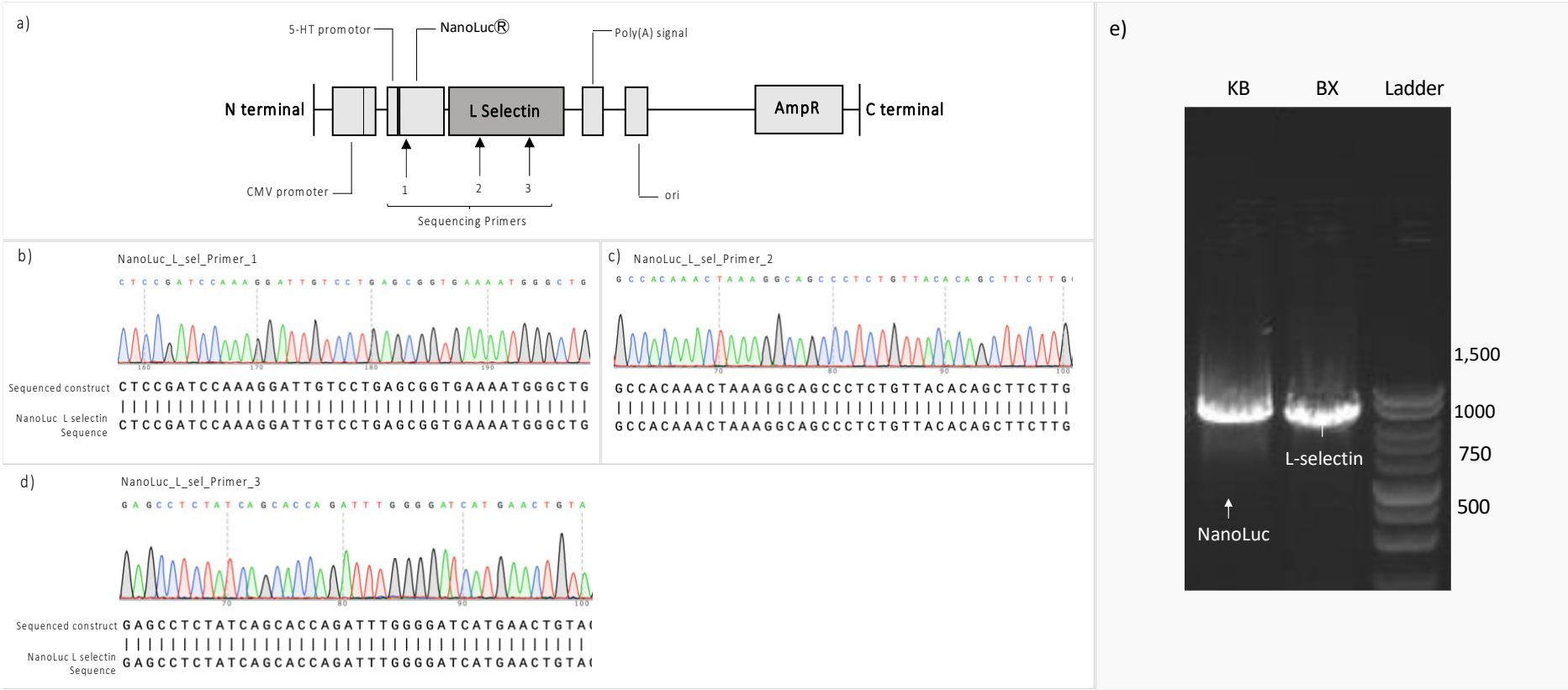

Figure 5.7 ***Sanger sequencing and restriction enzyme digestion verification for the NanoLuc L-selectin construct.*** *a) Structure of SNAP-tag L-selectin and localization for where primers 1-3 are complementary to the SNAP-tag L-selectin sequence. b) c) and d) A 40bp snapshot of sanger sequencing results for each primer; showcasing individual, sharp and evenly spaced peaks which aligned with known sequence. e) Restriction enzyme incubation with KpNI (K) and BamHI (B) resulted in isolation of the NanoLuc sequence, in addition incubation with B + XhoI (X) resulted in restriction enzyme cutting and isolation of the L-selectin sequence for the NanoLuc L-selectin construct.*

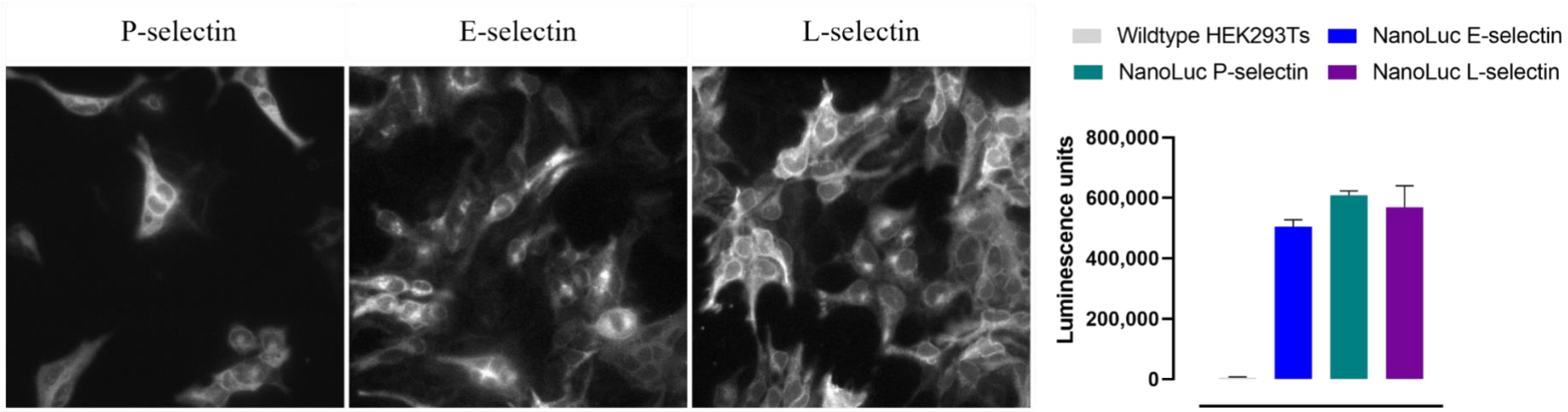

Figure 5.8 ***Transfection of NanoLuc-Selectin constructs resulted in membrane expressed E-selectin which reached luminescence units >450,000.*** *a) NanoLuc P-/E-/L-selectin stable cell lines were imaged using LV200 widefield microscope after addition of furimazine. b) average luminescence intensity for NanoLuc cell lines were 505,449 (E-selectin), 609.260 LU (P-selectin) and 569,383 (L-selectin), >155-fold increase from units measured for un-transfected WT HEK293Ts using the BMG PHERAstar plate reader. N=3, error bars = SEM*

5.2.2 Fluorescent-Esbp saturable binding assays

No saturable binding was observed after addition of increasing concentrations of either Alexa Fluor 633 conjugated Esbp (AF633-Esbp) nor for Alexa Fluor 488 conjugated Esbp (AF488-Esbp) in NanoLuc E-selectin stable cell line or clone C8 HiBiT E-selectin TERT2 HUVEC cell line following the addition of purified LgBiT (see figures 5.9 – 5.17).

Investigations began after AF633-Esbp showed no saturable specific binding or displacement after addition of 10 µM Esbp (Figure 5.9a). A linear increase in baseline corrected BRET ratio could be observed with increasing concentrations of AF633-Esbp, due to the occurrence of non-specific BRET. Alongside, a positive control experiment showcased saturable binding of a red-shifted fluorescent CXCR4 agonist (BODIPY 630/650 labelled SD131) to a N terminal NanoLuc tagged CXCR4 stably expressed in HEK293T cells (Figure 5.9b). In this case, the BRET ratio increased in a hyperbolic curve after addition of increasing concentrations of the fluorescent CXCR4 antagonist SD131, which was displaced after 10 µM addition of a specific CXCR4 unlabelled antagonist (AMD3100). Specific binding was then calculated, from which the maximum binding capacity (Bmax: 123.9) and affinity of SD131 (Kd: 165 nM) was calculated.

To further confirm that no binding of fluorescently labelled Esbp was occurring to E-selectin, addition of AF633-Esbp at concentrations 100 nM and 1000 nM did not result in any co-localisation with SNAP-tag E-selectin when expressed in HEK293T cells (Figure 5.10). Red ‘specks’ could be visualised in the images which represent non specific accumulation of the AF633-Esbp ligand.

It is known that for some peptide ligands, addition of higher concentrations of BSA is required for it to remain in solution. To check whether the concentration of BSA used in the vehicle buffer affected the final concentration of AF633-Esbp in the well and therefore binding, 0% BSA, 0.1% BSA and 1% BSA in HBSS buffer was used in saturable binding assays. There was no saturable binding observed nor displacement with unlabelled Esbp (Figure 5.11). Finally, AF633-Esbp was tested for binding with other NanoLuc selectin cell lines (P and L), but no saturable binding was observed for any selectin construct at low and high AF633-Ebp concentrations (Figure 5.12).

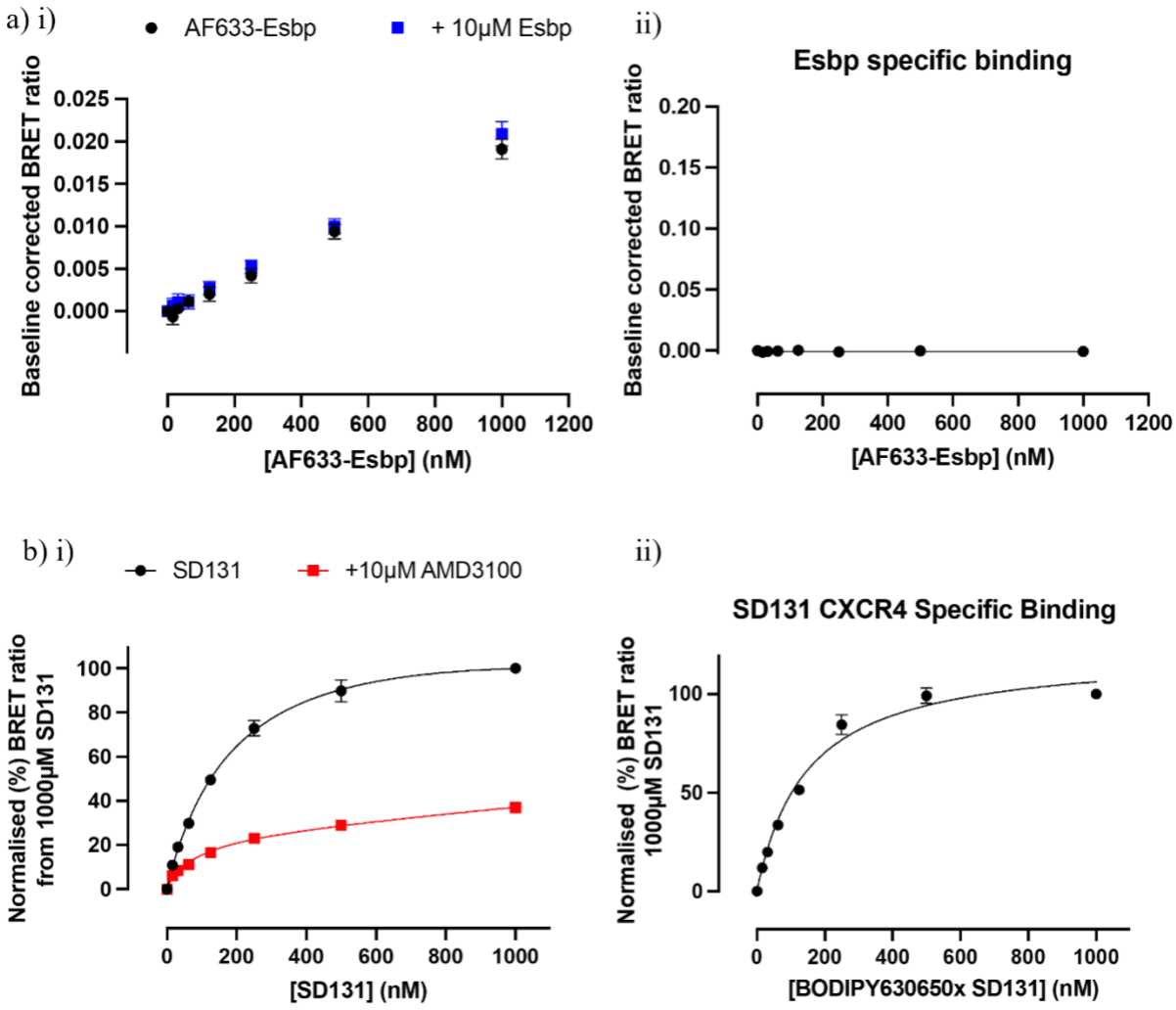

Figure 5.9 ***AF633-Esbp did not bind to NanoLuc-E-selectin.*** *a) i) AF633- Esbp did not display saturable binding to NanoLuc-E-selectin, and there was no displacement with addition of unlabelled Esbp (10 μM), resulting in ii) no specific binding calculated. b) i) a positive control was used to test the NanoBRET system. NanoLuc CXCR4 cell line was plated with addition of BODIPY 630/650 conjugated SD131 in the presence of the antagonist AMD3100 (10μM). Saturable binding was seen with increasing concentrations of SD131 0 - 1000 nM. There was significant displacement of fluorescent SD131 with 10μM addition of AMD3100, resulting in ii) specific binding calculated successfully. This positive control gave confidence on the NanoBRET system and experimental competency. N=5, error bars = SEM.*

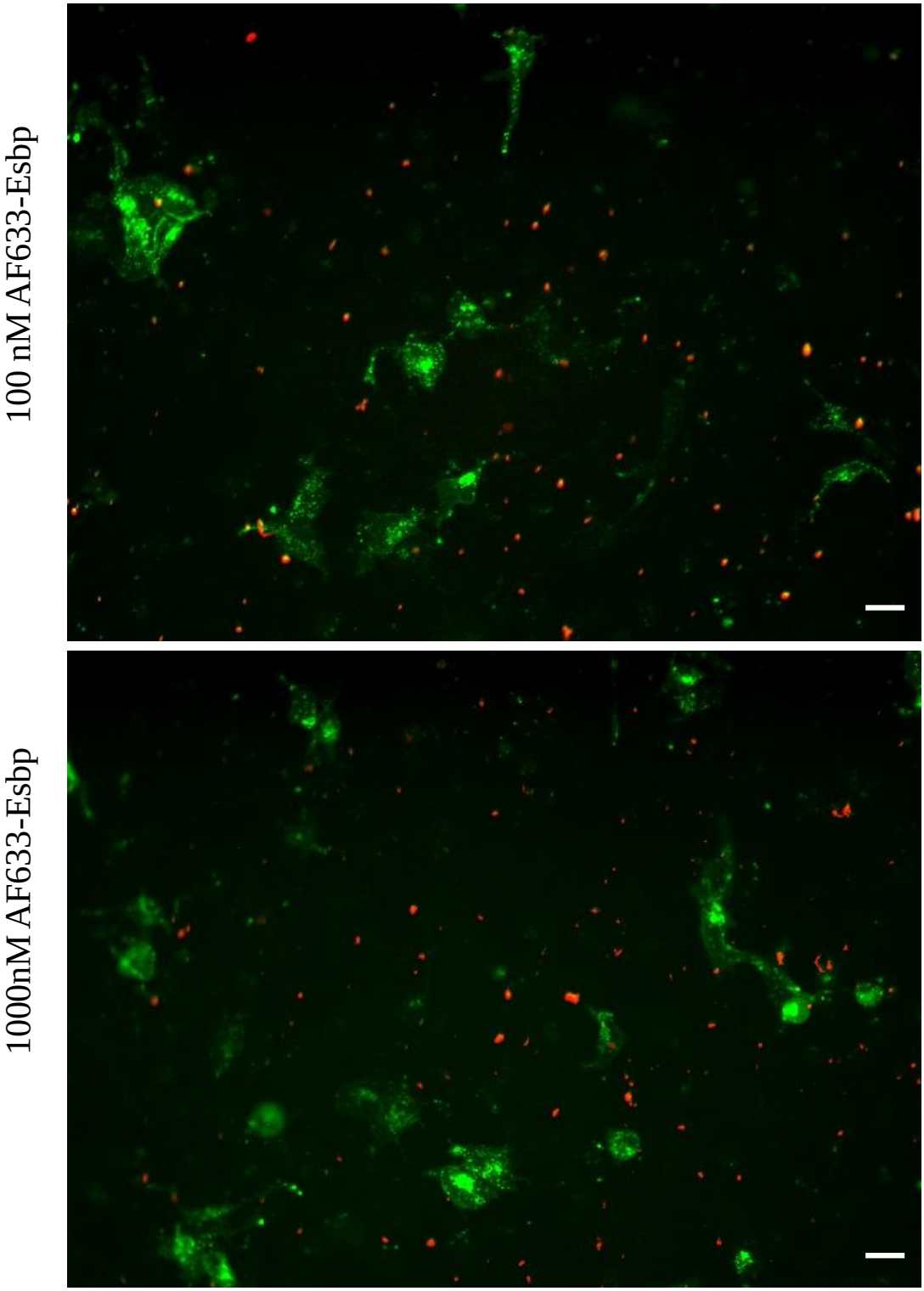

Figure 5.10 ***No co-localization of AF633-Esbp with SNAP-tag E-selectin was seen in HEK293Ts.*** *100 nM and 1000 nM of AF633-Esbp was incubated with SNAP-tag E-selectin (membrane impermeable label) transiently transfected in HEK293T cells (1 hr, 37C 5% CO2). The plate was then imaged used an IX micro widefield platereader and no co-localization of SNAP-tag E-selectin (green signal) with AF633-Esbp (red signal) was visualized, confirming that there is no binding happening between the selectin and ligand. (n=3) Scale bar = 50 µm*

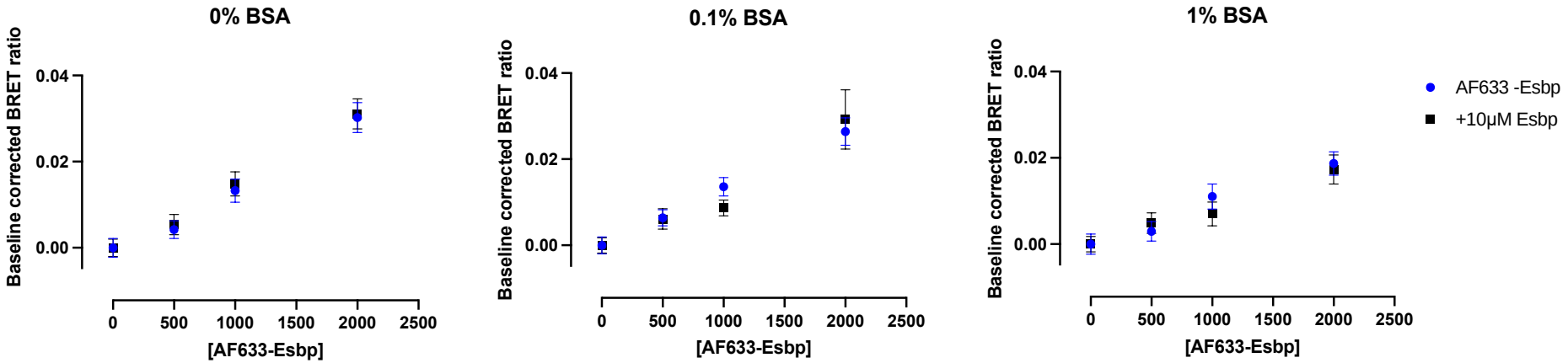

Figure 5.11 ***Addition of bovine serum albumin (BSA) into the vehicle did not result in specific binding of AF633-Esbp to E-selectin.*** *Saturable binding of AF633-Esbp was attempted with differing BSA concentrations added to the vehicle buffer (HBSS) in HEK293Ts stably expressing NanoLuc E-selectin (1 hr incubation with 0 – 2000 nM AF633-Esbp in the absence and presence of 10μM Esbp). There was no saturable binding or displacement due to addition of unlabelled Esbp observed with any concentration of BSA used. N=5, error = SEM.*

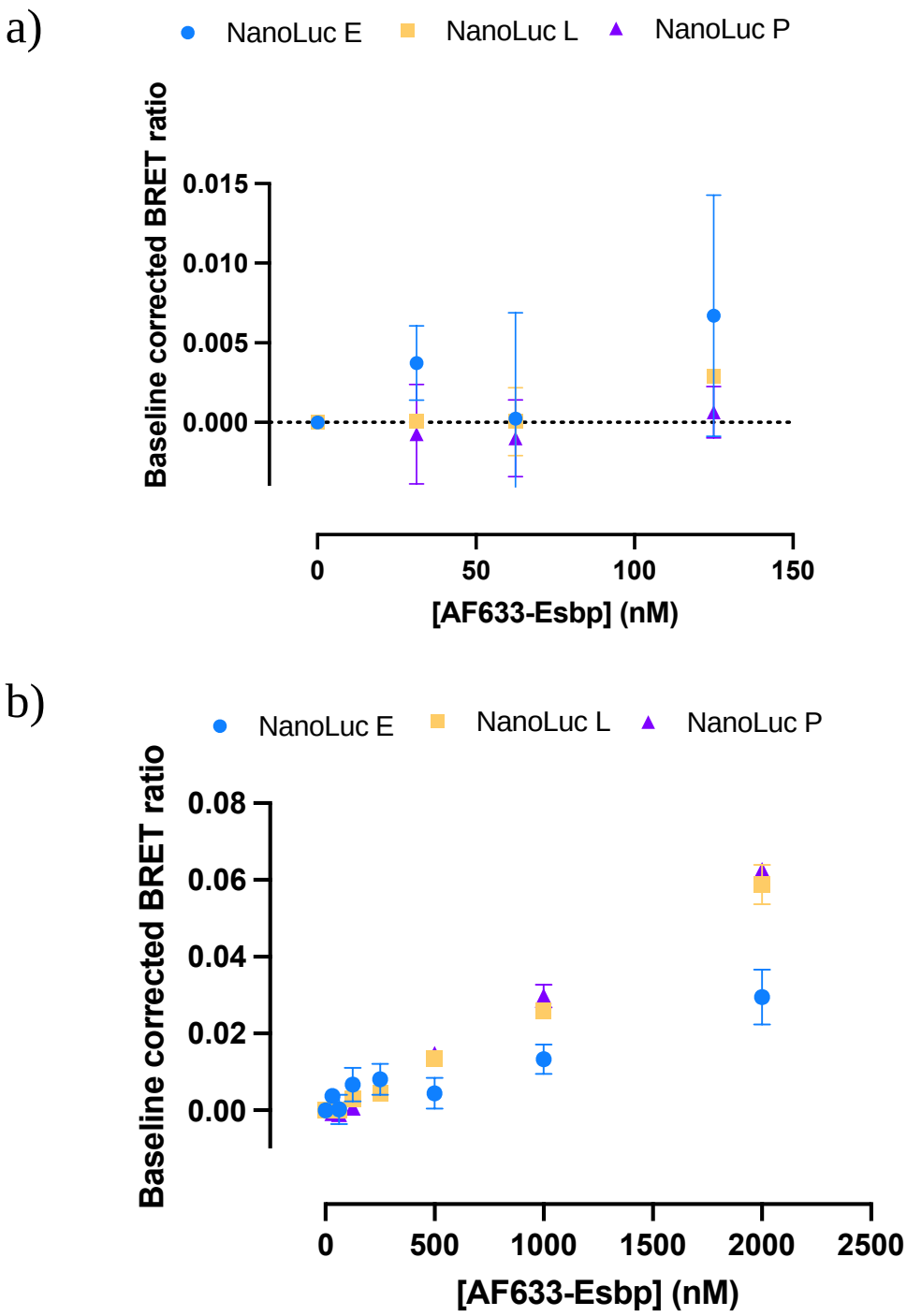

Figure 5.12 ***AF633-Esbp showed no specific binding to any selectin family member at low or high concentrations of probe.*** *NanoLuc-Selectin HEK293T stable cell lines were plated on the same 96-well plate and addition of increasing concentrations of AF633-Esbp (1 hr, 37C) did not show saturable binding at a a) low concentration range (0 – 125 nM) and b) high concentration range (0 – 2000 nM) Error bars = SEM, n=3.*

Due to the hypothesis that there was no E-selectin binding due to the absence of a linker between the Esbp pharmacophore and the fluorescent moiety, the peptide was re-synthesised with a GGGG linker. This peptide was also designed with an Alexa Fluor 488 fluorophore. Unfortunately, no saturable binding to NanoLuc E-selectin could be detected with AF488-Esbp (Figure 5.13). In this case, fluorescence intensity was quantified to verify accurate addition of increasing fluorescent Esbp and a linear increase was observed. AF488-Esbp binding was tested in the same manner using transiently transfected NanoLuc E-selectin in HEK293T cells (Figure 5.14) and TNF alpha stimulated TERT2 HUVEC HiBiT E-selectin clone C8 following addition of purified LgBiT (Figure 5.15) with no saturable binding observed for either cell population.

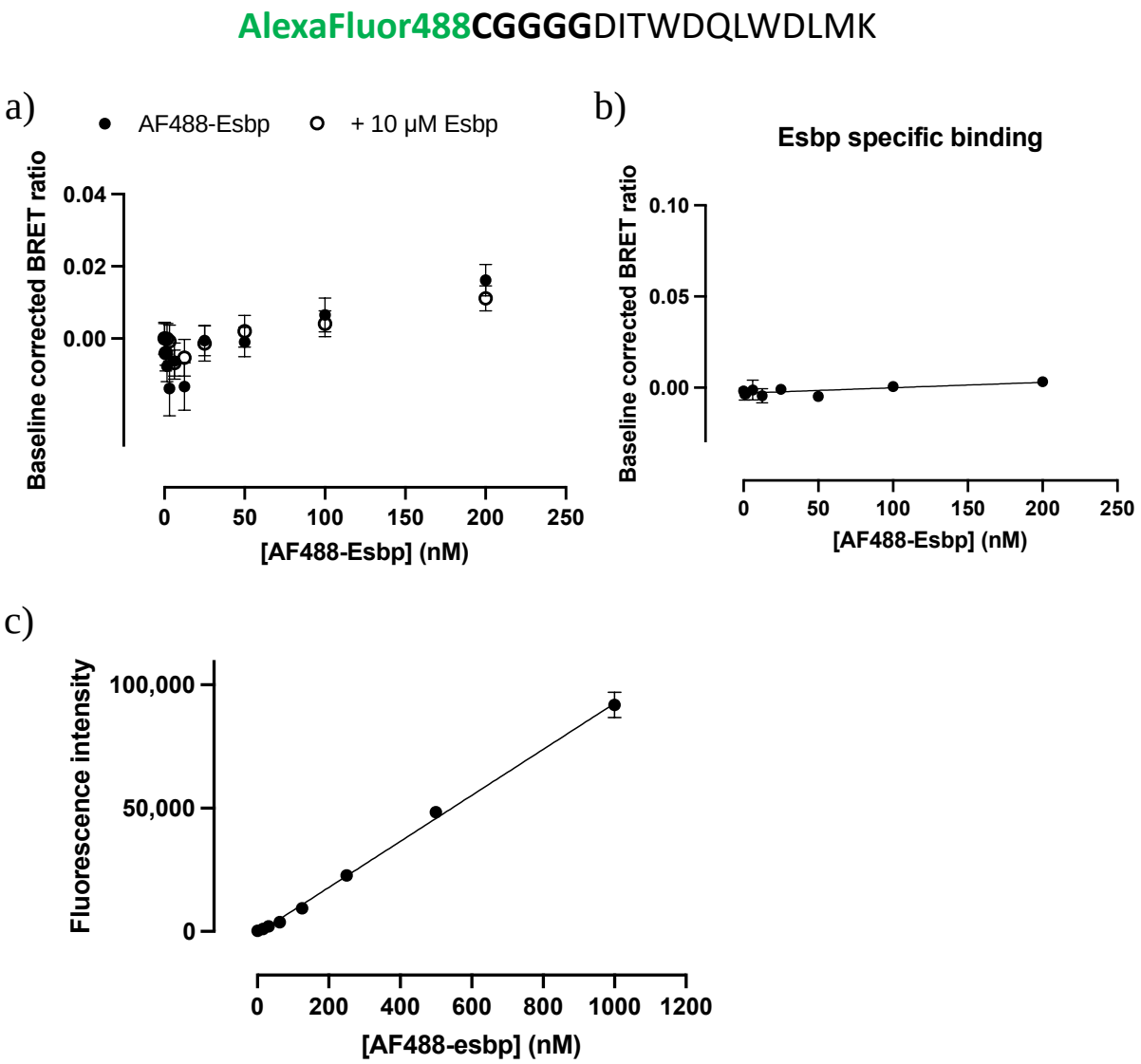

Figure 5.13 ***AF488—Esbp did not bind to NanoLuc E-selectin.*** *The change of fluorophore and additional peptide linker in comparison to AF633-Esbp, did not affect the ability of Esbp to bind to E-Selectin. a) No saturable binding, or displacement was seen for AF488-Esbp (0 – 200 nM, 1hr, 37C 5% CO2) in the absence and presence of unlabelled Esbp, leading to b) no specific binding being calculated. c) in this instance, fluorescence intensity was measured using a BMG PHERAstar 485/520 filter, gain 200. to assess whether addition of increasing concentrations AF488-Esbp was accurate – a correlation was quantified as expected. N=5, error bars = SEM.*

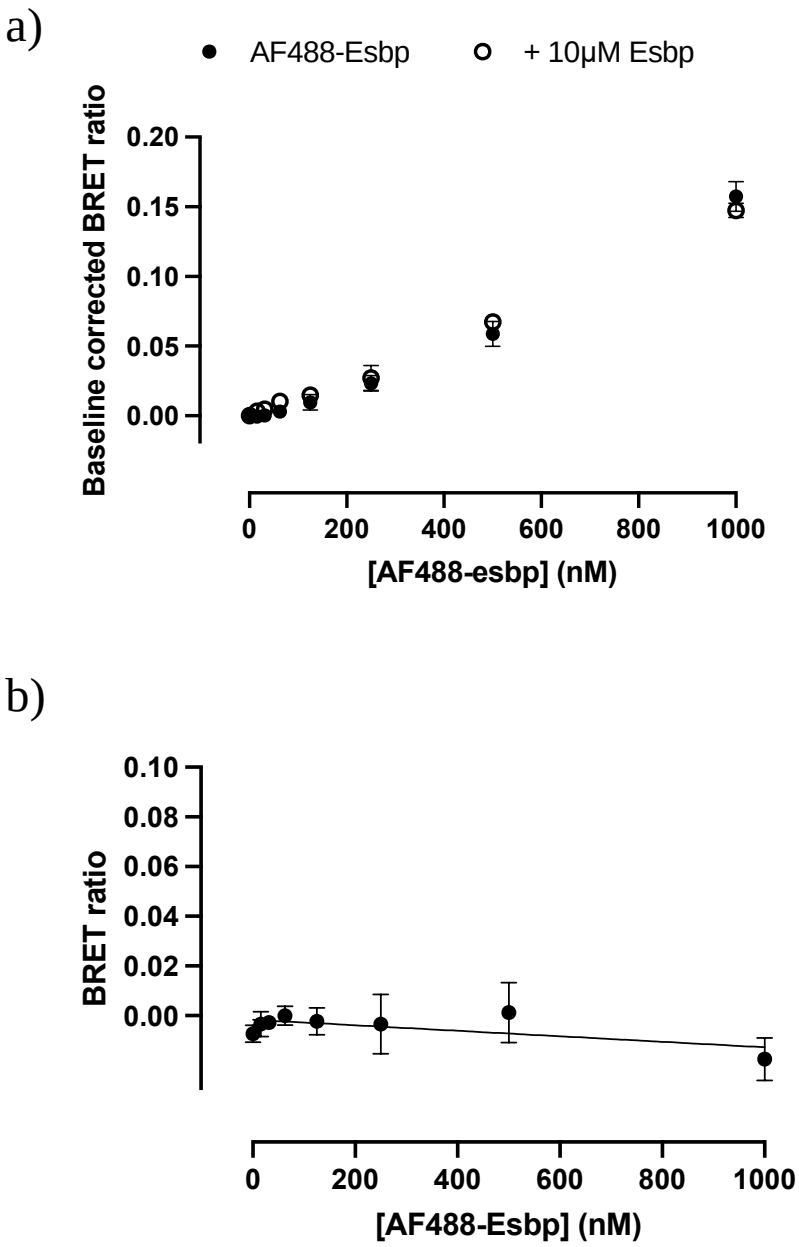

Figure 5.14 . ***AF488—Esbp did not bind to transiently transfected NanoLuc E-selectin.*** *Transiently expression of NanoLuc E-selectin did not affect the saturation of AF488-Esbp. a) No saturable binding, or displacement was seen for AF488-Esbp (0 – 1000 nM, 1hr, 37C 5% CO2) in the absence and presence of unlabelled Esbp, leading to b) no specific binding being calculated. N=1, error bars = SD*

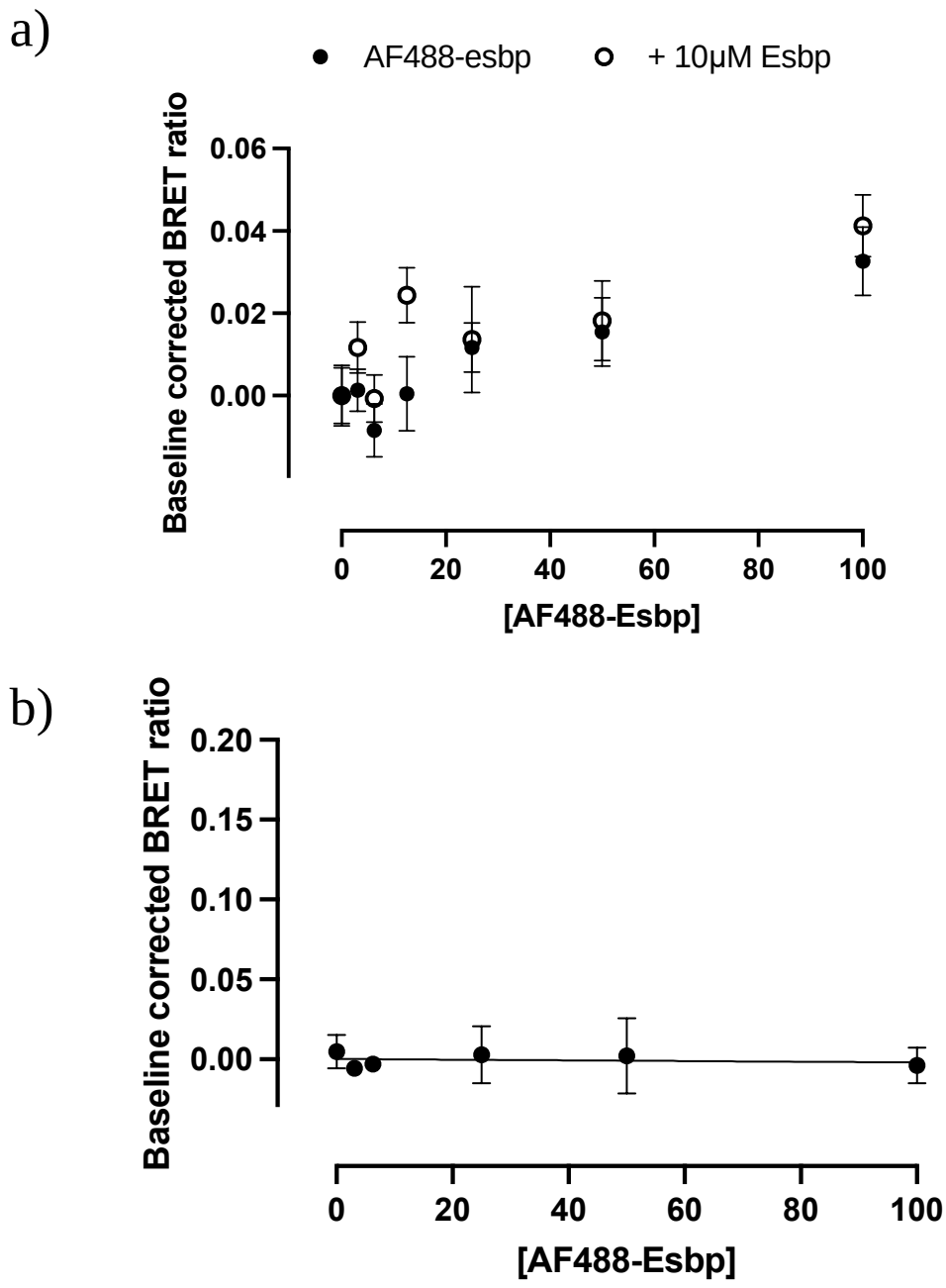

Figure 5.15 ***AF488—Esbp showed no specific binding to HiBiT E-selectin****. HiBiT E-selectin clone C8 TERT2 HUVECs were stimulated with 1 nM TNF alpha (6 hr, 37℃ 5% CO2), followed by addition of purified LgBiT (1:400, 20 min 37℃). AF488-Esbp was incubated with cells at increasing concentrations (0 – 100 nM) in the presence or absence of 10 μM Esbp (1 hr, 37℃ 5% CO2). a) There was no saturable binding or displacement after addition of unlabelled Esbp, meaning b) no specific binding was visualized in clone C8. n=1, error bars = SD.*

Finally, AF488-Esbp binding was tested in membranes prepared from HEK293T cells stably expressing NanoLuc E-selectin. First, membrane buffer was tested in the absence and presence of 0.25% Saponin, to test whether there was any spontaneous vesicle formation of membranes in the assay buffer which could have prevented binding of peptide (Figure 5.16). Presence of saponin only had an affect when using 1 µg per well of membranes, as a significant increase in BRET ratio was only observed in the presence of saponin (two-way ANOVA with Tukey's post hoc test ** $p<0.01$). In all other cases, a difference in BRET ratio was not observed compared to vehicle (ns, $p>0.05$). In addition, a significant difference in BRET ratio after addition of AF488-Esbp (200 nM) compared to vehicle was only observed using 1 µg or 2 µg membrane per well. Because of this, 2 µg membranes per well was used for subsequent saturation binding experiments. Unfortunately, no saturable binding was observed for AF488-Esbp using 2 µg membrane per well in the presence or absence of 0.25% Saponin (Figure 5.17).

a)

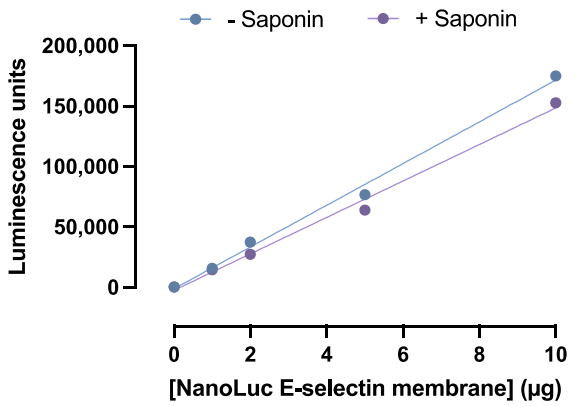

b)

	Mean Δ BRET ratio from vehicle - saponin	Mean Δ BRET ratio from vehicle + saponin
1 µg	0.0311	0.0613
2 µg	0.0517	0.0683
5 µg	0.0247	0.03145
10 µg	0.0333	0.0465

c)

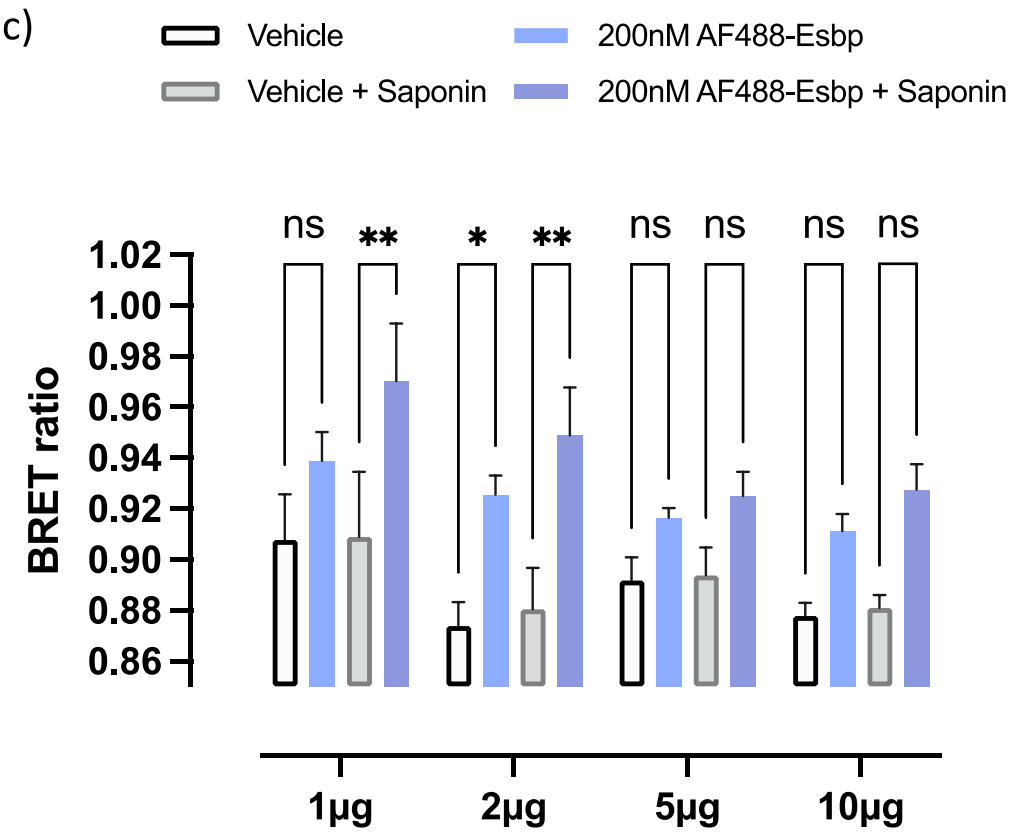

Figure 5.16 ***Changes in BRET ratio were seen with changes in NanoLuc E-selectin membrane concentrations.*** *Membranes were isolated from the NanoLuc E-selectin stable cell line and seeded onto 96 well plate in triplicate at amounts of 1 µg, 2 µg, 5 µg and 10 µg per well. Buffer consisted of 0.1% BSA HBSS in the absence or presence of 0.25% Saponin. a) The luminescence units correlated with the amount of membrane as expected with or without Saponin. b) AF488-Esbp was then incubated with membranes (200 nM, 1 hr, 37℃ 5% CO2). The change in BRET ratio was calculated for each membrane concentration in the presence or absence of saponin. c) The BRET ratio was analysed for a statistically significant increase from vehicle using two-way ANOVA with Tukey's post-hoc test. A statistically significant increase in BRET was only seen with lower membrane concentrations 1µg in the presence of Saponin (* $p<0.05$) and at concentration of 2 µg membrane in the presence ($p<0.01$) or absence ($p<0.05$) of Saponin. In all other cases a statistically significant increase was not calculated (ns). N=3, error bars = SEM.*

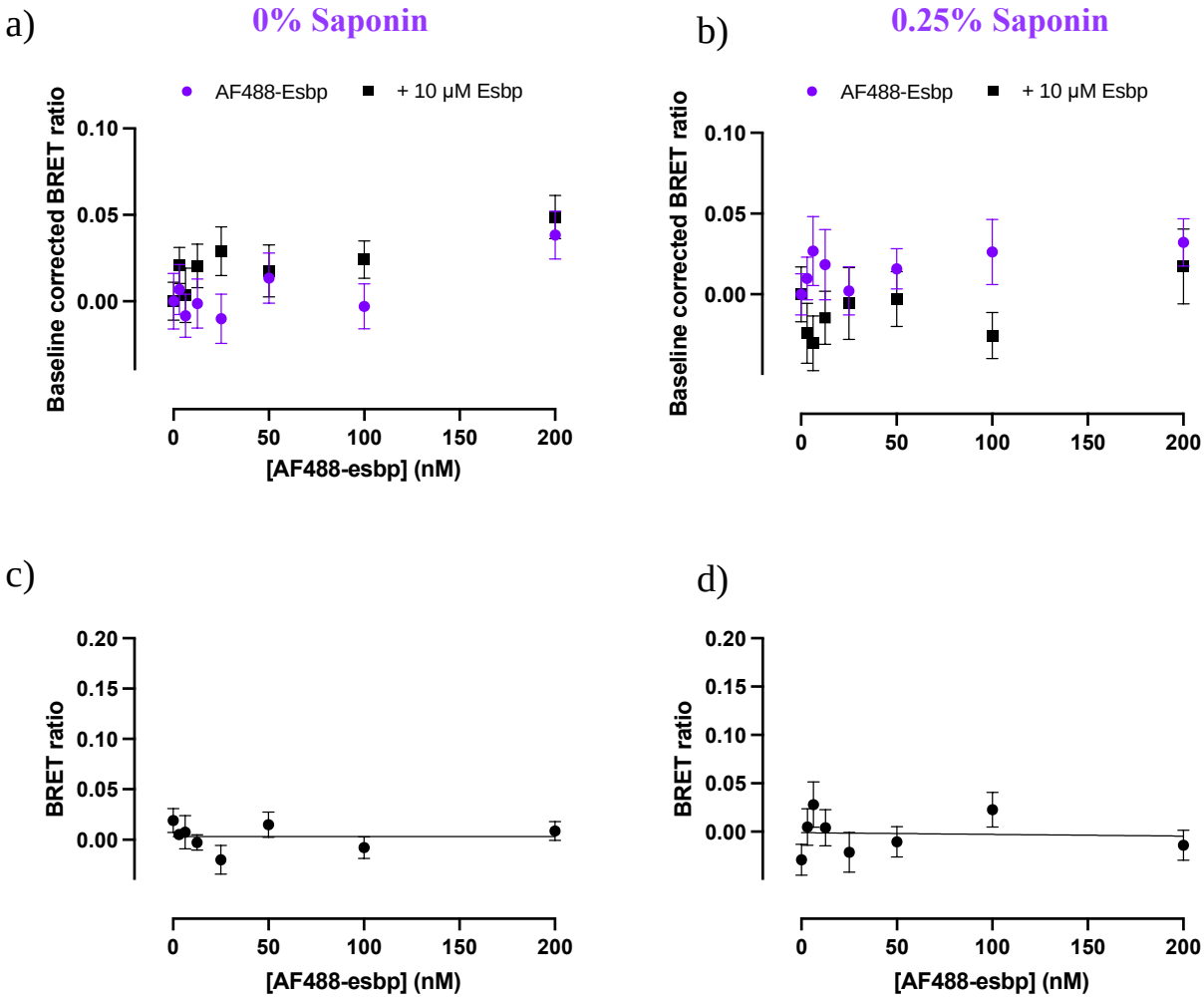

Figure 5.17 ***AF488-Esbp did not bind to NanoLuc E-selectin membranes in the presence or absence of 0.25% Saponin.*** *NanoLuc E-selectin membranes (2 µg) were plated onto each well of a 96 well plate, before addition of increasing concentrations AF488-Esbp (0– 200 nM) in the presence or absence of 10 µM Esbp (37℃, 1 hr). This was done a) and c) in the absence of Saponin and b) and d) in the presence of 0.25% Saponin in the 0.1% BSA HBSS buffer. In all cases, a) and b) there was no saturable binding observed, or displacement observed after addition of 10 µM unlabelled Esbp, resulting in c) and d) no specific binding being calculated. N=5, where each repeat used membranes isolated from a separate T175 flask, error bars = SEM*

Due to the hypothesis that the presence of the fluorophore was potentially preventing E-selectin binding, unlabelled Esbp was tested for its ability to internalise SNAP-tag E-selectin (Figure 5.18). A time dependent increase in internalisation was observed after 60 min of exposure with unlabelled Esbp. This was quantified using MetaXpress analysis, and a linear increase in the percentage of cells positive for internalised SNAP-tag E-selectin increased after 60 min Esbp incubation. SNAP-tag Beta 2 receptor was used in these experiments as a negative control as Esbp should not be able to bind and internalise this receptor. No increase in SNAP-tag Beta 2 receptor internalisation was measured over the course of 60 min Esbp stimulation (Figure 5.18). Esbp-induced internalisation was also quantified at TERT2 HUVEC HiBiT E-selectin clone C8 (Figure 5.19). Here, a 25% decrease in membrane expressed HiBiT E-selectin was observed after 1 hr exposure with unlabelled Esbp following addition of membrane impermeable purified LgBiT (One-way ANOVA with Tukey's post hoc test **** $p<0.0001$ $n=5$).

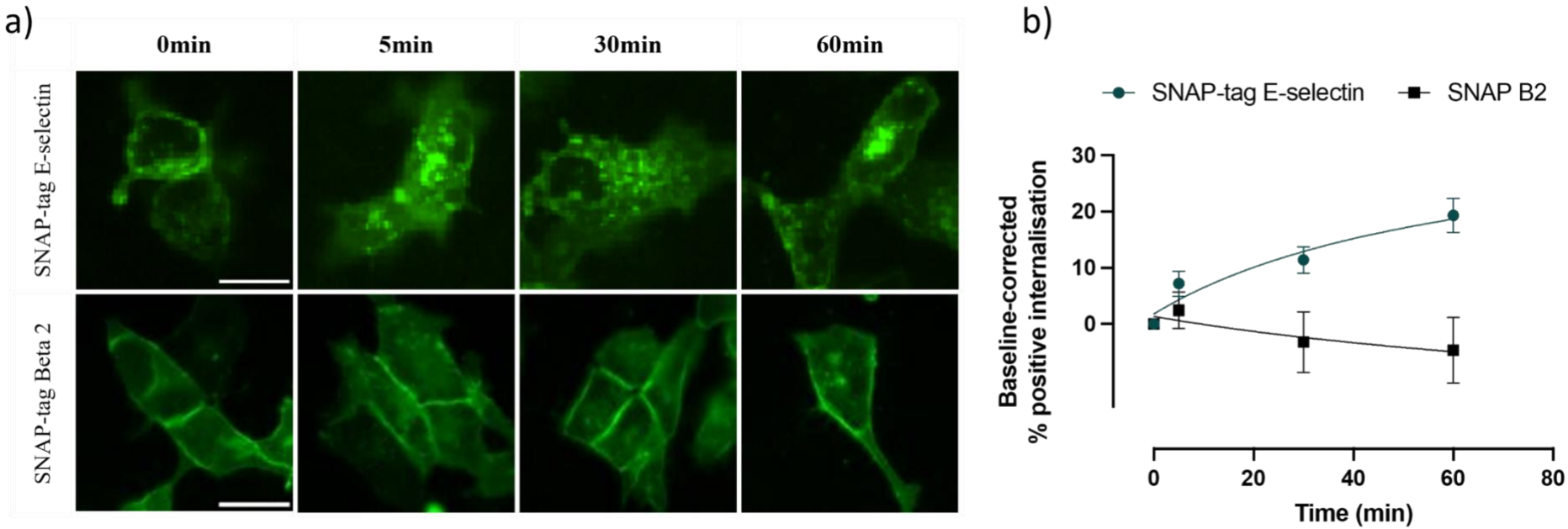

Figure 5.18 ***Esbp induced SNAP-tag E-selectin internalization.*** *a) SNAP-tag E-selectin or SNAP-tag beta 2 receptor were transiently transfected in HEK293T cells (100 ng total cDNA per well). Transfected cells were labelled with membrane impermeable SNAP-surface 488 substrate (30 min, 37℃ 5% CO2), before cells were incubated with Esbp (100 nM) for 5 min, 30 min, 60 min. Esbp induced an increase in internalization of SNAP-tag E-selectin but not SNAP-tag beta 2 receptor. Images were taken using IX micro widefield platereader and regions of interest were isolated (100x100pixel). Scale bar = 50 µm. b) % positive internalization was calculated using MetaXpress anaylsis and quantified on a per cell basis to to show an increase in SNAP-tag E-selectin localized within the cell compared to vehicle, N=5, error bars= SEM*

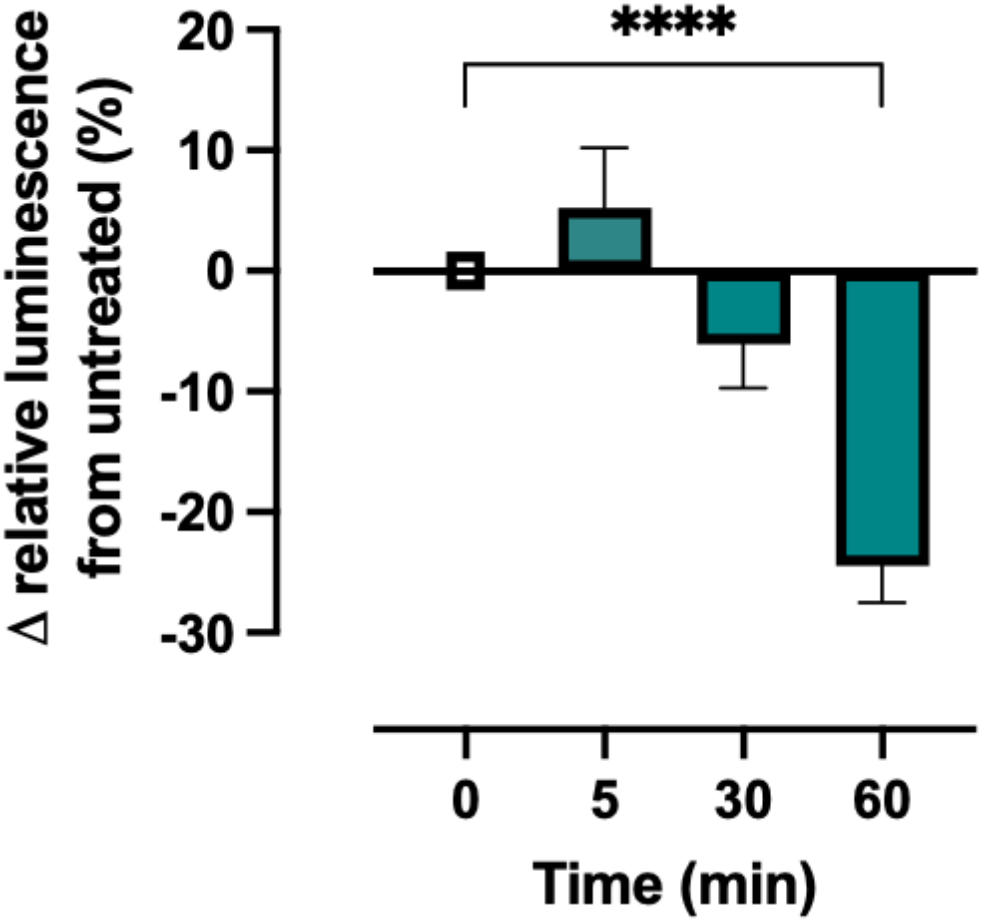

Figure 5.19 ***Unlabelled Esbp induced time-dependent internalization of HiBiT E-selectin.*** *TERT2 HUVEC HiBiT E-Selectin clone C8 was stimulated with TNF alpha to induce HiBiT E-selectin expression (1 nM, 6 hr 37℃ 5% CO2). Unlabeled Esbp (100 nM) was then added for 0 – 60 min at 37℃. Membrane impermeable purified LgBiT was then added (1:400, 20 min) followed by Furimazine (1:400). Luminescence emissions were then read using a BMG PHERAstar platereader. A significant decrease in luminescence indicative of a decrease in surface expressed HiBiT E-selectin was quantified after 60 min of Esbp stimulation (One-way ANOVA with Tukey's post-hoc test, **** P<0.0001). N=5, error bars = SEM.*

5.2.3 NanoBRET interactions between membrane expressed NanoLuc E-selectin and SNAP-tag labelled selectins/receptors

Interactions of NanoLuc E-selectin with AF488-SNAP surface labelled SNAP-tag E-/P-/L-selectin were investigated using NanoBRET. An increase in fluorescence intensity after addition of increasing amounts of cDNA (0 -100 ng) of acceptor SNAP-tag DNA was verified by measuring fluorescence intensity (FI) before the NanoLuc substrate furimazine was added and dual luminescence and fluorescence emissions subsequently measured (BRET). An increase in FI was observed with increasing addition of acceptor DNA encoding for SNAP-tagged proteins (Figure 5.20). In addition, a NanoLuc NRP-1 and SNAP-tag NRP-1 pairing was included as a positive control alongside each experiment (Figure 5.20a). NRP-1 is a transmembrane protein that has a well established interaction with VEGFR2 on the surface of endothelial cells and has been shown to form homodimers (King *et al.*, 2018). NanoLuc E-selectin and SNAP-tag Adenosine-3 (A3) receptor exhibit no interactions on the membrane, therefore was used as a negative control. The ratio of fluorescence:luminescence (BRET ratio) revealed that there was no saturable binding between E-selectin and P-selectin (EP) (Figure 5.20c), however hyperbolic curves were observed after addition of increasing concentrations of L-selectin and E-selectin indicating saturable binding (Figure 5.20d/e).

NanoLuc E-selectin was then tested for saturable binding with Halotag VEGFR2 and SNAP-tag NRP-1. Using NanoLuc NRP-1 and SNAP-tag NRP1 as a positive control in both cases, no saturable binding could be detected between E-selectin and NRP-1 (Figure 5.21) nor for E-selectin and VEGFR2 (Figure 5.22).

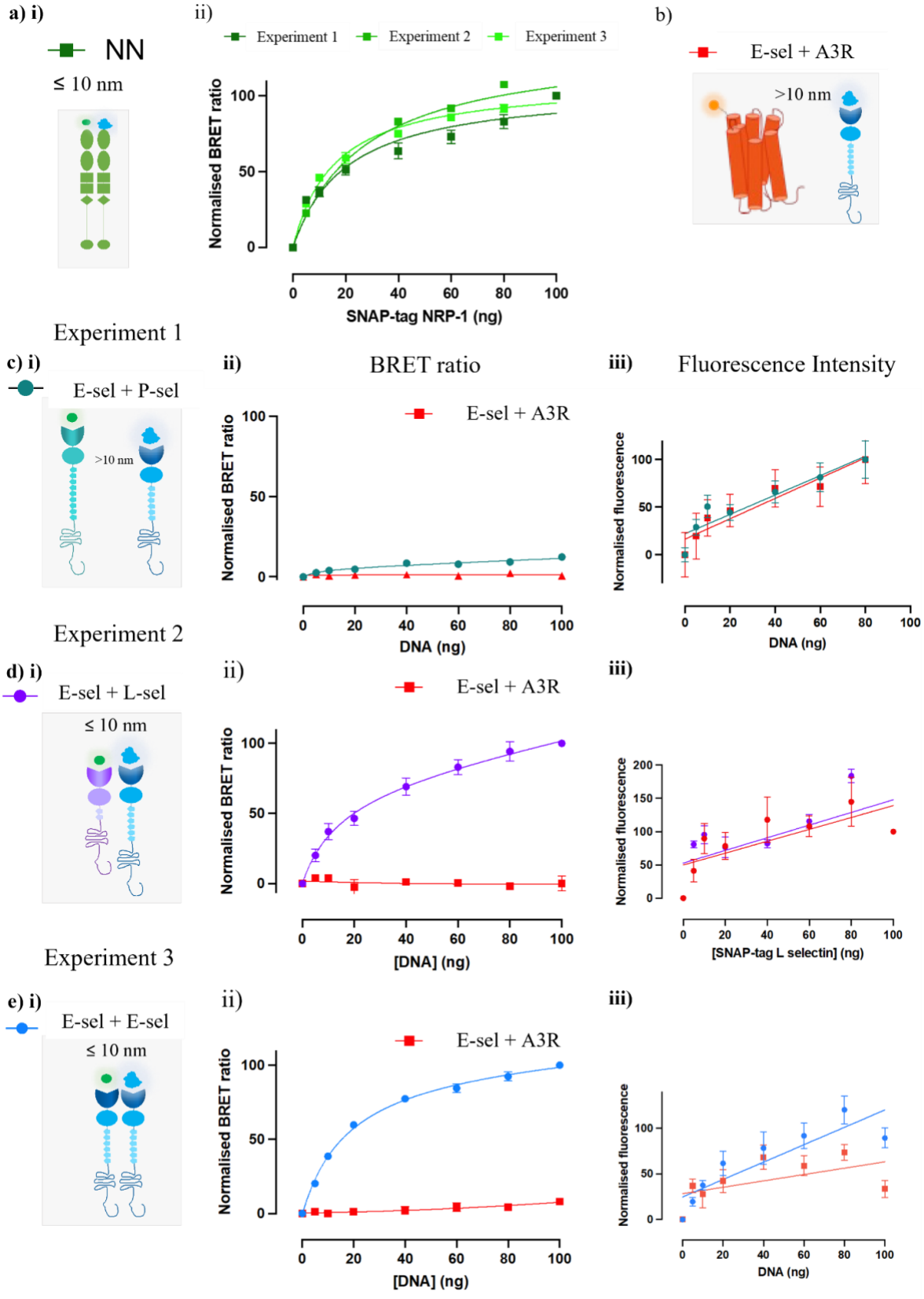
a) i)
NN
≤ 10 nm
ii)
Experiment 1
Experiment 2
Experiment 3
Normalised BRET ratio
SNAP-tag NRP-1 (ng)
b)
E-sel + A3R
>10 nm
Experiment 1
c) i)
E-sel + P-sel
>10 nm
ii)
BRET ratio
E-sel + A3R
Normalised BRET ratio
DNA (ng)
iii)
Fluorescence Intensity
Normalised fluorescence
DNA (ng)
Experiment 2
d) i)
E-sel + L-sel
≤ 10 nm
ii)
E-sel + A3R
Normalised BRET ratio
[DNA] (ng)
iii)
Normalised fluorescence
[SNAP-tag L selectin] (ng)
Experiment 3
e) i)
E-sel + E-sel
≤ 10 nm
ii)
E-sel + A3R
Normalised BRET ratio
[DNA] (ng)
iii)
Normalised fluorescence
DNA (ng)

Figure 5.20 ***E-selectin formed homodimers, and heterodimers with L-selectin but not P-selectin as measured using BRET.*** *A constant amount of donor cDNA (NanoLuc E-selectin, 20 ng per well on 96 well plate) was transfected in HEK293Ts in the presence of increasing concentrations of acceptor cDNA (SNAP-tag P-/L-/E-selectin) to investigate interactions using BRET. All i) Schematics representing no BRET due lack of proximity between the fluorophore and NanoLuc tags. a)ii) Neuropilin homodimer formation was used as a positive control for each experiment 1, 2 and 3 investigating selectin interactions. In all cases saturable binding was observed. b) schematic to describe the negative control for selectin binding with adenosine A3 receptor (A3R). c) ii) Experiment 1, SNAP-tag P-selectin did not show saturable binding with NanoLuc- E-selectin indicative of no interaction (E-sel + P-sel, turquoise). b) ii) Experiment 2 and c) ii) Experiment 3; NanoLuc E-selectin displayed saturable binding with SNAP-tag L-selectin (E-sel +L-sel, purple) and SNAP-tag E-selectin (E-sel + E-sel, blue), as seen in the positive controls for all experiments shown in a) ii) Neuropilin-Neuropilin (NN) homodimer. All iii) fluorescence intensity increased as the concentration of SNAP-tag-selectin increased. Error bars = SEM, n=5.*

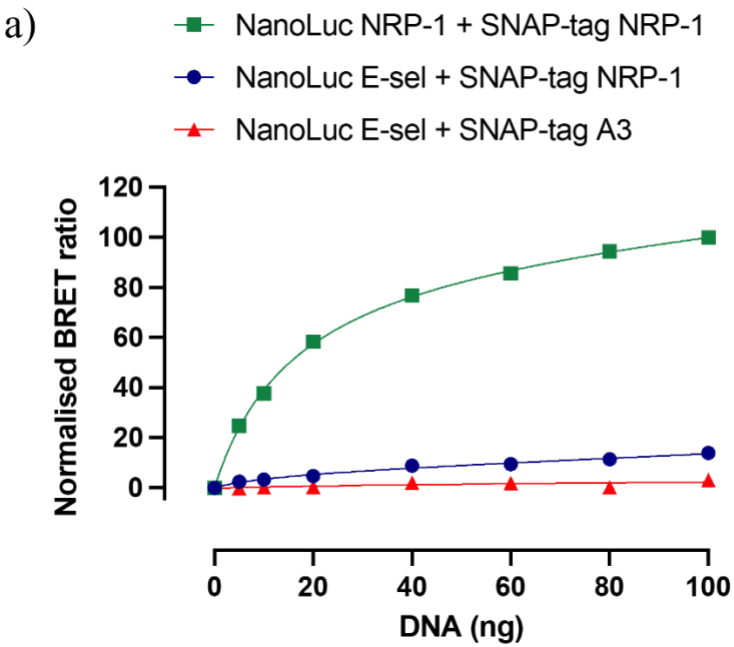

Figure 5.21 ***There was no interaction between E-selectin and NRP-1.*** *a) saturation can only be seen for the NanoLuc NRP-1- SnapTag NRP-1 (NN, green) positive control. Interaction was similar to SnapTag A3 negative control or SnapTag E-selectin (EA, red) for E-selectin and NRP-1 (EN, blue). b) fluorescence intensity correlated with increased addition of acceptor SNAP-tag DNA for i) SNAP-tag NRP-1 addition in positive control (NN), ii) SNAP-tag NRP-1 addition in EN test, and iii) SNAP-tag A3 addition in negative control (EA).*

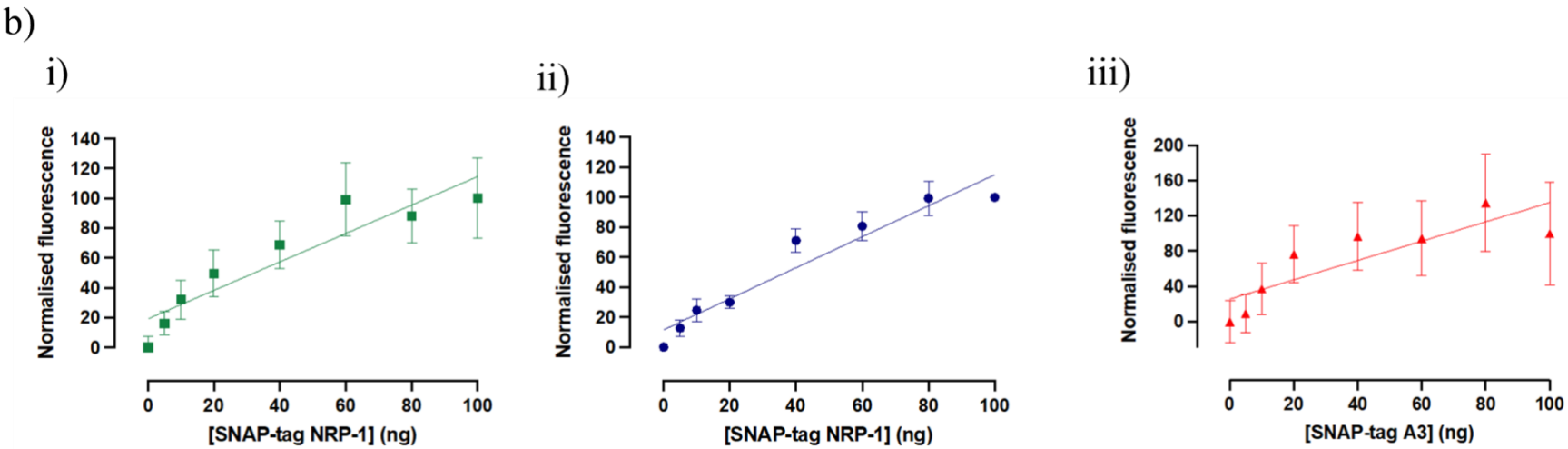

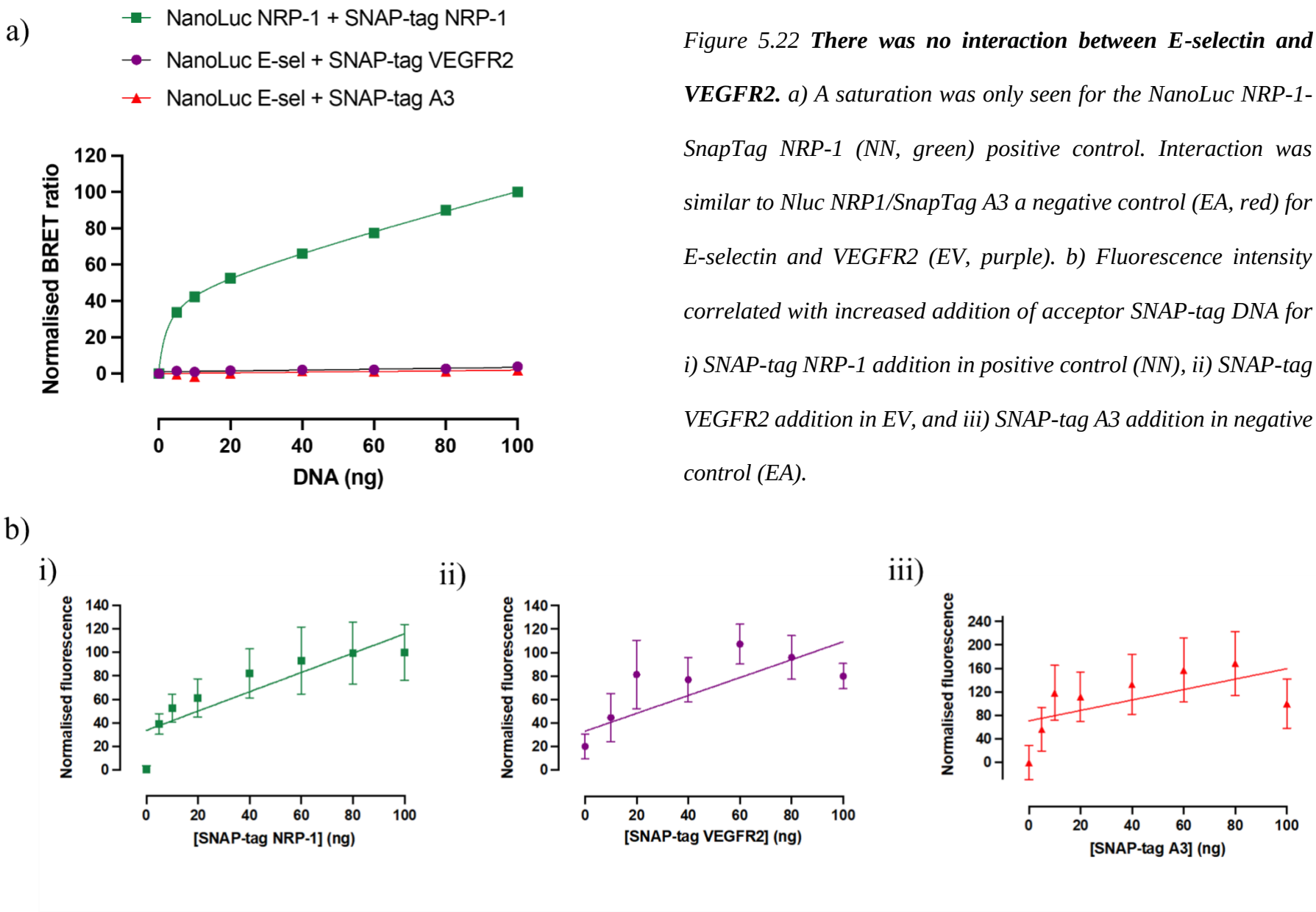

Figure 5.22 ***There was no interaction between E-selectin and VEGFR2.*** *a) A saturation was only seen for the NanoLuc NRP-1-SnapTag NRP-1 (NN, green) positive control. Interaction was similar to Nluc NRP1/SnapTag A3 a negative control (EA, red) for E-selectin and VEGFR2 (EV, purple). b) Fluorescence intensity correlated with increased addition of acceptor SNAP-tag DNA for i) SNAP-tag NRP-1 addition in positive control (NN), ii) SNAP-tag VEGFR2 addition in EV, and iii) SNAP-tag A3 addition in negative control (EA).*

5.3 Discussion

This chapter investigated binding of a fluorescent labelled version of an E-selectin targeting peptide (Esbp) using NanoBRET. Two versions of a fluorescently labelled peptide; AF633-Esbp and AF488-Esbp were used with neither showing specific binding to NanoLuc E-selectin whole cell assays. This was not due to the assay set up, as a positive control exhibited saturable binding of a fluorescently tagged CXCR4 agonist to NanoLuc CXCR4, which was displaced by an unlabelled CXCR4 antagonist. Here, saturable binding could be detected after addition of increasing concentrations of fluorescent CXCR4 agonist, where binding increased to a maximum plateau. As increasing concentrations of AF633- or AF488- Esbp were added, a linear increase in BRET ratio was detected, indicative of nonspecific BRET. Non-specific BRET, or bystander BRET, occurs when the signal is a result of non-specific interactions of the fluorescent ligand, for example colocalization in the same membrane region due to random collisions, which commonly occurs when excessive concentrations of acceptor are added (Pfleger and Eidne, 2006).

The ability of the fluorescent peptide to specifically bind to E-selectin was not affected by BSA concentration, fluorophore conjugation, selectin family member investigated, or by reducing the concentration of donor. This last assay was chosen, as it was possible that the NanoLuc E-selectin expression was too high in the stable cell lines to be saturated by the concentrations of fluorescent peptide used. To investigate this, NanoLuc E-selectin was transiently transfected into HEK293T cells, however this lower expression of NanoLuc E-selectin did not make a difference to Esbp-AF633 binding. In addition, membranes were isolated from the stable HEK293 NanoLuc E-selectin cell line, and a consistent amount of membrane per well (1 µg – 10 µg) was added in the presence of a fixed concentration of fluorescent peptide. Here, a difference was noticed where a significant increase in BRET was observed when using lower concentrations (1 – 2 µg per well) of membrane which wasn't seen with higher concentrations (5 – 10 µg per well). However further experiments investigating binding using 2 µg membrane per well still exhibited no saturable binding of the fluorescent peptide. Lack of binding to NanoLuc E-selectin could be due to a multitude of reasons stemming from either the fluorescent modification of Esbp or the luminescent protein modification of E-selectin affecting binding (Figure 5.23).

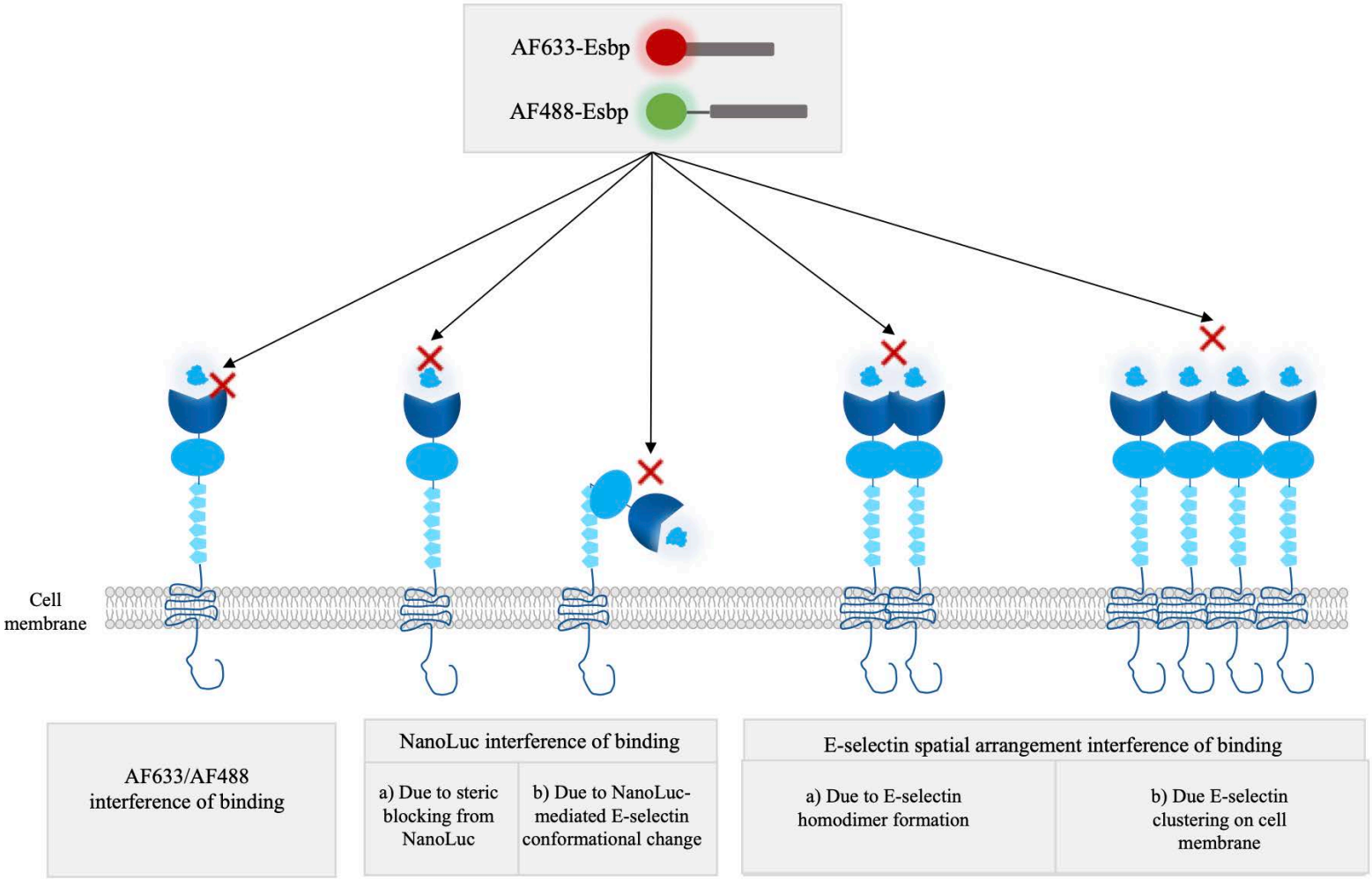

Figure 5.23 ***The possible reasoning for no binding of fluorescently labelled Esbp to NanoLuc E-selectin.*** *Firstly, the addition of a fluorophore could have blocked the binding domain of Esbp and inhibited binding. Alternatively, the NanoLuc tag on E-selectin could have interfered with binding via directly blocking the binding site, or by causing conformational change of the E-selectin protein therefore disabling access to the Esbp binding site. In addition, the spatial arrangement on the cell membrane could have contributed towards Esbp blockade, due to homodimer formation or clustering of E-selectin proteins on the membrane occluding the Esbp binding site.*

Previous studies found that truncation of the N-terminal D and I amino acids of the Esbp **DI**TWDQLWDLMK sequence, inhibited binding significantly (Martens *et al.*, 1995). Therefore, it was stipulated that the conjugation of AF633 to Esbp could be inhibiting this functional domain's ability to bind E-selectin. This theory was further warranted, as in the absence of fluorophore conjugation, Esbp seemed to be interacting with E-selectin as there was increased internalisation of SNAP-tag and HiBiT tagged E-selectin in HEK293T cells and TERT2 HUVECs respectively (Figure 5.18 and Figure 5.19). Despite this, an AF488 conjugated Esbp peptide designed with a flexible glycine (G) linker (GGGG) on the N-terminus still exhibited no binding to NanoLuc E-selectin. Potentially, a larger linker is required, or the location of the fluorophore on the N-terminus needed to be switched to the C-terminus to facilitate binding.

Esbp-conjugate binding has been performed before for polymer-drug carriers, as well as Alexa Fluor 488 labelled Esbp and both have reported success in E-selectin targeting when conjugated to both the N-terminus or the C-terminus with and without a GGG-cysteine (C) linker (Shamay *et al.*, 2009b; Goel *et al.*, 2022). The difference between these assays however, were that they measured binding to recombinant E-selectin coated plates as opposed to whole cells in most cases. Goel et al., (2022) did utilise a whole-cell binding assay however here, they modified neuroprogenitor cells (NPCs) to present Esbp. They measured a significant increase in binding to TNF alpha activated human aortic endotheial cells (HAoECs). In this case, there was no N-terminal modification of E-selectin with a tag, suggesting that this may also be a contributing factor towards the lack of detectable specific binding to NanoLuc E-selectin. Previously, HiBiT addition to E-selectin has been shown to inhibit antibody binding (see Chapter 4, Figure 4.11), suggesting that edits at the N-terminus of E-selectin could be blocking N terminal binding sites for E-selectin. Alternatively N-terminal edits could be causing conformational change in the E-selectin protein, disabling peptide access. As mentioned in Chapter 4 discussion, investigation of the structure of E-selectin with and without N-terminal tags would be extremely informative on this issue.

In addition, NanoBRET interactions between NanoLuc and SNAP-tag E-selectin revealed homodimeric complexes forming between E-selectins. This membrane arrangement alone, or in conjunction with NanoLuc tags, and fluorescent tags, could be sterically inhibiting binding of the fluorescent Esbp conjugates. Clustering of multiple interacting E-selectins could be

occurring on the membrane surface further complicating binding. Induced dimerization of E-selectin facilitated by a C-terminal Fc region was shown to enhance binding of the dimeric ligand PSGL-1 and monomeric ligand HCELL (Aleisa *et al.*, 2020), therefore to follow this theory, Esbp could bind to a different site than these endogenous ligands if there was a decrease in binding.

The location for Esbp binding to E-selectin has not been mapped, however but it has been suggested that it can't be binding to the lectin domain as it did not act as a sialyl lewis x (sLe^x) binding glycomimetic. This was concluded as unlike sLe^x, Esbp binding was Ca^{2+} independent, and sLe^x did not inhibit binding of radiolabelled-Esbp to E-selectin (Martens *et al.*, 1995). Binding could be occurring at a site distinct from this, such as the EGF domain or CR units responsible for extending the lectin-binding domain beyond the crowded glycocalyx of the cell surface (Bevialacqua *et al.*, 1989). Aleisa et al., (2020) synthesised multiple forms of E-selectin using the silkworm expression system, including forms with differing number of CR units (6, 2 and 0) to evaluate their role in binding to their endogenous ligands PSGL-1 and HCELL. They found that both the association and dissociation rate of binding to these ligands was dependent on the number of CR domains, where a reduction in CR units resulted in a decline in functional binding. In contrast, the lectin and EGF domains were only affecting the ligand dissociation rate. This could simply be due to the fact that full-length E-selectin would be in closer proximity to cells and enhancing chance of binding. It was also stipulated that increased CR units increases the association rate by interacting with other regions of the ligands, or that the number of CR units presents the lectin and EGF domains in the proper confirmation thus improving binding. An increased size of the lectin-EGF interdomain angle has been shown to exhibit stronger binding for mouse E-selectin compared to human-E-selectin which did not have this confirmational change (Rocheleau *et al.*, 2016). This was replicated by mutating the lectin domain at position A28H and significantly improved binding of E-selectin was observed (Aleisa *et al.*, 2020). Knowing that the CR units play a significant role in binding affinity to ligands, the Esbp peptide could be interacting with these regions to inhibit or reduce leukocyte rolling which was observed in previous studies (Martens *et al.*, 1995; Shamay *et al.*, 2009b, 2015b) by affecting the ligand-lectin interactions. If this is the binding site, it could explain why dimerization or clustering of E-selectins would reduce accessibility for the peptide as CR domains are more hidden. No increase in binding was seen where a reduction in E-selectin was controlled in transient transfections and membranes, however potentially a further decrease in expression, and therefore clustering, needs to be tested in future experiments. The inducement

or prevention of E-selectin dimerization could be tested by modifying C-terminal regions of E-selectin as described before (Aleisa *et al.*, 2020), and the effect on binding could be tested for the fluorescent peptides.

The interaction of NanoLuc E-selectin with VEGFR2 and NRP-1 was investigated, however no interaction was observed using BRET. This was investigated as the VEGFR2 and NRP1 endogenous ligand $VEGF_{165}a$ had been shown to induce E-selectin expression previously (see Chapter 3 and Chapter 4) and like E-selectin, VEGFR2 and NRP1 have been shown to be expressed at high levels on endothelial cells and endothelial primary cells (HUVECs, TERT2-HUVECs) (Mehta *et al.*, 2018). NanoLuc E-selectin interaction with SNAP-tag E- P- and L-selectin was also investigated. BRET revealed close proximity of NanoLuc and SnapTag E-selectin indicative of homodimer formation. Homodimeric E-selectin complexes have been shown to increase binding affinity and strength of binding with leukocyte receptors such as dimeric PSGL-1 (Aleisa *et al.*, 2020). This induces slow rolling with leukocytes and this stage precedes firm adhesion and diapedesis via differential endothelial cell receptor binding (see Chapter 1 Introduction). It would be interesting to investigate whether homodimer formation was an initial and inherent mechanism for E-selectin or whether it is mediated by number of molecules present on the endothelium, the life-time of expression of E-selectin (are these homodimeric complexes pre-formed during cell surface translocation) or by any other exogenous or internal signaling that could be occurring. In addition, E-selectin showed no specific BRET signal and hence proximity with the endothelial cell localised selectin family member P-selectin, which highlights a potential significant difference in their roles in the two different phases of inflammation. One could argue that the taller P-selectin's SNAP-tag was too far or in an incorrect orientation to enable optimal energy transfer, especially if dimeric formation was occurring at C-terminal regions and if there were conformational changes in selectins causing further distance between SNAP-tag and NanoLuc tags. However, these potential issues did not exist between the equally different sizes of L-selectin and E-selectin. Close proximity of E-selectin and L-selectin in these BRET experiments further solidifies the theory that EL interaction between leukocytes and endothelial cells is occurring. Because of this, potentially an E-L-selectin inhibitor could be more effective in ameliorating inflammatory disease symptoms by increased inhibition of leukocyte extravasation. These binding studies not only elucidated the potential role of E-selectin physiologically, but also showed that interactions can be measured between selectins using NanoBRET and the absence of NanoBRET binding between fluorescent Esbp was more likely due to steric hindrance. It is

likely that dimerization occurs at a different site to Esbp binding, but this could be tested in the future by measuring the ability of Esbp to inhibit E-selectin homodimer formation and/or EL heterodimer formation.

The NanoBRET experiments only investigated E-selectin interactions in over-expressed HEK293Ts, which is likely not reflective of their native interactions in endothelial cells. In response to inflammatory cytokines TNF alpha, IL-1 beta and LPS, endothelial cells also express other adhesion molecules such as ICAM-1 and VCAM-1. Other adhesion molecules are constitutively expressed on endothelial cells such as vascular endothelial (VE)-cadherins which are presented in endothelial cell-cell junctions, integrins which are largely expressed in their inactive form and Syndecans which expression is increased by inflammatory cytokines (Silva *et al.*, 2008; Vestweber, 2008; Gopal, 2020). All of these adhesion molecules that HEK293Ts do not express, could be supporting selectin interactions, therefore investigating NanoBRET in endothelial cells could shed light on whether interactions can occur in their native cells. In addition, an inflammatory environment could be affecting E-selectin membrane activity, and VEGFR2 stimulation with $VEGF_{165}a$ could be altering interactions with E-selectin. Future experiments could therefore see whether change in inflammatory environment alters selectin-selectin, selectin-VEGFR2 or selectin-NRP-1 interactions.

5.4 Conclusions

To conclude, no specific binding was observed for two fluorescently labelled E-selectin-targeting peptides using NanoBRET. This was likely due to steric interference of the peptides N-terminal fluorophore, or the N-terminal NanoLuc E-selectin tag, occluding binding, as unlabelled Esbp was able to induce SNAP-tag and HiBiT E-selectin internalisation. However, NanoBRET interactions could provide information on homodimer formation of E-selectin and heterodimer formations between E-selectin and L-selectin. This interplay could explain interference of Esbp binding due to E-selectin clustering. In addition, this suggests that the binding sites enabling dimerization between selectins were different to the orthosteric binding site of Esbp. Future experimentation could look at differential N-terminal location of tags with HiBiT or NanoLuc to see whether this affects interference of Esbp binding, or conformational changes in selectins.

Chapter 6 General Discussion

E-selectin is a key player in vascular inflammation due to its role in extravasating leukocytes into tissue. As a consequence it has been treated as a biomarker for early vascular disease diagnosis and targeted for inhibition to prevent disease progression. Understanding E-selectin expression dynamics, membrane organisation and binding of potential therapeutics is pivotal when approaching drug design and drug testing. Therefore this project aimed to characterise differential cytokine inducements of surface E-selectin expression as well as create an *in vitro* model that could be used in drug discovery programmes to pharmacologically quantify E-selectin targeting therapeutics.

Chapter 3 characterised E-selectin expression in fixed HUVECs using anti E-selectin monoclonal antibody labelling with confocal microscopy and ELISA quantification in response to a potent inflammatory mediator (TNF alpha) as well as weak stimulants ($VEGF_{165}$a and histamine). In addition, $VEGF_{165}$a and histamine worked synergistically with TNF alpha to significantly further increase induced E-selectin expression compared to TNF alpha alone.
Chapter 4 further characterised and replicated WT HUVEC data for E-selectin expression in CRISPR edited HUVECs and TERT2 immortalised HUVECs. Here, a rank order of potency for inflammatory cytokines was quantified for TNF alpha, LPS, IL-1 alpha/beta, $VEGF_{165}$a and histamine. NanoBiT was used to measure the dynamics of cell surface expression of E-selectin in live cells over the course of 15 hr with greater temporal sensitivity than has been previously possible with techniques used to investigate E-selectin expression.
Chapter 5 began to explore binding kinetics of a novel E-selectin peptide Esbp, using free and fluorescent-conjugated versions with HiBiT, NanoLuc and SNAP-tag E-selectin in TERT2 HUVECs and HEK293Ts respectively. Here, only free-Esbp could induce HiBiT-E-selectin internalisation as a result of 60 min incubation, and NanoBRET could not detect any specific binding with fluorescent conjugated Esbp. Here the importance of investigating steric hindrance of fluorophores was discussed. In addition, membrane expressed selectin interactions were explored using NanoBRET and E-selectin homodimer formation, as well as E- and L-selectin heterodimer interactions were confirmed.

6.1 What is the relevance of differential cytokine regulation for E-selectin?

Here we found that many cytokines act as a messenger signalling ECs to produce and express E-selectin, however some cytokines were more potent in their E-selectin induction than others. This difference in expression would likely drive localised regions of high densities of E-

selectin or low densities of E-selectin on the membrane (Levin, Ting-Beall and Hochmuth, 2001), which could directly control leukocyte behaviour. For example, low expression and therefore low E-selectin site densities has been shown to result in rapid association and dissociation rates for leukocyte-E-selectin bonds resulting in fast rolling along the endothelium (McEver and Zhu, 2010; Li et al., 2015). Contrary to this, high expression and consequential clustering of E-selectins has been shown to stabilise and reduce rolling velocity by increasing the number of selectin-leukocyte bonds and reducing the force on individual bonds (McEver and Zhu, 2010). In addition, slow rolling and increased selectin binding increases signalling events occurring in leukocytes, which ready them for the next stage of activation and adhesion, which precedes leukocyte diapedesis (See Chapter 1 Introduction). One could therefore speculate that TNF alpha, a rapid and potent inducer of E-selectin would promote leukocyte slow rolling, activation, firm adhesion and diapedesis whereas weaker stimulants of E-selectin expression such as $VEGF_{165}$a, Histamine and IL-1 alpha/beta would promote fast rolling velocities of leukocytes in an inactivated state due to the decreased E-selectin surface densities. One could also suggest therefore that it would be physiologically logical for TNF alpha activated ECs to be nearer to the inflamed site compared to for example IL-1 alpha activated ECs.

Kinetics data in Chapter 4 could also support TNF alpha's role in influencing leukocyte activation for long periods of time (15 hr) compared to interleukins, $VEGF_{165}$a, histamine and LPS whereby peak expression of cell surface E-selectin declined from 6-8 hours. Cytokine induced selectin-leukocyte tethering and rolling has the potential to exacerbate the excessive recruitment of leukocytes, which is characteristic in diseases such as atherosclerosis, atherothrombosis, DVT, arthritis, psoriasis, chronic inflammation, COPD, stroke, asthma and reperfusion injury (Kerr *et al.*, 2000b; Ohta *et al.*, 2001b; Ulbrich *et al.*, 2006b; Japp *et al.*, 2013b). Because E-selectin is induced by TNF alpha for prolonged periods of time (>15 hr) this could suggest TNF alpha's role in the chronic leukocyte extravasation in diseases. TNF alpha inducement of E-selectin has been stipulated as additionally regulated by IL-4 which down regulates E-selectin expression (Stocker *et al.*, 2000), and our studies revealed expression is further upregulated in the presence of $VEGF_{165}$a and Histamine. Tuneable expression via additional stimuli could suggest interplay between receptors, and future experiments could investigate interactions between TNFR and VEGFR2, H1 and IL1R receptors.

Furthermore, the known role of VEGF in angiogenesis could theoretically reconcile with E-selectin's involvement in cell replication. For example, the pro-angiogenic VEGF splice variant ($VEGF_{165}a$) and not the anti-angiogenic splice variant ($VEGF_{165}b$) induced E-selectin expression at low levels. This was only in a few endothelial cells in the field of view and it was noticed that of the cells expressing, a large proportion were undergoing replication (Chapter 3). E-selectin expression in the context of cell replication has been explored before in HDMECs after stimulation with basic fibroblast growth factor, and E-selectin expression was 5x higher in proliferating cells in comparison to confluent HDMECs (Jianying Luo, Paranya and Bischoff, 1999), however no further studies had investigated E-selectin expression within the cell cycle. Inducement by $VEGF_{165}a$ could suggest a role of E-selectin in aiding $VEGF_{165}a$ induced angiogenesis. *In vitro* and *in vivo* studies have shown that E-selectin is associated with endothelial proliferation, migration and tube formation (Parikh *et al.*, 2018). Interestingly, promotion of these same physiological outcomes are also well established as signalling consequences of VEGFR2 activation by VEGF in endothelial cells (Peach *et al.*, 2018). In addition, like E-selectin, NRP-1 exclusively binds $VEGF_{165}a$, can modulate VEGFR2 driven signalling and has higher localisation at cell-cell junctions (Shintani *et al.*, 2006; Koch *et al.*, 2014; Mehta *et al.*, 2018; Domingues and Fantin, 2021).

Therefore, E-selectin and NRP-1 have commonalities in that they are expressed in endothelial cells in instances of cell replication and a pro-angiogenic environment. There were no interactions observed between NanoLuc E-selectin and SNAP-tag NRP-1, nor for SNAP-tag VEGFR2 in an overexpressed HEK293T assay, however their interaction could depend on being expressed in their native endothelial cells where there is also expression of other native receptors and differential cell bodies such as WPBs that do not exist in HEK293Ts. Future experimentation could investigate membrane interactions in ECs, using colocalization assays by immunolabeling E-selectin and VEGFR2/NRP-1 with different fluorophore-conjugated antibodies.

In addition, correlation of E-selectin expression in hyper-angiogenic environments has been observed previously in diseases such as cancer. Liu et al., (2011) found that E-selectin knock-down in melanoma cells significantly inhibited SDF-1 alpha (CXCL12) induced endothelial progenitor cell (EPC) homing in tumour angiogenesis, and significantly decreased melanoma growth *in vivo*. Borentain et al., (2016) found that inhibition of E-selectin expression using E-selectin inhibitors Cimetidine and Amiloride, inhibited 75% of HepG2 tumour growth in vivo. One hypothesised pathway for angiogenesis induction was due to the E-selectin mediated increase in PMN leukocytes. This is because PMNs induce angiogenesis via transcription

factor Ets-1, and E-selectin inhibition had been shown to reduce PMN induced angiogenesis (Yasuda *et al.*, 2002). In addition, the presence of soluble E-selectin within the blood stream after expression has also been hypothesised to promote angiogenesis via the Src-P13K pathway (Koch *et al.*, 1995; Kumar *et al.*, 2003). Aoki *et al.*, (2001) suggested that E-selectin mediates angiogenesis via VEGF activity; in high metastatic and low metastatic RCT clones, E-selectin inhibition suppressed tube formation induced by VEGF, and E-selectin expression was inhibited by a VEGF monoclonal antibody. In addition, $VEGF_{165}$a increased the TNF alpha induced response, which could suggest a role of expression in inflamed areas which also require neovascularlation, which include disease states such as cancer, rheumatoid arthritis and atherosclerosis.

6.2 The future of efficacy testing for anti-inflammatory therapeutics using E-selectin

The in vitro models I have developed to quantify E-selectin cell surface expression, were able to deduce cytokine induced E-selectin expression and E-selectin interactions on the cell surface, but further have the potential to answer more specific questions in the context of ligand binding, association and dissociation and localised internalisation, all of which are relevant with combatting the issue of lack of specific drug binding and amelioration of inflammatory symptoms in disease. Therefore, how this *in vitro* model, could act as first stage testing of the affinity, potency and efficacy (in respect to E-selectin inhibition) for therapeutics will be discussed.

In vitro efficacy testing should ideally be as close to the endogenous system as possible, that can confidently pinpoint specific binding or inhibition of down-stream events before exploring their effects in an *in vivo* system and eventually for Phases 0 – IV clinical trials. This starting point for testing binding and understanding E-selectin membrane dynamics can greatly aid drug design and drug testing. Our system utilised a CRISPR-Cas9 edited primary endothelial cell line to monitor E-selectin expression. To utilise this assay system to measure specific E-selectin binding not only will be the first study to do so in an endogenous EC, but also powerfully considers binding in the context of the other membrane expressed adhesion molecules such as P-selectin which is stored in EC specific WPBs, VCAM-1, ICAM-1 and integrins in activated ECs. Specific binding in the context of differential cytokine induced membrane expression of E-selectins and other vascular inflammation relevant EC proteins and receptors can also be assessed.

Although it has been made evident that the tagging of E-selectin with HiBiT or NanoLuc, or fluorescent tags of E-selectin targeting ligand needs to be fully assessed and optimised, once successful, these versions of protein and ligand can aid high throughput testing systems for E-selectin targeting in drug discovery. Previously, recombinant versions of E-selectin in cell-isolated systems, and the ability of therapeutics to inhibit selectin-mediated leukocyte binding in endothelial cells were used to grade the efficacy of drugs (Spragg *et al.*, 1997b; Shamay *et al.*, 2009b, 2015b; Kawano *et al.*, 2011; Barra *et al.*, 2016b; Ma *et al.*, 2016b; Hu *et al.*, 2018b). These systems lack integration in whole cell models and do not necessarily discriminate specificity of E-selectin binding versus other selectin family members. It is important to

discriminate between E-selectin, P-selectin and L-selectin, as although they all mediate leukocyte binding, each have additional separate functions in platelet coagulation, cancer metastasis and leukocyte signaling (Brenner *et al.*, 1996; McEver, 2015b; Borentain *et al.*, 2016; Au and Josefsson, 2017), therefore specifically targeting E-selectin could help reduce off target side effects. In addition E-selectin has been identified to bind to the largest range of ligands/proteins presented on leukocytes (Hidalgo *et al.*, 2007), therefore is a more attractive target for inhibiting leukocyte tethering.

The TERT2 HUVEC HiBiT E-selectin clone (Clone C8) generated did not detect binding to E-selectin with fluorescent Esbp. However there is still potential for this assay system to detect binding with other fluorescent E-selectin targeting ligands using the NanoBiT and NanoBRET systems. As mentioned in Chapter 5, one possible issue for lack of NanoBRET interactions between fluorescent Esbp and NanoLuc E-selectin could be due to lack of proximity of the AF488/AF633-Esbp binding site compared to N-terminal HiBiT. The location of the Esbp binding site, as well as other potential E-selectin targeting therapeutics, could be explored by using different PAM sites to CRISPR edit HiBiT at different points along the E-selectin N terminus and assessing consequential increase in NanoBRET (Figure 6.1a). After the binding site is determined, a single experiment can detect cytokine induced E-selectin expression (as described in Chapter 4), and further, confirm binding using NanoBRET to fluorescently conjugated E-selectin ligands. The kinetics of binding can be defined by change in NanoBRET signal, and further experimentation can define drug induced internalisation of E-selectin via fluorescence and luminescence microscopy (Figure 6.1 b-d).

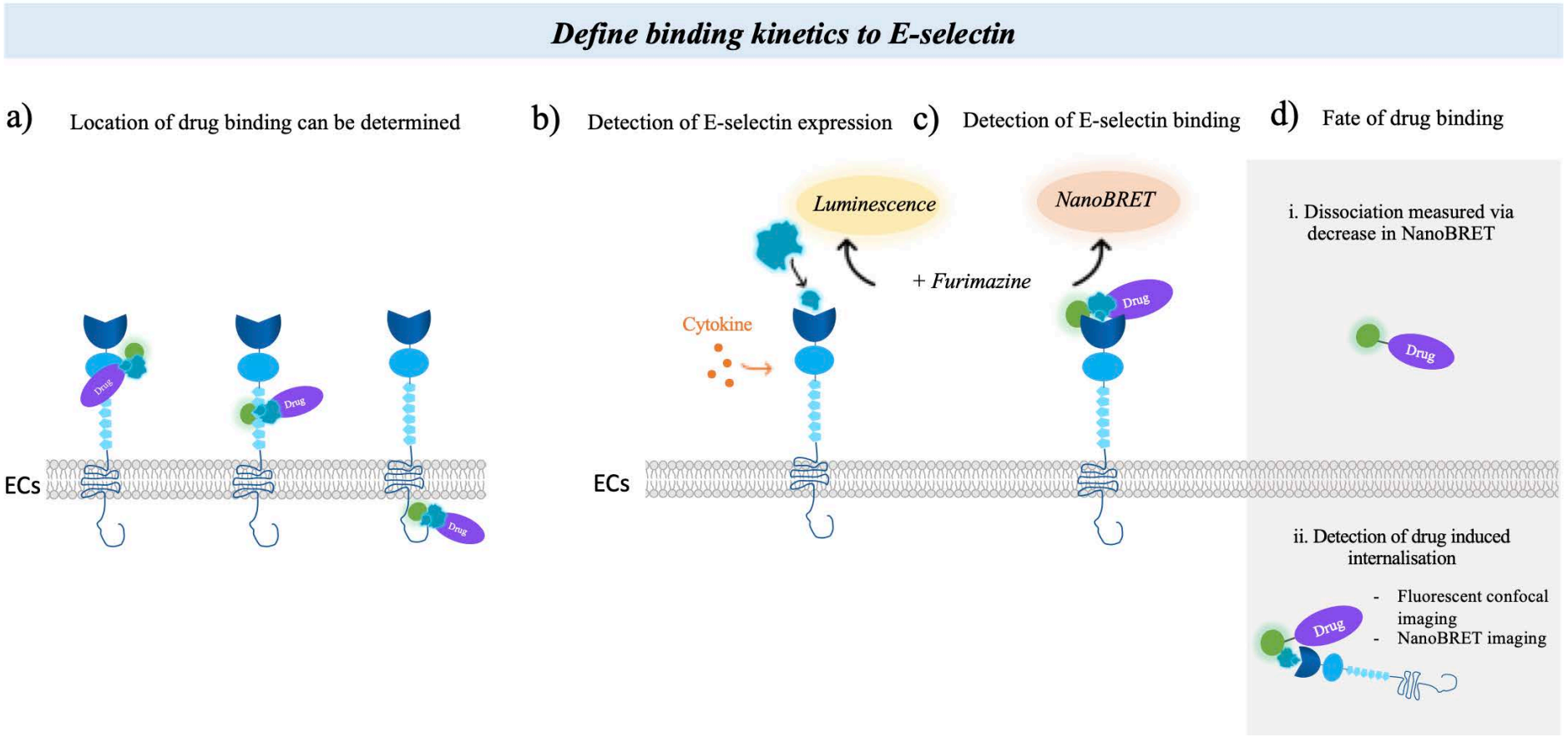

Figure 6.1 ***E-selectin expression, fluorescent drug binding and kinetics can be defined using CRISPR edited HiBiT E-selectin TERT2 HUVECs (Clone C8).*** *a) Location of drug binding can be defined by HiBiT addition to different sites along E-selectin sequence by measuring NanoBRET interactions. b) Cytokine induced E-selectin expression (as previously described in Chapter 4) induces E-selectin expression, quantified using NanoBiT complementation with LgBiT and addition of furimazine. c) Theoretically, addition of fluorescent conjugations of drugs can measure specific drug binding of E-selectin using NanoBRET, and kinetics experiments can determine d) the fate of drug binding i.e. i) dissociation rates of drugs and ii) possible drug–induced E-selectin internalisation. This can be imaged using fluorescent microscopy and by imaging BRET.*

Endogenous E-selectin homodimer formation can be defined using the NanoBiT system, however using small bit (SmBiT) in the place of HiBiT. LgBiT-HiBiT complementation and consequential luminescence output in this system would be indicative of binding, however this isn't desirable as the high affinity of HiBiT for LgBiT could be driving luminescence detection instead of being an indication of a genuine specific selectin-selectin interaction. Instead, SmBiT could be used; a fragment with lower affinity for LgBiT (K_D = 190 μM) yet retains the bright signal of NanoLuc at saturation when recomplemented (Kozielewics and Schulte, 2022). If homodimer formation is confirmed in ECs (as homodimeric E-selectin was confirmed before in over-expressed HEK293T cell line), the effect of fluorescent drug binding could then be assessed at defined E-selectin homodimers identified using NanoBRET (Figure 6.2a). Furthermore, E-selectin localised density can be controlled by treating ECs with increasing concentrations of cytokine (see Chapter 4 concentration response and kinetics experiments and Figure 6.2b), and the effect of drug binding can be investigated using NanoBRET. These experiments have the potential to answer whether E-selectin homodimer formation, and clustering is promoting or inhibiting binding for different E-selectin targeting drugs.

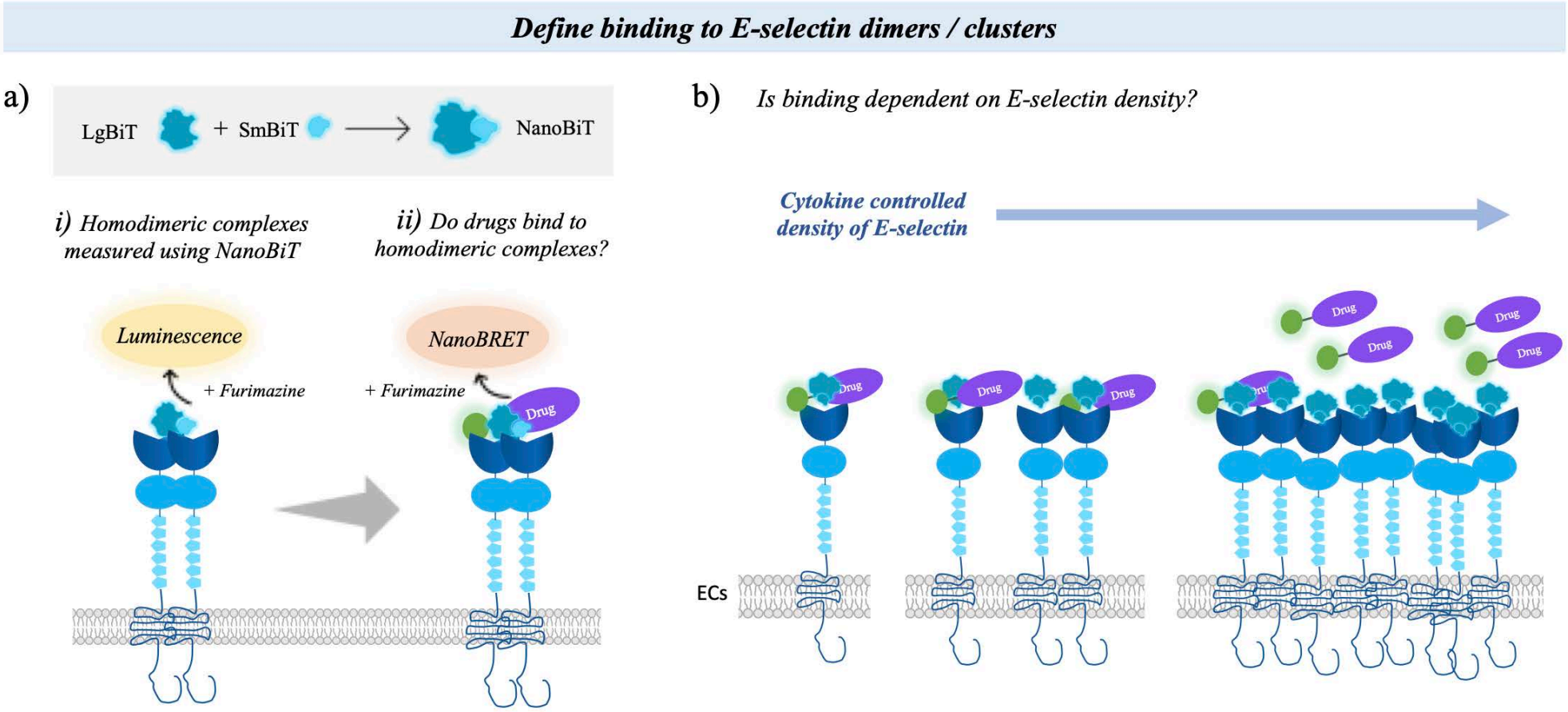

Figure 6.2 ***Binding to E-selectin homodimers, and high site densities of E-selectin can be investigated*** *a) investigation of homodimeric complexes can be investigated by co-transfecting SmBiT E-selectin and LgBiT E-selectin in HEK293Ts, and addition of fluorescent drug can deduce whether binding occurs in homodimers by measuring NanoBRET. b) a gradient of E-selectin membrane densities can be controlled by cytokine stimulation (i.e. using 0 – 0.05 nM TNF alpha), and resultant ability of drug binding can be measured using NanoBRET.*

One step further can be taken to define the ability of fluorescent-E-selectin therapeutics to bind to homodimers in a controlled format. Technologies such as supramolecular system-induced dimerization exist which induce reversible dimerization of proteins in cells (Summarised in Figure 6.3). This technology makes use of supramolecular host molecules, such as naturally-derived sugar-based cone-shaped ß-cyclodextrin which selectively binds the hydrophobic guest molecule lithocholic acid with high affnity (Ka – 10^6 m^{-1}) at 1:1 ratio (Uhlenheuer et al., 2011, Dang 2022). This reaction can be reversed by inhibiting dimerization with free ß-cyclodextrin. The system can be further tweaked by enhancing the affinity of synthetic host-guest complex by molecular upgrading of beta-cyclodextran side chains (Uhlenheuer et al., 2011). This technology therefore enables induced dimer formation and breakage, as well as inducement of 'loosely' or 'tightly' bound dimers. Furthermore, trimers can be induced using the host molecular Curcibit [8]uril (8 membered omologue of cucribit [n]uril) which binds two synthetic guest molecules simultaneously (Dang, 2022). This modulation of protein assembly can help further define how drugs are interacting with E-selectin in monomeric, dimeric or trimeric states. The disadvantage of this system however is the consideration that E-selectin homodimer formation could still be occurring in the presence of host/guest molecule inhibition, however this can be detected early on using NanoBRET.

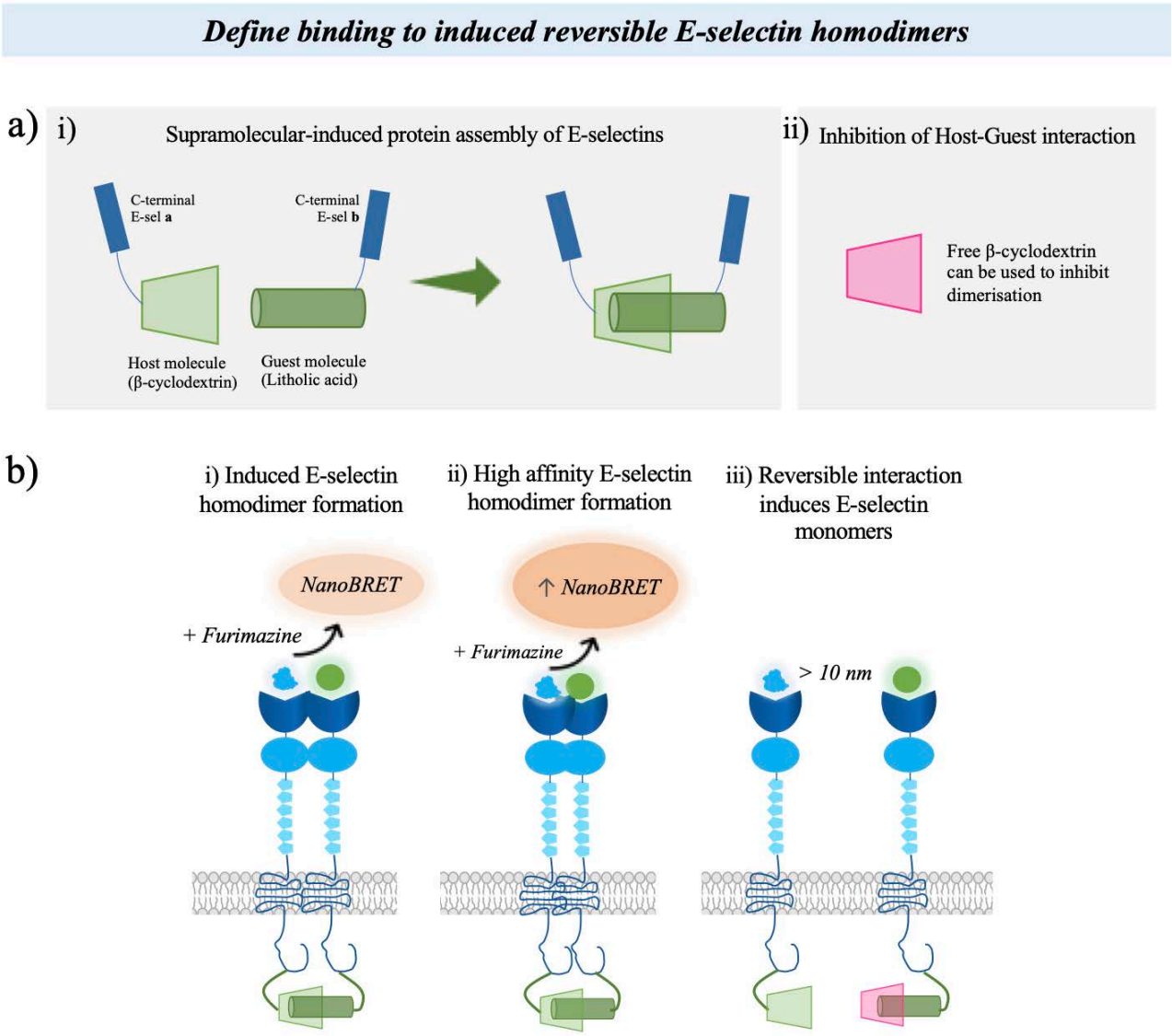

Figure 6.3 ***Proposal for use of supramolecular-induced dimerization of E-selectin to study the effect of E-selectin dimerization on Drug binding.*** *a) i) The Supramolecular-induced protein assembly is achieved by conjugating E-selectin C-termini with either a host molecule (e.g. β-cyclodextrin) or a guest molecule (e.g. Litholic acid) which binds reversibly with addition of ii) free host molecule which displaces E-selectin conjugated host molecule. b) NanoBRET can be used to validate homodimer formation using co-transfection of NanoLuc E-selectin and SNAP-tag E-selectin with assigned host/guest conjugates. c) NanoLuc E-selectin host/guest conjugates can determine fluorescent-drug binding affinities in dimer and monomer states.*

Moreover, the ability of E-selectin targeting drugs to inhibit E-selectin and L-selectin interactions could be further explored using inhibition of leukocyte interactions as an experimental readout. Just because a drug can bind E-selectin, doesn't necessarily mean that it's physiological role for tethering leukocytes is inhibited and the first step to investigating this could be to use the model I have developed during this project. Co-transfection of NanoLuc E-selectin and SNAP-tag L-selectin has previously resulted in potential heterodimer formation (Chapter 5), therefore the ability of a drug to inhibit this interaction can be tested by measuring decrease in NanoBRET in the presence of increasing concentrations of drug (Figure 6.4a). Further investigation could then be undertaken using a more physiologically relevant assay by measuring the interaction between E-selectin on endothelial cells with a separate L-selectin presenting leukocyte. To do this, NanoLuc E-selectin presenting cells could be co-cultured with SNAP-tag L-selectin presenting cells, as described in Figure 6.4b. This was attempted in the latter half of this project, however was unsuccessful as many parameters of optimisation were required that were ultimately time prohibitive; from the amount of construct to transfect to the cell seeding densities to use and a positive control is not yet available for this set up. Moreover, cell-cell distance and orientation was difficult to control with both factors known to substantially adversely affect BRET efficiency (Weihs *et al.*, 2020).

In addition to specific E-selectin targeting, the TERT2 HUVEC HiBiT E-selectin clone C8 *in vitro* model offers the possibility to test the efficacy of cytokine targeting therapeutics to a high degree of sensitivity. The cytokines used in Chapter 3 and Chapter 4; TNF alpha, IL-1 alpha and beta, LPS, histamine and $VEGF_{165}a$ all have distinctive and quantifiable effects on inducing E-selectin cell surface expression which could be scrutinised in the presence of specific inhibitors. As opposed to specific drug binding, this system could measure inhibition of this early biomarker of inflammation to discriminate between successful inhibitors in a high throughput format, with the capability of measuring inhibition over more than 15 hr using longer acting NanoLuc substrates (for example, endurazine).

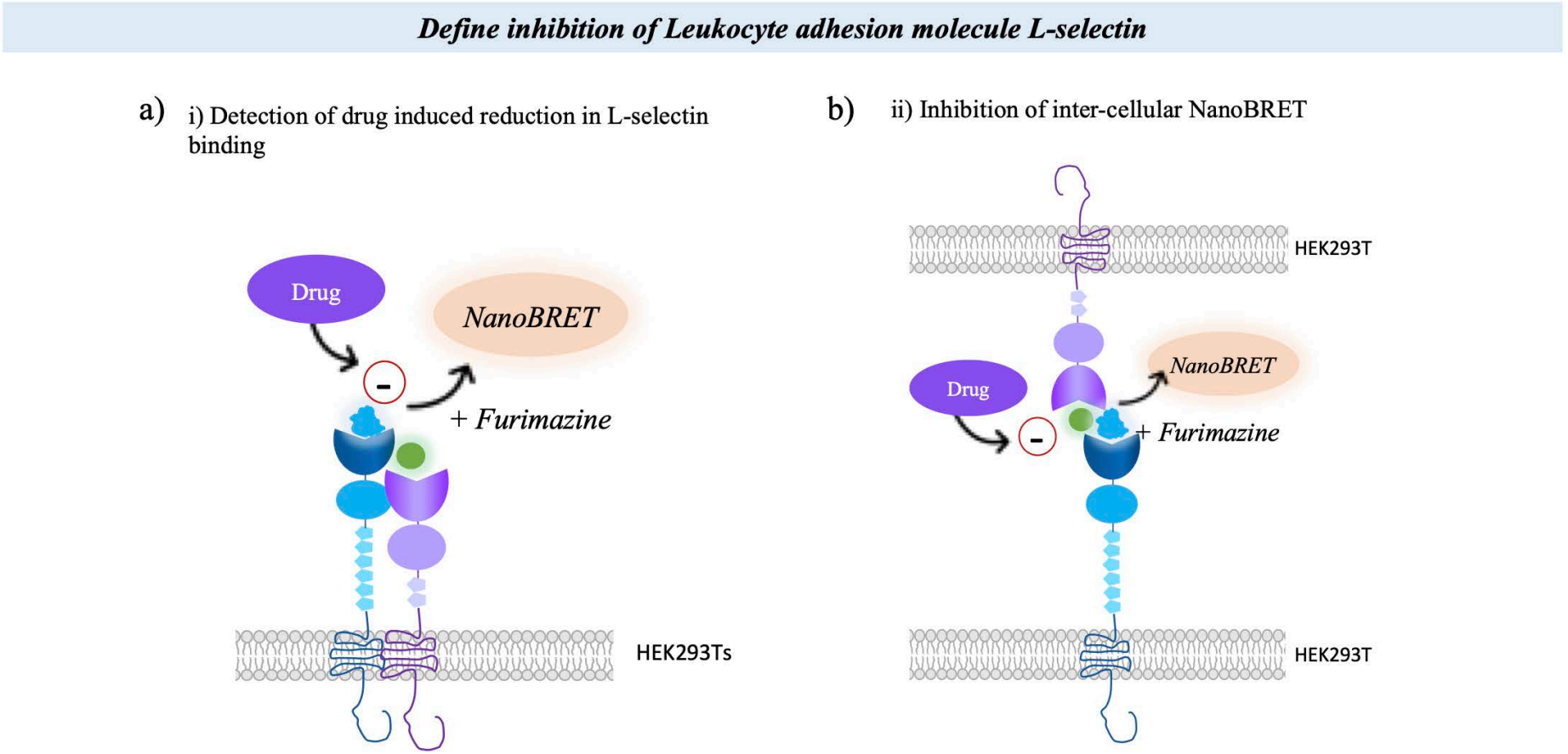

Figure 6.4 ***Drug induced inhibition of L-selectin binding can be investigated in a single cell, and inter-cellular format.*** *a) co-transfection of NanoLuc E-selectin and SNAP-tag L-selectin has previously resulted in heterodimerization of selectins. The ability of drug induced inhibition of this interaction can shed light on whether this will inhibit leukocyte adherence. b) the concept of intercellular nanoBRET between two cells. In theory, E and L selectin binding would occur and the ability of drug to inhibit this interaction would be more physiologically relevant in the context of inhibiting leukocyte binding.*

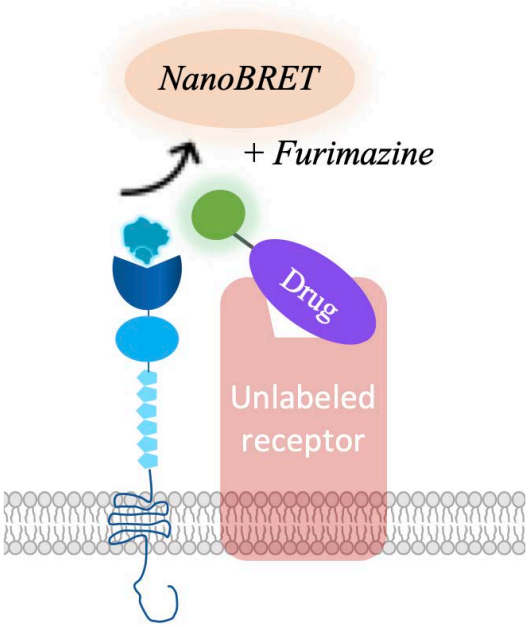

Figure 6.5 ***By-stander BRET between unlabelled receptors and fluorescent ligands on endothelial cells could be investigated using the TERT2 HUVEC HiBiT E-selectin clone.*** *Fluorescent ligand binding to an unlabelled receptor would lead to fluorescent ligand accumulation at the plasma membrane, which results in the increase of bystander BRET between the E-selectin luciferase and the fluorescent ligand. Further binding of unlabelled ligand will prevent this signal.*

Finally, the high expression of the HEK293T NanoLuc E-selectin stable cell line, or TERT2 HUVEC HiBiT E-selectin clone has the potential to act as a by-stander BRET system to measure binding of fluorescent ligands to un-modified receptors in close proximity to E-selectin. A disadvantage of measuring ligand-receptor binding using BRET is that one has to modify the receptor of interest with a luciferase donor or fluorophore acceptor, which can affect conformation, cell surface expression or ligand binding at the receptor. Recently, a model of by-stander BRET to measure binding of carboxytetramethylrhodamine (TAMRA) conjugated angiotensin II (AngII) to unmodified overexpressed AT_1 angiotensin receptor (AT_1R) has been shown using a plasma membrane localised *Gaussia* luciferase (a luciferase isolated from the marine *Gaussia princeps* which has the same molecular weight as NanoLuc) (Tóth *et al.*, 2021). Here, an increase in by-stander BRET was measured due to specific binding of AngII-TAMRA to AT_1R that occurred in sufficiently close enough proximity to the membrane localised GLuc. A similar approach could be used with my TERT2 HUVEC homozygous clone for HiBiT E-selectin or the similarly bright NanoLuc E-selectin HEK293T stable cell line that could theoretically measure ligand binding at many endothelial cell or embryonic kidney cell expressed receptors.

Although the receptor of interest would be required to be in the correct orientation and in close proximity to HiBiT /NanoLuc E-selectin, once optimised this assay has the potential to assess

ligand binding at multiple unmodified receptors; either in an overexpressed HEK293T system (using for example, GPCRs) or endogenously expressed EC receptors which naturally have high expression (such as receptor tyrosine kinases (RTKs)). The highly sensitive HiBiT E-selectin TERT2 HUVEC clone will help with by-stander BRET detection as there is a large dynamic range with cytokine controlled high expression of E-selectin.

6.3 Key conclusions

The data presented in this thesis identified differential expression dynamics of E-selectin in response to cytokines involved in vascular inflammation using immunolabelling and luciferase based techniques. CRISPR-Cas9 editing in TERT2 HUVECs enabled the production of a HiBiT E-selectin homozygous clone which allowed quantification of membrane expressed E-selectin in live cells with high sensitivity. The live monitoring of endogenous expression patterns enabled further understanding of expression kinetics and suggested the key players involved in inducing membrane expression and consequential leukocyte extravasation pathway such as TNF alpha, LPS, IL-1 alpha and IL-1 beta. TNF alpha induced E-selectin expression was enhanced by co-stimulation with pro-angiogenic $VEGF_{165}a$, which like histamine could also induce low E-selectin expression in the absence of TNF alpha. Membrane expressed E-selectin was then investigated for interactions with the other selectin family members with, consequentially putative E-selectin homodimer and E-selectin – L-selectin heterodimers observed. Esbp induced E-selectin internalisation was then quantified and visualised using HiBiT and SNAP-tag labelling of E-selectin in TERT2 HUVECs and HEK293Ts respectively. Specific binding of fluorescently conjugated Esbp was unable to be detected in NanoLuc E-selectin stable cell line using NanoBRET. This was possibly due to proximity issues with Esbp binding site, inhibition of binding from fluorophore, or NanoLuc/SNAP-tag tags inhibiting Esbp binding. The model created will allow investigation of specific ligand binding in endothelial cells/HEK293Ts using NanoBRET and NanoBiT technologies in the future.

Chapter 7 References

Abram, C.L. and Lowell, C.A. (2009) 'The ins and outs of leukocyte integrin signaling', *Annual Review of Immunology*, 27, pp. 339–362. Available at: https://doi.org/10.1146/annurev.immunol.021908.132554.
AbuSamra, D.B. *et al.* (2015) 'Quantitative characterization of E-selectin interaction with native CD44 and P-selectin glycoprotein ligand-1 (PSGL-1) using a real time immunoprecipitation-based binding assay', *Journal of Biological Chemistry*, 290(35), pp. 21213–21230. Available at: https://doi.org/10.1074/jbc.M114.629451.
Acuner Ozbabacan, S.E. *et al.* (2014) 'The Structural Pathway of Interleukin 1 (IL-1) Initiated Signaling Reveals Mechanisms of Oncogenic Mutations and SNPs in Inflammation and Cancer', *PLoS Computational Biology*, 10(2). Available at: https://doi.org/10.1371/journal.pcbi.1003470.
Addis, R. *et al.* (2014) 'Human umbilical endothelial cells (HUVECs) have a sex: Characterisation of the phenotype of male and female cells', *Biology of Sex Differences*, 5(1). Available at: https://doi.org/10.1186/s13293-014-0018-2.
Aggarwal, V. *et al.* (2019) 'Role of reactive oxygen species in cancer progression: Molecular mechanisms and recent advancements', *Biomolecules*. MDPI AG. Available at: https://doi.org/10.3390/biom9110735.
Aleisa, F.A. *et al.* (2020) 'Functional binding of E-selectin to its ligands is enhanced by structural features beyond its lectin domain', *Journal of Biological Chemistry*, 295(11), pp. 3719–3733. Available at: https://doi.org/10.1074/jbc.RA119.010910.
Alhayaza, R. *et al.* (2020) 'The Relationship Between Reactive Oxygen Species and Endothelial Cell Metabolism', *Frontiers in Chemistry*. Frontiers Media S.A. Available at: https://doi.org/10.3389/fchem.2020.592688.
Alwan, B. Al *et al.* (2021) 'Single-molecule imaging and microfluidic platform reveal molecular mechanisms of leukemic cell rolling', *Communications Biology*, 4(1). Available at: https://doi.org/10.1038/s42003-021-02398-2.
Au, A.E. and Josefsson, E.C. (2017) 'Regulation of platelet membrane protein shedding in health and disease', *Platelets*, 28(4), pp. 342–353. Available at: https://doi.org/10.1080/09537104.2016.1203401.
Aydt, E.M., Bock, D. and Wolff, G. (2010) 'Selectin antagonists and their potential impact for the treatment of inflammatory lung diseases', *New Drugs and Targets for Asthma and COPD*, 39, pp. 175–184. Available at: https://doi.org/10.1159/000320817.
Banerjee, E. (2011) 'Triple selectin knockout (ELP-/-) mice fail to develop OVA-induced acute asthma phenotype', *Journal of Inflammation*, 8. Available at: https://doi.org/10.1186/1476-9255-8-19.
Banquy, X. *et al.* (2008) 'Selectins ligand decorated drug carriers for activated endothelial cell targeting', *Bioconjugate Chemistry*, 19(10), pp. 2030–2039. Available at: https://doi.org/10.1021/bc800257m.
Barra, P.A. *et al.* (2016a) 'Discovery of New E-Selectin Inhibitors by Virtual Screening , Fluorescence Binding Assays , and STD NMR Experiments', pp. 1008–1014. Available at: https://doi.org/10.1002/cmdc.201600058.
Barra, P.A. *et al.* (2016b) 'Discovery of New E-Selectin Inhibitors by Virtual Screening , Fluorescence Binding Assays , and STD NMR Experiments', pp. 1008–1014. Available at: https://doi.org/10.1002/cmdc.201600058.

Barthel, S.R. *et al.* (2007a) 'Targeting selectins and selectin ligands in inflammation and cancer', 11(11), pp. 1473–1491. Available at: https://doi.org/10.1517/14728222.11.11.1473.Targeting.
Barthel, S.R. *et al.* (2007b) 'Targeting selectins and selectin ligands in inflammation and cancer', 11(11), pp. 1473–1491. Available at: https://doi.org/10.1517/14728222.11.11.1473.Targeting.
Bendas, G. *et al.* (1998) 'Selectins as new targets for immunoliposome-mediated drug delivery. A potential way of anti-inflammatory therapy', *Pharmaceutica Acta Helvetiae*, 73(1), pp. 19–26. Available at: https://doi.org/10.1016/S0031-6865(97)00043-5.
Bendas, G. *et al.* (1999) 'Targetability of novel immunoliposomes prepared by a new antibody conjugation technique', *International Journal of Pharmaceutics*, 181(1), pp. 79–93. Available at: https://doi.org/10.1016/S0378-5173(99)00002-2.
Berridge, B.R., Van Vleet, J.F. and Herman, E. (2018) *Cardiovascular System, Fundamentals of Toxicologic Pathology: Third Edition*. Elsevier Inc. Available at: https://doi.org/10.1016/B978-0-12-809841-7.00009-5.
Bevialacqua, M.P. *et al.* (1989) 'Endothelial Leukocyte Adhesion Molecule 1: An Inducible Receptor for Neutrophils Related to Complement Reglatory Proteins and Lectins', *Science*, 243, pp. 1160–1165. Available at: https://doi.org/10.1002/prot.21847.
Bevilacqua, M.P. *et al.* (1987) 'Identification of an inducible endothelial-leukocyte adhesion molecule.', *Proceedings of the National Academy of Sciences of the United States of America*, 84(24), pp. 9238–42. Available at: http://www.ncbi.nlm.nih.gov/pubmed/2827173%0Ahttp://www.pubmedcentral.nih.gov/articlerender.fcgi?artid=PMC299728.
Bhaskar, V. *et al.* (2003) 'E-selectin up-regulation allows for targeted drug delivery in prostate cancer', *Cancer Research*, 63(19), pp. 6387–6394.
Bhushan, M. *et al.* (2002) 'Anti-e-selectin is ineffective in the treatment of psoriasis: A randomized trial', *British Journal of Dermatology*, 146(5), pp. 824–831. Available at: https://doi.org/10.1046/j.1365-2133.2002.04743.x.
Blackwell, J.E. *et al.* (2001) 'Ligand coated nanosphere adhesion to E- and P-selectin under static and flow conditions', *Annals of Biomedical Engineering*, 29(6), pp. 523–533. Available at: https://doi.org/10.1114/1.1376697.
Bochner, B.S. *et al.* (1994) 'Differences between human eosinophils and neutrophils in the function and expression of sialic acid-containing counterligands for E-selectin.', *Journal of immunology (Baltimore, Md. : 1950)*, 152(2), pp. 774–82.
Borentain, P. *et al.* (2016) 'Inhibition of E-selectin expression on the surface of endothelial cells inhibits hepatocellular carcinoma growth by preventing tumor angiogenesis', *Cancer Chemotherapy and Pharmacology*, 77(4), pp. 847–856. Available at: https://doi.org/10.1007/s00280-016-3006-x.
Borroto-Escuela, Dasiel O. MarcFlajolet Agnati, L.F., Greengard, P. and Fuxe, K. (2013) *Methods in Cell Biology*.
Boscaro, C. *et al.* (2020) 'Sex Differences in the Pro-Angiogenic Response of Human Endothelial Cells: Focus on PFKFB3 and FAK Activation', *Frontiers in Pharmacology*, 11. Available at: https://doi.org/10.3389/fphar.2020.587221.
Bradley, J.R. (2008) 'TNF-mediated inflammatory disease', *Journal of Pathology*, pp. 149–160. Available at: https://doi.org/10.1002/path.2287.
Branco, A.C.C.C. *et al.* (2018) 'Role of Histamine in Modulating the Immune Response and Inflammation', *Mediators of Inflammation*. Hindawi Limited. Available at: https://doi.org/10.1155/2018/9524075.

Braverman, I.M. (2000) ‘The cutaneous microcirculation’, *Journal of Investigative Dermatology Symposium Proceedings*, 5(1), pp. 3–9. Available at: https://doi.org/10.1046/j.1087-0024.2000.00010.x.
Brenner, B. *et al.* (1996) ‘L-Selectin activates the Ras pathway via the tyrosine kinase p56lck’, *Proceedings of the National Academy of Sciences of the United States of America*, 93(26), pp. 15376–15381. Available at: https://doi.org/10.1073/pnas.93.26.15376.
British Heart Foundation (2022) *Heart statistics publications, British Heart Foundation*.
Brozovich, F. V. *et al.* (2016) ‘Mechanisms of vascular smooth muscle contraction and the basis for pharmacologic treatment of smooth muscle disorders’, *Pharmacological Reviews*, 68(2), pp. 476–532. Available at: https://doi.org/10.1124/pr.115.010652.
Campbell, H.K., Maiers, J.L. and DeMali, K.A. (2017) ‘Interplay between tight junctions & adherens junctions’, *Experimental Cell Research*. Elsevier Inc., pp. 39–44. Available at: https://doi.org/10.1016/j.yexcr.2017.03.061.
Campbell, J.J. *et al.* (1998) ‘Chemokines and the Arrest of Lymphocytes Rolling Under Flow Conditions’, *SCIENCE*, 279. Available at: https://www.science.org.
Cappenberg, A., Kardell, M. and Zarbock, A. (2022) ‘Selectin-Mediated Signaling—Shedding Light on the Regulation of Integrin Activity in Neutrophils’, *Cells*. MDPI. Available at: https://doi.org/10.3390/cells11081310.
Carraway, M.S. *et al.* (1998) ‘Antibody to E- and L-selectin does not prevent lung injury or mortality in septic baboons’, *American Journal of Respiratory and Critical Care Medicine*, 157(3 PART I), pp. 938–949.
Chan, W.T. *et al.* (2013) ‘A comparison and optimization of methods and factors affecting the transformation of Escherichia coli’, *Bioscience Reports*, 33(6). Available at: https://doi.org/10.1042/BSR20130098.
Chang, J. *et al.* (2010) ‘GMI-1070, a novel pan-selectin antagonist, reverses acute vascular occlusions in sickle cell mice’, *Blood*, 116(10), pp. 1779–1786. Available at: https://doi.org/10.1182/blood-2009-12-260513.
Chang, M.W.F. *et al.* (2005) ‘Comparison of early passage, senescent and hTERT immortalized endothelial cells’, *Experimental Cell Research*, 309(1), pp. 121–136. Available at: https://doi.org/10.1016/j.yexcr.2005.05.002.
Chen, F., Alphonse, M. and Liu, Q. (2020) ‘Strategies for nonviral nanoparticle-based delivery of CRISPR/Cas9 therapeutics’, *Wiley Interdisciplinary Reviews: Nanomedicine and Nanobiotechnology*. Wiley-Blackwell. Available at: https://doi.org/10.1002/wnan.1609.
Chen, J., Raouf, A. and Khalil, I. (2017) *Matrix Metalloproteinases and Tissue Remodeling in Health and Disease: Target Tissues and Therapy*. 4th edn. Edited by I. Mani and V. Singh.
Clinicaltrial.gov (2007) *GI-270384 Study In Patients With Mild To Moderate Ulcerative Colitis, GlaxoSmithKline*.
Clinicaltrial.gov (2014) ‘Placebo-controlled Single Dose Study to Evaluate Safety and Pharmacokinetics of GMI-1271 in Healthy Volunteers’.
Clinicaltrial.gov (2016) ‘A Study to Determine the Efficacy, Safety and Pharmacokinetics of GMI-1271 as Adjunct to Standard of Care for the Treatment of Multiple Myeloma’.
Clinicaltrial.gov (2018) ‘Study to Determine the Efficacy of Uproleselan (GMI-1271) in Combination With Chemotherapy to Treat Relapsed/Refractory Acute Myeloid Leukemia’.
Cole, N.B. (2013) ‘Site-specific protein labeling with SNAP-tags’, *Current Protocols in Protein Science*, 2013, pp. 30.1.1-30.1.16. Available at: https://doi.org/10.1002/0471140864.ps3001s73.
Collins, R.G. *et al.* (2000) *P-Selectin or Intercellular Adhesion Molecule (ICAM)-1 Deficiency Substantially Protects against Atherosclerosis in Apolipoprotein E-deficient Mice, J. Exp. Med*. Available at: http://www.jem.org.

Collins, R.G. *et al.* (2001) 'Dermal and pulmonary inflammatory disease in E-selectin and P-selectin double-null mice is reduced in triple-selectin-null mice', *Blood*, 98(3), pp. 727–735. Available at: https://doi.org/10.1182/blood.V98.3.727.
Concordet, J.P. and Haeussler, M. (2018) 'CRISPOR: Intuitive guide selection for CRISPR/Cas9 genome editing experiments and screens', *Nucleic Acids Research*, 46(W1), pp. W242–W245. Available at: https://doi.org/10.1093/nar/gky354.
Culmer, D.L. *et al.* (2017) 'E-selectin inhibition with GMI-1271 decreases venous thrombosis without profoundly affecting tail vein bleeding in a mouse model', pp. 1171–1181.
Dale, N.C. *et al.* (2019) 'NanoBRET: The bright future of proximity-based assays', *Frontiers in Bioengineering and Biotechnology*, 7(MAR), pp. 1–13. Available at: https://doi.org/10.3389/fbioe.2019.00056.
Dang, D.T. (2022) 'Molecular Approaches to Protein Dimerization: Opportunities for Supramolecular Chemistry', *Frontiers in Chemistry*. Frontiers Media S.A. Available at: https://doi.org/10.3389/fchem.2022.829312.
DeAngelo, D. *et al.* (2019) 'A phase III trial to evaluate the efficacy of uproleselan (GMI-1271) with chemotherapy in patients with relapsed/refractory acute myeloid leukemia.', *Journal of Clinical Oncology* [Preprint].
Dembic, Z. (2015) 'Cytokines Important for Growth and/or Development of Cells of the Immune System', *The Cytokines of the Immune System*, pp. 263–281. Available at: https://doi.org/10.1016/b978-0-12-419998-9.00008-0.
Dembo, M. *et al.* (1988) 'The reaction-limited kinetics of membrane-to-surface adhesion and detachment', *Proc R Soc Lof B Biol Sci.*, 234(1274), pp. 55–83.
Devata, S. *et al.* (2020) 'Use of GMI-1271, an E-selectin antagonist, in healthy subjects and in 2 patients with calf vein thrombosis', *Research and Practice in Thrombosis and Haemostasis*, 4(2), pp. 193–204. Available at: https://doi.org/10.1002/rth2.12279.
Diacovo, T.G. *et al.* (1996) 'Interactions of Human alpha/beta and gamma/delta T Lymphocyte Subsets in Shear Flow with E-Selectin and P-Selectin', *J. Exp. Med*, 183, pp. 1193–1203.
Dickerson, J.B. *et al.* (2001) 'Limited adhesion of biodegradable microspheres to E- and P-selectin under flow', *Biotechnology and Bioengineering*, 73(6), pp. 500–509. Available at: https://doi.org/10.1002/bit.1085.
Dijon, N., Nesheva, D. and Holliday, N. (2022) 'Luciferase Complementation Approaches to Measure GPCR Signaling Kinetics and Bias', in. Humana Press, pp. 249–274. Available at: http://www.springer.com/series/7651.
Dixon, A.S. *et al.* (2016) 'NanoLuc Complementation Reporter Optimized for Accurate Measurement of Protein Interactions in Cells', *ACS Chemical Biology*, 11(2), pp. 400–408. Available at: https://doi.org/10.1021/acschembio.5b00753.
Domingues, A. and Fantin, A. (2021) 'Neuropilin 1 regulation of vascular permeability signaling', *Biomolecules*. MDPI AG. Available at: https://doi.org/10.3390/biom11050666.
Dong, Z.M. *et al.* (1998) *Absence of P-and E-Selectins Reduces Atherosclerosis in Mice The Combined Role of P-and E-Selectins in Atherosclerosis, J. Clin. Invest*. Available at: http://www.jci.org.
Doudna, J.A. and Charpentier, E. (2014) 'The new frontier of genome engineering with CRISPR-Cas9', *Science*. American Association for the Advancement of Science. Available at: https://doi.org/10.1126/science.1258096.
Doulias, P.T. and Tenopoulou, M. (2020a) 'Endothelial nitric oxide synthase-derived nitric oxide in the regulation of metabolism', *F1000Research*. F1000 Research Ltd. Available at: https://doi.org/10.12688/f1000research.19998.1.

Doulias, P.T. and Tenopoulou, M. (2020b) ‘Endothelial nitric oxide synthase-derived nitric oxide in the regulation of metabolism’, *F1000Research*. F1000 Research Ltd. Available at: https://doi.org/10.12688/f1000research.19998.1.
Dunlop, L.C. (2004) ‘Characterization of GMP-140 (P-selectin) as a circulating plasma protein’, *Journal of Experimental Medicine*, 175(4), pp. 1147–1150. Available at: https://doi.org/10.1084/jem.175.4.1147.
Ear, T. *et al.* (2001) *High efficiency transient transfection of genes in human umbilical vein endothelial cells by electroporation, Journal of Immunological Methods*. Available at: www.elsevier.comrlocaterjim.
Ehrhardt, C., Kneuer, C. and Bakowsky, U. (2004a) ‘Selectins - An emerging target for drug delivery’, *Advanced Drug Delivery Reviews*, 56(4), pp. 527–549. Available at: https://doi.org/10.1016/j.addr.2003.10.029.
Ehrhardt, C., Kneuer, C. and Bakowsky, U. (2004b) ‘Selectins - An emerging target for drug delivery’, *Advanced Drug Delivery Reviews*, 56(4), pp. 527–549. Available at: https://doi.org/10.1016/j.addr.2003.10.029.
El-Kattan, M.M. *et al.* (2022) ‘Relation of serum level of tumor necrosis factor-alpha to cognitive functions in patients with Parkinson’s disease’, *Egyptian Journal of Neurology, Psychiatry and Neurosurgery*, 58(1). Available at: https://doi.org/10.1186/s41983-022-00460-2.
England, C.G., Ehlerding, E.B. and Cai, W. (2016) ‘NanoLuc: A Small Luciferase Is Brightening Up the Field of Bioluminescence’, *Bioconjugate Chemistry*. American Chemical Society, pp. 1175–1187. Available at: https://doi.org/10.1021/acs.bioconjchem.6b00112.
Eriksson, E.E. *et al.* (2005) ‘Powerful inflammatory properties of large vein endothelium in vivo’, *Arteriosclerosis, Thrombosis, and Vascular Biology*, 25(4), pp. 723–728. Available at: https://doi.org/10.1161/01.ATV.0000157578.51417.6f.
Esposito, M. *et al.* (2019) ‘Bone vascular niche E-selectin induces mesenchymal–epithelial transition and Wnt activation in cancer cells to promote bone metastasis’, *Nature Cell Biology*, 21(5), pp. 627–639. Available at: https://doi.org/10.1038/s41556-019-0309-2.
Eustice, D.C. and Wilhelm, J.M. (1984) ‘Mechanisms of action of aminoglycoside antibiotics in eucaryotic protein synthesis’, *Antimicrobial Agents and Chemotherapy*, 26(1), pp. 53–60. Available at: https://doi.org/10.1128/AAC.26.1.53.
Fan, F. *et al.* (2008) ‘Novel genetically encoded biosensors using firefly luciferase’, *ACS Chemical Biology*, 3(6), pp. 346–351. Available at: https://doi.org/10.1021/cb8000414.
Faryammanesh, R. *et al.* (2014) ‘SDA , a DNA Aptamer Inhibiting E- and P-Selectin Mediated Adhesion of Cancer and Leukemia Cells , the First and Pivotal Step in Transendothelial Migration during Metastasis Formation’, 9(4). Available at: https://doi.org/10.1371/journal.pone.0093173.
Festuccia, C. *et al.* (2020) ‘with Docetaxel in Prostate Cancer Cell Intraosseous Growth’, 4.
Filippi, M.-D. (2016) ‘Mechanism of Diapedesis’, pp. 25–53. Available at: https://doi.org/10.1016/bs.ai.2015.09.001.
Förstermann, U. and Sessa, W.C. (2012) ‘Nitric oxide synthases: Regulation and function’, *European Heart Journal*. Available at: https://doi.org/10.1093/eurheartj/ehr304.
Friedl, J. *et al.* (2002) *Induction of permeability across endothelial cell monolayers by tumor necrosis factor (TNF) occurs via a tissue factor-dependent mechanism: relationship between the procoagulant and permeability effects of TNF*. Available at: http://ashpublications.org/blood/article-pdf/100/4/1334/1685960/h81602001334.pdf.
Gainetdinov, R.R. *et al.* (2004) ‘Desensitization of G protein-coupled receptors and neuronal functions’, *Annual Review of Neuroscience*, 27, pp. 107–144. Available at: https://doi.org/10.1146/annurev.neuro.27.070203.144206.

Galley, H.F. and Webster, N.R. (2004) 'Physiology of the endothelium', *British Journal of Anaesthesia*, 93(1), pp. 105–113. Available at: https://doi.org/10.1093/bja/aeh163.
Garibyan, L. and Avashia, N. (2013) 'Research Techniques Made Simple: Polymerase Chain Reaction (PCR)', *Eurosurveillance*, 133(4), pp. 1–8. Available at: https://doi.org/10.2807/ese.18.04.20382-en.
Gholizadeh, S. *et al.* (2018a) 'E-selectin targeted immunoliposomes for rapamycin delivery to activated endothelial cells', *International Journal of Pharmaceutics*, 548(2), pp. 759–770. Available at: https://doi.org/10.1016/j.ijpharm.2017.10.027.
Gholizadeh, S. *et al.* (2018b) 'E-selectin targeted immunoliposomes for rapamycin delivery to activated endothelial cells', *International Journal of Pharmaceutics*, 548(2), pp. 759–770. Available at: https://doi.org/10.1016/j.ijpharm.2017.10.027.
Godo, S. and Shimokawa, H. (2017) 'Endothelial Functions', *Arteriosclerosis, Thrombosis, and Vascular Biology*. Lippincott Williams and Wilkins, pp. e108–e114. Available at: https://doi.org/10.1161/ATVBAHA.117.309813.
Goel, I. *et al.* (2022) 'Enhancement of intercellular interaction between iPSC-derived neural progenitor cells and activated endothelial cells using cell surface modification with functional oligopeptides', *Biomaterials Science*, 10(4), pp. 925–938. Available at: https://doi.org/10.1039/d1bm01503f.
Goldfarb, R.D. *et al.* (2010) 'Targeting host E-selectin expression by antisense oligodeoxynucleotides as potential antiendotoxin therapy in vivo', *Oligonucleotides*, 20(5), pp. 253–261. Available at: https://doi.org/10.1089/oli.2010.0229.
Gopal, S. (2020) 'Syndecans in Inflammation at a Glance', *Frontiers in Immunology*. Frontiers Media S.A. Available at: https://doi.org/10.3389/fimmu.2020.00227.
Hadi, H.A.R., Carr, C.S. and Al Suwaidi, J. (2005) 'Endothelial dysfunction: cardiovascular risk factors, therapy, and outcome.', *Vascular health and risk management*, 1(3), pp. 183–198.
Haeussler, M. *et al.* (2016) 'Evaluation of off-target and on-target scoring algorithms and integration into the guide RNA selection tool CRISPOR', *Genome Biology*, 17(1). Available at: https://doi.org/10.1186/s13059-016-1012-2.
Hall, M.P. *et al.* (2012) 'Engineered luciferase reporter from a deep sea shrimp utilizing a novel imidazopyrazinone substrate', *ACS Chemical Biology*, 7(11), pp. 1848–1857. Available at: https://doi.org/10.1021/cb3002478.
Hamada, K., Osaka, M. and Yoshida, M. (2014) 'Cell density impacts epigenetic regulation of cytokine-induced E-selectin gene expression in vascular endothelium', *PLoS ONE*, 9(4). Available at: https://doi.org/10.1371/journal.pone.0090502.
Hammer, D.A. and Apte, S.M. (1992) 'Simulation of cell rolling and adhesion on surfaces in shear flow: general results and analysis of selectin-mediated neutrophil adhesion', *Biophysical Society*, 53, pp. 35–37.
Hanahan, D., Jessee, J. and Bloom, F.R. (1991) 'Plasmid transformation of Escherichia coli and other bacteria', *Methods in Enzymology*, 204(C), pp. 63–113. Available at: https://doi.org/10.1016/0076-6879(91)04006-A.
He, X. *et al.* (1998) 'Humanization and Pharmacokinetics of a Monoclonal Antibody with Specificity for Both E- and P-Selectin'.
Henriques, G.M.O. *et al.* (1996) 'Selectins mediate eosinophil recruitment in vivo: A comparison with their role in neutrophil influx', *Blood*, 87(12), pp. 5297–5304. Available at: https://doi.org/10.1182/blood.v87.12.5297.bloodjournal87125297.
Hidalgo, A. *et al.* (2007) 'Complete Identification of E-Selectin Ligands on Neutrophils Reveals Distinct Functions of PSGL-1, ESL-1, and CD44', *Immunity*, 26(4), pp. 477–489. Available at: https://doi.org/10.1016/j.immuni.2007.03.011.

Hu, J.B. *et al.* (2018a) ‘An E-selectin targeting and MMP-2-responsive dextran-curcumin polymeric prodrug for targeted therapy of acute kidney injury’, *Biomaterials Science*, 6(12), pp. 3397–3409. Available at: https://doi.org/10.1039/c8bm00813b.
Hu, J.B. *et al.* (2018b) ‘An E-selectin targeting and MMP-2-responsive dextran-curcumin polymeric prodrug for targeted therapy of acute kidney injury’, *Biomaterials Science*, 6(12), pp. 3397–3409. Available at: https://doi.org/10.1039/c8bm00813b.
Hubert, M., Larsson, E. and Lundmark, R. (2020) ‘Keeping in touch with the membrane; Protein- And lipid-mediated confinement of caveolae to the cell surface’, *Biochemical Society Transactions*. Portland Press Ltd, pp. 155–163. Available at: https://doi.org/10.1042/BST20190386.
Hunt, M.A. *et al.* (2010) *Optimizing Transfection of Primary Human Umbilical Vein Endothelial Cells Using Commercially Available Chemical Transfection Reagents*.
Inoue, A. *et al.* (2019) ‘Illuminating G-Protein-Coupling Selectivity of GPCRs’, *Cell*, 177(7), pp. 1933-1947.e25. Available at: https://doi.org/10.1016/j.cell.2019.04.044.
Ivetic, A., Green, H.L.H. and Hart, S.J. (2019) ‘L-selectin: A major regulator of leukocyte adhesion, migration and signaling’, *Frontiers in Immunology*, 10(MAY), pp. 1–22. Available at: https://doi.org/10.3389/fimmu.2019.01068.
Jacob, M.C., Favre, M. and Bensa, J. -C (1991) ‘Membrane cell permeabilisation with saponin and multiparametric analysis by flow cytometry’, *Cytometry*, 12(6), pp. 550–558. Available at: https://doi.org/10.1002/cyto.990120612.
Jacobsen, L.B., Calvin, S.A. and Lobenhofer, E.K. (2009) ‘Transcriptional effects of transfection: The potential for misinterpretation of gene expression data generated from transiently transfected cells’, *BioTechniques*, 47(1), pp. 617–624. Available at: https://doi.org/10.2144/000113132.
Jang, D.I. *et al.* (2021) ‘The role of tumor necrosis factor alpha (Tnf-α) in autoimmune disease and current tnf-α inhibitors in therapeutics’, *International Journal of Molecular Sciences*. MDPI AG, pp. 1–16. Available at: https://doi.org/10.3390/ijms22052719.
Japp, A.G. *et al.* (2013a) ‘Effect of PSI-697, a novel P-selectin inhibitor, on platelet-monocyte aggregate formation in humans.’, *Journal of the American Heart Association*, 2(1), pp. 1–6. Available at: https://doi.org/10.1161/JAHA.112.006007.
Japp, A.G. *et al.* (2013b) ‘Effect of PSI-697, a novel P-selectin inhibitor, on platelet-monocyte aggregate formation in humans.’, *Journal of the American Heart Association*, 2(1), pp. 1–6. Available at: https://doi.org/10.1161/JAHA.112.006007.
Jianying Luo, B., Paranya, G. and Bischoff, J. (1999) ‘Noninflammatory Expression of E-Selectin Is Regulated by Cell Growth’, *The American Society of Hematology*, 93(11), pp. 3785–3791. Available at: http://ashpublications.org/blood/article-pdf/93/11/3785/1653932/3785.pdf.
Jiao, A. *et al.* (2007) ‘A role for endothelial selectins in allergic and nonallergic inflammatory disease’, *Annals of Allergy, Asthma and Immunology*, 98(1), pp. 83–88. Available at: https://doi.org/10.1016/S1081-1206(10)60864-2.
Jin, Y. and Marquardt, S. (2020) ‘Dual sgRNA-based Targeted Deletion of Large Genomic Regions and Isolation of Heritable Cas9-free Mutants in Arabidopsis’, *BIO-PROTOCOL*, 10(20). Available at: https://doi.org/10.21769/bioprotoc.3796.
Jinek, M. *et al.* (2014) *Structures of Cas9 Endonucleases Reveal RNA-Mediated Conformational Activation*, *Science*. Available at: www.sciencemag.org/content/343/6176/1247997/suppl/DC1.
Jubeli, E. *et al.* (2012) ‘Preparation of E-selectin-targeting nanoparticles and preliminary in vitro evaluation’, *International Journal of Pharmaceutics*, 426(1–2), pp. 291–301. Available at: https://doi.org/10.1016/j.ijpharm.2012.01.029.

Jung, U. and Ley, K. (1999) ‘Mice lacking two or all three selectins demonstrate overlapping and distinct functions for each selectin.’, *Journal of immunology (Baltimore, Md. : 1950)*, 162(11), pp. 6755–62.
Jutila, M. *et al.* (1994) ‘Cell surface P- and E-selectin support shear-dependent rolling of bovine gamma/delta T cells.’, *The Journal of Immunology*, 153(9), pp. 3917–3928.
Kaneko, N. *et al.* (2019) ‘The role of interleukin-1 in general pathology’, *Inflammation and Regeneration*. BioMed Central Ltd. Available at: https://doi.org/10.1186/s41232-019-0101-5.
Kany, S., Vollrath, J.T. and Relja, B. (2019) ‘Cytokines in inflammatory disease’, *International Journal of Molecular Sciences*. MDPI AG. Available at: https://doi.org/10.3390/ijms20236008.
Kappelmayer, J. and Nagy, B. (2017a) ‘The Interaction of Selectins and PSGL-1 as a Key Component in Thrombus Formation and Cancer Progression’, *BioMed Research International*, 2017, pp. 1–18. Available at: https://doi.org/10.1155/2017/6138145.
Kappelmayer, J. and Nagy, B. (2017b) ‘The Interaction of Selectins and PSGL-1 as a Key Component in Thrombus Formation and Cancer Progression’, *BioMed Research International*, 2017, pp. 1–18. Available at: https://doi.org/10.1155/2017/6138145.
Kawano, S.K. *et al.* (2011) ‘Identification of a Novel Carbohydrate-Mimicking Octapeptide from Chemical Peptide Library and Characterization as Selectin Inhibitor’, 34(June).
Kerr, K.M. *et al.* (2000a) ‘The use of Cylexin (CY-1503) in prevention of reperfusion lung injury in patients undergoing pulmonary thromboendarterectomy’, *American Journal of Respiratory and Critical Care Medicine*, 162(1), pp. 14–20. Available at: https://doi.org/10.1164/ajrccm.162.1.9712142.
Kerr, K.M. *et al.* (2000b) ‘The use of Cylexin (CY-1503) in prevention of reperfusion lung injury in patients undergoing pulmonary thromboendarterectomy’, *American Journal of Respiratory and Critical Care Medicine*, 162(1), pp. 14–20. Available at: https://doi.org/10.1164/ajrccm.162.1.9712142.
Kessner, S. *et al.* (2001) ‘Investigation of the cellular uptake of E-Selectin-targeted immunoliposomes by activated human endothelial cells’, *Biochimica et Biophysica Acta - Biomembranes*, 1514(2), pp. 177–190. Available at: https://doi.org/10.1016/S0005-2736(01)00368-6.
Kim, I. *et al.* (2001) ‘Vascular Endothelial Growth Factor Expression of Intercellular Adhesion Molecule 1 (ICAM-1), Vascular Cell Adhesion Molecule 1 (VCAM-1), and E-selectin through Nuclear Factor-κB Activation in Endothelial Cells’, *Journal of Biological Chemistry*, 276(10), pp. 7614–7620. Available at: https://doi.org/10.1074/jbc.M009705200.
Kim, W. *et al.* (2003) ‘Adrenomedullin reduces VEGF-induced endothelial adhesion molecules and adhesiveness through a phosphatidylinositol 3′-kinase pathway’, *Arteriosclerosis, Thrombosis, and Vascular Biology*, 23(8), pp. 1377–1383. Available at: https://doi.org/10.1161/01.ATV.0000081740.65173.D1.
King, C. *et al.* (2018) ‘Interactions between NRP1 and VEGFR2 molecules in the plasma membrane’, *Biochim Biophys Acta Biomembr.* [Preprint]. Available at: https://doi.org/10.1016/j.bbamem.
Klopocki, A.G. *et al.* (2008) ‘Replacing a lectin domain residue in L-selectin enhances binding to P-selectin glycoprotein ligand-1 but not to 6-sulfo-sialyl Lewis x’, *Journal of Biological Chemistry*, 283(17), pp. 11493–11500. Available at: https://doi.org/10.1074/jbc.M709785200.
Koch, A.E. *et al.* (1995) ‘Angiogenesis mediated by soluble forms of E-selectin and vascular cell adhesion molecule-1’, *Nature*, 376.
Koch, S. *et al.* (2014) ‘NRP1 Presented in trans to the endothelium arrests VEGFR2 endocytosis, preventing angiogenic signaling and tumor initiation’, *Developmental Cell*, 28(6), pp. 633–646. Available at: https://doi.org/10.1016/j.devcel.2014.02.010.

Kostov, K. (2021) ‘The causal relationship between endothelin-1 and hypertension: Focusing on endothelial dysfunction, arterial stiffness, vascular remodeling, and blood pressure regulation’, *Life*. MDPI. Available at: https://doi.org/10.3390/life11090986.
Kozielewics, P. and Schulte, G. (2022) ‘NanoBRET and NanoBiT/BRET-Based Ligand Binding AssaysPermit Quantitative Assessment of Small Molecule LigandBinding to Smoothened’, in Xiaochin Li (ed.) *Hedgehog Signaling*. Humana Press. Available at: http://www.springer.com/series/7651.
Krüger-Genge, A. *et al.* (2019) ‘Vascular endothelial cell biology: An update’, *International Journal of Molecular Sciences*. MDPI AG. Available at: https://doi.org/10.3390/ijms20184411.
Kumar, P. *et al.* (2003) ‘Src and phosphatidylinositol 3-kinase mediate soluble E-selectin-induced angiogenesis’, *Blood*, 101(10), pp. 3960–3968. Available at: https://doi.org/10.1182/blood-2002-04-1237.
Kurata, M. *et al.* (2018) ‘Highly multiplexed genome engineering using CRISPR/Cas9 gRNA arrays’, *PLoS ONE*, 13(9). Available at: https://doi.org/10.1371/journal.pone.0198714.
Kurtovic, N. and Halilovic, E. (2022) ‘Serum Levels of Tumor Necrosis Factor - alpha in Patients With Psoriasis’, *Materia Socio Medica*, 34(1), p. 40. Available at: https://doi.org/10.5455/msm.2022.33.40-43.
Laferrière, J. *et al.* (2001) ‘Transendothelial Migration of Colon Carcinoma Cells Requires Expression of E-selectin by Endothelial Cells and Activation of Stress-activated Protein Kinase-2 (SAPK2/p38) in the Tumor Cells’, *Journal of Biological Chemistry*, 276(36), pp. 33762–33772.
Lampugnani, M.G. (2012) ‘Endothelial cell-to-cell junctions: Adhesion and signaling in physiology and pathology’, *Cold Spring Harbor Perspectives in Medicine*, 2(10), pp. 1–14. Available at: https://doi.org/10.1101/cshperspect.a006528.
Läubli, H. and Borsig, L. (2010) ‘Selectins as Mediators of Lung Metastasis’, in *Cancer Microenvironment*, pp. 97–105. Available at: https://doi.org/10.1007/s12307-010-0043-6.
Lawrence, M. and Springer, T. (1991) ‘Leukocytes roll on a selectin at physiologic flow rates: distinction from and prerequisite for adhesion through integrins’, *CellPress*, 65(5), pp. 859–873.
Lee, P.Y. *et al.* (2012) ‘Agarose gel electrophoresis for the separation of DNA fragments’, *Journal of Visualized Experiments*, (62), pp. 1–5. Available at: https://doi.org/10.3791/3923.
Leeuwenberg, J.F.M. *et al.* (1992) *E-selectin and intercellular adhesion molecule-1 are released by activated human endothelial cells in vitro*, *Immunology*.
Leroy, E. *et al.* (2019) ‘Differential effect of inhibitory strategies of the V617 mutant of JAK2 on cytokine receptor signaling’, *Journal of Allergy and Clinical Immunology*, 144(1), pp. 224–235. Available at: https://doi.org/10.1016/j.jaci.2018.12.1023.
Levin, J.D., Ting-Beall, H.P. and Hochmuth, R.M. (2001) ‘Correlating the kinetics of cytokine-induced E-selectin adhesion and expression on endothelial cells’, *Biophysical Journal*, 80(2), pp. 656–667. Available at: https://doi.org/10.1016/S0006-3495(01)76046-8.
Ley, K. *et al.* (2007) ‘Getting to the site of inflammation: The leukocyte adhesion cascade updated’, *Nature Reviews Immunology*, pp. 678–689. Available at: https://doi.org/10.1038/nri2156.
Li, Q. *et al.* (2015) ‘A method for surface E-selectin site density determination’, *Frontiers in Life Science*, 8(3), pp. 294–299. Available at: https://doi.org/10.1080/21553769.2015.1033654.
Liang, X. *et al.* (2015) ‘Rapid and highly efficient mammalian cell engineering via Cas9 protein transfection’, *Journal of Biotechnology*, 208, pp. 44–53. Available at: https://doi.org/10.1016/j.jbiotec.2015.04.024.

Liao, H. *et al.* (2014) 'Effects of long-term serial cell passaging on cell spreading, migration, and cell-surface ultrastructures of cultured vascular endothelial cells', *Cytotechnology*, 66(2), pp. 229–238. Available at: https://doi.org/10.1007/s10616-013-9560-8.
Litwin, M. *et al.* (1997) *Novel Cytokine-independent Induction of Endothelial Adhesion Molecules Regulated by Platelet/Endothelial Cell Adhesion Molecule (CD31), The Journal of Cell Biology*. Available at: http://www.jcb.org.
Liu, T. *et al.* (2017) 'NF-κB signaling in inflammation', *Signal Transduction and Targeted Therapy*. Springer Nature. Available at: https://doi.org/10.1038/sigtrans.2017.23.
Loenen, W.A.M. *et al.* (2014) 'Highlights of the DNA cutters: A short history of the restriction enzymes', *Nucleic Acids Research*, 42(1), pp. 3–19. Available at: https://doi.org/10.1093/nar/gkt990.
Lorenz, T.C. (2012) 'Polymerase chain reaction: Basic protocol plus troubleshooting and optimization strategies', *Journal of Visualized Experiments*, (63), pp. 1–15. Available at: https://doi.org/10.3791/3998.
Lorenzon, P. *et al.* (1998) *Endothelial Cell E-and P-Selectin and Vascular Cell Adhesion Molecule-1 Function as Signaling Receptors, The Journal of Cell Biology*. Available at: http://www.jcb.org.
Luís, R. *et al.* (2022) 'Chapter 13 - Nanoluciferase-based methods to monitor activation, modulation and trafficking of atypical chemokine receptors', in A. Shulka (ed.) *Methods in Cell Biology*. 1st edn, pp. 279–294.
Luo, B.-H., Carman, C. V and Springer, T.A. (2007) 'Structural Basis of Integrin Regulation and Signaling', *Annu Rev Immunol*, 25, pp. 619–647.
Ma, S. *et al.* (2016a) 'E-selectin-targeting delivery of microRNAs by microparticles ameliorates endothelial inflammation and atherosclerosis', *Scientific Reports*, 6(November 2015), pp. 1–11. Available at: https://doi.org/10.1038/srep22910.
Ma, S. *et al.* (2016b) 'E-selectin-targeting delivery of microRNAs by microparticles ameliorates endothelial inflammation and atherosclerosis', *Scientific Reports*, 6(November 2015), pp. 1–11. Available at: https://doi.org/10.1038/srep22910.
Ma, Y. *et al.* (2012) 'Human CMV transcripts: an overview', *Future Microbiol*, 7(5), pp. 577–93.
Mai, J. *et al.* (2013) 'An evolving new paradigm: Endothelial cells - Conditional innate immune cells', *Journal of Hematology and Oncology*, 6(1), pp. 1–13. Available at: https://doi.org/10.1186/1756-8722-6-61.
Mann, A.P. *et al.* (2010) 'Identification of thioaptamer ligand against E-selectin: Potential application for inflamed vasculature targeting', *PLoS ONE*, 5(9), pp. 1–11. Available at: https://doi.org/10.1371/journal.pone.0013050.
Marshall, B.T. *et al.* (2003) *Direct observation of catch bonds involving cell-adhesion molecules*. Available at: www.nature.com/nature.
Martens, C.L. *et al.* (1995) 'Peptides which bind to E-selectin and block neutrophil adhesion', *Journal of Biological Chemistry*, 270(36), pp. 21129–21136. Available at: https://doi.org/10.1074/jbc.270.36.21129.
Matthaeus, C. and Taraska, J.W. (2021) 'Energy and Dynamics of Caveolae Trafficking', *Frontiers in Cell and Developmental Biology*. Frontiers Media S.A. Available at: https://doi.org/10.3389/fcell.2020.614472.
McEver, Rodger.P. (1997) 'Regulation of Expression of E-selectin and P-selectin', in D. Vestweber (ed.) *The Selectins. Initiators of Leukocyte Endothelial Adhesion* . 1st edn. Münster: Harwood academic publishers, pp. 31–36.
McEver, R.P. *et al.* (1989) 'GMP-140, a platelet α-granule membrane protein, is also synthesized by vascular endothelial cells and is localized in Weibel-Palade bodies', *Journal of Clinical Investigation*, 84(1), pp. 92–99. Available at: https://doi.org/10.1172/JCI114175.

McEver, R.P. (2015a) ‘Selectins: Initiators of leucocyte adhesion and signalling at the vascular wall’, *Cardiovascular Research*, 107(3), pp. 331–339. Available at: https://doi.org/10.1093/cvr/cvv154.
McEver, R.P. (2015b) ‘Selectins: Initiators of leucocyte adhesion and signalling at the vascular wall’, *Cardiovascular Research*, 107(3), pp. 331–339. Available at: https://doi.org/10.1093/cvr/cvv154.
McEver, R.P. and Zhu, C. (2010) ‘Rolling cell adhesion’, *Annual Review of Cell and Developmental Biology*, pp. 363–396. Available at: https://doi.org/10.1146/annurev.cellbio.042308.113238.
Mehta, V. *et al.* (2018) ‘VEGF (vascular endothelial growth factor) induces NRP1 (neuropilin-1) cleavage via ADAMs (a disintegrin and metalloproteinase) 9 and 10 to generate novel carboxy-terminal NRP1 fragments that regulate angiogenic signaling’, *Arteriosclerosis, Thrombosis, and Vascular Biology*, 38(8), pp. 1845–1858. Available at: https://doi.org/10.1161/ATVBAHA.118.311118.
Di Meo, S. and Venditti, P. (2020) ‘Evolution of the Knowledge of Free Radicals and Other Oxidants’, *Oxidative Medicine and Cellular Longevity*. Hindawi Limited. Available at: https://doi.org/10.1155/2020/9829176.
Michel, T. and Vanhoutte, P.M. (2010) ‘Cellular signaling and NO production’, *Pflugers Archiv European Journal of Physiology*, 459(6), pp. 807–816. Available at: https://doi.org/10.1007/s00424-009-0765-9.
Miki, I. *et al.* (1996) ‘Histamine enhanced the TNF-α-induced expression of E-selectin and ICAM-1 on vascular endothelial cells’, *Cellular Immunology*, 171(2), pp. 285–288. Available at: https://doi.org/10.1006/cimm.1996.0205.
Minaguchi, J. *et al.* (2008) ‘Transvascular accumulation of sialyl lewis X conjugated liposome in inflamed joints of collagen antibody-induced arthritic (CAIA) mice’, *Archives of Histology and Cytology*, 71(3), pp. 195–203. Available at: https://doi.org/10.1679/aohc.71.195.
Modur, V. *et al.* (1997) ‘Oncostatin M Is a Proinflammatory Mediator’, *Journal of Clinical Investigations*, 100(1), pp. 158–168.
Molenaar, T.J.M. *et al.* (2002) ‘Specific inhibition of P-selectin-mediated cell adhesion by phage display-derived peptide antagonists’, *Blood*, 100(10), pp. 3570–3577. Available at: https://doi.org/10.1182/blood-2002-02-0641.
Morita, Y. *et al.* (2016) ‘E-selectin Targeting PEGylated-thioaptamer Prevents Breast Cancer Metastases’, *Molecular Therapy - Nucleic Acids*, 5(December), p. e399. Available at: https://doi.org/10.1038/mtna.2016.103.
Moya-García, A.A. *et al.* (2021) ‘Histamine, Metabolic Remodelling and Angiogenesis:A Systems Level Approach’, *biomolecules*, 11(415). Available at: https://doi.org/10.3390/biom.
Myers, D. *et al.* (2002) ‘Selectins Influence Thrombosis in a Mouse Model of Experimental Deep Venous Thrombosis’, *Journal of Surgical Research*, 108(2), pp. 212–221.
Myers, D. *et al.* (2019) ‘From the American Venous Forum A new way to treat proximal deep venous thrombosis using E-selectin inhibition’, pp. 268–278. Available at: https://doi.org/10.1016/j.jvsv.2019.08.016.
Myrset, A.H. *et al.* (2011) ‘Design and characterization of targeted ultrasound microbubbles for diagnostic use’, *Ultrasound in Medicine and Biology*, 37(1), pp. 136–150. Available at: https://doi.org/10.1016/j.ultrasmedbio.2010.10.010.
Nishimasu, H. *et al.* (2014) ‘Crystal structure of Cas9 in complex with guide RNA and target DNA’, *Cell*, 156(5), pp. 935–949. Available at: https://doi.org/10.1016/j.cell.2014.02.001.
Noori, N.M. *et al.* (2017) *Serum Levels of Tumor Necrosis Factor-α and Interleukins in Children with Congenital Heart Disease*, *J Teh Univ Heart Ctr*. Available at: http://jthc.tums.ac.ir.

Oh-hashi, K. *et al.* (2017) 'Application of a novel HiBiT peptide tag for monitoring ATF4 protein expression in Neuro2a cells', *Biochemistry and Biophysics Reports*, 12, pp. 40–45. Available at: https://doi.org/10.1016/j.bbrep.2017.08.002.
Ohta, S. *et al.* (2001a) 'Inhibition of P-selectin specific cell adhesion by a low molecular weight, non-carbohydrate compound, KF38789', *Inflammation Research*, 50(11), pp. 544–551. Available at: https://doi.org/10.1007/PL00000232.
Ohta, S. *et al.* (2001b) 'Inhibition of P-selectin specific cell adhesion by a low molecular weight, non-carbohydrate compound, KF38789', *Inflammation Research*, 50(11), pp. 544–551. Available at: https://doi.org/10.1007/PL00000232.
O'Neill, S. and Knaus, U. (2022) 'Bioluminescence-Based Complementation Assayto Correlate Conformational Changes in Membrane-BoundComplexes with Enzymatic Function', in Sig-Bae Kim (ed.) *Bioluminescence*. 4th edn. Humana Press, pp. 123–137. Available at: http://www.springer.com/series/7651.
Ostadfar, A. (2016) 'Macrocirculation System', *Biofluid Mechanics*, pp. 61–86. Available at: https://doi.org/10.1016/b978-0-12-802408-9.00002-8.
Ourradi, K. *et al.* (2017) 'VEGF isoforms have differential effects on permeability of human pulmonary microvascular endothelial cells', *Respiratory Research*, 18(1). Available at: https://doi.org/10.1186/s12931-017-0602-1.
Panicker, S. *et al.* (2017) 'Circulating soluble P-selectin must dimerize to promote inflammation and coagulation in mice', *Blood*, 130(2), pp. 181–191. Available at: https://doi.org/10.1182/blood-2017-02-770479.
Parikh, P.P. *et al.* (2018) 'Intramuscular E-selectin/adeno-associated virus gene therapy promotes wound healing in an ischemic mouse model', *Journal of Surgical Research*, 228, pp. 68–76. Available at: https://doi.org/10.1016/j.jss.2018.02.061.
Peach, C.J. *et al.* (2018) 'Molecular pharmacology of VEGF-A isoforms: Binding and signalling at VEGFR2', *International Journal of Molecular Sciences*. MDPI AG. Available at: https://doi.org/10.3390/ijms19041264.
Peach, C.J. *et al.* (2021) 'Use of NanoBiT and NanoBRET to monitor fluorescent VEGF-A binding kinetics to VEGFR2/NRP1 heteromeric complexes in living cells', *British Journal of Pharmacology*, 178(12), pp. 2393–2411. Available at: https://doi.org/10.1111/bph.15426.
Pfleger, K.D. and Eidne, K.A. (2006) 'Illuminating insights into protein-protein interactions using bioluminescence resonance energy transfer (BRET)', *Nature Methods*, 3, pp. 165–174.
Pober, J.S. and Sessa, W.C. (2007) 'Evolving functions of endothelial cells in inflammation', *Nature Reviews Immunology*, 7(10), pp. 803–815. Available at: https://doi.org/10.1038/nri2171.
Podolnikova, N.P. *et al.* (2015) 'Ligand recognition specificity of leukocyte integrin αmβ2 (Mac-1, CD11b/CD18) and its functional consequences', *Biochemistry*, 54(6), pp. 1408–1420. Available at: https://doi.org/10.1021/bi5013782.
Popa, C. *et al.* (2007) 'The role of TNF-α in chronic inflammatory conditions, intermediary metabolism, and cardiovascular risk', *Journal of Lipid Research*, pp. 751–752. Available at: https://doi.org/10.1194/jlr.R600021-JLR200.
Promega Corporation (2018a) 'Nano-Glo® Luciferase Assay System', *Nld.Promega.Com* [Preprint]. Available at: https://nld.promega.com/products/reporter-assays-and-transfection/reporter-assays/nano_glo-luciferase-assay-system/?catNum=N1110.
Promega Corporation (2018b) *Nano-Glo ® Endurazine™ and Vivazine™ Live Cell Substrates Instructions for Use of*. Available at: www.promega.com.
Promega Corporation. (2018) 'Technical Manual: Nano-Glo® Endurazine™ and Vivazine ™ Live Cell Substrates'. Available at: https://www.promega.de/-/media/files/resources/protocols/technical-manuals/500/nano-glo-endurazine-and-vivazine-live-cell-substrates-technical-manual.pdfp.

Qin, L. *et al.* (2013) 'The vascular permeabilizing factors histamine and serotonin induce angiogenesis through TR3/Nur77 and subsequently truncate it through thrombospondin-1', *Blood*, 121(11), pp. 2154–2164.
Rahman, A. *et al.* (1998) *E-selectin expression in human endothelial cells by TNF-induced oxidant generation and NF-B activation*.
Rajendran, P. *et al.* (2013) 'The vascular endothelium and human diseases', *International Journal of Biological Sciences*, 9(10), pp. 1057–1069. Available at: https://doi.org/10.7150/ijbs.7502.
Ramachandran, V. *et al.* (2004) 'Dynamic alterations of membrane tethers stabilize leukocyte rolling on P-selectin', *Proceedings of the National Academy of Sciences of the United States of America*, 101(37), pp. 13519–13524. Available at: https://doi.org/10.1073/pnas.0403608101.
Rashid, M. ur and Coombs, K.M. (2019) 'Serum-reduced media impacts on cell viability and protein expression in human lung epithelial cells', *Journal of Cellular Physiology*, 234(6), pp. 7718–7724. Available at: https://doi.org/10.1002/jcp.27890.
Read, M.A. *et al.* (1997) 'Tumor necrosis factor α-induced E-selectin expression is activated by the nuclear factor-κB and c-JUN N-terminal kinase/p38 mitogen-activated protein kinase pathways', *Journal of Biological Chemistry*, 272(5), pp. 2753–2761. Available at: https://doi.org/10.1074/jbc.272.5.2753.
Reyes-Alcaraz, A. *et al.* (2022) 'A NanoBiT assay to monitor membrane proteins trafficking for drug discovery and drug development', *Communications Biology*, 5(1). Available at: https://doi.org/10.1038/s42003-022-03163-9.
Robb, G.B. (2019) 'Genome Editing with CRISPR-Cas: An Overview', *Current Protocols in Essential Laboratory Techniques*, 19(1), pp. 1–20. Available at: https://doi.org/10.1002/cpet.36.
Rocheleau, A.D. *et al.* (2016) 'Comparison of human and mouse E-selectin binding to Sialyl-Lewisx', *BMC Structural Biology*, 16(1). Available at: https://doi.org/10.1186/s12900-016-0060-x.
Rodrigues, R.M. *et al.* (2022) 'E-Selectin-Dependent Inflammation and Lipolysis in Adipose Tissue Exacerbate Steatosis-to-NASH Progression via S100A8/9', *CMGH*, 13(1), pp. 151–171. Available at: https://doi.org/10.1016/j.jcmgh.2021.08.002.
Roitt, Ivain.M. *et al.* (2017) *Roitt's essential immunology*. 13th edn.
Rossi, R. *et al.* (1997) 'Functional characterization of the T4 DNA ligase: A new insight into the mechanism of action', *Nucleic Acids Research*, 25(11), pp. 2106–2113. Available at: https://doi.org/10.1093/nar/25.11.2106.
Sakhalkar, H.S. *et al.* (2003) 'Leukocyte-inspired biodegradable particles that selectively and avidly adhere to inflamed endothelium in vitro and in vivo', *Proceedings of the National Academy of Sciences of the United States of America*, 100(26), pp. 15895–15900. Available at: https://doi.org/10.1073/pnas.2631433100.
Sandoo, A. *et al.* (2010) 'The Endothelium and Its Role in Regulating Vascular Tone', *The Open Cardiovascular Medicine Journal*, 4(1), pp. 302–312. Available at: https://doi.org/10.2174/1874192401004010302.
Sarangapani, K.K. *et al.* (2004) 'Low Force Decelerates L-selectin Dissociation from P-selectin Glycoprotein Ligand-1 and Endoglycan', *Journal of Biological Chemistry*, 279(3), pp. 2291–2298. Available at: https://doi.org/10.1074/jbc.M310396200.
Sawant, D.A. *et al.* (2013) 'Regulation of tumor necrosis factor-α einduced microvascular endothelial cell hyperpermeability by recombinant B-cell lymphoma-extra large', *Journal of Surgical Research*, 184(1), pp. 628–637. Available at: https://doi.org/10.1016/j.jss.2013.04.079.

Schimmel, L., Heemskerk, N. and van Buul, J.D. (2017) 'Leukocyte transendothelial migration: A local affair', *Small GTPases*. Taylor and Francis Inc., pp. 1–15. Available at: https://doi.org/10.1080/21541248.2016.1197872.
Schleiffenbaum, B., Spertini, O. and Tedder, T.F. (1992) 'Soluble L-selectin is present in human plasma at high levels and retains functional activity', *Journal of Cell Biology*, 119(1), pp. 229–238. Available at: https://doi.org/10.1083/jcb.119.1.229.
Schmidtke, D.W. and Diamond, S.L. (2000) *Direct Observation of Membrane Tethers Formed during Neutrophil Attachment to Platelets or P-selectin under Physiological Flow*, *The Journal of Cell Biology*. Available at: http://www.jcb.org.
Schön, M.P. (2005) 'Inhibitors of selectin functions in the treatment of inflammatory skin disorders.', *Therapeutics and clinical risk management*, 1(3), pp. 201–8.
Shamay, Y. *et al.* (2009a) 'E-selectin binding peptide-polymer-drug conjugates and their selective cytotoxicity against vascular endothelial cells', *Biomaterials*, 30(32), pp. 6460–6468. Available at: https://doi.org/10.1016/j.biomaterials.2009.08.013.
Shamay, Y. *et al.* (2009b) 'E-selectin binding peptide-polymer-drug conjugates and their selective cytotoxicity against vascular endothelial cells', *Biomaterials*, 30(32), pp. 6460–6468. Available at: https://doi.org/10.1016/j.biomaterials.2009.08.013.
Shamay, Y. *et al.* (2009c) 'Multivalent display of quinic acid based ligands for targeting E-selectin expressing cells', *Journal of Medicinal Chemistry*, 52(19), pp. 5906–5915. Available at: https://doi.org/10.1021/jm900308r.
Shamay, Y. *et al.* (2015a) 'Inhibition of primary and metastatic tumors in mice by E-selectin-targeted polymer-drug conjugates', *Journal of Controlled Release*, 217, pp. 102–112. Available at: https://doi.org/10.1016/j.jconrel.2015.08.029.
Shamay, Y. *et al.* (2015b) 'Inhibition of primary and metastatic tumors in mice by E-selectin-targeted polymer-drug conjugates', *Journal of Controlled Release*, 217, pp. 102–112. Available at: https://doi.org/10.1016/j.jconrel.2015.08.029.
Shao, J.Y., Ting-Beall, H.P. and Hochmuth, R.M. (1998) 'Static and dynamic lengths of neutrophil microvilli', *Proceedings of the National Academy of Sciences of the United States of America*, 95(12), pp. 6797–6802. Available at: https://doi.org/10.1073/pnas.95.12.6797.
Shintani, Y. *et al.* (2006) 'Glycosaminoglycan modification of neuropilin-1 modulates VEGFR2 signaling', *EMBO Journal*, 25(13), pp. 3045–3055. Available at: https://doi.org/10.1038/sj.emboj.7601188.
Silva, R. *et al.* (2008) 'Integrins: The keys to unlocking angiogenesis', *Arteriosclerosis, Thrombosis, and Vascular Biology*, pp. 1703–1713. Available at: https://doi.org/10.1161/ATVBAHA.108.172015.
Soave, M., Heukers, R., *et al.* (2020) 'Monitoring Allosteric Interactions with CXCR4 Using NanoBiT Conjugated Nanobodies', *Cell Chemical Biology*, 27(10), pp. 1250-1261.e5. Available at: https://doi.org/10.1016/j.chembiol.2020.06.006.
Soave, M., Kellam, B., *et al.* (2020) 'NanoBiT Complementation to Monitor Agonist-Induced Adenosine A1 Receptor Internalization', *SLAS Discovery*, 25(2), pp. 186–194. Available at: https://doi.org/10.1177/2472555219880475.
Sonar, S.A. and Lal, G. (2019) 'The iNOS activity during an immune response controls the CNS pathology in experimental autoimmune encephalomyelitis', *Frontiers in Immunology*, 10(APR). Available at: https://doi.org/10.3389/fimmu.2019.00710.
Spivak, I. *et al.* (2016) 'Low-Dose Molecular Ultrasound Imaging with E-Selectin-Targeted PBCA Microbubbles', (September 2015), pp. 180–190. Available at: https://doi.org/10.1007/s11307-015-0894-9.
Spragg, D.D. *et al.* (1997a) 'Immunotargeting of liposomes to activated vascular endothelial cells: A strategy for site-selective delivery in the cardiovascular system', *Proceedings of the*

National Academy of Sciences of the United States of America, 94(16), pp. 8795–8800. Available at: https://doi.org/10.1073/pnas.94.16.8795.
Spragg, D.D. *et al.* (1997b) 'Immunotargeting of liposomes to activated vascular endothelial cells: A strategy for site-selective delivery in the cardiovascular system', *Proceedings of the National Academy of Sciences of the United States of America*, 94(16), pp. 8795–8800. Available at: https://doi.org/10.1073/pnas.94.16.8795.
Stadtmann, A. *et al.* (2011) 'Rap1a activation by CalDAG-GEFI and p38 MAPK is involved in E-selectin-dependent slow leukocyte rolling', *European Journal of Immunology*, 41(7), pp. 2074–2085. Available at: https://doi.org/10.1002/eji.201041196.
Stadtmann, A. *et al.* (2013a) 'The PSGL-1-L-selectin signaling complex regulates neutrophil adhesion under flow', *Journal of Experimental Medicine*, 210(11), pp. 2171–2180. Available at: https://doi.org/10.1084/jem.20130664.
Stadtmann, A. *et al.* (2013b) 'The PSGL-1-L-selectin signaling complex regulates neutrophil adhesion under flow', *Journal of Experimental Medicine*, 210(11), pp. 2171–2180. Available at: https://doi.org/10.1084/jem.20130664.
Stahn, R. *et al.* (1998) 'Multivalent sialyl Lewis x ligands of definite structures as inhibitors of E-selectin mediated cell adhesion', *Glycobiology*, 8(4), pp. 311–319. Available at: https://doi.org/10.1093/glycob/8.4.311.
Stannard, A.K. *et al.* (2007) 'Vascular endothelial growth factor synergistically enhances induction of E-selectin by tumor necrosis factor-α', *Arteriosclerosis, Thrombosis, and Vascular Biology*, 27(3), pp. 494–502. Available at: https://doi.org/10.1161/01.ATV.0000255309.38699.6c.
Stocker, C.J. *et al.* (2000) 'TNF-α, IL-4, and IFN-γ Regulate Differential Expression of P- and E-Selectin Expression by Porcine Aortic Endothelial Cells', *The Journal of Immunology*, 164(6), pp. 3309–3315. Available at: https://doi.org/10.4049/jimmunol.164.6.3309.
Stocker, C.J. *et al.* (2014) 'TNF- , IL-4, and IFN- Regulate Differential Expression of P- and E-Selectin Expression by Porcine Aortic Endothelial Cells', *The Journal of Immunology*, 164(6), pp. 3309–3315. Available at: https://doi.org/10.4049/jimmunol.164.6.3309.
Sturtzel, C. (2017a) 'Endothelial Cells', in *The Immunology of Cardiovascular Homeostasis and Pathology*. The Immunology of Cardiovascular Homeostasis and Patholog, pp. 77–91. Available at: https://doi.org/10.1007/978-3-319-57613-8.
Sturtzel, C. (2017b) 'Endothelial Cells', in *The Immunology of Cardiovascular Homeostasis and Pathology*. The Immunology of Cardiovascular Homeostasis and Patholog, pp. 77–91. Available at: https://doi.org/10.1007/978-3-319-57613-8.
Subramaniam, M., Koedam, J.A. and Wagner, D.D. (1993) *Divergent Fates of P-and E-Selectins After Their Expression on the Plasma Membrane*, *Molecular Biology of the Cell*.
Sukriti, S. *et al.* (2014) 'Mechanisms regulating endothelial permeability', *Pulmonary Circulation*, 4(4), pp. 535–551. Available at: https://doi.org/10.1086/677356.
Sullivan, V. *et al.* (2003) 'Decrease in fibrin content of venous thrombi in selectin-deficient mice', *Journal of Surgical Research*, 109(1), pp. 1–7.
Sun, H., Hu, L. and Fan, Z. (2021) 'β2 integrin activation and signal transduction in leukocyte recruitment', *American Journal of Physiology - Cell Physiology*. American Physiological Society, pp. C308–C316. Available at: https://doi.org/10.1152/ajpcell.00560.2020.
Sundd, P. *et al.* (2012) 'Slings enable neutrophil rolling at high shear', *Nature*, pp. 399–403. Available at: https://doi.org/10.1038/nature11248.
Tammara, B.K. *et al.* (2017) 'Lack of Effect of Rivipansel on QTc Interval in Healthy Adult African American Male Subjects', *Journal of Clinical Pharmacology*, 57(10), pp. 1315–1321. Available at: https://doi.org/10.1002/jcph.924.

Telen, M. *et al.* (2015) 'Randomized phase 2 study of GMI-1070 in SCD: reduction in time to resolution of vaso-occlusive events and decreased opioid use', *Blood*, 125(17), pp. 2656–2664.
Tinoco, R. *et al.* (2017) 'PSGL-1: A New Player in the Immune Checkpoint Landscape', *Trends in Immunology*, 38(5), pp. 323–335. Available at: https://doi.org/10.1016/j.it.2017.02.002.
Tomioka, H. *et al.* (1999) 'Relaxation in Different-Sized Rat BloodVessels Mediated by Endothelium-Derived Hyperpolarizing Factor: Importance of Processes Mediating Precontractions', *Journal of Vascular Research*, 36, pp. 311–320.
Tóth, A.D. *et al.* (2021) 'A general method for quantifying ligand binding to unmodified receptors using Gaussia luciferase', *Journal of Biological Chemistry*, 296. Available at: https://doi.org/10.1016/j.jbc.2021.100366.
Tremblay, P.L., Auger, F.A. and Huot, J. (2006) 'Regulation of transendothelial migration of colon cancer cells by E-selectin-mediated activation of p38 and ERK MAP kinases', *Oncogene*, 25(50), pp. 6563–6573. Available at: https://doi.org/10.1038/sj.onc.1209664.
Tsoref, O. *et al.* (2018) 'E-selectin-targeted copolymer reduces atherosclerotic lesions, adverse cardiac remodeling, and dysfunction', *Journal of Controlled Release*, 288(May), pp. 136–147. Available at: https://doi.org/10.1016/j.jconrel.2018.08.029.
Tu, L. *et al.* (2002) 'A functional role for circulating mouse L-selectin in regulating leukocyte/endothelial cell interactions in vivo.', *Journal of immunology (Baltimore, Md. : 1950)*, 169(4), pp. 2034–43. Available at: https://doi.org/10.4049/jimmunol.169.4.2034.
Tucker, W. and Mahajan (2019) *Anatomy, Blood Vessels*. Edited by WD. Tucker and K. Mahajan. StatPearls.
Ulbrich, H.K. *et al.* (2006a) 'A novel class of potent nonglycosidic and nonpeptidic pan-selectin inhibitors', *Journal of Medicinal Chemistry*, 49(20), pp. 5988–5999. Available at: https://doi.org/10.1021/jm060468y.
Ulbrich, H.K. *et al.* (2006b) 'A novel class of potent nonglycosidic and nonpeptidic pan-selectin inhibitors', *Journal of Medicinal Chemistry*, 49(20), pp. 5988–5999. Available at: https://doi.org/10.1021/jm060468y.
Ushiyama, S. *et al.* (1993) 'Structural and functional characterization of monomeric soluble P-selectin and comparison with membrane P-selectin', *Journal of Biological Chemistry*, 268(20), pp. 15229–15237.
Vestweber, D. (2008) 'VE-cadherin: The major endothelial adhesion molecule controlling cellular junctions and blood vessel formation', *Arteriosclerosis, Thrombosis, and Vascular Biology*, pp. 223–232. Available at: https://doi.org/10.1161/ATVBAHA.107.158014.
Vinogradova, T.M., Roudnik, V.E., Bystrevskaya, V.B., *et al.* (2000) 'Centrosome-directed translocation of Weibel-Palade bodies is rapidly induced by thrombin, calyculin A, or cytochalasin B in human aortic endothelial cells', *Cell Motility and the Cytoskeleton*, 47(2), pp. 141–153. Available at: https://doi.org/10.1002/1097-0169(200010)47:2<141::AID-CM5>3.0.CO;2-U.
Vinogradova, T.M., Roudnik, V.E., Bystrevskaya, V., *et al.* (2000) 'Centrosome-directed translocation of Weibel-Palade bodies is rapidly induced by thrombin, calyculin A, or cytochalasin B in human aortic endothelial cells', *Cell Motility and the Cytoskeleton*, 47(2), pp. 141–153. Available at: https://doi.org/10.1002/1097-0169(200010)47:2<141::AID-CM5>3.0.CO;2-U.
Wacker, I. *et al.* (1997) 'Microtubule-dependent transport of secretory vesicles visualized in real time with a GFP-tagged secretory protein.', *Journal of cell science*, 110 (Pt 1, pp. 1453–63.
Wallez, Y. and Huber, P. (2008) 'Endothelial adherens and tight junctions in vascular homeostasis, inflammation and angiogenesis', *Biochimica et Biophysica Acta* -

Biomembranes, 1778(3), pp. 794–809. Available at: https://doi.org/10.1016/j.bbamem.2007.09.003.
Wayman, A.M. *et al.* (2010) 'Triphasic force dependence of E-selectin/ligand dissociation governs cell rolling under flow', *Biophysical Journal*, 99(4), pp. 1166–1174. Available at: https://doi.org/10.1016/j.bpj.2010.05.040.
Weber, C. (2003) 'Novel mechanistic concepts for the control of leukocyte transmigration: Specialization of integrins, chemokines, and junctional molecules', *Journal of Molecular Medicine*, 81(1), pp. 4–19. Available at: https://doi.org/10.1007/s00109-002-0391-x.
Weihs, F. *et al.* (2020) 'Experimental determination of the bioluminescence resonance energy transfer (BRET) Förster distances of NanoBRET and red-shifted BRET pairs', *Analytica Chimica Acta: X*, 6. Available at: https://doi.org/10.1016/j.acax.2020.100059.
van Wetering, S. *et al.* (2013) 'VCAM-1-mediated Rac signaling controls endothelial cell-cell contacts and leukocyte transmigration', *American Journal of Physiology-Cell Physiology*, 285(2), pp. C343–C352. Available at: https://doi.org/10.1152/ajpcell.00048.2003.
Wheater, P.R., Burkitt, H.G. and Daniels, V.G. (1982) *Functional Histology*. 1st edn. Churchill Livingstone.
White, C.W. *et al.* (2020) 'CRISPR-Mediated Protein Tagging with Nanoluciferase to Investigate Native Chemokine Receptor Function and Conformational Changes', *Cell Chemical Biology*, 27(5), pp. 499-510.e7. Available at: https://doi.org/10.1016/j.chembiol.2020.01.010.
Wildeman, A.G. (1988) 'Regulation of SV40 early gene expression', *Biochemistry and Cell Biology*, 66(6).
De Wit, T.R. *et al.* (2003) 'Real-time imaging of the dynamics and secretory behavior of Weibel-Palade bodies', *Arteriosclerosis, Thrombosis, and Vascular Biology*, 23(5), pp. 755–761. Available at: https://doi.org/10.1161/01.ATV.0000069847.72001.E8.
Wodicka, J.R. *et al.* (2019) 'Selectin-Targeting Peptide–Glycosaminoglycan Conjugates Modulate Neutrophil–Endothelial Interactions', *Cellular and Molecular Bioengineering*, 12(1), pp. 121–130. Available at: https://doi.org/10.1007/s12195-018-0555-6.
Woltmann, G. *et al.* (2000) 'Interleukin-13 induces PSGL-1/P-selectin-dependent adhesion of eosinophils, but not neutrophils, to human umbilical vein endothelial cells under flow', *Blood*, 95(10), pp. 3146–3152.
Wong, D. and Dorovini-Zis, K. (1996) 'Regulation by Cytokines and lipopolysaccharide of E-selectin Expression by Human Brain Microvessel Endothelial Cells in Primary Culture', *Journal of Neuropathology and Experimental Neurology*, 55(2), pp. 225–235.
Woo, J., Hong, J. and Dinesh-Kumar, S.P. (2017) 'Bioluminescence resonance energy transfer (BRET)-based synthetic sensor platform for drug discovery', *Current Protocols in Protein Science*, 2017, pp. 1–12. Available at: https://doi.org/10.1002/cpps.30.
Wun, T. *et al.* (2014) 'Phase 1 study of the E-selectin inhibitor GMI 1070 in patients with sickle cell anemia', *PLoS ONE*, 9(7), pp. 1–12. Available at: https://doi.org/10.1371/journal.pone.0101301.
Wyble, C. *et al.* (1996) 'Physiologic Concentrations of TNFα and IL-1β Released from Reperfused Human Intestine Upregulate E-Selectin and ICAM-1', 63(1), pp. 333–338.
Wyble, C.W. *et al.* (1997) 'TNF-alpha and IL-1 Upregulate Membrane-Bound and Soluble E-Selectin through a Common Pathway', *JOURNAL OF SURGICAL RESEARCH*, 73, pp. 107–117.
Xu, C. *et al.* (2015) 'TNF causes changes in glomerular endothelial permeability and morphology through a Rho and myosin light chain kinase-dependent mechanism', *Physiological Reports*, 3(12). Available at: https://doi.org/10.14814/phy2.12636.

Xu, X.L. *et al.* (2019) 'Highly Integrated Nanoplatform Based on an E-Selectin-Targeting Strategy for Metastatic Breast Cancer Treatment', *Molecular Pharmaceutics*, 16(8), pp. 3694–3702. Available at: https://doi.org/10.1021/acs.molpharmaceut.9b00616.
Yago, T. *et al.* (2004) 'Catch bonds govern adhesion through L-selectin at threshold shear', *Journal of Cell Biology*, 166(6), pp. 913–923. Available at: https://doi.org/10.1083/jcb.200403144.
Yasuda, M. *et al.* (2002) 'Differential roles of ICAM-1 and E-selectin in polymorphonuclear leukocyte-induced angiogenesis'. Available at: https://doi.org/10.1152/ajpcell.00223.2001.-Ets-1.
Yu, L. *et al.* (2009) 'Phage display screening against a set of targets to establish peptide-based sugar mimetics and molecular docking to predict binding site', *Bioorganic & Medicinal Chemistry*, 17(13), pp. 4825–32.
Zarbock, A. *et al.* (2008) 'PSGL-1 engagement by E-selectin signals through Src kinase Fgr and ITAM adapters DAP12 and FcRγ to induce slow leukocyte rolling', *Journal of Experimental Medicine*, 205(10), pp. 2339–2347. Available at: https://doi.org/10.1084/jem.20072660.
Zarbock, A. *et al.* (2011a) 'Leukocyte ligands for endothelial selectins: Specialized glycoconjugates that mediate rolling and signaling under flow', *Blood*, 118(26), pp. 6743–6751. Available at: https://doi.org/10.1182/blood-2011-07-343566.
Zarbock, A. *et al.* (2011b) 'Leukocyte ligands for endothelial selectins: Specialized glycoconjugates that mediate rolling and signaling under flow', *Blood*, 118(26), pp. 6743–6751. Available at: https://doi.org/10.1182/blood-2011-07-343566.
Zhang, X.H. *et al.* (2015) 'Off-target effects in CRISPR/Cas9-mediated genome engineering', *Molecular Therapy - Nucleic Acids*. Nature Publishing Group, p. e264. Available at: https://doi.org/10.1038/mtna.2015.37.
Zhu, Q. *et al.* (2020) 'Serum concentrations of TNF-α and its soluble receptors in graves' disease', *Endocrine Connections*, 9(7), pp. 736–746. Available at: https://doi.org/10.1530/EC-20-0162.